CRANFIELD INSTITUTE OF TECHNOLOGY

SCHOOL OF INDUSTRIAL SCIENCE

PhD Thesis

Academic Year 1980 - 1982

J.W.C. THOMPSON

Phenomenological investigation of the influence of Cathodic Protection on corrosion fatigue crack propagation behaviour, in a BS 4360 50D type structural steel and associated weldment microstructures, in a marine environment

Supervisor : B.S. Hockenhull

June 1984

ABSTRACT

The influence of Cathodic Protection potential upon corrosion fatigue crack propagation rates in a medium-strength ferritic-pearlitic structural steel (BS 4360 grade 50D) and associated weldment microstructures in simulated sea-water was studied and the results were presented in bi-modal da/dN vs ΔK curves. Above transition propagation rate data was satisfactorily described by the Paris relationship $da/dN = C.\Delta K^m$ and a relationship of the form $m = A\ln C + D$ between Paris exponent m and constant C was confirmed. In all microstructures the influence of cathodic protection on crack propagation rate was found to be dependent upon the level of cathodic potential applied and crack depth. A critical crack depth of approximately 5.0mm was identified.

Optical crack monitoring combined with graphical data processing,was found to be particularly effective for the characterisation of corrosion fatigue crack propagation behaviour and resulted in minimal data scatter. The phenomena of transition which was evident in the bi-modal da/dN vs ΔK curves was found to be associated with secondary or branched-crack activity. Back-extrapolation of below transition data was used to estimate ΔK_{TH} values and showed that the weldment heat-affected zone microstructure was a major potential source of fatigue or corrosion fatigue fracture.

The effect of a single cycle of simulated overload, to storm-load levels, on both fatigue and corrosion fatigue crack propagation behaviour in parent plate material was studied and the phenomenon of retardation was confirmed.

ACKNOWLEDGEMENTS

I would like to thank my supervisor, Mr. B.S. Hockenhull, for his advice and guidance throughout this project and for his help during the period I have been at Cranfield.

My thanks are also due to :-

(i) Mr. R. Hardwicke and Mr. A. Baldwin and their staff, for the high standard of engineering support which was provided by the departmental workshops.

(ii) Mr. R. Smith, for maintenance and development of the electronic control system for the electrohydraulic fatigue testing machine.

(iii) Mr. D. Timpson, Mr. P. Cook and Mr. C. Mathews for laboratory services.

(iv) Mrs. Ann Hills for her careful typing of this thesis.

Finally, I would like to express my gratitude and appreciation to my wife, for all her support and encouragement, throughout the period of my studies at Cranfield.

INDEX

PAGE NUMBERING AS ORIGINAL

LIST OF FIGURES

14. Fractographs of fracture surfaces in weld metal in air, exhibiting ductile striation-type surface markings.

15. Fractograph of fracture surface in BS 4360 50D plate material in air, exhibiting ductile striation-type surface markings.

16. Graphs of log da/dN Vs log ΔK, for crack growth in BS 4360 50D plate material in environments of laboratory air, nominal correct cathodic protection, nominal cathodic overprotection and free corrosion.

17. Graphs of Environmental Enhancement Factor Vs ΔK, for crack growth in BS 4360 50D plate material.

18. Fractographs of fracture surfaces in BS 4360 50D plate material, in an environment of free corrosion.

19. Fractographs of fracture surfaces in BS 4360 50D plate material, in an environment of nominal correct cathodic protection.

20. Fractographs of fracture surfaces in BS 4360 50D plate material, in an environment of nominal cathodic overprotection.

21. Graphs of log da/dN Vs log ΔK, for crack growth in weld metal in environments of laboratory air, nominal correct cathodic protection, nominal cathodic overprotection and free corrosion.

22. Graphs of Environmental Enhancement Factor Vs ΔK, for crack growth in weld metal.

23. Fractographs of fracture surfaces in weld metal, in an environment of free corrosion.

24. Fractographs of fracture surfaces in weld metal, in an environment of nominal correct cathodic protection.

25. Fractographs of fracture surfaces in weld metal, in an environment of nominal cathodic over-protection.

26. Graphs of log da/dN Vs log ΔK for crack growth in heat affected zone microstructure in environments of laboratory air, nominal correct cathodic protection, nominal cathodic overprotection and free corrosion.

27. Graphs of Environmental Enhancement Factor Vs ΔK, for crack growth in heat affected zone microstructure.

28. Graphs of log da/dN Vs log ΔK, for crack growth in weld fusion-line microstructure, in environments of laboratory air, nominal correct cathodic protection, nominal cathodic overprotection and free corrosion.

29. Graphs of Environmental Enhancement Factor Vs ΔK, for crack growth in weld fusion-line microstructure.

30. Graph of a Vs N for crack growth in BS 4360 50D plate material in an environment of simulated tidal immersion.

31. Graph of a Vs N for crack growth in weld metal in an environment of simulated tidal immersion.

32. Graph of log da/dN Vs log ΔK for crack growth in BS 4360 50D plate material, in an environment of simulated splash-zone.

33. Graph of log da/dN Vs log ΔK for crack growth in weld metal, in an environment of simulated splash-zone.

34. Graphs of da/dN Vs a , for crack growth in BS 4360 50D plate material in environments of laboratory air, nominal correct cathodic protection, nominal cathodic overprotection and free corrosion.

35. Graphs of da/dN Vs a , for crack growth in weld metal in environments of laboratory air, nominal correct cathodic protection, nominal cathodic overprotection and free corrosion.

36. Graphs of da/dN Vs a , for crack growth in heat affected zone microstructure in environments of laboratory air, nominal correct cathodic protection, nominal cathodic overprotection and free corrosion.

37. Graphs of da/dN Vs a , for crack growth in weld fusion-line microstructure in environments of laboratory air, nominal correct cathodic protection, nominal cathodic overprotection and free corrosion.

38. Graph of Paris exponent m Vs Paris constant C.

TABLES

LIST OF APPENDICES

NOTATION

a	Crack length
N	Number of load cycles
ΔK	Stress intensity factor range
K	Stress intensity factor
K_{max}	The maximum value of stress intensity factor per load cycle
K_{min}	The minimum value of stress intensity factor per load cycle
R	The ratio of K_{min} to K_{max}
K_{1c}	The critical stress intensity factor in plane-strain
K_{1scc}	The threshold stress intensity factor for stress corrosion cracking
ΔK_{TH}	The threshold stress intensity factor range for corrosion fatigue crack propagation
B	Specimen thickness
W	Specimen depth
σ_y	Material yield stress
da/dN	Crack growth rate per cycle of fatigue loading
δ	Crack tip opening displacement (C.T.O.D.)
da/dt	Crack growth rate per unit time
r_σ	Radius of the critically stressed plastic zone
r_y	Radius of the crack tip plastic zone under conditions of plane strain

CHAPTER 1

INTRODUCTION

Corrosion fatigue is a term used to describe the synergistic effect of fatigue crack propagation in the presence of an aggressive or corrosive environment. It is a major cause of loss of integrity in a variety of systems from the nuclear to the oil industry offshore structures. It therefore has an adverse effect upon safety. This was tragically demonstrated by the Alexander Kielland disaster (1), which resulted in the loss of 123 lives. It must be noted, however, that the adverse effects of corrosion fatigue are not confined to the offshore industry. A recent non-offshore example is corrosion fatigue cracking in the suspension links of the Severn Estuary road bridge (2).

The study of corrosion fatigue in the United Kingdom is an important element in the scientific and technological base of the UK offshore industry as a whole. Such studies are significant in the maintenance of existing offshore installations, particularly those of the jacket and semi-submersible types and in the design and development of stressed-hull tethered type installations such as the tension leg platform (3). At present 80% of UK offshore installations are of the jacket type and are subjected to extensive inspection and structural maintenance for safe and cost-effective operation (4).

Due to the complex structural design of steel jacket installations, fusion welding of carbon-manganese structure steels has evolved as the principal means of fabrication, accounting for 80% of North Sea installations. Any weldment may create a mechanical discontinuity in stress path, irrespective of joint design; a microstructural discontinuity or 'metallurgical notch' in relation to the grain structure through the cross section and residual stresses from the process of welding which are in addition to the operational design stresses in the joint. Further, the process of welding can create a variety of defects within the joint, many of which are capable of initiating fatigue or corrosion fatigue failure. It is in this context that a common undesirable feature of jacket design can be identified. Namely the concentration of weldments in areas of enhanced stress within the primary load paths, termed 'Nodal joints'.

The application of fracture mechanics concepts to jacket structural design appraisal has established the design philosophies of 'safe life' and 'damage tolerance' and rendered the assessment of structural integrity independent of traditional 'S - N curve' analysis methods. For 'safe life' design, inherent structural integrity is demonstrated at all stages of structural life by fracture mechanics analysis of crack growth rate data. Damage tolerance is achieved by providing the structure with a degree of redundancy.

Application of safe-life design philosophy generally relies on integration of the Paris crack propagation law (5) for assessment of residual fatigue life, given a known size of defect at any time t, a_t, and known 'Paris parameters' c and m. Initial defect size a_o, generally corresponds to the minimum size detectable by non destructive

examination methods. Final or maximum acceptable defect size, a_+, is based upon material crack tolerance. Between limits of crack length, life cycles are obtained by integration of the Paris relationship $da/dN = C.\Delta K^m$ where da/dN represents crack propagation per cycle of fatigue, ΔK is the stress intensity range and C and m are constants.

Integration of the Paris relationship is a powerful tool in offshore structural design, as data produced can be applied directly to damage summation. It is a U.K. statutory certification requirement (6) that at all times structural integrity complies with the Palmgren-Miner cumulative damage law (6) for the in-service load spectrum. Palmgren-Miner requires that a damage summation is carried out over the load spectrum, as shown below :-

$$\frac{n_1}{N_1} + \frac{n_2}{N_2} + \frac{n_3}{N_3} + \ldots\ldots\ldots\Sigma \frac{n_i}{N_i} \leq 1 \text{ for no failure}$$

where n_i is the number of cycles applied at a given stress range and N_i is the number of cycles allowed at the given stress range. The sum is to be less than or equal to unity for no failure, based on Design curves.

Assessment of residual life based upon integration of Paris type power law relationships is subject to a number of constraints, the more significant of which include :-

(a) Adequate determination of stress intensity factor, K, for joint detail and geometry. This is particularly important in respect of Nodal joints .

(b) The Paris parameters 'C' and 'm' must be determined for the relevant mechanical, metallurgical and environmental conditions.

(c) Integration of the Paris relationship is not valid at extremely low levels of stress intensity factor, in the 'threshold region' nor indeed when K_{max} approaches K_{Ic}, as shown schematically below :-

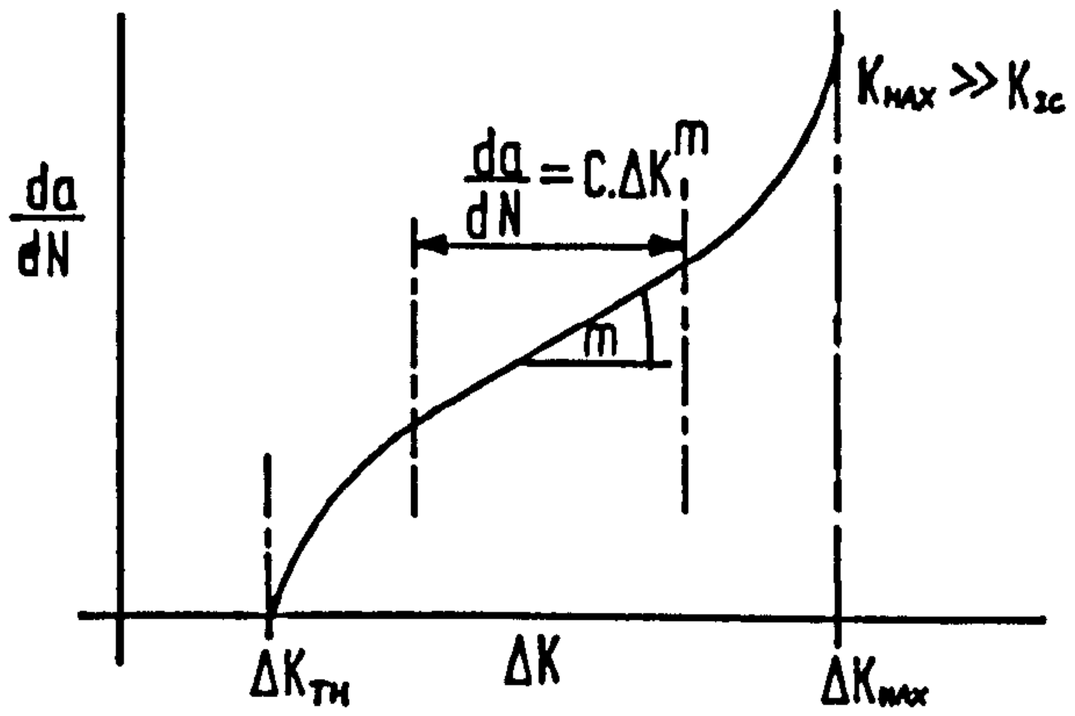

Schematic of the Significant Limitation of the Paris Crack Propagation Rates Relationship

A further significant consideration arises from the statutory requirement (6), that all U.K. certified offshore structures must have fitted, an effective cathodic protection system, as an anti-corrosion measure. Investigation of the influence of cathodic protection on corrosion fatigue crack propagation rates in structural steels is therefore necessary if confidence in residual life assessment, based on integration of the Paris relationship, is to be maintained. Against this background, the project reported herein was established to investigate the phenomenological aspects of cathodic protection, on corrosion fatigue crack propagation rates in a specific, well known structural steel with particular regard to the influence of weld joint microstructure.

CHAPTER 2

LITERATURE SURVEY

A general review of literature relevant to the investigation reported herein is presented as follows :-

2.1 Corrosion fatigue significant variables

2.2 Fracture mechanics aspects

2.3 Corrosion processes and corrosion control

2.4 Cathodic protection current data

2.5 Data reduction and crack measurement

2.1 CORROSION FATIGUE (SIGNIFICANT) VARIABLES

Variables or parameters which influence corrosion fatigue behaviour of structural steels, can be grouped under the general headings of :-

(a) Mechanical variables

(b) Metallurgical variables

(c) Environmental variables

Within each group the relative importance of individual parameters or variables is often dictated by experimental design and overall project objectives. For the project reported herein, a distinction was made between parameters considered to be of importance to corrosion fatigue studies in general and those of particular note in respect of project objectives. A general review of published data was made in respect of the latter group.

2.1.1 Significant Mechanical Variables

Barsom (7) was one of the first to demonstrate that crack growth can occur by means of stress corrosion or corrosion fatigue processes. Dependent upon the level of crack tip stress intensity present in relation to a threshold value defined as K_{ISCC}, Barsom proposed that corrosion fatigue crack propagation behaviour below K_{ISCC} was dominated by the precise nature of the stress waveform and in particular the rise time to peak load. Further, no environmental attack occurred during constant load portions of the fatigue cycle (square wave) for frequencies of the order of 0.1 Hz.

In the context of the present investigation, it must be noted that Barsom used a marageing steel in a test environment of standard salt water solution, not simulated sea water. Therefore care must be exercised in relating Barsom's results directly to corrosion fatigue

crack propagation in BS 4360 50D type structural steels in simulated sea water.

Radon (8) has proposed that for high strength Aluminium alloy, K(mean) and ΔK exert a distinct but separate influence on propagation rate, as shown below :-

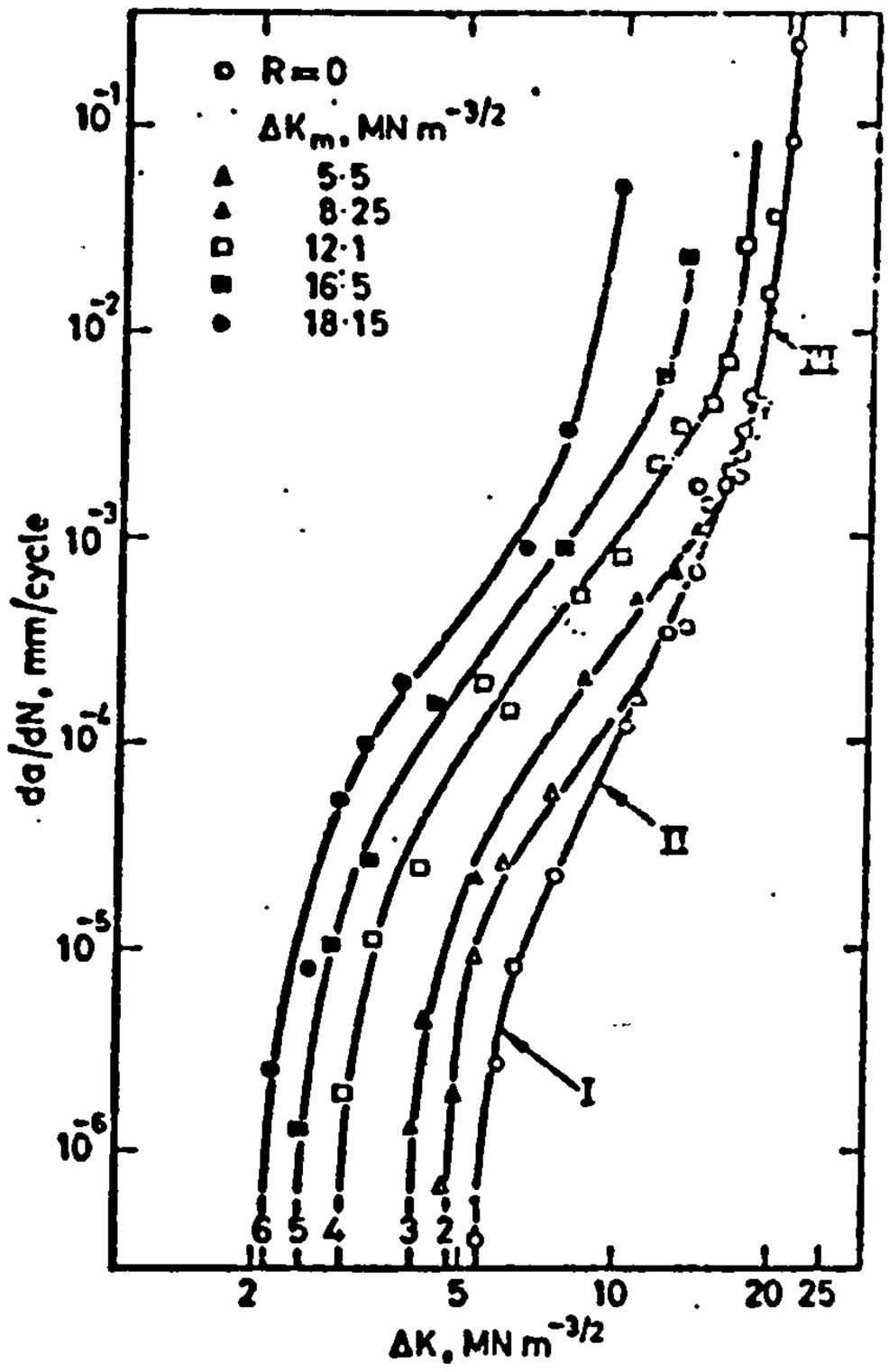

Crack propagation rate Vs ΔK for increasing levels of Km : frequency constant (after Ref. 8)

The above data is unusual in its classical fracture mechanics treatment. However, if growth rates in the Paris region only are considered and re-drawn in a conventional presentation, the underlying trend of enhancement of propagation rate for increase in K(mean) remains, but in a practical sense is shown to be of questionable significance. The implied effect of K(mean) on ΔK(threshold) is possibly of more interest to offshore related studies. However, as before, the relatively low magnitude of the effect may be insignificant in consideration of the nature of offshore fatigue loading and the superior crack tolerance of structural steel. Lastly, the reference to the effects of ΔK on propagation rate can be considered to be superfluous, as the effect has been widely documented from a number of previous studies (8). Overall, Radon can be considered to have emphasized an interesting effect of K(mean), but one which has

little significance in the context of offshore related corrosion fatigue crack propagation studies.

Specifically, for low alloy high strength steel, Stewart (9) has proposed that the stress ratio R and yield strength have dominant influences on the level of ΔK (threshold), as shown below :-

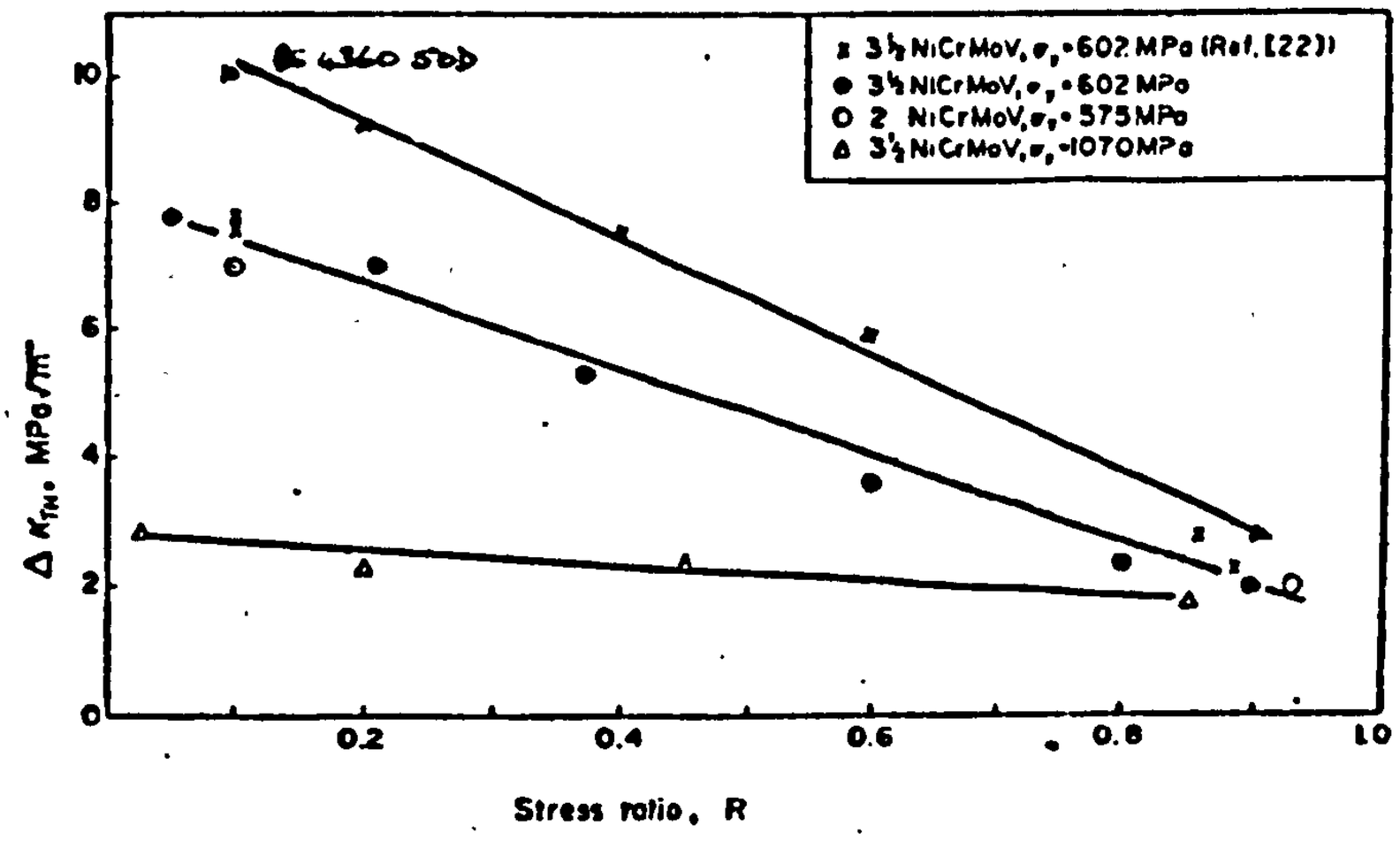

The influence of stress ratio and yield stress on ΔK_{TH} for low alloy high strength steels in laboratory air (after Ref. 9)

The above data is interesting for two reasons. First, for very high strength steel (σ_y = 1070 M.Pa), ΔK_{TH} is shown to be sensibly independent of R ratio. Second, for a given medium strength steel (σ_y = 575 M.Pa), stress ratio R as it varies from 0.8 to 0.1 changes the level of ΔK_{TH} by a factor of approximately four for values of R ratio $\geq$ 0. The magnitude of this effect is significant and should be considered in the design of fatigue and corrosion fatigue crack propagation experiments. Further development of this work, to provide similar threshold data for conditions of corrosion fatigue would be particularly beneficial.

By use of the relationship $\Delta K_{TH_o} = \overset{o}{K}_{TH}(1 - R)^{\gamma}$ proposed by Austen (10) for BS 4360 50D steel (where $\overset{o}{K}_{TH}$ = 10.76, γ = 0.637) it can be seen that the in-air calculated values of ΔK_{TH} are comparable and can be superimposed on Stewart's data. It is interesting to note that the effect of reducing yield stress is to raise the level of ΔK_{TH} for a given level of stress ratio. The common trend, however, remains in that ΔK_{TH} is reduced with increasing stress ratio; an effect which can be considered to have particular significance for the early stages of fatigue crack propagation in the vicinity of welded joints, in that the influence of geometrical stress concentration factors and enhanced levels of residual stress could together be expected to locally

increase the effective level of R ratio.

Further, the extrapolated value of ΔK_{TH} derived from data reported herein, correlates well with the calculated value of 10.08, M.Pa.$\sqrt{m}$. This indicates that the relationship proposed by Austen is valid and can be readily applied to BS 4360 50D steel. It must, however, be remembered that the relationship proposed by Austen is empirical and is limited to plate material and an air environment. Therefore it cannot be used, for instance, to determine threshold levels in welded plate, under conditions of corrosion fatigue, as the empirical relationship has no provision for the influence of an aggressive environment on the early stages of fatigue crack growth in an inhomogeneous grain structure of the kind present in structural steel weldments.

There is no doubt that frequency of loading is a dominant influence upon fatigue and corrosion fatigue crack propagation rates in structural steel with maximum values tending to occur at low frequency (f < 1 Hz). This is illustrated by the data shown below :-

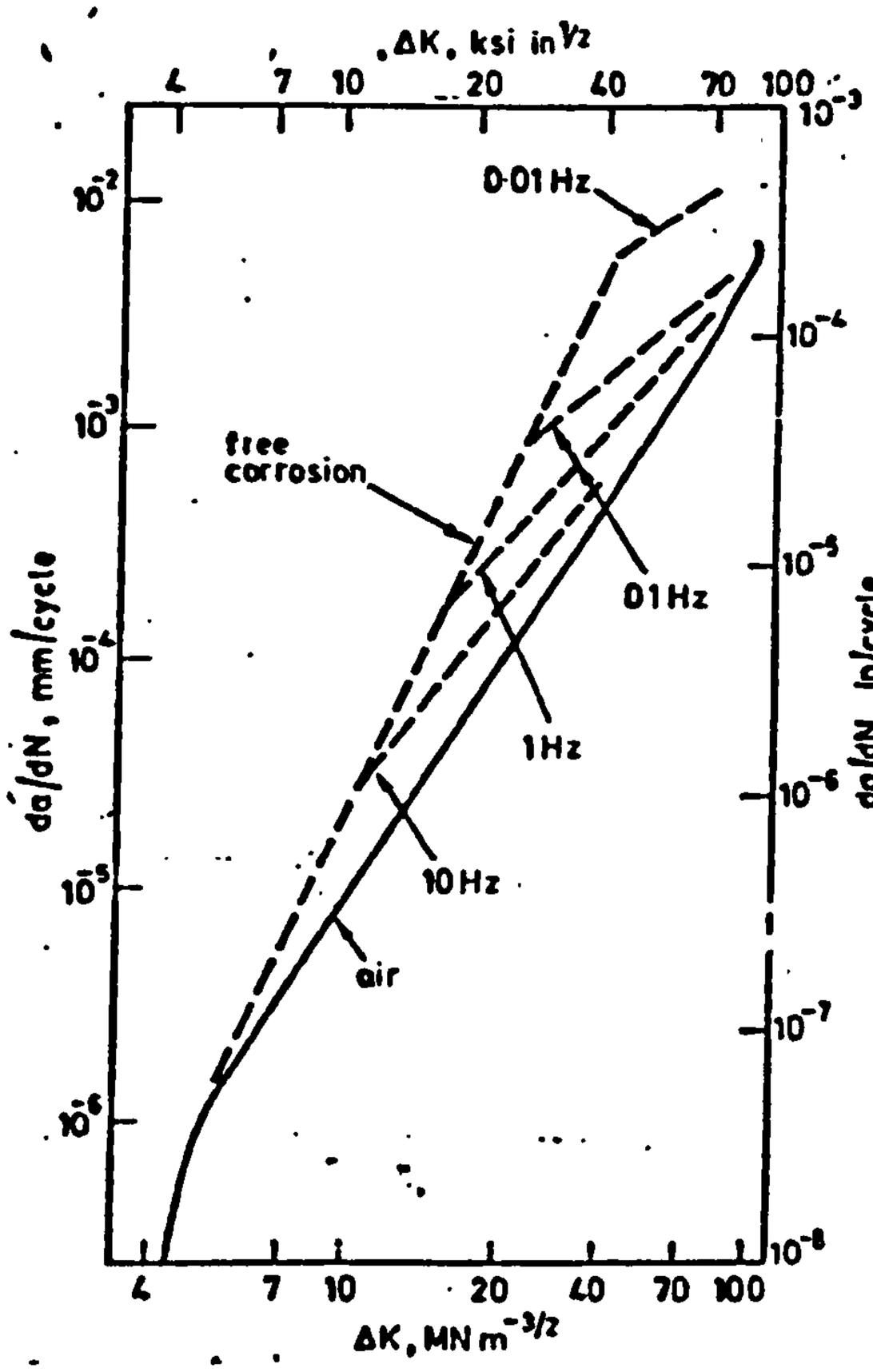

Effect of frequency on corrosion fatigue crack growth rate of line-pipe steel.
(after Ref. 11)

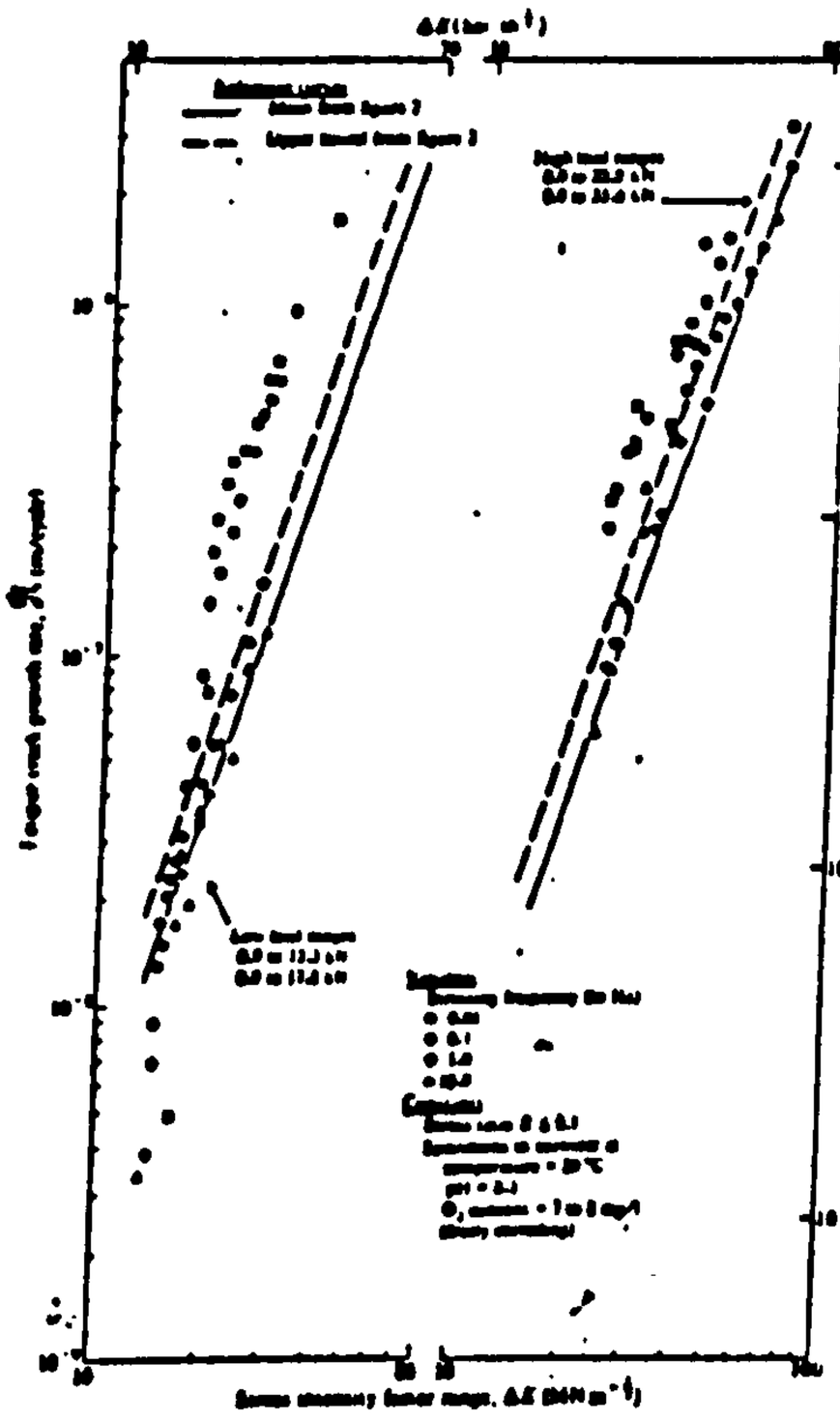

Fatigue crack propagation data as a function of frequency of stressing in seawater.
(after Ref. 12)

A significant feature of the above data, is the contrast in the style of presentation. Vosikovsky (11) omits all data points and thereby precludes comparison or meaningful appraisal with data from other sources. In contrast, the graphs presented by Scott and Sylvester (12) have a wealth of data points but lack definition. Interpretation is left to the reader save for reference to 'tramlines' representative of 'upper' and 'lower bound' conditions based on regression analysis methods for in-air data at fixed frequency.

It is a common feature of Scott and Sylvester results generally that data points are enclosed within upper and lower bound lines, defined by regression analysis methods.

In view of the mass of data presented, the use of bound lines is possibly overcautious and can be considered to represent gross smoothing, to the detriment of identification of specific detail. This is particularly important in respect of implied multi-modal behaviour, which is shown by data for specific frequencies. Further, the 'upper and lower bound' type treatment of the data does not encourage discussion of possible trends which is particularly undesirable in view of the widespread application of this and similar data in structural appraisal. Without doubt, the data produced by Scott and Sylvester is of considerable value to the continued development of U.K. offshore technology. However, the overcautious presentation must be regarded as a significant shortcoming.

2.1.2 Significant Metallurgical Variables

Microstructure is a significant metallurgical variable in relation to fatigue or corrosion fatigue crack propagation behaviour in structural steels. The influence of microstructure on fracture propagation mechanisms generally has been summarised by Lindley and McCartney (13), as shown overleaf.

It must be noted, however, that the above proposals are generalised and should be interpreted with caution to avoid misleading conclusions. It is unrealistic to expect an abrupt change in fracture mechanism at a specific value of ΔK in the way that the schematic might imply. Nor can the effects of environment be considered to be confined to the immediate threshold region only or material response to be independent of frequency. Overall, the schematic proposed by Lindley and McCartney is useful as a summary of possible influences, but should not be viewed without qualification.

A significant influence of microstructure on fatigue crack propagation in ferritic pearlitic steels has been proposed by Barsom (14). He suggests thatiron carbide platelets present in pearlite locally increase the strength of pearlite colonies relative to the bulk ferrite matrix. This increase in strength reduces ductility and as a consequence the preferred fracture path is through the more ductile ferrite phase with pearlite acting as a barrier to crack advance. Barsom's proposals are interesting, but lack important detail. As an example, no discussion is offered as to the possible influence of pearlite orientation on its ability to act as a mechanical barrier. Nor of the possible interaction between crack tip

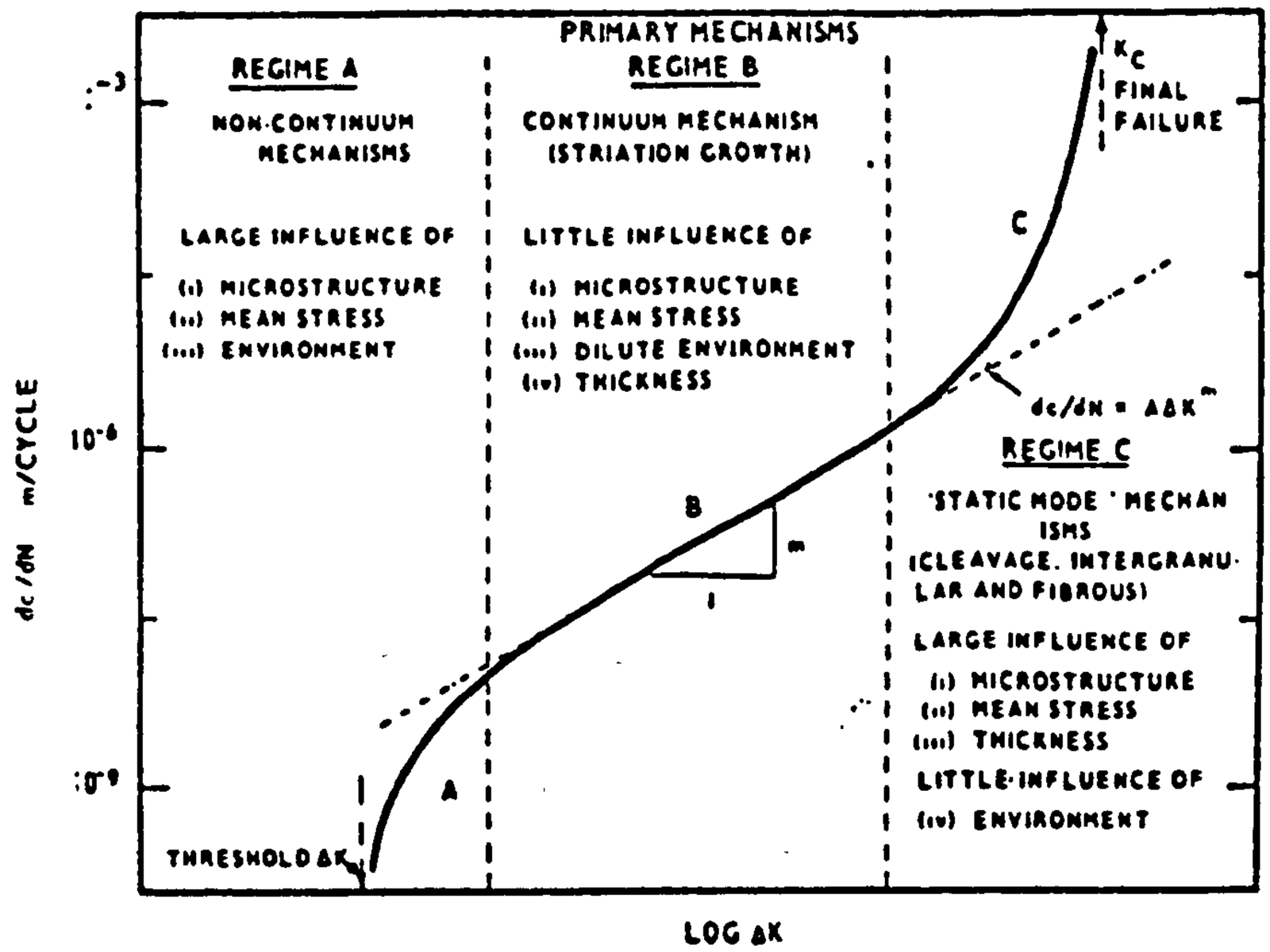

Summary diagram showing the primary fracture mechanisms associated with fatigue crack propagation rate dc/dN and range of stress intensity ΔK (after Ref. 13)

plasticity and individual pearlite bands in respect of the nature of the distortion caused to the crack tip plastic-zone. Similarly, no mention is made of possible effects due to volume fraction of pearlite present or of pearlite band spacing. These shortcomings could have in part been satisfied by the use of microhardness surveys. Overall the proposals have value, but are deficient in detail and do not clearly define the nature of the phenomenon. They are, however, worthy of further study, particularly as the majority of structural steels, BS 4360 50D included, are of the ferrite-pearlite type.

One influence of volume fraction of pearlite or brittle micro-constituent on fatigue crack propagation has been illustrated by Aita and Weertman (15), by reference to the data shown overleaf.

Aita and Weertman (15) propose that the influence of pearlite volume fraction on fatigue crack propagation rate can be described by response to changes in the value of the 'Paris' exponent m. For levels of pearlite content commonly associated with structural steels of the BS 4360 50D type (30 - 40%), this data indicates that the effect is sensibly constant and of little significance. Greater influence is indicated for pearlite content of the order of 80% which is shown to increase the value of m by approximately 25%.

In isolation, this particular result appears to be significant but in practice can be argued to represent a steel that would generally not be acceptable for structural use on the grounds of

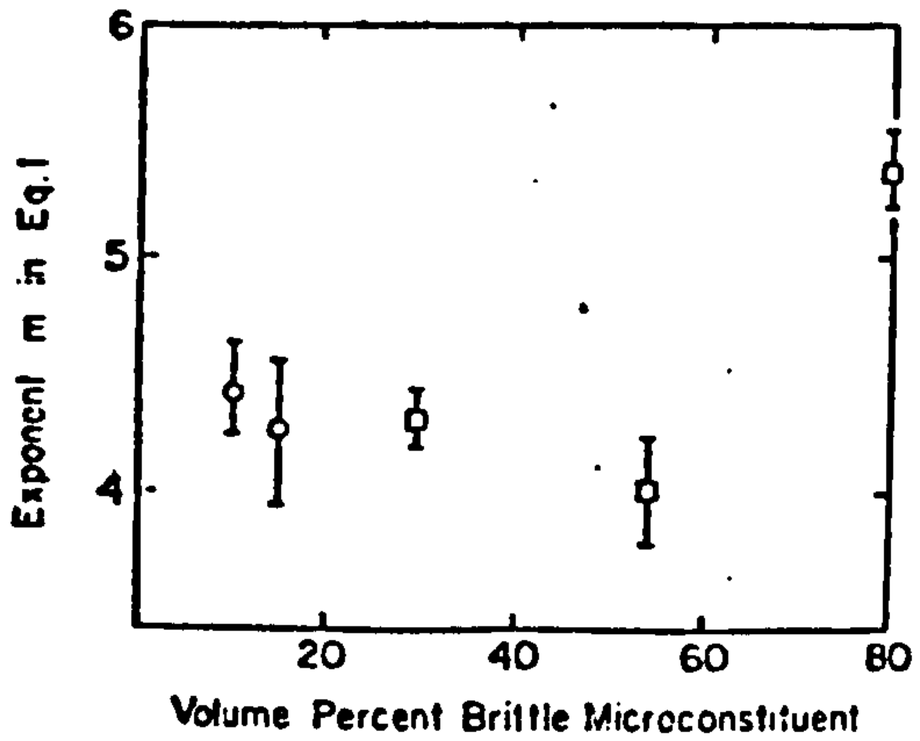

Variation of the exponent m with the volume fraction of brittle microconstituent contained in Fe - C alloys (□ indicates pearlite, O indicates iron carbide). (after Ref. 15)

possible reduced crack tolerance. In this respect, data on critical C.T.O.D. values at 80% pearlite, would have been of considerable value.

Overall the data presented by Aita and Weertman is useful and indicates that at moderate levels, pearlite content has an insignificant effect upon fatigue crack propagation rates. However, their report is deficient in data on the comparable values of the Paris constant C, for the various values of exponent m. Consideration of both parameters together is ultimately a better measure of significance, therefore the omission of this data must be regarded as a major shortcoming in what is otherwise a useful paper.

Finally it is interesting to note that in recent years a number of authors (16, 17, 18, 19, 20), have investigated the influence of microstructure on fatigue crack propagation rate and have generally agreed with Barsom's original proposals.

The effect of microstructure on fatigue crack propagation rate is particularly significant in the region of a welded joint. For mild steel, Dowse and Richards (21), have shown that fatigue crack propagation is strongly influenced by the effect of heat affected zone (h.a.z.) on the size and shape of the plastic zone ahead of the crack tip. Their data shows that variation in hardness and orientation of the h.a.z. to the tensile axis, can produce deviations in crack path towards softer and, by implication, tougher material, in addition to a reduction in crack propagation rate. An important implication from this data is that the integrity of a welded joint may depend upon the toughness of the metallurgical component with the lowest flow stress. It also creates an element of uncertainty in prediction of crack path in the vicinity of welded joints.

It must be noted, however, that Dowse and Richards obtained their data under carefully tailored conditions, designed to ensure plane stress type crack tip plasticity only, i.e. very thin material, acute angle of attack of crack front to h.a.z. and 'pure' mode I crack tip opening. Under these conditions, for specific orientations of crack front to h.a.z., deviation was observed in the manner described above. In view of the deliberate 'plane stress' tailoring present in their experimental design, it would be unwise to infer that similar results would occur for unconstrained material thickness, h.a.z. orientation or mode of crack tip opening. Particularly as away from plane stress conditions, significant changes are introduced in the shape of the crack tip plastic zone. A further limitation is that the model proposed by Dowse and Richards contains no provision for the effects of residual mechanical stresses arising from welding processes , which have been shown (22, 23) to significantly reduce fatigue crack propagation rates, irrespective of metallurgical structure.

For fatigue crack propagation in mild steel weldments, Maddox (24) has shown that data can be adequately described by a bi-modal presentation which exhibits two distinct values of exponent m, either side of a change point, the position of which is dependent upon applied stress and can be correlated with a change in fracture surface appearance. Bi-modal presentation is a significant departure from accepted practice and is worthy of detailed consideration. Unfortunately Maddox does not consider the wider implications of this form of presentation nor its practical significance. Instead discussion is limited to consideration of possible causes for the change in slope with no reference to significance or comparison with conventional Paris graphs from other sources. Overall, the superficial treatment of the data and mode of presentation is unjustified and is a major deficiency in what is otherwise an interesting paper.

2.1.3 Significant Environmental Variables

The following environmental variables are considered to have a significant influence on corrosion fatigue crack propagation rates in structural steel :-

(a) Temperature

(b) Hydrogen content

(c) Electrical potential

Temperature. For low alloy steels in an aqueous environment, Misawa et al (25) have proposed that the corrosion fatigue crack propagation rate is significantly influenced by temperature and that the variation of rate with temperature implies that a thermally activated process is possibly the rate controlling step in corrosion-fatigue. This proposal is considered to be particularly interesting, as it supports proposals made by Tomkins (26), namely that for structural steels, anodic dissolution at the crack tip is a significant factor in corrosion fatigue crack growth behaviour.

Smith and Stewart (27) have reported that corrosion fatigue crack propagation rates in low alloy steel increase with temperature and have proposed that frequency of loading is also a significant influence, in the manner shown below :-

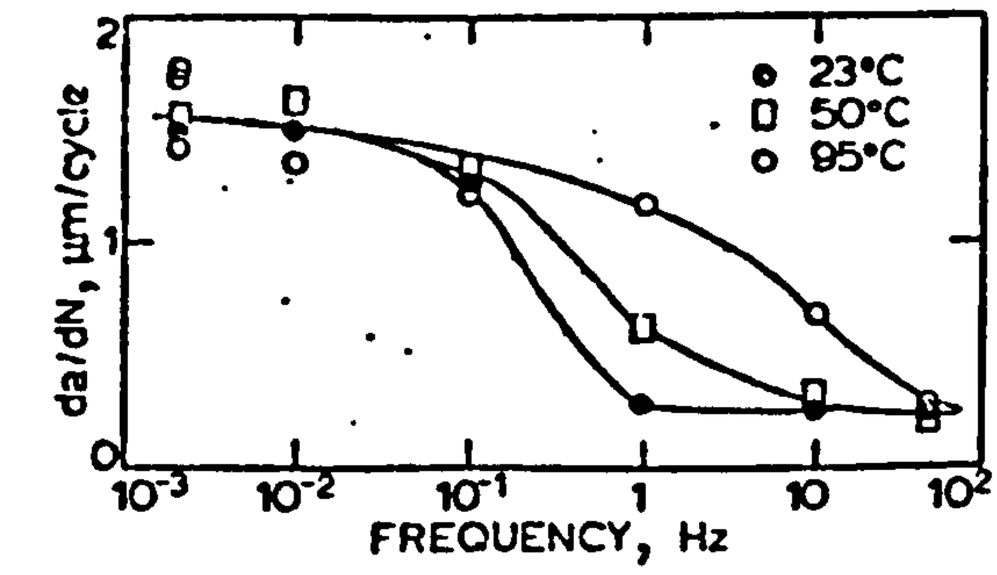

Effect of temperature and frequency on fatigue crack growth rate in water with sine wave loading (after Ref. 27)

A feature of this data is that at low frequency ($f \lesssim 0.1$ Hz), crack propagation rate is shown to be sensibly independent of temperature. For frequencies > 0.1 Hz an effect is shown, but of relatively low magnitude and therefore of little significance to offshore studies applied to North Sea conditions, where sea water surface temperature is generally within the range 0^{o} - 12^{o}C.

The data shown above can, however, be used for limited validation of the proposals made by Misawa et al (25).

Thus , if the mechanism of corrosion fatigue crack propagation in sea water is a thermally activated process, then the rate limiting step could be described by Arrhenius' equation, expressed as

$$da/dt = A.e^{-\frac{Q}{R.T}}$$

where Q is the apparent process activation energy, R is the Universal Gas Constant and T is the absolute temperature. In order to simplify the derivation of Q, two important assumptions have to be made. First, the complex quantity A is assumed to be constant for small temperature ranges and hence can be ignored. Second, if the overall process of propagation is assumed to involve more than a single mechanism, then the process with the lowest activation energy can be considered to be the dominant component. From the application of Arrhenius' Equation to Smith and Stewart's data (27), the apparent process activation energy for corrosion fatigue was found to be approximately 40 K.J. mole^{-1}. Similar treatment of data, reproduced overleaf, which was reported by Ryder and Gallagher (28), yielded an apparent process activation energy of 41.5 K.J. mole^{-1}.

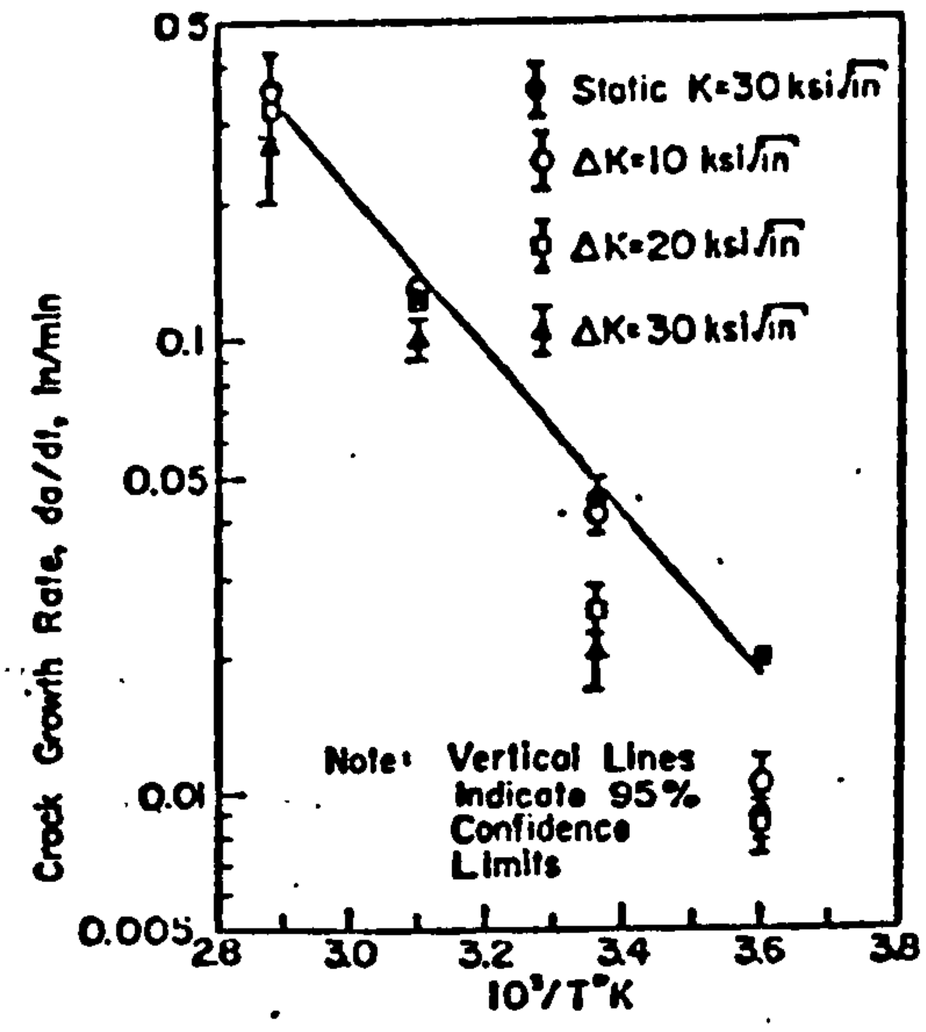

Comparison of cyclic and static crack-growth rates showing temperature dependence (after Ref. 28)

In this context it should be noted that for low alloy steel, Miawa et al (25) have reported values of an apparent process activation energy, Q, in the range 20 - 55 K.J. mole^{-1} for a ΔK value of 14 M.Pa $\sqrt{m}$ and have also proposed that 'Q' is largely independent of ΔK, for values of ΔK less than approximately 23 M.Pa $\sqrt{m}$.

The low level of apparent process activation energy, derived above, is considered to indicate that a thermally activated dislocation transport mechanism such as climb , or an atomistic transport mechanism, such as self-diffusion , is unlikely to be operative in corrosion fatigue. In circumstances where the value of Q is low and the corrosion fatigue crack propagation rate is found to increase with temperature (27, 28), Smith and Stewart (27) have proposed that hydrogen diffusion is the rate controlling process. This proposal is particularly interesting and can be considered to have a number of significant implications which include :-

(a) Identification of hydrogen diffusion as a significant factor in corrosion fatigue crack propagation mechanisms in steel. Indirectly, Smith and Stewart (27) can be considered to corroborate the proposals made by Tomkins (26); namely that anodic dissolution reactions at the crack tip are a critical feature of crack growth under conditions of corrosion fatigue.

(b) Hydrogen enhancement of crack propagation rates could be expected to be a significant feature of corrosion fatigue crack propagation in structural steels.

(c) Offshore in the North Sea, whose annual range of sea water

temperature at the surface is 0 - 12°C (91), sufficient thermal energy for activation of corrosion fatigue processes can be assumed at all times, i.e. it is simple to show that $e^{-\frac{4000}{8.2\times273}}$ and $e^{-\frac{4000}{8.2\times285}}$ are greater than zero.

In view of the comparative ease with which it is possible to estimate the apparent process activation energy for corrosion fatigue, it is considered to be a surprising feature of the literature survey reported herein, that the technique does not enjoy wider popularity.

Hydrogen. Corrosion fatigue crack propagation rates in structural steel are undoubtedly influenced by material or microstructure sensitivity to alternative crack growth mechanisms and, in particular, those encouraged by the presence of hydrogen. It is popularly accepted that rate of hydrogen entry into structural steel is greater in harder materials and is increased by tensile strain and rise in temperature. There is, however, no basis for the assumption that hydrogen embrittlement of structural steel might only take place above a critical hardness level. Microstructure sensitivity to the entry (adsorption and absorption) of hydrogen, is therefore a significant parameter in respect of the overall fatigue performance of offshore structures and is significant in respect of fabricated nodal joints. Particularly since under conditions of cathodic protection, an overall increase in susceptibility to hydrogen ingress can be expected, accompanied by a significant reduction in fatigue endurance.

A possible overall hydrogen embrittlement process for structural steel has been proposed by Smith and Stewart (27), shown below in schematic :-

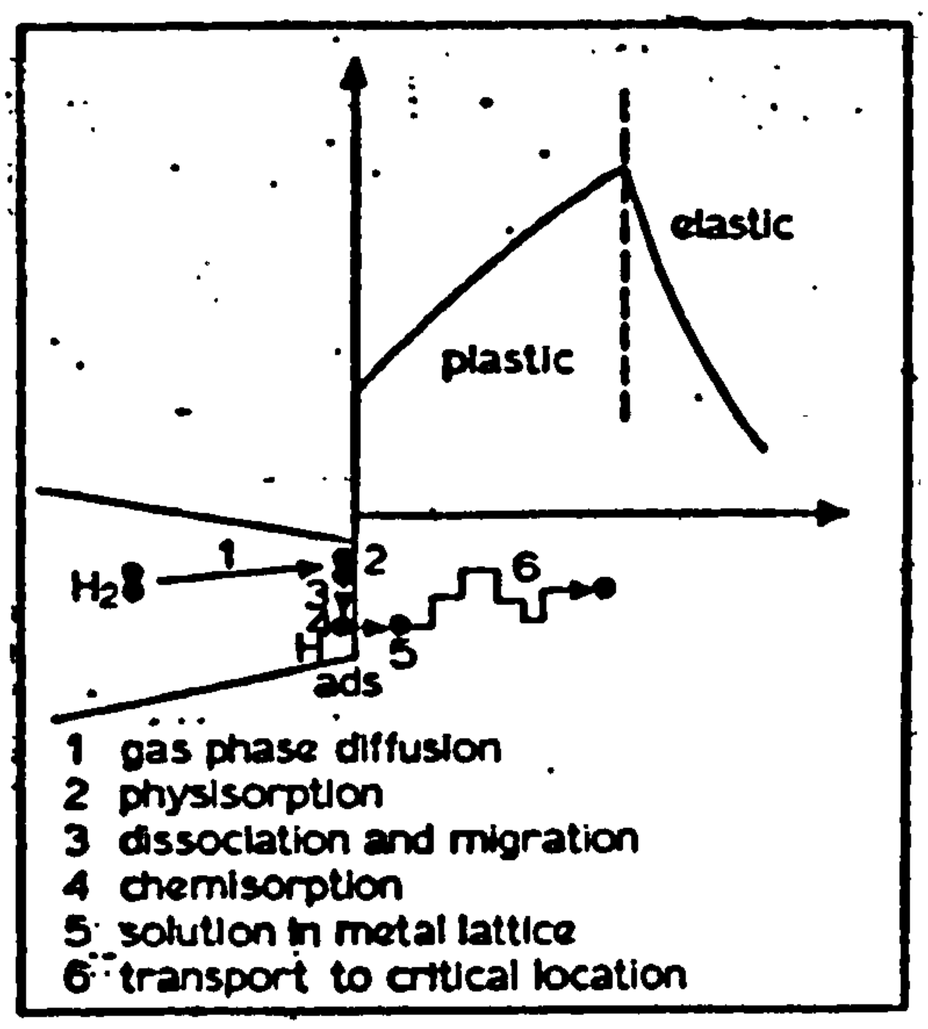

Schematic model of possible overall process leading to hydrogen embrittlement of steel (after Ref. 27)

In view of the previously derived level of apparent activation energy, for corrosion fatigue crack propagation, the above model has significance as it can be inferred that various hydrogen transport mechanisms constitute the rate determining step in hydrogen enhancement of corrosion fatigue crack propagation rates. Mechanisms which involve adsorption of molecular hydrogen and its dissociation into atomic species, absorption into the metal lattice and diffusion through the lattice to the region or site of embrittlement.

A concise examination of the practical implications of diffusion or transport type models for hydrogen embrittlement of structural steels has been made by Tomkins (26), the essential features of which are shown below :-

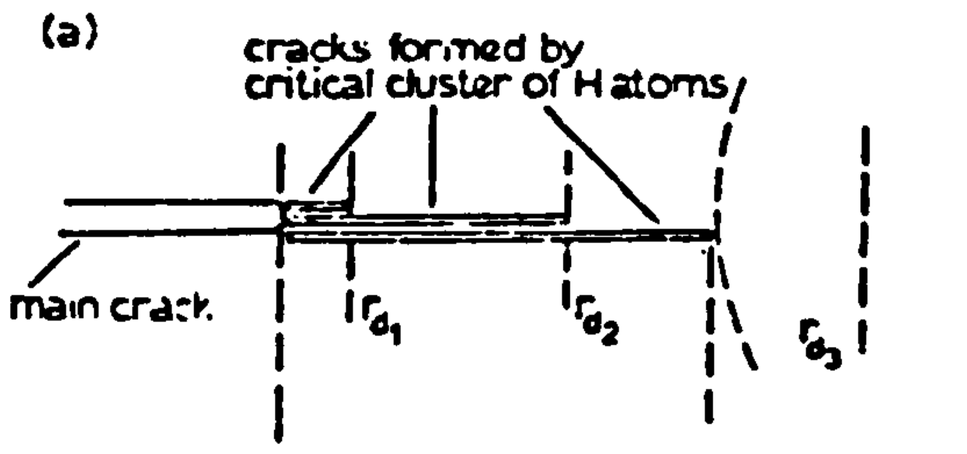

r_{d_1}, r_{d_2}, r_{d_3}: effective H diffusion distances for crack formation depends on H concentration and time: r_σ is threshold stress boundary

Schematic of hydrogen assisted fatigue crack growth (after Ref. 26)

Tomkins proposes that the position or depth of any hydrogen concentration, t_d, ahead of a crack tip, in relation to the radius of critically stressed plastic zone, r_σ, is the essential feature of hydrogen embrittlement in steel subjected to fatigue loading. However, similar arguments could be applied to the case for stress corrosion cracking, especially as the schematic can also be interpreted as presenting crack propagation response in the manner of idealised

K_{ISCC} behaviour, a possibility which Tomkins fails to acknowledge or discuss.

A further notable feature of the model is that limited access of environment to the crack tip during stage I growth is considered not to stop any electrochemically produced hydrogen along the crack flanks from diffusing to the region ahead of the crack tip. As a result, the threshold for hydrogen-assisted growth is less sharply defined than might otherwise be expected. Overall, the requirement remains for a mechanistic theory or model, capable of quantitative prediction of the effects of hydrogen on corrosion fatigue crack propagation rates.

Electrical Potential. For BS 4360 50D steel in sea water, it has been shown (12) that specimen potential has a significant effect on corrosion fatigue crack propagation rates, through a reduction in crack tip opening displacement. In general, cathodic polarisation to just below free corrosion potential (- 0.70 V_{SCE}) is shown to produce the maximum reduction in propagation rate and to provide the closest approach to in air values. The data (12) is summarised below :-

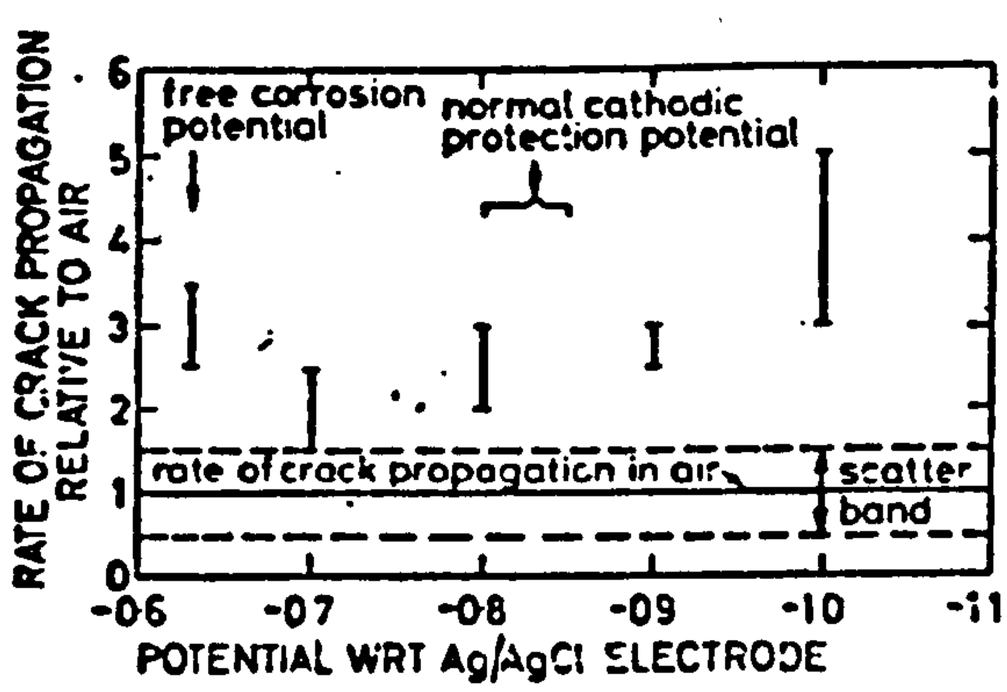

Effect of electrical potential on corrosion fatigue crack propagation rate for structural steel stressed at 0.1 Hz in sea water at 20°C and R≤ 0.1 (after Ref. 12)

In the above data C.T.O.D. is considered to be controlled by ΔK which has a limiting value of 18 M.Pa.$\sqrt{m}$. At values of ΔK < 18 M.Pa$\sqrt{m}$ and potential in the range - 0.8 to - 1.00 V Ag/Ag Cl, reduction in propagation rate is attributed to reduction in effective level of crack tip stress intensity range, caused by inhibited crack closure due to the precipitation of calcareous deposits on the fracture surfaces. At levels of ΔK > 18 M.Pa.$\sqrt{m}$ retardation is not present and propagation rates are accelerated by the environment at all potentials. An interesting feature of the data is that propagation rate is shown to be greater for specimens freely corroding and at a potential of - 1.00 V Ag/Ag Cl. than for intermediate potentials. It is a

notable feature of the paper, that having proposed the concept of 'crack blocking', the authors fail to discuss the wider implications, in particular :-

(a) Is the effect of crack blocking confined to the plastic zone and dependent upon 'near-threshold' propagation conditions?

(b) Does crack propagation rate represent a 'dynamic' limiting condition away from the threshold region, such that, the rate at which fresh fracture surface is formed exceeds the rate at which the nucleation and growth of the calcareous layer can take place to firstly passivate the fracture surface and secondly to produce a layer of sufficient depth to mechanically interfere with crack closure.

(c) Is the mechanical strength of the calcareous deposits such that they will remain intact and in place during crack closure and not be crushed and subsequently ejected from the crack by natural pumping action ?

(d) What depth of calcareous layer would be required to produce a reduction in level of ΔK to give the in-air properties rates?

Overall there can be no doubt that calcareous deposits are formed by the action of cathodic protection. However, in the absence of independent appraisal, the significance of the phenomenon as proposed by the authors must remain subject to debate.

2.2 *FRACTURE MECHANICS ASPECTS*

The application of fracture mechanics in the investigation reported herein is limited to description of corrosion fatigue crack propagation behaviour by use of the Paris relationship (5) $da/dN = C.(\Delta K)^m$. Therefore the limitations and constraints of this relationship are worthy of review. For a specific frequency of loading, the Paris equation is generally presented in schematic as shown overleaf.

It can be seen from this schematic that areas of uncertainty exist in the range of application at extreme levels of ΔK. At very low levels of ΔK, an apparent threshold level, ΔK_{TH}, is considered to exist, below which crack propagation is assumed not to occur, i.e. $da/dN \rightarrow 0$ for $\Delta K \lesssim \Delta K_{TH}$. For comparatively high levels of ΔK, rapid failure occurs when K_{max} closely approaches or exceeds the material fracture toughness K_{1c}. As a result, the relationship is only valid for ranges of ΔK away from the extremes. To maximise the range of application and improve linearity, the original relationship has been subjected to considerable development.

A recent survey (29) has noted in excess of seventy crack propagation relationships, which relate fatigue crack advance per load cycle to some function of stress applied, while attempting to include variables such as frequency of loading f and stress ratio R.

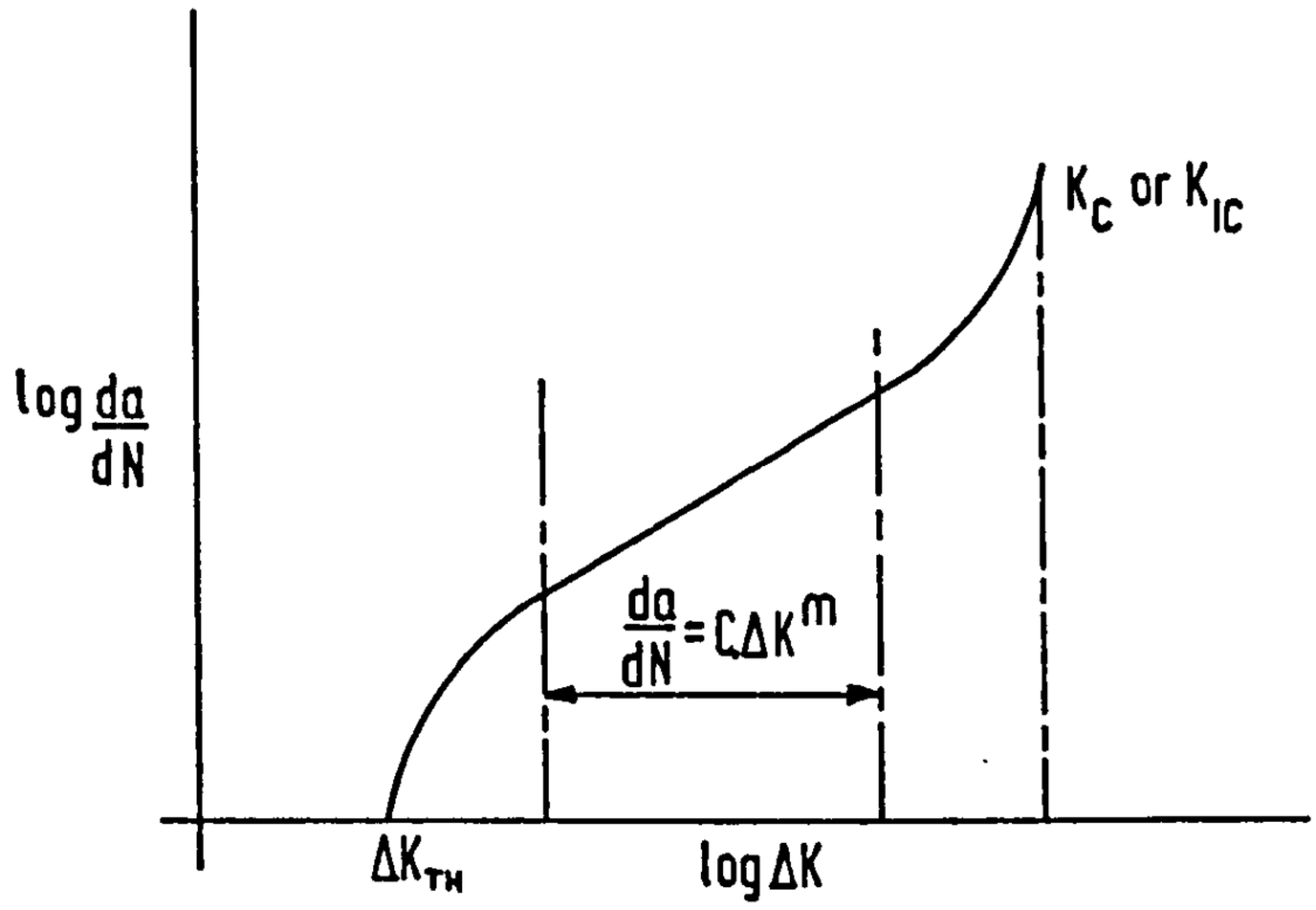

Schematic of fatigue crack propagation in accordance with the 'Paris equation' for a fixed frequency (after Ref. 5)

Examples include :-

$$da/dN = f \times \left| \frac{\Delta K^m}{(1 - R)^{1-m}} \right| \qquad (30)$$

where f = frequency of loading

$$da/dN = \frac{C.\Delta K^m}{(1 - R)K_c - \Delta K} \qquad (31)$$

$$da/dN = \frac{\Delta K^2}{4.\pi.\sigma_y.E} \left| \frac{\Delta K - \Delta K_{TH}}{K_{1c} - \Delta K/(1 - R)} \right|^{\frac{1}{2}} \qquad (10)$$

For the Paris relationship and those presented above, it must be noted that the following assumptions and simplifications have been included :-

(a) Relationships of the form da/dN α a function of (applied stress) are empirical, invariably based on a pure metal or specific alloy and have no general application.

(b) In the majority of cases, the fatigue crack is assumed to open in Mode I only.

(c) The relationships are adjusted by regression analysis techniques for agreement with observed data trends and ignore the effects of environment, frequency and secondary cracking.

It can be argued that the omission of secondary cracking effects

is an undesirable over-simplification, as the phenomenon is frequently observed on fatigue fracture surfaces in structural steel. However, in practice, the development of Paris type relationships to include alternative modes of crack opening displacement, inevitably generates further complexity in the final expression, as shown below :-

For pure Mode II opening

$$\frac{da}{dN} = \frac{C_2(\Delta K_{II})^{n_2}}{K_{II_c} - K_{II_{max}}} \qquad (32)$$

which when combined with Mode I opening, yields :-

$$\frac{da}{dN} = \frac{-C_1(\Delta K_I)^{n_1} + C_2(\Delta K_{II})^{n_2}}{|(K_{I_{max}}/K_{1c})^2 + (K_{II_{max}}/K_{II_c})^2 - 1|} \qquad (32)$$

Mode I, II and III stress intensity factors have been shown by Knott (33) to be related in the form :-

$K^2 = E.G. = (1 - \nu^2)K_I^2 + (1 - \nu^2)K_{II}^2 + (1 + \nu)K_{III}^2$ for plane strain and

$K^2 = E.G. = K_I^2 + K_{II}^2 + (1 + \nu)K_{III}^2$ for plane stress, where E is Youngs Modulus and G is the strain energy release rate.

It is interesting to note, however, that despite advances in analysis of the kind presented above, the original Paris relationship continues to enjoy widespread popularity in the field of offshore engineering. It is therefore pertinent to question if the modified equations offer any significant improvement in the general level of confidence related to the prediction of structural fatigue life offshore.

For corrosion fatigue, a notable feature of recent crack propagation concepts is reduction of the overall propagation rate into mechanical and environmental components, generally expressed as :-

$$(da/dN)_{CF} = (da/dN)_{MECH} + (da/dN)_{ENV}$$

Based on the known temperature dependence of corrosion fatigue crack propagation rates in aqueous environments (34, 28, 25), Atkinson and Lindley (35) have proposed that $(da/dN)_{CF}$ can be given by :-

$$(da/dN)_{CF} = (da/dN)_{MECH} + f/2(da/dt)_{ENV}.$$

where $(da/dt)_{ENV}$ is given by Arrhenius' equation $A.e^{-Q/R.T.}$

This relationship is interesting in that it implies a time dependent element by reference to da/dt, but then converts to a cycle dependency, factored by 0.5.

A possible inference is, that the authors consider that time dependent environmental enhancement mechanisms are only operative over one half of the loading cycle. This would agree with proposals from other authors (36), who consider that for the mechanical component of fatigue, crack propagation only occurs over the rising-load part of each fatigue cycle. Unfortunately Atkinson and Lindley provide only limited discussion in this area.

It is interesting to note that Parkins and Greenwell (34) propose that composite type propagation models can be improved by specific reference to stress corrosion crack propagation, where the overall crack propagation rate is expressed as :-

$$(da/dt)_{CF} = (da/dt)_{SCC} + f(da/dn)_{F}$$

It must be noted, however, that two major assumptions are present in the above relationship. First, the environmentally assisted growth only occurs as stress corrosion cracking, therefore by implication the model can only be applied to susceptible materials. Second, the environmental enhancement occurs over the full fatigue cycle, but remains time dependent. Therefore, for a decrease in frequency, an increase in relative environmentally assisted component of crack propagation could be expected. An effect which is known to occur in high strength steels (37, 38), but is not generally found in relatively low strength structural steels.

Based on the composite type of model discussed above, Austen (10), has proposed that the overall phenomenon of corrosion fatigue crack propagation can be described by reference to a 'process competition model', which can be stated as :- 'At a particular ΔK value, a crack will grow either at the fatigue crack growth rate or the average stress corrosion crack growth rate during the fatigue stressing cycle, whichever is the faster.' In this model, 'true corrosion fatigue' is defined as the conjoint action of mechanical and environmental components over the full range of ΔK values. 'Stress corrosion fatigue' is defined as only occurring when the crack tip stress intensity factor exceeds K_{ISCC}, as shown schematically overleaf.

In respect of the general model presented overleaf, for BS 4360 50D steel, Austen reiterates the widely reported view that structural steels in general are not susceptible to stress corrosion related crack propagation mechanisms. There is no doubt that structural steels in general are not susceptible for 'classic' stress corrosion crack propagation. However, it must be noted that there is a considerable amount of recent data (39, 40, 41, 11) which implies that this is not necessarily true under all circumstances, in particular conditions of cathodic polarisation or cathodic protection. For conditions of enforced cathodic polarisation, i.e. cathodic protection, steel and environment combinations which normally exhibit true corrosion

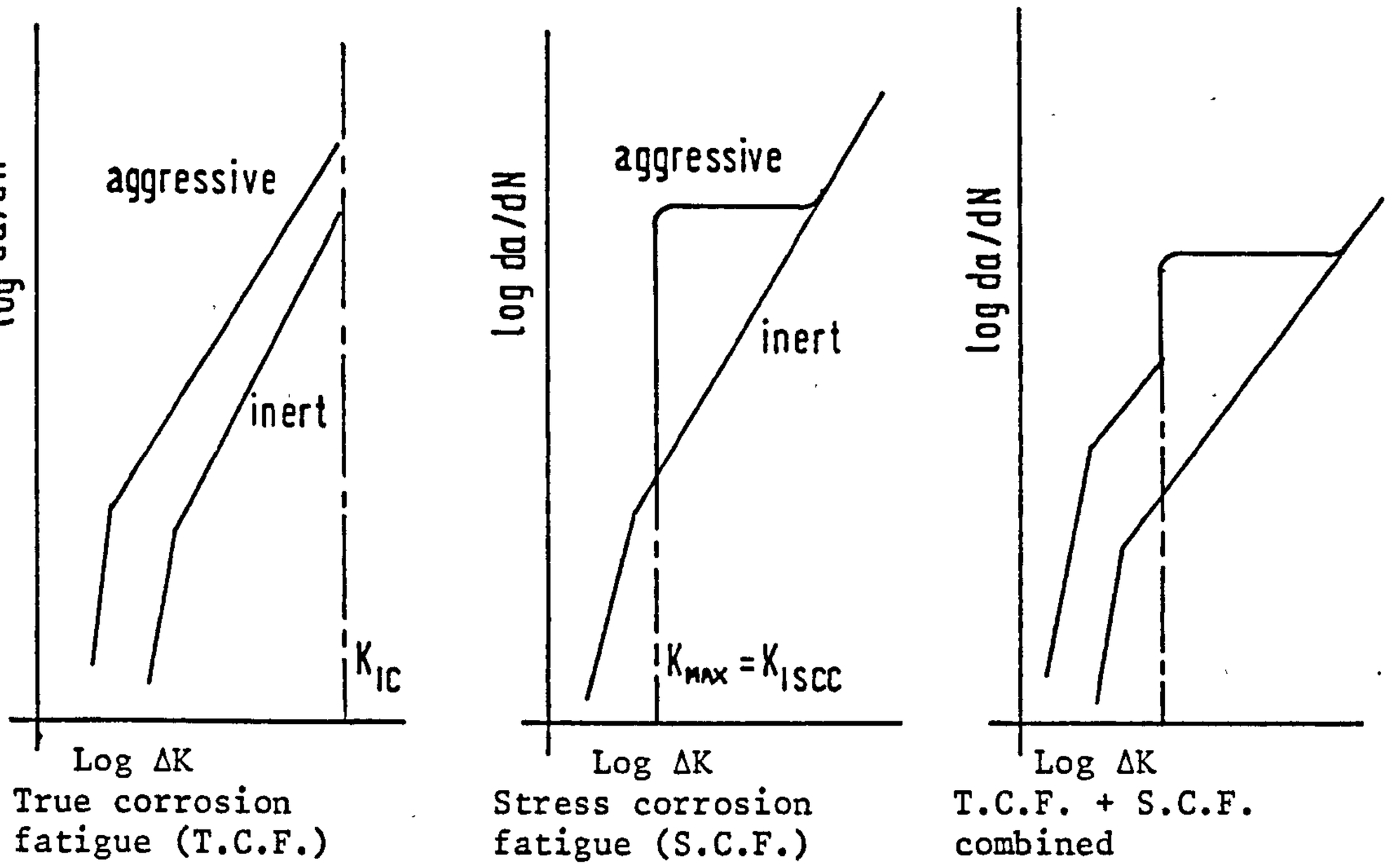

Schematic of basic types of corrosion fatigue crack propagation mechanism according to the process competition model (after Ref. 10)

fatigue behaviour have been found to show effects characteristic of stress corrosion related propagation mechanisms. This generalised view will be discussed further later in this report, specifically in the context of BS 4360 50D steel in a simulated sea water environment, where at a cathodic protection potential of - 1100mV my data exhibits distinct s.c.c. trends.

From the general model presented above, it can be inferred that if the dependence of $(da/dN)_{MECH}$ on K is a steeper function than that of $(da/dN)_{ENV}$, then a corrosion fatigue crack could be expected to propagate by essentially mechanical, rather than corrosion related mechanisms.

However, an alternative interpretation is also possible, which is founded on my data. Namely that plasticity related mechanisms which cause the formation of striations could be expected to be less in evidence for crack propagation under combined processes, which are increasingly influenced by corrosion or stress-corrosion related mechanisms, such as under conditions of enforced cathodic polarisation. Under these circumstances, the formation of striations could be expected to be less, with more evidence of intergranular or quasi-cleavage facets.

It is therefore perhaps significant that the majority of corrosion fatigue crack propagation rate data continues to be presented in terms of conventional Paris type relationships. The above comments could easily be proved or disproved, if more authors in corrosion fatigue studies carried out scanning microscopy of their fracture surfaces.

Given that crack propagation relationships in whatever form, provide a common basis for analysis of experimental data, selection of the relationship to be used might be aided by critical appraisal in the manner indicated below :-

(a) Is ΔK, the crack-tip stress intensity range, a major variable?

(b) On a plot of log da/dN against log ΔK , what is the value of exponent m found experimentally, and does it lie in the range $2 < m < 4$?

(c) Does the relationship or law predict mean load effects and increase of exponent m values to $m > 4$ as K approaches K_c or K_{1c}?

(d) Does the relationship or law contain provision for environmental effects?

(e) Does the relationship or law predict a threshold level of ΔK for fatigue crack propagation and the effects of material variables?

2.2.1 Plasticity Effects

Crack tip plasticity influences fracture mechanics relationships associated with fatigue and corrosion fatigue crack propagation studies, in the following ways :-

(a) Through control of crack propagation by plastic blunting processes at the crack tip.

(b) Through the effects of plasticity induced crack closure arising from the existence of a reverse plastic zone at the crack tip region.

The significance of crack-tip plasticity in relation to fatigue crack propagation has been summarised by Tomkins (26), with reference to the schematic shown overleaf.

For the project reported herein, interest is centred on crack propagation rates in the range 10^{-8} to 10^{-6} m/cycle which are shown in the schematic overleaf to be in the region of change from Stage I threshold or near threshold growth to Stage II steady state propagation. For Stage II growth, Tomkins proposes that intense localised shear deformation in flowbands near the crack tip leads to the creation of new fracture surfaces by shear decohesion at the crack tip itself.

It must be noted, however, that the above schematic can be considered to represent idealised behaviour of a relatively clean metal. As a consequence, therefore, it should not be inferred that it rigidly defines within the same limits of propagation rate, the fracture mechanisms active in structural steel alloys of the BS 4360 50D type. As

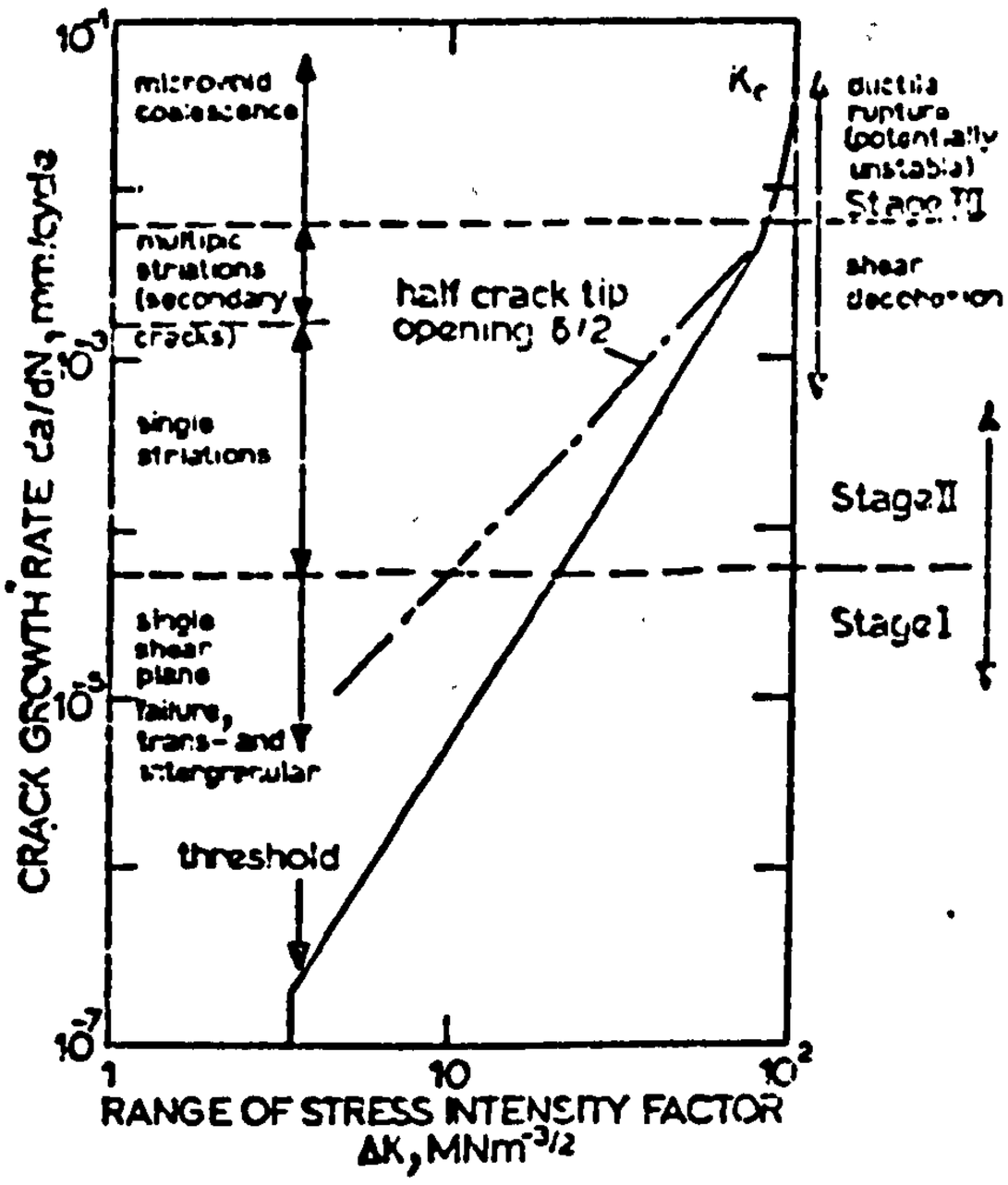

Schematic illustration of fatigue crack propagation mechanisms (after Ref. 26)

discussed later, this was the case observed for the project reported herein.

For Stage II growth, Tomkins has proposed that shear decohesion at the crack tip can be regarded as the process of crack blunting by which the strain singularity which exists at the tip is relieved. Overall blunting of the crack is to the extent of C.T.O.D. (δ) and the amount of new fracture surface formed Δa is $\leq \delta/2$. The general model presented above is supported by Miller (42), who has proposed that fatigue crack propagation is dependent on fracture after a specific amount of crack tip plastic deformation which may be equated to a critical value of δ. Branco et al (43) have developed the concept of a critical value of δ and have proposed that the crack propagation rate da/dN can be expressed in terms of δ, by the empirical relationship :

$$\frac{da}{dN} = A.\left(\frac{\Delta\delta - \Delta\delta_{TH}}{\delta_c - \delta_{max}}\right)$$

where $\Delta\delta = \delta_{max} - \delta_{min}$, $\Delta\delta_{TH} = \delta_{max_{TH}} - \delta_{min_{TH}}$ and δ_c is the critical value of δ for unstable fracture.

Formulae which relate δ to da/dN are no doubt valuable in theoretical analyses of laboratory data obtained from the fatigue of specimens whose stress and loading systems and threshold performance are known. However, it must be noted that for practical application of the

relationship presented above, values of $\Delta\delta_{TH}$ and δ_c are required to be determined for any material, material loading system, joint design and joint geometry relevant to offshore structures, supported by a reliable and acceptable means for the in-field measurement of δ under service conditions. Therefore the correlation of da/dN to δ can be regarded as an interesting scientific exercise, but one which is unlikely to gain widespread acceptance due to inherent practical difficulties.

Reverse Plasticity . Cyclic loading of a ductile material such as aluminium or steel has been found (44) to produce forward and reverse plastic deformation at the crack tip during the loading and unloading parts of the fatigue cycle which gives rise to residual strains in the area of the crack tip. Elber (44) has proposed that this phenomena results in an effective range of stress intensity at the crack tip which can be expressed as :- $\Delta K_{EFF} = A.\Delta\sigma_{EFF}\sqrt{\pi}.a$ where A is a constant and $\Delta\sigma_{EFF}$ is given by U.ΔK and U is known as the 'effective stress range factor'. Schematically, the phenomenon of crack closure can be represented as shown below :

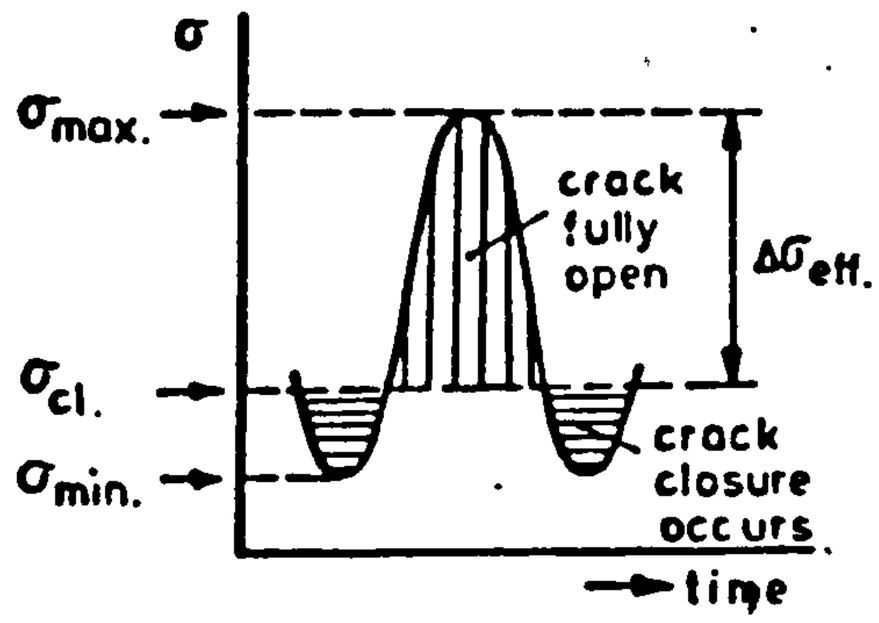

Schematic illustration of crack closure (after Ref. 44).

For the model presented above $U = \frac{(\sigma_{max} - \sigma_{cl})}{\Delta\sigma}$ where σ_{cl} is the crack opening stress. For aluminium, σ_{cl} has been shown to be approximately constant which implies that σ_{cl} is independent of crack length a. It is interesting to note that the definition of ΔK_{EFF} presented above implies that crack propagation can be described by a relationship of the form $da/dN = A(\Delta K_{EFF})^n$ where $\Delta K_{EFF} = K_{max} - K_{OP}$. However, in general there is little agreement in closure measurement data between authors (45 - 50) who have reported data obtained by a variety of techniques, usually on differing alloy systems, specimen designs and environments.

The present generally high level of overall uncertainty connected with the measurement of crack closure prompts the view that considerable development is required before the concept can be applied to structural appraisal. The concept has, however, been applied successfully to analysis of experimental data (50) where it has demonstrated that crack closure effects during pre-fatigue crack propagation can

influence threshold and near-threshold crack propagation behaviour. In this application, relative significance is determined by experimental design and objectives.

Plasticity Related Overload Effects. Of particular general interest to the project reported herein is possible interaction between plasticity and reverse plasticity which might result in the often observed phenomena of retarded crack propagation following overload of a growing crack. Within the framework of fracture mechanics, the following types of phenomenological model can be identified :-

(a) Residual compressive stresses at or near the crack tips (51, 52) and associated yield zone interaction effects (53).

(b) Crack closure effects (54, 55, 56).

(c) Crack tip blunting (57).

(d) Crack tip strain hardening (58).

The range of models identified above indicates that a considerable diversity of opinion exists as to the precise nature of overload phenomena.

It must be noted, however, that a comparable range of techniques, materials and experimental designs etc. was present as previously found for investigation of reverse plasticity. Therefore differences of opinion as to the mechanism responsible is not unexpected. There is, however, general agreement that retardation occurs, to some degree, as a result of overload and that it is a most significant effect.

A major practical implication irrespective of model, is that if a component or structure containing 'active' fatigue cracks is overloaded, an increase in fatigue life can be expected. This would be particularly relevant to pressure vessels which might be subject to inadvertent 'overpressure' during service in addition to over-pressure 'proof testing' during the commissioning phase and to off-shore structures subjected to storm loading.

Bernard et al (59) have proposed that five major phenomenological effects on fatigue crack propagation can be identified in steel, following overload, they are :-

(a) *No effect* : Small overloads have no detectable influence on fatigue crack propagation. The lack of retardation is characterised by reference to an 'apparent threshold level'. For steel overload threshold level is generally assumed to be in the range 40 - 60% of baseline K_{1max}, i.e.

$$\% \text{ OVERLOAD} = \frac{(K_{overload} - K_{1max})}{K_{1max}}$$

(b) *Retardation* : Retardation of crack propagation occurs above the apparent threshold overload level. Effect of retardation can be quantified by empirical relationships

for specific geometries, materials and loading conditions.

(c) *Delayed retardation* : Either an increase in propagation rate immediately following an overload application followed by retardation or delay in propagation following an overload, prior to retardation.

(d) *Lost retardation* : Retardation of propagation rate followed by acceleration to a rate higher than pre-overload rate, before returning to the original rate.

(e) *Arrest* : Complete arrest of crack propagation or crack propagation at a rate too slow to be detected by currently available crack monitoring techniques.

Of particular interest to the project reported herein is the overload propagation rate data reported by the above author for Ducol type steels, as shown below :-

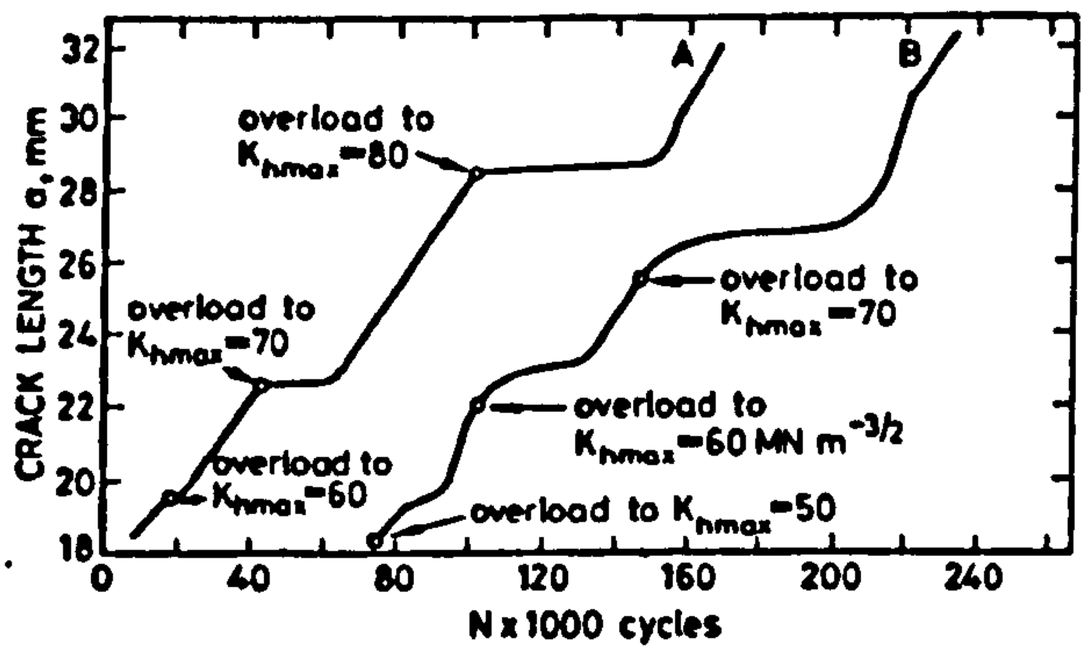

Crack-growth retardation curves for (A) FV 520 B and (B) W 30 B Ducol steels. (after Ref. 59).

For the above data Bernard et al propose that overload retardation in Ducol steels is primarily due to residual compressive stresses generated in the crack tip region in association with crack closure effects. They suggest that the effect can be rationalised in terms of fatigue crack propagation through overload plastic zones subjected to influences arising from plane-stress and plane-strain deformations.

The results presented above are particularly interesting, as data presented later in this report for BS 4360 50D steel show similar overall trends, but for a different experimental technique. It is therefore a disappointment that the authors provide little detailed discussion of their results or experimental technique. In particular there is no discussion to justify the reported increase in $K_{OVERLOAD}$ with increase in crack length a; a feature which it can be argued, confuses the time effect of overload as discussed later in this report.

2.3 *CORROSION PROCESSES AND CORROSION CONTROL*

Aqueous Corrosion. Aqueous corrosion of structural steel in sea water is popularly modelled by reference to chemical reactions arising from the dissolution of iron in a dilute acid. It should be noted, however, that two significant assumptions are made. First, the overall corrosion performance of structural steel, an alloy of iron, is assumed to be dominated by the chemical reactions involving iron only. Reactions involving the alloying elements are assumed to be insignificant. Second, sea water is assumed to behave chemically as a dilute acid, which by inference limits the range of pH values to 1 - 7.

The dissolution of iron in a dilute acid produces a soluble cation and hydrogen gas by the reaction :-

$$Fe + 2H.Cl \rightarrow Fe.Cl_2 + H_2$$

If it is assumed that the acid and ferrous chloride are fully ionized and that chloride ions are common to both sides and can therefore be omitted, the reaction becomes :-

$$Fe + 2H^+ \rightarrow Fe^{2+} + H_2$$

If the corrosion reaction is further simplified by separation of the metallic and non-metallic reactants, then the overall reaction can be presented in two parts as :-

$$Fe \rightarrow Fe^{2+} + 2\bar{e} \qquad (a)$$

$$2H^+ + 2\bar{e} \rightarrow 2H \rightarrow H_2 \qquad (b)$$

For corrosion fatigue crack propagation studies in general and for the project reported herein in particular, the significant reaction is considered to be given by equation (b) above, reduction or cathodic reaction of ionic hydrogen to form hydrogen gas. For structural steel under conditions of free corrosion in sea water, it can be inferred from the above equation that hydrogen enhanced fatigue crack propagation is likely to be an active mechanism. The significance of this circumstance is that hydrogen enhancement of crack propagation rate is therefore not limited to conditions of cathodic overprotection only, as proposed by the majority of investigations. For the project reported herein, a possible influence of hydrogen under conditions of free corrosion potential will be discussed further in a later chapter.

An interesting development in the study of aqueous corrosion related to offshore applications has been provided by Strutt and Turner (60), by investigation of corrosion morphology for BS 4360 50D weldments in sea water, using an accelerated corrosion testing

technique. They proposed that weld corrosion morphology is dependent upon weld heat input and hence indirectly upon the type of welding process used, as shown below :-

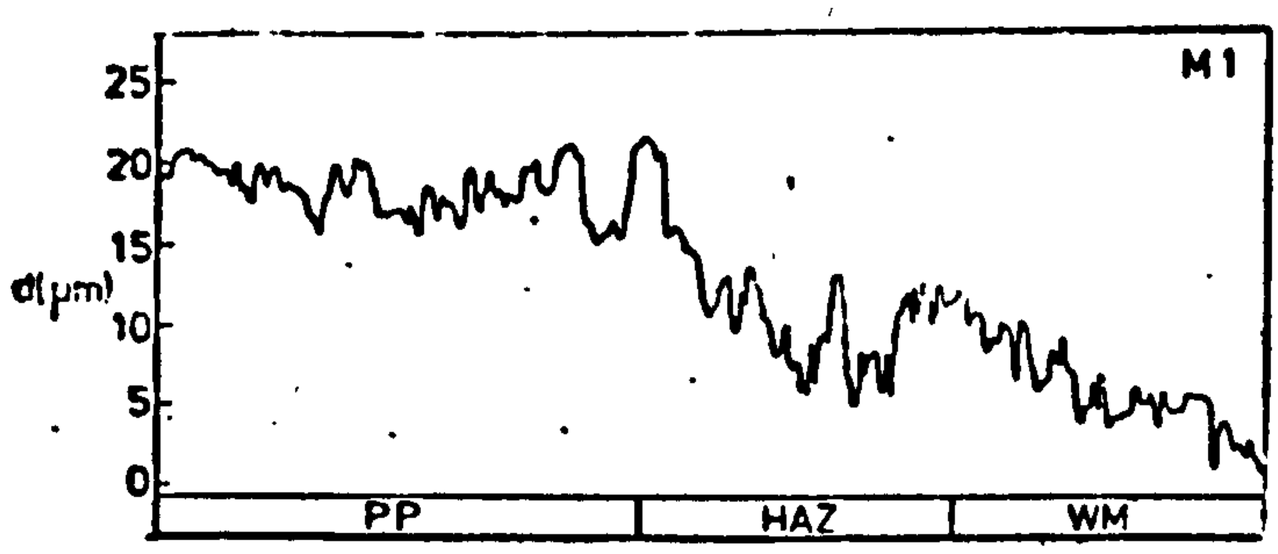

Talysurf trace across corroded weld in BS 4360 50D plate using manual metal arc welding (after Ref. 60)

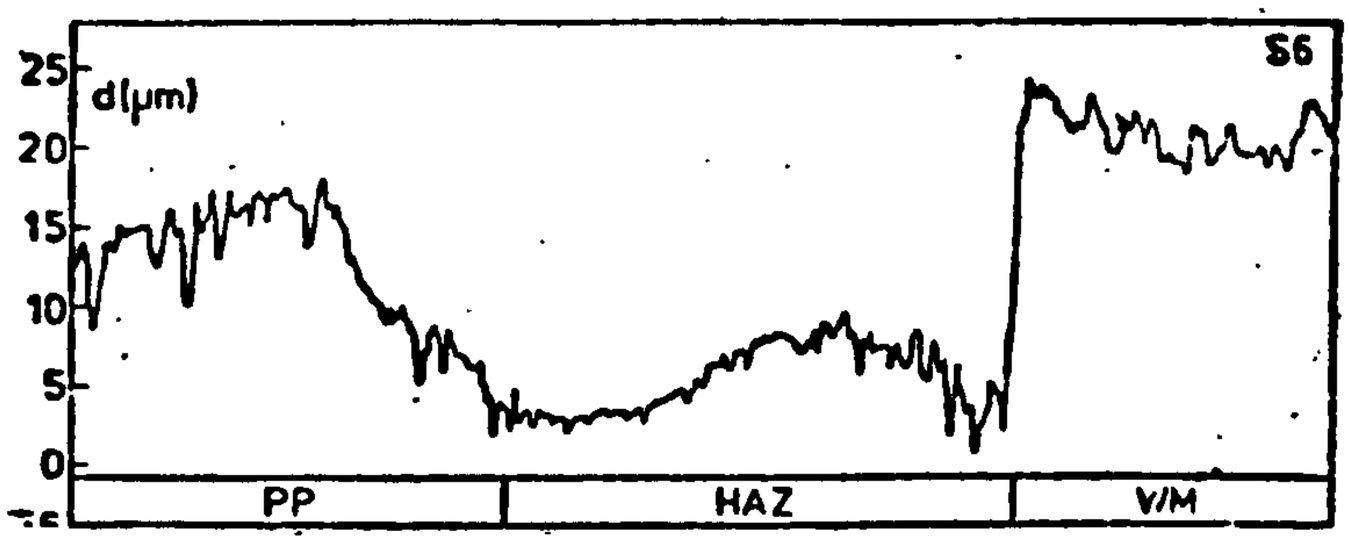

Talysurf trace across corroded weld in BS 4360 50D plate using submerged arc welding (after Ref. 60)

The results presented above indicate that the general effect of an increase in weld heat input on corrosion morphology is to encourage anodic behaviour in the heat affected zone microstructure. It is notable in Strutt and Turner's results, that post weld heat treatment is shown to modify the electrochemical corrosion behaviour of a welded joint by rendering the weld metal and heat affected zone anodic to approximately the same degree.

It must be noted, however, that the above results were obtained under conditions of accelerated corrosion, which under normal circumstances, are not truly representative of offshore service conditions. Further, the maximum material loss was shown to be of the order of 10 μm depth, which can be argued to be insignificant in respect of full size structures.

Overall, the value of the data is considered to lie in the trends which are indicated and not in quantitative levels. As an example, the results presented above can be considered to indicate a possible

basis for the widely held view that corrosion fatigue crack propagation in a welded joint preferentially takes place in the heat affected zone, irrespective of where initiation occurs. Of more interest to the project reported herein are possible influences of preferential corrosion attack in weld microstructure on corrosion fatigue crack propagation rates in the presence of cathodic protection. To date in the literature, the implications of preferential corrosion attack on the fatigue endurance of welded joints has received little attention. In relation to this deficiency, a limited discussion is presented in a later chapter based on data obtained from the project reported herein.

Corrosion Control and Calcareous Deposits. It has been shown (61) that application of Le Chatelier's principle to the anodic and cathodic reactions of aqueous corrosion, causes the expectation that if an electrical intervention is made in the corrosion reaction,changes in the relative rates of reaction should occur. Thus if electrons are supplied to the metal from an external power source, the cathodic reaction rate will increase and electron release or anodic dissolution will decrease. As a consequence, the rate of hydrogen evolution increases, rate of metal dissolution decreases and electrical potential falls. Thus by the supply of electrons from an external source, rate of dissolution is reduced, an effect which is sometimes referred to as 'the principle of Cathodic Protection', development of which has resulted in the techniques of impressed current and sacrificial anode cathodic protection, widely used for corrosion protection of the submerged zones of offshore structures.

The action of cathodic protection is generally considered to be significant in respect of the cathodic reaction where it causes a local rise of pH level, at the surface of the protected steel. In sea water this local rise in pH, precipitates compounds of calcium carbonate and magnesium hydroxide (61). Theoretical calculations have shown that under typical protective current densities, the pH level could be expected to attain pH 11 (62, 63). Calcareous deposits are also considered to influence the electrical properties of the metal surface by allowing the protective potential to be attained at lower current densities. Corrosion behaviour of the protected steel may also be modified either by the coating or by the raised pH within the porous alkaline deposits (64).

Hartt and Wolfson (63) have proposed that mechanistically, the most significant effect is that of a surface with an active area reduced by partly impervious scale or deposits with oxygen arriving at the protected surface at a diffusion limited rate. This can encourage a current density at the scale/metal interface which is high enough to bring the local potential into the range for hydrogen evolution. Potentially this is a most significant feature of calcareous deposits,; particularly for investigation of corrosion fatigue crack propagation rates in the presence of cathodic protection. For the project reported herein, possible influences will be discussed further in a later chapter.

It is interesting to note that a number of authors have reported that the protective value of calcareous scale or deposits does not increase indefinitely with formation current density or negative

potential. With overprotection , calcareous deposits are reported to become more porous (65, 66, 67, 64) and also less adherent to the metal surface (68), where loss of adherence is attributed to increased hydrogen evolution within the porous deposits. It is a notable feature in literature on calcareous deposits that investigations are inevitably biased towards consideration of electrical aspects arising from scale formation. Investigation of mechanical properties, particularly those associated with possible crack blocking have been ignored. This deficiency is significant, in view of the general popularity of mechanical crack blocking concepts based on the formation of calcareous scales, in explanation of the alleged beneficial effects of cathodic protection.

In practice, the most significant effect of calcareous scales and deposits is generally considered to be reduction in current density required for protection. However, on a 'full size' offshore installation, it is probable that scale formation will not be uniform or consistent throughout the 'protected area'; as locally the structure may simultaneously experience a current density that is initially high with the attendant risk of 'spalling', followed by a period when it is low with the risk of increased porosity. From currently available literature, it is not known how calcareous scales react to changes in current density. As an example, information is not available as to whether scale properties reflect some overall aspect of the formation period, e.g. total charge passed or whether after sufficient time a scale adopts the protective properties corresponding to the current density last imposed upon it.

In view of the mechanical influences attributable to calcareous deposits which are popularly used to explain the influence of cathodic protection on corrosion fatigue crack propagation, it is significant that historically the general trend in investigations of calcareous deposits has been concerned with electrical and electrochemical properties, not mechanical. Therefore, if the dominant effect of calcareous scales is indeed mechanical, then the greater part of research to date has been misdirected. Further, the situation is created whereby an overall effect is explained by reference to an unsubstantiated model. This apparent contradiction will be discussed further in a subsequent chapter.

2.4 CATHODIC PROTECTION CURRENT DATA

At strength levels associated with structural steels, S - N tests on plain specimens have generally shown cathodic protection to be beneficial (69), particularly under low stress-range, high cycle conditions appropriate to long service lives. The effect of cathodic protection seems to be less clearly defined for high strain, short life tests (life < 10^3 cycles) where fatigue endurance has been found to be reduced, compared to in-air performance (70). However, beneficial effects from cathodic protection have been reported for various configurations of structural steel welded joints (71, 72 and 73). Early studies indicated that relatively high levels of current density were required to obtain the full benefit of cathodic protection (of the order of 220 mA/m^2) (69). Later studies have, however, shown that current demands are reduced to economic levels by the deposition of calcareous deposits on the surface of the protected steel. In

general, cathodic protection to a value sufficient to arrest weight loss, has been shown to produce optimum improvement in fatigue endurance to approximate in-air values (74).

Such favourable effects of cathodic protection appear to be not so apparent from tests employing pre-cracked specimens. Early studies using pre-cracked specimens in salt water environments with cathodic protection, tended to be based on high strength steels (75) and showed that cathodic protection had an adverse effect. However, this is possibly not an unexpected result, in view of the well known susceptibility of high strength steels to hydrogen embrittlement and stress corrosion cracking.

At levels of material yield strength and hardness commonly present in offshore structures, structural steels are not normally considered to be susceptible to hydrogen related crack propagation mechanisms, particularly under static load conditions. However, for specific conditions of cathodic protection, significant increases in corrosion fatigue crack propagation rate have been observed (12, 72, 76). For BS 4360 50D type structural steel, Scott and Silvester (12) have proposed that cathodic polarisation to just below the free corrosion potential, produces the optimum reduction in corrosion fatigue crack propagation rate, although not to the level derived from corresponding air tests. Reduction in crack propagation rate is attributed to the effects of crack blocking due to calcareous deposits on the fracture surfaces and to a reduced contribution to crack growth from anodic dissolution. However, at more negative potentials, crack propagation rate was reported to increase significantly.

A notable exception to the popularly accepted view of 'overprotection' is proposed by Bardal et al (77). For BS 4360 50D type steel, they propose that no significant differences in corrosion fatigue crack propagation rate arise as a result of overprotection. The influence of cathodic protection on crack propagation rate is considered to be dependent upon crack depth with a relatively small influence for deep cracks, a $\geq$ 3mm, and maximum effect for shallow cracks, a $\leq$ 3mm. Unfortunately the authors do not include in their model consideration of fracture mechanics parameters, in particular ΔK. As a result, the relationship between crack depth and threshold ΔK levels cannot be assessed from their data. If shallow crack depths are considered to be equivalent to threshold or near threshold conditions, then the results are in accord with the general body of data. However, if the influence of crack depth is truly independent of ΔK and threshold, then the results assume considerable significance.

Therefore, by correlation of influence of cathodic protection to crack depth with no consideration of fracture mechanics parameters. The authors are considered to have introduced an unnecessary and unhelptul complication, particularly as they further propose that cathodic overprotection of structural steel has no significant influence on corrosion fatigue crack propagation rate. A result which is contradictory to the majority of published data.

To date in published literature, much valuable research has been reported into specific aspects of calcareous deposits and cathodic

protection in general. However, the situation remains that the precise influence of cathodic protection on corrosion fatigue crack propagation rates in structural steel remains ill-defined. It is in this area that the project reported herein is intended to make a major contribution.

2.5 *CRACK LENGTH MEASUREMENT AND DATA PROCESSING TECHNIQUES*

Measurement of crack length under conditions of corrosion fatigue and subsequent presentation of crack propagation rate data can be considered to be fundamental to any fracture mechanics based study of corrosion fatigue crack propagation behaviour in structural steel. Techniques for both monitoring/measurement of corrosion fatigue crack length and for subsequent presentation of Paris type crack propagation rate data are therefore worthy of particular consideration.

In general, techniques for monitoring/measurement of corrosion fatigue crack length can be classed as being either optically or electrically based. A simple measurement technique and historically one which has tended to be least used, is optical crack measurement by use of a Vernier type travelling microscope. The comparative merits of this technique are summarised in Table 10A, together with those of a representative electrically based technique which are summarised in Table 10B. Currently for fatigue crack propagation in air, a popular method of crack length measurement is based upon measurement of electrical (D.C.) potential change with increase in crack length. Of late, a similar technique using (A.C.) has also been developed (98). The fundamental principles of the D.C. technique have been extensively reviewed by Wei and Brazill (78) and Aronson and Ritchie (79). From these reviews, it is evident that electrical potential monitoring type techniques for measurement of crack length, are technically complex and subject to significant constraints for accurate and reproducible measurements of crack length. A calibration between measured voltage and crack length must be established, based on either empirical (80, 81) or analytical (79, 82, 83, 84) methods and verified experimentally.

Further, the geometry of the test specimen and the location of the measurement probes must be arranged to :-

(a) optimise the absolute potential signal, compared to instantaneous instrument resolution,

(b) optimise the change in potential per unit crack depth/length, compared to long-term instrument stability,

(c) minimise variations between crack depths predicted from the calibration and actual values.

In this context, Gangloff (85), has proposed that small errors in probe location significantly influence the relationship between potential and crack depth and therefore negates empirical calibration. As a consequence, Gangloff argues that analytical calibration procedures only should be used to relate measured potential to crack size and to specific initial crack and probe dimensions. It should be noted, however, that Gangloff's research was concerned with cracks

less than 1.00 mm deep. Moreover, he reported values of calculated crack depth, based on electrical potential measurements, of the order of ± 15% of optically measured values, which necessitated the application of electric current to the specimen in the range 10 - 20 amperes.

Overall, both types of crack measurement/monitoring technique can be considered to have significant limitations. Optical measurement techniques can only give the surface crack length, which for 'thick' specimens in particular, may be markedly different from that in the centre of the specimen due to the effect of 'crack tunnelling'. In addition, many corrosion environment systems have opaque solutions or produce surface corrosion products and coatings, which interfere with satisfactory observation of the specimen surfaces.

In contrast, electrical potential measurement techniques can produce reasonably accurate and repeatable measurements of crack length, for fatigue cracks in air. However, in aqueous corrosion environments and in particular sea-water, calibration can be extremely difficult to achieve, due to the presence of an electrically conductive medium within the crack. Further, a significant constraint in respect of corrosion fatigue studies is that the presence of inherently high levels of electric current can establish electric potential gradients in the region of the crack tip and can promote unwanted interference with electrochemical corrosion processes.

Against this background, a technique for corrosion fatigue crack monitoring, based on change in specimen compliance with increase in crack length, has been developed by Scott and Silvester (12) and Misawa, Ringshall and Knott (25). Within the elastic range, the specimen compliance is considered to be a unique function of the a/w ratio and hence of crack length. It should be noted, however, that both groups of authors (12, 25) obtained initial specimen compliance calibration in-air by use of optical crack monitoring, to verify crack length measurements obtained by use of electrical potential drop techniques. Further, the discussion presented (12, 25) can be considered to be deficient in the following areas :-

(a) For conditions of corrosion fatigue, the relative accuracy of crack length measurement by change in specimen compliance compared to measurements obtained optically, is not discussed.

(b) Reliability of equipment and repeatability of data produced by the change in specimen compliance technique is not discussed.

(c) The change in specimen compliance technique is not critically appraised with a view to establishment of practical constraints. As an example, the technique may not be applicable in circumstances where displacement at the crack mouth cannot be accurately measured.

Based on the foregoing discussion, a suspicion is created that the popularity of the change in specimen compliance technique is founded on ease of automation in conjunction with reduced labour re-

quirements, particularly as the technique can be readily incorporated into computerised data acquisition, processing and analysis systems.

In this context, it must be noted that crack monitoring is not the only significant consideration in experimental investigation of corrosion fatigue crack propagation behaviour in structural steel. Of equal importance is the significance of the variables associated with the processing, analysis and presentation of crack propagation rate data. Specific variables involved are the data processing methods used to convert, the crack length versus elapsed cycles test data (a vs N) into crack growth rate data, expressed as a function of stress intensity factor range (da/dN vs ΔK) in conjunction with the analytical methods subsequently used to evaluate data scatter and present the test results in a form suitable for use in design.

The analytical methods which can be used to characterise corrosion fatigue crack growth rate performance can be summarised as shown below:

SUMMARY OF ANALYTICAL METHODS USED TO CHARACTERISE FATIGUE CRACK GROWTH RATE.

Data Processing

(a vs N to log da/dN vs log ΔK)

Method used to compute da/dN

(1) Graphical techniques

(2) Finite difference methods

(3) Numerical curve fitting techniques

Evaluation of Data Scatter

(determination of upper-bound limits for Design Data)

(4) Visual determination of upper-bound

(5) Upper bound Regression line

(6) Confidence bands based upon Standard Deviation

(1) The graphical method, described by Knott (86) is simple and easily applied and involves visually fitting a smooth curve through the plotted a vs N data and estimation of the rate of growth at a given crack length, a_i, from the slope of a tangent to the curve at a_i. The corresponding ΔK value is computed using the crack length a_i.

(2) A commonly used finite difference method is the 'secant' or 'point-to-point' technique (87). The crack growth rate is calculated from the slope of a straight line, connecting two adjacent points on the a vs N curve. This can be expressed simply as :-

$$da/dN = \frac{a_{(i+1)} - a_i}{N_{(i+1)} - N_i}$$

Thus da/dN is the average crack growth rate over the increment a_i to $a_{(i+1)}$, the mean crack length $\frac{1}{2}(a_{i+1} + a_i)$ is used to calculate ΔK.

(3) Numerical curve fitting methods currently in use include several sophisticated techniques for fitting data with complex polynomial expressions (88). Of these, a popular method is the 'incremental polynomial technique', in which a 2nd order polynomial (parabola) expression is fitted to sets of successive data points (usually 5 or 7 data points). A typical form is :-

$$a = b_o + b_1\left(\frac{N - C_1}{C_2}\right) + b_2\left(\frac{N - C_1}{C_2}\right)^2$$

where b_o, b_1 and b_2 are regression parameters, determined by the least squares criterion over the local range of crack lengths. The parameters C_1 and C_2 are scaling factors. The rate of crack growth at (a_o, N_i) is given by the derivative of the 2nd order expression which has the form :-

$$da/dN = \frac{b_1}{c_2} + 2b_2(N_i - C_1)/C_2^2 \qquad (99)$$

Generally the ΔK value corresponding to the derived growth rate is computed for a fitted crack length, $\hat{a}_i$, which corresponds to the median number of cycles $\hat{N}_i$, over the local elapsed cycle range. A variation of this method is to fit a higher order polynomial to all the data points and differentiate as before to determine growth rate.

The important feature of the foregoing, brief description of analysis techniques is that each technique can be considered to have inherent limitations, likely to have an adverse effect upon the characterisation of corrosion fatigue crack growth behaviour. For example, graphical analysis methods can be considered to be subjective by nature, and therefore might tend to produce inconsistent and unreproducible results. Whereas finite difference methods, which are based on point-to-point differences can be considered to enhance variations in a vs N test data and consequently may yield excessive scatter in the processed data where the variability is sensitive to crack length measurement interval. Conversely, numerical curve fitting methods can be considered to generally involve a least squares regression analysis, which may induce excessive smoothing of the data and consequently may mask important material behaviour. The adverse effect of excessive smoothing of data is particularly relevant where a single polynomial expression is fitted to all data points.

Given the range of limitations of data processing methods, briefly discussed above, it is noted with interest that from previous evaluation of actual test data (89), Clark and Hudak (90) have proposed that the data processing technique used has a relatively small and, by inference, insignificant effect on the central tendency behaviour of data, but has a significant influence upon the extent of data scatter. It should be noted, however, that for the survey of literature reported herein, Clark and Hudak (90) were the sole source of recently published findings on the comparison of the overall performance of selected data processing techniques. As a consequence, their findings are considered to be uncorroborated, as they have thus far not been subjected to independent critical appraisal. Lack of critical appraisal is considered to be significant, because data scatter is an acknowledged feature of crack growth rate testing, but is not determined solely by the particular data processing technique applied. Also, discussion of the possible influence of data processing technique on the central tendency of data, has generally been omitted from the majority of contemporary published literature.

In practical terms, it is considered that the major consideration from the foregoing brief review, is the potential degree of scatter promoted by a given data processing method. As noted previously, there are a number of techniques currently in use for analysis of data scatter, which vary significantly in their approach and degree of sophistication. The simplest technique involves visually fitting a straight line through all the data points to establish a mean-growth bound as through the upper data points only, to establish an upper-bound. A more sophisticated method involves the determination of a least-squares regression line for a given group of data, which is subsequently used to establish an upper-bound, where the upper-bound is established either by drawing a line parallel to the regression line at a location which encompasses all of the data points, or the estimated standard deviation about the regression line is established statistically and an upper bound is determined on the basis of two or three standard deviations. The estimated standard deviation can also be used to establish any one of several types of upper confidence bounds, to a level required for a given application. It should be noted, however, that the establishment of estimated standard deviation bounds are not confidence statements and cannot be used to make inferences concerning the probability that all data will occur within the bounds. Additional, more complex statistical analyses would be required to establish confidence bands, suitable for use in design applications.

CHAPTER 3

OBJECTIVES

The notional objectives for this investigation were defined as follows :-

1. To assess the phenomenological effects of cathodic protection on low frequency corrosion fatigue crack propagation in BS 4360 50D structural steel, immersed in sea water for microstructures associated with parent plate and welded joint configurations.

2. To assess the phenomenological effects of low frequency corrosion fatigue crack propagation in BS 4360 50D structural steel in environments of intermittent immersion and simulated splash zone for microstructures associated with parent plate and welded joint configurations.

3. To assess the phenomenological effects of single cycle overload on low frequency corrosion fatigue crack propagation in BS 4360 50D structural steel in air and in sea water.

4. To assess the suitability of the Paris crack propagation relationship when used to characterise low frequency corrosion fatigue crack propagation in BS 4360 50D structural steel, in the presence of cathodic protection for microstructures associated with parent plate and welded joint configurations.

5. To determine the nature of surface deposits generated by cathodic protection and to assess their influence on corrosion fatigue crack propagation rates in BS 4360 50D structural steel, for microstructures associated with parent plate and welded joint configurations.

6. To assign significance to the influence of cathodic protection on low frequency corrosion fatigue crack propagation rates in BS 4360 50D structural steel, for microstructures associated with parent plate and welded joint configurations.

CHAPTER 4

EXPERIMENTAL

4.1 TEST MACHINE

A general view of the fatigue testing machine used for this project is given in Figure 1A. A view of the associated load control panel is given in Figure 1B. The test machine shown in Figure 1 is a specialised development of a general purpose, three point bend fatigue testing machine that was designed and built at Cranfield. In its original form, this type of machine was used primarily for the fatigue testing of steels in air at frequencies in the range 1 - 15 Hz.

For the project reported herein, the testing machine provided for experimental use had been previously modified by the addition of an electrically isolated specimen tank in the machine's working section, as shown in Figure 1A. The arrangements used to electrically isolate the tank assembly from the bulk of the test machine are shown in Appendix 1.

Two fixed steel rollers were mounted on a Paxolin insulation block. The load was applied to the specimen by a central lower steel roller. The central lower roller was pillar mounted onto the specimen tank bottom and was sealed against the loss of aqueous test solution by the use of clear silicone sealant. As supplied, the specimen tank had a clear perspex observation port cut into one side only, to permit optical crack measurement. This arrangement was subsequently modified by the addition of a viewing port in the opposite tank side, as shown schematically in Appendix 3. The complete specimen tank assembly was mounted via a Paxolin spacer to a steel balance plate which was, in turn, assembled to an adaptor plate which was fixed to the end of the hydraulic ram extension piece. The load cell that was used to provide closed-loop load control, was mounted in series between the hydraulic ram extension piece and the main hydraulic ram. In operation the main hydraulic ram, ram extension piece, load cell, balance plate and specimen tank assembly, were all subject to sinusoidal vertical displacement.

The test machine was originally designed to operate in the load-control mode and it was this control method that was utilised throughout the project. Load control was achieved by means of a simple closed-loop servo hydraulic control system. The system used for this project is shown schematically in Appendix 15, where the shaded features are modifications to the original system design which were initiated by pre-commissioning of the test machine. The modifications made and their justification are discussed in more detail in later paragraphs.

In operation, the output from the Function Generator was a sinusoidal waveform or signal whose frequency, amplitude and mean level were variable. Control of frequency, amplitude and mean level was exercised via the variable resistance potentiometer's marked frequency, amplitude and offset respectively, shown in Figure 1B.

The output from the Function Generator was passed via an error

measuring circuit, to the servo-amplifier which was connected as a summing amplifier. The output from the servo-amplifier was in turn passed to the servo hydraulic control valve (Moog valve) which controlled the rate and direction of flow of hydraulic fluid into the main hydraulic ram.

Under the influence of hydraulic pressure, the hydraulic ram moved until resistance to movement was encountered due to the presence of the specimen in the machine's working section. When resistance to movement was encountered, load was progressively applied to the specimen with the load magnitude being measured by the load cell. Under load, the load cell produced an output voltage which was amplified by the load cell amplifier and was then fed to the error measuring circuit.

The revised output from the error measuring circuit was in turn used to reduce the input to the servo-amplifier. The reduced input was amplified and loading was continued until the signal fed back from the load cell, via the load cell amplifier, was sufficient to cancel out the signal from the function generator and thus reduce the input to the servo amplifier to zero. By this means, sinusoidal loading under closed-loop load control was applied to the specimen.

In operation, the magnitude of vertical displacement of the main hydraulic ram and associated moving masses was negligible and therefore the system as a whole was considered to have inherently low inertia.

Prior to the start of scheduled project activity, the test machine was pre-commissioned and its performance was assessed against the stated project objectives. As a result, the following deficiencies were noted :-

4.1.1. Load sensitivity was poor and unacceptable, particularly at load levels of the order of 2KN or less. This was a significant feature in view of the intended use of an R ratio of 0.1.

4.1.2. The output frequency from the Function Generator was found to be erratic, particularly at frequencies of less than 10 Hz. Again, this was a significant feature in view of the intended loading frequency of 0.5 Hz.

4.1.3. Load control generally was found to be poor with a marked time-dependent upward drift in load levels during machine operation.

4.1.4. Random voltage peaks or 'spikes' in the electrical mains supply to the test machine were found to result invariably in catastrophic specimen failure.

4.1.5. The action of starting and stopping adjacent hydraulically powered testing machines in the same laboratory was found to result invariably in catastrophic specimen failure due to the effect of 'hydraulic surge'.

4.1.6. The industrial 'Chiller Unit' that was provided for temperature control of the test solution was found to be incapable of maintaining the desired solution temperature of nominally $10^{o}C$.

4.1.7. The specimen tank was found to be severely corroded both internally and externally with evidence of substantial leakage around all penetrations through the tank shell, i.e. central pillar mounting holes in the tank bottom and the observations port cut in one tank side.

4.1.8. In operation, the test machine was found to encourage significant unequal crack growth on opposite specimen faces.

In view of the deficiencies detailed above, the following remedial works were carried out to the test machine and its associated services, prior to the start of the scheduled experimental programme.

4.1.9. The noted poor load sensitivity was attributed to the existing load cell fitted to the test machine which was rated at 66 KN maximum capacity. This load cell was removed and it was replaced by a down-rated load cell of 22 KN maximum capacity which was connected to the test machine load control panel by a specially lengthened and shielded umbilical cable.

This arrangement enabled the load cell to be calibrated (full range) in an adjoining Denison machine with the minimum of electrical disconnections from the test machine load control panel. The only disconnection/reconnection required was the Cannon connector onto the load cell itself. In subsequent service, the load cell was re-calibrated at three monthly intervals.

4.1.10. The unstable low frequency output from the Function Generator was attributed to the basic design of the frequency generator circuit which was originally intended to generate a maximum frequency of 50 Hz.

The circuit design for use in this project was subsequently modified by the addition of a dividing circuit with the incorporation of a higher value potentiometer control which was used to fine tune the output frequency. In its modified form, the Function Generator produced a maximum output frequency of 4 Hz at full scale setting.

The sinusoidal output waveform was checked using an oscilloscope and the output frequency was calibrated against potentiometer settings, using an electronic digital frequency counter. In subsequent service, the output waveform was checked and the frequency generator was re-calibrated at three monthly intervals.

4.1.11. The phenomenon of load drift was attributed to instability in voltage inputs to the essential control system elements, namely the load cell amplifier, the servo amplifier and the function generator. There was also some effect from degradation of the hydraulic oil, due to overtemperature and contamination.

The observed instability in voltage inputs was remedied by the addition of three high quality stabilised power supplies, one down-stream of each essential control system element as shown schematically in the shaded features in Appendix 15. These units replaced the single stabilised power supply originally provided with the test machine. Protection from the adverse effects of voltage peaks in the mains

electrical supply was provided by the addition of a capacitive filter in the supply line to the test machine. The general arrangement is shown schematically in the shaded features in Appendix 15.

The deficiencies in the hydraulic oil supply to the test machine were remedied as follows :-

(i) The test machine used for this project was removed from a common hydraulic power supply, used by other laboratory machines, and was re-connected to an isolated hydraulic power pack. This dedicated power pack remained with the test machine for the duration of the project.

(ii) The air-cooling arrangements for the hydraulic power pack were modified to provide increased air flow through the oil-cooler matrix. Also a previously unserviceable oil high temperature alarm and trip were reinstated.

(iii) The existing hydraulic oil was drained and flushed and was replaced by new oil of an uprated specification. The hydraulic ram assembly contained within the test machine was removed, dismantled, thoroughly cleaned and was reinstated with new seals and a new flow control valve (Moog Valve).

4.1.12. The lack of effective temperature control for the test solution was attributed to failure of the refrigeration equipment contained within the Chiller Unit. This unit was subsequently overhauled by the manufacturers and a new refrigerant circulation pump was installed. Also the test solution reservoir tank was externally clad with 50mm thick expanded polystyrene sheet on all surfaces, including the tank bottom. In service these arrangements were found to readily and consistently maintain the required test solution temperature of $10^{o}C \pm 1^{o}$.

4.1.13. The severe corrosion attack present on the specimen tank was attributed to failure of the surface paint coating combined with ineffective sealing of all through-wall penetrations.

The specimen tank was removed from the test machine and was stripped of its original paint coating down to a bright metal finish. At this time, a second observation port was cut in the tank side to allow observation of both specimen faces. This arrangement is shown schematically in Appendix 3.

The specimen tank was subsequently repainted using a chlorinated rubber paint specification of the type used extensively offshore for structural protection in the splash zone region. Modified perspex covers to the observation ports were fitted. These improved covers, incorporated larger diameter 'O' ring seals and reduced pitch of attachment fastenings which significantly improved the distribution of the clamping load .

The central pillar and its mounting bolts were sealed using a standard commercial quality silicone rubber sealant.

The measures outlined above were successful in preventing further corrosion attack of the specimen tank for the duration of the project.

4.1.14. The phenomenon of unequal crack growth on opposite specimen faces was attributed to the adverse effect of uneven contact pressure between the upper and lower specimen edges and the respective load applicationand load reaction rollers. This was considered to arise from general machine mis-alignment coupled with wear and out of roundness of the rollers themselves.

The existing rollers were therefore removed and were replaced by new items. Also the vertical alignment of the hydraulic ram assembly was adjusted such that the longitudinal axis of the load application roller was parallel to the longitudinal axes of the two upper load reaction rollers. These measures were found to be satisfactory for the duration of the project.

4.2 TEST ENVIRONMENT : ESSENTIAL CONDITIONS

The Project objectives detailed in Chapter 3 were considered to define effectively the scope of experimentation required and also to establish the essential environmental conditions. Given that the stated bias of the project was essentially phenomenological in nature, the measurement of fatigue crack growth behaviour in pre-cracked, single edge notched specimens, loaded in three point bending, was selected as the most suitable experimental vehicle.

The simulation of an offshore corrosion fatigue environment, was based broadly upon a low frequency of loading with the specimens wholly contained in a temperature controlled simulated sea water environment. The frequency of loading used throughout the project was 0.5 Hz ± 0.1% with the temperature of the simulated sea water consistently maintained in the range 10°C ± 1°.

It is acknowledged that in practice, the wave loading of offshore structures in fatigue is of random amplitude and frequency. However, the underlying trend has been shown to be sinusoidal in nature with an effective average wave period of nominally 14 secs. (91). Rigorous experimental simulation of this feature would dictate that a loading frequency of 0.1 Hz be used.

However, given the limited period of time that was available for completion of the project, a loading frequency of nominally 0.1 Hz was not considered to be viable. Therefore for expediency, a fatigue loading frequency of nominally 0.5 Hz was selected, in order to maximise the acquisition of data in the limited amount of time available. This decision was justified by the criterion that for fatigue of steels in general, a fatigue frequency of nominally 0.5 Hz has been shown to be the highest frequency that can legitimately be considered to be representative of the low frequency fatigue regime (92).

The test environment of simulated sea water was made in accordance with the manufacturer's instructions from a proprietory salt compound supplied by B.D.H. Chemicals Ltd., under the tradename 'Sea Water Corrosion Test Mixture'. The chemical composition of this salt is given in Appendix 2. In use, the solution was found to have a consistent pH value of 6 which was slightly acidic with respect to natural sea water which is generally accepted to be neutral to alkalise with a pH of 7 - 8. This minor difference in pH values was not consid-

ered to be significant and was probably due to dissolved CO_2.

In service, 100 litres of the simulated sea water test solution was contained in a specially lagged reservoir tank (previously described in paragraph 4.1), which was situated at the rear of the test machine. This solution was renewed at three monthly intervals, to avoid any possible electrochemical interference, promoted by the build-up of corrosion products within the test solution and any other contamination. As a further aid to averting unwanted electrochemical interference, polymer components were used throughout the test solution circulation system. This included all fittings, pipework and the circulation pump itself.

The temperature controlled test solution was circulated through the specimen tank at a rate of approximately 2 litres/minute. It entered at the bottom of the tank, through a single inlet fitting under pressure from the circulating pump and was removed from the top of the tank through twin overflow pipes. These pipes carried the test solution back to the reservoir tank. The position of the twin overflow outlets was arranged such that the specimen was consistently submerged in an adequate depth of test solution. These arrangements are shown schematically in Appendix 3.

The test solution was assumed to be fully aerated at all times. Full aeration was maintained by a continuous supply of low pressure compressed air that was injected into the test solution within the reservoir tank.

The desired test solution temperature of $10^{o}C \pm 1^{o}$ was maintained by use of a specially adapted industrial Chiller Unit with a remote copper cooling coil. The remote cooling coil was located inside the reservoir tank and was connected to the Chiller Unit by polymer pipework. Throughout the project, this arrangement successfully maintained the test solution within the desired temperature range.

4.3 TEST SPECIMENS

The single edge notched test specimens were manufactured in the form of blanks in three basic material configurations, in order to provide the desired range of microstructural features. The design of specimen blank used was common to all tests and microstructures and is given in Appendix 4.

The specimen dimensions detailed in Appendix 4 were developed from the basic requirements contained in BS 5447 : 1977, 'Methods of test for plain strain fracture toughness of metallic materials'. At the outset it was acknowledged that for this project, there was no requirement for valid K_{1c} data. As a consequence, the relationship for minimum specimen thickness, $B \geq 2.5 (K_{1c}/\sigma_y)^2$, given in BS 5447, was considered to be not strictly applicable.

It was, however, considered that the relationship $B \geq 2.5(K_{1c}/\sigma_y)^2$ could justifiably be modified, to indicate a notional specimen thickness for essentially plain strain stress conditions at the crack tip, in a test specimen where the expected value of K_{max} was significantly less than the associated value of K_{1c}.

As a consequence, for this project, the highest calculated experimental value of K_{max} was substituted for K_{1c} and the relationship for B was rewritten as $B \geq 2.5(K_{max}/\sigma_y)^2$ for essentially plain-strain stress conditions at the crack tip. For the planned experimental maximum load amplitude at the longest crack length, application of the modified relationship for B yielded a notional minimum specimen thickness value of approximately 20.00mm.

By reference to BS 5447 and the recommended thickness (B) to width (W) ratio (B/W) of 0.5, it was evident that for the 40 mm thick, BS 4360 50D plate material provided for project use, a notional test specimen thickness of 20 mm could not be accommodated, as the corresponding width dimension became 40 mm which was equivalent to the as-supplied plate thickness.

It was therefore considered acceptable to use a specimen thickness (B) of 15.00mm with a corresponding width (W) dimension of 30 mm. This arrangement was considered to provide for the largest practicable size of test specimen for the given size of as-supplied plate. It was also consistent with the overall guidance given in BS 5447, as to test specimen dimensional ratios necessary to ensure that essentially plain strain stress conditions are generated at the crack tip.

The required variation in test microstructural features was achieved by specific joint design. The test specimen configurations used were as follows :

Group A : Parent plate. The specimens in this group were manufactured from 40 mm thick BS 4360 50D plate in the 'as received' condition, with the longitudinal axis of the specimen parallel to the rolling direction. In this way, fatigue crack propagation normal to the direction of rolling in the short transverse direction was assured. The direction of rolling was identified from metallographic examination of the parent plate. The mechanical properties of the steel used are given in Appendix 5 with the results from a chemical analysis given in Appendix 6.

Group B : Welded plate. The specimens in this group were manufactured using a single Vee groove weld preparation, in accordance with the requirements of AWS. Code D1.1, as shown in Appendix 7. The details of the weld procedure and filler metal used are given in Appendix 8.

Group C : Welded plate. The specimens in this group were manufactured using a single bevel groove, weld preparation in accordance with the requirements of AWS Code D1.1, as shown in Appendix 9. The details of the weld procedure and filler metal used are given in Appendix 10.

For welded plate specimens in group B, a single edge notch was machined on the centre line of the weld, through the weld root area. The notch configuration used is given in detail A in Appendix 4. The machining of the notch in the specimen blank, followed non-symmetric removal of material by milling, to attain the depth dimension of 30 mm. Approximately 8.0 mm depth of material was removed from the edge which contained the weld 'root run' (top edge) and approximately 2.0 mm depth of material was removed from the surface which contained the weld capping runs (bottom edge).

The non-symmetric removal of material and the positioning of the single edge notch in the weld root area, was intended to minimise any possible adverse mechanistic influences upon crack-tip plasticity, arising from variations in material hardness. The results from a typical hardness survey for a welded plate in group B are given in Appendix 11.

For welded plate specimens in group C, a single edge notch was machined through the root area in one of two positions : either at the nominally vertical fusion line or in the vertical heat affected zone microstructure, approximately 1.0mm away from the fusion line; for the heat affected zone specimens, the correct position for the notch was determined by polishing and etching of the weld prior to machining. In all cases, the test specimens were machined using the procedure described for group B above.

The specimens were tested in the conditions of stress relieved and non-stress relieved as appropriate, for all microstructures. Stress relief was achieved by slow heating in a recirculating air-furnace to a temperature of 550°C with holding at temperature for 1½ hours, followed by furnace cooling to ambient temperature. The absence of any microstructural changes as a result of stress relief was confirmed by metallographic examination of the grain structure from a representative sample of specimens.

In addition, the yield and ultimate tensile strength of the weld metal used was established by standard tensile testing methods, using test specimens to the design given in Appendix 12. The tensile tests were carried out for both stress relieved and non-stress relieved material conditions.

4.4 EXPERIMENTAL GROUPS

Experimental investigations were carried out in seven groups, as listed below :-

Group 1 : Fatigue crack initiated in and propagated through plate material, stress relieved.

Group 2 : Fatigue crack initiated in and propagated through weld metal material, stress relieved.

Group 3 : Fatigue crack initiated in and propagated through heat affected zone material, stress relieved.

Group 4 : Fatigue crack initiated in and propagated through heat affected zone material, not stress relieved.

Group 5 : Fatigue crack initiated in and propagated along the weld fusion line in stress relieved material.

Group 6 : Fatigue crack initiated in and propagated along the weld fusion line in material not stress relieved.

Group 7 : Fatigue crack initiated in weld metal and propaged through and across weld metal fusion line into parent plate material, not stress relieved. Fatigue crack initiated in parent plate material and propagated through weld heat affected zone and across weld fusion line into the body weld metal, not stress relieved.

The environments listed below, were common to all experiments conducted in groups 1 to 6 inclusive :-

(a) *Laboratory air*, at ambient temperature, pressure and relative humidity. NOTE : One experiment in group 1 was conducted in air at 0% R.H.

(b) *Free corrosion potential* - absence of cathodic protection. For all specimens, the free corrosion potential was found to be of the order of - 0.700 Vs.c.ε ± 0.01 Vs.c.ε.

(c) *Nominal correct protection potential* - cathodic protection to a potential of - 0.780 Vs.c.ε ± 0.01 Vs.c.ε.

(d) *Nominal overprotection potential* - cathodic protection to a potential of - 1.100 Vs.c.ε ± 0.01 Vs.c.ε.

For environments (b), (c) and (d) above, the simulated sea water environment was maintained at a temperature of $10^{o}C \pm 1^{o}C$.

In addition to the environments listed above, the following were selectively applied by groups, as follows :-

Group 1 : (a) Simulated tidal immersion of nominally 6 hours at free corrosion potential and 6 hours in ambient air conditions.
(b) Simulated splash zone conditions, generated by the use of low pressure compressed air, in the manner shown in Appendix 13.
(c) Simulated splash zone combined with simulated tidal immersion of 6 hours at free corrosion potential.
(d) Single cycle overload to simulated storm loading level in ambient air conditions. Repeated for conditions of free corrosion potential.

Group 2 : (a) Simulated tidal immersion as for Group 1(a) above.
(b) Simulated splash zone as for Group 1(b) above.

Group 3 : (a) Simulated tidal immersion as for Group 1(a) above.

Group 4 : (a) Simulated tidal immersion as for Group 1(a) above.

Group 7 : Aqueous and cathodic protection environments were not used, with the exception of two experiments conducted at free corrosion potential. The majority of experiments in this group were conducted in laboratory air, at ambient pressure, temperature and relative humidity.

A Master Index list of the experiments carried out during this project is given in Table 11.

4.5 EXPERIMENTAL PROCEDURE

4.5.1 Test Specimen Preparation

Prior to each test, the appropriate test specimen was positively identified, marked with scribed reference lines as shown schematically in Appendix 16 and was hard stamped with an identification code that was recorded in the experimental log.

The specimen was then mounted on a surface table and the depth of the machined starter notch was measured optically, using a Vernier travelling microscope in accordance with the following procedure; Appendix 16 also refers.

(a) The microscope base was checked and adjusted for level as necessary and the microscope cross-wire was focussed in the eyepiece.

(b) The microscope cross-wire top edge was aligned with and focussed on the upper edge of the specimen, adjacent to the mouth of the machined starter notch, surface A in Appendix 16. The Vernier scale reading was noted.

(c) The microscope was then traversed and the cross-wire top edge was aligned with and focussed on the scribed reference line B in Appendix 16. The Vernier scale reading was noted.

(d) The depth of the machined starter notch was subsequently determined by subtraction of the scale readings noted at (b) and (c) above. The notch depth was then recorded in the experimental log. For comments on accuracy of measurement, see later in the text.

4.5.2 Loading of Test Specimens into the Test Machine

All loading of test specimens into three point bend test machines, either for pre-fatigue or experimental crack growth purposes, was carried out in accordance with the following procedure.

(a) The Amplitude, Mean Load and Frequency controls on the test machine function generator panel, were set to zero.
NOTE : The mains electrical supply to the test machine was continuously on and was only disconnected for safety reasons during essential machine maintenance activities.

(b) The test specimen was placed on the lower load application roller with the scribed reference line C aligned as shown schematically in Appendix 16. The test specimen was held in position by hand and the mean load control was then used to slowly 'inch up' the main hydraulic ram/specimen tank/load roller assembly under the action of hydraulic pressure.

(c) 'Inching' of the load roller assembly was continued until contact was established between the specimen upper edge and the upper load reaction rollers. At this stage adjustment of the mean load control ceased.

(d) The test specimen was then adjusted in position such that it was centrally placed on the load application roller with its longitudinal axis normal to the axes of the load/reaction rollers, as shown schematically in Appendix 16.

(e) With the test specimen correctly positioned in the working section of the test machine, the mean load control was adjusted to provide a small static 'pinch' load on the specimen of nominally 0.22 KN.

4.5.3 Experimental Procedure for Pre-Fatigue Crack Growth

For all crack growth experiments for this project, pre-fatigued test specimens without side compression were used. The initiation and subsequent limited growth of a 'sharp' pre-fatigue crack was carried out as follows :

(a) The appropriate test specimen was prepared for test in accordance with the procedure given in sub-section 4.5.1 and was subsequently loaded into a standard three point bond test machine in accordance with the procedure given in sub-section 4.5.2.

(b) With the test specimen held in position by a small 'pinch load', the mean load control was adjusted to increase slowly the static load on the specimen, up to the nominal calculated pre-fatigue mean load level. When the calculated mean load was attained, loading was halted.

NOTE : Throughout the project, the actual value of the load applied to the test specimen was determined by reference to the appropriate load cell calibration curve. Where the calibration curve related the test machine panel meter voltage reading to the magnitude of load transmitted through the load cell, the resolution of the panel meters was ± 10mV which was equivalent to ± 48 N. At the maximum experimental load level this produced an accuracy of load measurement of ± 0.55%, whereas at the minimum experimental load level, the accuracy of load measurement was ± 5.5%.

(c) With the mean load applied to the test specimen, the amplitude and frequency controls were simultaneously adjusted to provide the required pre-fatigue loading at a frequency of 20 Hz. The load levels indicated by the peak and trough meters on the test machine load control panel were continuously monitored and minor adjustments to the mean and amplitude controls were made as necessary, to compensate for electronic drift. A maximum pre-fatigue load level of 1.25 x the experimental maximum fatigue load was used to initiate pre-fatigue crack growth.

(d) Subsequent to initiation of a fatigue crack, the mean and amplitude controls were adjusted, to reduce the maximum load applied to the specimen down to the experimental maximum load. At the revised load setting, the load levels were again continuously monitored and minor adjustments were made as necessary.

(e) At the experimental fatigue load setting, the pre-fatigue crack growth on both specimen faces was continuously monitored using a

Vernier travelling microscope. Pre-fatigue was continued until a nominal crack growth of 1.50mm had occurred, at this stage pre-fatigue was stopped.

NOTE : Identical pre-fatigue load levels were used throughout the project.

(f) To stop pre-fatigue of the specimen, the amplitude and frequency controls were simultaneously reduced to zero, followed by the mean load control. The test specimen was then removed from the test machine and was stored in a Dessicator, pending experimental use in order to preserve a sharp crack front.

4.5.4 Measurement of Crack Lenath

4.5.4.1 Optical method

Throughout the project, all measurements of crack length were made optically, by means of a travelling Vernier microscope with a basic scale resolution of 10 μm and magnification x 10.

At the pre-commissioning stage of the project, it was noted that there were several electrically based potential drop crack monitoring techniques available for monitoring crack growth in metals. These techniques were commonly based, on the detection and measurement of the change in electrical potential within a metal, caused by the presence of a fracture within the bulk of the material. These techniques have been reviewed earlier in Chapter 1.

A particularly significant feature of this project, is that there is no requirement to produce absolute or design data as such. As a consequence, it was acknowledged at the project planning stage that the pursuit of absolute accuracy in the measurement of essential experimental data, such as crack length, was not justified.

With this in mind, the possible use of an AC potential drop crack measurement system was rejected on the grounds of cost and complexity balanced against a low level of potential enhancement in the quality of crack length data produced. Similarly, the possible use of a D.C. potential drop system was assessed and was rejected in view of the unacceptably high levels of electrical current required. This particular feature of the D.C. technique was considered to be incompatible with the monitoring of corrosion fatigue crack growth in a sea water environment, where electrochemical corrosion reactions within the growing fatigue crack could reasonably be expected to exert a significant influence upon the overall crack growth behaviour.

The inherent level of accuracy associated with the measurement of crack length by use of a Vernier travelling microscope was assessed in the manner described in the following. At the outset it was acknowledged that the lack of inbuilt compensation for crack front curvature effects might prove to be a significant limitation.

From pre-commissioning tests of the test machine, using actual test specimens and experimental fatigue loading values, it was established that the optimum crack measurement interval for experimental

purposes was every 2000 cycles with a maximum final crack length limited to nominally 18.00 mm. This value of final crack length was found to provide a sufficient safety margin against the potential adverse influence of plastic hinge effects, that were likely to be present at very long crack lengths in three point bend type specimens, of the size used for this project.

From trial measurements made on the Vernier travelling microscope itself, it was established that the thickness of the microscope cross-wire was of the order of 5 μm. This apparent thickness was increased by the adverse effect of backlash or general wear, present in the microscope screw thread. It was however established, that in practice both potential sources of inherent error have a negligible influence on the accuracy of measurement, provided that the correct practical technique is adopted. Namely, that all experimental measurements of crack length are consistently made to the same side of the cross-wire, at each observation the full length of the fatigue crack is measured and not just the increment in length from the previous reading and lastly, that all traversing of the microscope for experimental observations is consistently carried out in the same direction. This last proviso is essential to nullify any adverse effects arising from general wear in the microscope thread or carriage mechanism.

It is also particularly important to note that the quoted basic microscope resolution of ± 10 μm strictly refers to the minimum scale division present in the Vernier scale plate. The practical significance of this value, is that the effective resolution of any given scale reading is ± 5 μm, where this value represents the physical scale limits, by which the alignment of any two nearest scale lines may be resolved at the point of reference in the Vernier scale.

From pre-commissioning tests, the minimum expected value of crack propagation rate was found to be of the order of 1.0×10^{-8} m/cycle. Therefore for a given crack growth interval of 2000 cycles, the notional crack length increment would be 20 μm, which for an overall microscope resolution of ± 5 μm would produce a potential error in measurement of ± 25%.

At the nominal maximum crack length of 18.0 mm, crack propagation rates were found to be of the order of 5.0×10^{-7} m/cycle. Consequently, for a given crack growth interval of 2000 cycles, the notional increment in crack length would be 100 μm. For an overall microscope resolution of ± 5 μm, this would produce a potential error in measurement of ± 5%.

The significance of the errors determined above, is that for the measurement of a given crack incremental length, the accuracy of optical measurement is dependent directly upon the specific value of crack propagation rate, which for a fixed growth interval is not an unexpected result. This result does, however, serve to emphasize that when using optical crack measurement methods, the measurements of fatigue crack length should not be based upon the measurement of incremental growth.

In any experiment, the potential level of possible cumulative errors must be assessed and suitable corrective action taken to minimise their

effect. For this project the results of the pre-commissioning tests showed that in the worst case, more than 80 measurements of crack length might be made during a specimen's life. On a cumulative basis, this would introduce a potential error of the order of ± 2% at a crack length of nominally 18.0 mm.

However, provided the measurement technique discussed above is adopted, then the possibility of cumulative errors occurring becomes insignificant and can be disregarded. As a consequence, the only additional source of error to that calculated above, is the self-consistent component introduced by the operator.

Therefore for this project, the inherent errors arising from the use of optical crack monitoring are expressed in direct relation to a given crack length for an effective microscope resolution of ± 5 μm. At a minimum crack length of the order of 10.5 mm, this would produce an inherent error of ± 0.05%, whereas at the maximum nominal crack length of the order of 18.0 mm, the error produced is ± 0.03%.

The above level of inherent error is considered to be insignificant and to justify fully the use of optical crack monitoring for this project.

4.5.4.2 *Experiment procedure for the optical measurement of fatigue crack length in air*

Throughout the project, all measurements of fatigue crack length in air were made dynamically, i.e. with the test machine in operation. For each specimen, the initial crack length was measured at nominally 0 fatigue cycles and thereafter at every 2000 cycles. Measurements were completed within an average span of ± 50 cycles, relative to the scheduled measurement point. All measurements were made in accordance with the following :

(a) The external auxilliary lighting was adjusted to provide non-glare and shadow free illumination of the required specimen face.

(b) The microscope base was then checked and adjusted for level as necessary and the cross-wire was focussed in the eyepiece.

(c) The microscope cross-wire top edge was aligned and focussed on the upper edge of the specimen, adjacent to the mouth of the machined starter notch. The accurate positioning of the cross-wire was verified over a nominal span of five fatigue cycles, after which time the Vernier scale reading was noted.

(d) The microscope was then traversed and the cross-wire top surface was re-aligned and focussed on the tip of the fatigue crack. The accurate positioning of the cross-wire was again verified over a nominal span of five fatigue cycles, after which time the Vernier scale reading was noted.

NOTE : The microscope was always traversed in the same direction for each set of measurements.

(e) The length of the fatigue crack present was then determined by

subtraction of the reading recorded at (d) above from that recorded at (c) and was recorded in the experimental log.

(f) For measurement of the length of the fatigue crack present on the opposite specimen face, steps (a) to (e) above were repeated, using a separate dedicated Vernier travelling microscope.

(g) The assumed crack length at the specimen mid-thickness (B/2) was determined by calculation of the simple mean of the crack lengths recorded at (e) and (f) above. This value was recorded in the experimental log and was subsequently used as prime data in the development of the associated crack growth curve, a Vs N .

NOTE : The measurement of crack length within the period of ± 50 fatigue cycles was comfortably achieved by pre-positioning of the microscope cross-wire. This ensured that at the required time, only minor corrections to position were required for the actual experimental observation.

4.5.4.3 *Experimental procedure for the optical measurement of corrosion fatigue crack length in simulated sea water*

Throughout the project, all measurements of corrosion fatigue crack lengths for specimens in an environment of simulated sea water were made dynamically, i.e. with the test machine in operation. For all specimens, the initial crack length was measured at nominally 0 fatigue cycles and thereafter at every 2000 cycles. All measurements were made in accordance with the following :

(a) The external auxilliary lighting was adjusted to provide non-glare and shadow free illumination of the required specimen face.

(b) The microscope base was then checked and adjusted for level as necessary and the microscope cross-wire was focussed in the eye-piece.

(c) The specimen face in the immediate vicinity of the corrosion fatigue crack was gently cleaned to a clean metal finish, to remove surface films or corrosion products etc. The upper edge of the specimen immediately adjacent to the mouth of the machined starter notch was similarly cleaned.

(d) Subsequent to cleaning, the water in the specimen tank was allowed to settle and clear, prior to continuing with the measurement of crack length.

(e) With the water clear, the microscope cross-wire top surface was aligned and focussed on the upper edge of the specimen, adjacent to the mouth of the machined starter notch. The accurate positioning of the cross-wire was verified over a span of five fatigue cycles, after which time the Vernier scale reading was noted.

(f) The microscope was then traversed and the cross-wire top surface was re-aligned and focussed on the tip of the corrosion fatigue crack. The accurate positioning of the cross-wire was again

verified over a span of five fatigue cycles, after which time the Vernier scale reading was noted.

NOTE : The microscope was always traversed in the same direction for each set of measurements.

(g) The length of the corrosion fatigue crack present was then determined by subtraction of the reading recorded at (f) above from that recorded at (e) and was recorded in the experimental log.

(h) For measurement of the corrosion fatigue crack length present in the opposite specimen face, steps (a) to (g) above were repeated, using a separate dedicated Vernier travelling microscope.

(i) The assumed crack length at the specimen mid-thickness (B/2) was then determined by calculation of the simple mean of the crack lengths recorded at (g) and (h) above. This value was then recorded in the experimental log and was subsequently used as prime data in the development of the associated crack growth curve, a Vs N .

NOTE : 1. The cleaning of both specimen faces and top surface, was arranged such that the activity did not interfere with the nominal measurement span of ± 50 fatigue cycles.

2. The measurement of crack length within the period of ± 50 cycles was comfortably achieved by pre-positioning of the microscope cross-wire. This ensured that at the required time, only minor corrections to position were required for the actual experimental observation.

4.5.5 *Experimental Procedure for Fatigue Experiments in Air*

All fatigue experiments in air were carried out in accordance with the following :

(a) A test specimen having the required microstructure was selected and was prepared for use in accordance with the procedure given in sub-section 4.5.1.

(b) The test specimen was then loaded into the test machine in accordance with the procedure given in sub-section 4.5.2.

(c) With the test specimen held in position in the test machine under the action of a small pinch load, the mean load control was adjusted to increase slowly the static load on the specimen, up to the calculated nominal mean experimental load level. When this load level was attained, adjustment of the mean load control ceased.

(d) With the nominal mean experimental load applied to the specimen, the frequency and amplitude controls were simultaneously adjusted, to apply the required experimental fatigue load at a frequency of 0.5 Hz ± 1% and R ratio of nominally 0.1.

(e) Throughout the experiment, the fatigue load applied to the speci-

men was continuously monitored by regular observation of the peak and trough meters on the test machine load control panel. As a consequence, minor adjustments were made as necessary to the amplitude and mean load controls, to compensate for electronic drift in the associated control circuits. By this means, the required experimental fatigue load on the specimen was consistently maintained to within ± 0.55% at the maximum load and ± 5.5% at the minimum load.

NOTE : The peak and trough meter readings were in volts. The actual load applied was determined by referring the voltages to the appropriate load cell calibration curve.

(f) For all fatigue experiments in air, the fatigue crack length was first measured at nominally 0 fatigue cycles and thereafter at regular intervals of 2000 fatigue cycles, over the life of the test specimen. All measurements of fatigue crack length in air were made optically in accordance with the procedure given in sub-section 4.5.4.2.

(g) All fatigue specimens in air were terminated when the calculated crack length at the specimen mid-thickness (B/2) attained a value of 18.00 mm. At this point, the experiment was terminated in accordance with the procedure given in sub-section 4.5.11.

4.5.5.1 *Experimental procedure for fatigue experiments in air under conditions of single cycle overload*

A specimen from experimental group 1 was subjected to fatigue crack propagation in accordance with the procedure given in sub section 4.5.5 above, amended as follows :

Measurement of crack length was made every 2000 cycles until a nominal crack length of 13.00mm was attained. At this stage the specimen was subjected to a single cycle of overload to a K_{max} level which corresponded to $0.8\sigma_y$, an estimated storm loading case.

Following overload, measurement of crack length was again made every 2000 cycles, until a nominal crack length of 15.00mm was attained. At this stage the specimen was subjected to a further single cycle of overload to the level which corresponded to the simulated storm loading case.

Following this second overload, measurement of crack length was again made every 2000 cycles, to completion of the experiment.

4.5.6 *Experimental Procedure for Corrosion Fatigue Experiments at Free Corrosion Potential in an Environment of Simulated Sea Water*

All corrosion fatigue experiments at free corrosion potential were conducted in according with the following procedure.

(a) A test specimen having the required microstructure was selected and was prepared for use in accordance with the procedure given in sub-section 4.5.1. In addition, an insulated flying lead with a soldered eyelet end termination was fixed to the top edge of the

specimen, using a pre-drilled and threaded hole in the position shown in Appendix 4.

(b) The test specimen was then loaded into the test machine in accordance with the procedure given in sub-section 4.5.2. Care was exercised to ensure that the insulated flying lead was not trapped.

(c) With the test specimen held in position in the test machine under the action of a small pinch load, the sea water circulation pump was switched on and simulated sea water was pumped into the specimen tank. Correct circulation rate was confirmed by monitoring the outflow from the specimen tank, via the twin overflow pipes. Water temperature was continuously monitored by means of a mercury thermometer, suitably positioned inside the specimen tank.

(d) Prior to commencement of fatigue loading, the test specimen was allowed to stabilise its electrical potential at a notional free corrosion value for steel of - 700 mV_{SCE}. Stabilisation of potential was arbitrarily considered to have occurred when the target value of - 700 mV_{SCE} ± 10mV had been satisfactorily maintained for a period of one hour.

For all corrosion fatigue experiments at free corrosion potential reported herein, the specimen potential was continuously monitored with respect to a standard reference electrode. A saturated Calomel reference electrode was used, and was suspended from a retort stand positioned adjacent to the specimen tank. It was ¾ immersed inside the specimen tank and was arranged such that it sampled water from the immediate vicinity of the specimen by means of an attached glass 'J' tube. By connecting the specimen in circuit with the saturated Calomel reference electrode, via an independent digital voltmeter, the specimen potential was continuously monitored.

For all corrosion fatigue experiments at free corrosion potential reported herein, stabilisation was generally found to occur after approximately 5 hours.

(e) With the test specimen satisfactorily established at its free corrosion potential, the mean load control was adjusted to slowly increase the static load acting on the specimen, up to the calculated nominal mean experimental load level. When this load level was attained, adjustment of the mean load control ceased.

(f) With the calculated experimental mean load applied to the specimen, the frequency and amplitude controls were simultaneously adjusted to apply the required experimental fatigue load at a nominal frequency of 0.5 Hz ± 1% and R ratio of nominally 0.1.

(g) Throughout the experiment, the fatigue load applied to the specimen was continuously monitored by regular observation of the peak and trough meters on the test machine load control panel. As a consequence, minor adjustments were made as necessary to the amplitude and mean load controls, to compensate for electronic

drift in the associated control circuits. By this means the required experimental fatigue load in the specimen was consistently maintained to within ± 0.55% at the maximum load and ± 5.5% at the minimum load.

NOTE : The peak and trough meter readings were in volts. Actual load applied was determined by referring these voltages to the appropriate load cell calibration curve.

(h) For all corrosion fatigue experiments at free corrosion potential, the crack length was first measured at nominally 0 fatigue cycles and thereafter at regular intervals of 2000 fatigue cycles, over the life of the test specimen. All measurements of crack length were made optically in accordance with the procedure given in sub-section 4.5.4.3.

NOTE : All corrosion fatigue experiments at free corrosion potential were terminated when the calculated crack length at the specimen mid thickness (B/2) attained a nominal value of 18.00 mm.

(i) When the crack length of nominally 18.00 mm was attained at (h) above, the experiment was terminated in accordance with the procedure given in sub-section 4.5.12.

4.5.6.1 *Experimental procedure for corrosion fatigue experiment at free corrosion potential under conditions of single cycle overload*

A specimen from experimental group 1 was subjected to corrosion fatigue crack propagation in accordance with the procedure given in sub-section 4.5.6 above, amended as follows.

Measurement of crack length was made every 2000 cycles, until a nominal crack length of 13.00 mm was attained. At this stage the specimen was subjected to a single cycle of overload to a K_{max} level which corresponded to 0.8 σ_y, an estimated storm loading case.

Following overload, measurement of crack length was again made every 2000 cycles, until a nominal crack length of 15.00mm was attained. At this stage the specimen was subjected to a further single cycle of overload to the level which corresponded to the simulated storm loading case.

Following this second overload, measurement of crack length was again made every 2000 cycles, to completion of the experiment.

4.5.7 *Experimental Procedure for Corrosion Fatigue Experiments at a Cathodic Protection Potential of - 780 mV_{SCE}, in an Environment of Simulated Sea Water*

All corrosion fatigue experiments at a Cathodic Protection potential of - 780 mV_{SCE} were conducted in accordance with the following procedure.

(c) A test specimen having the required microstructure was selected and was prepared for use in accordance with the procedure given

in sub-section 4.5.1. In addition, an insulated flying lead with a soldered eyelet end termination was fixed to the top edge of the specimen, using a pre-drilled and threaded hole in the position shown in Appendix 4.

(b) The test specimen was then loaded into the test machine in accordance with the procedure given in sub-section 4.5.2. Care was exercised to ensure that the insulated flying lead was not trapped.

(c) With the test specimen held in position in the test machine under the action of a small pinch load, the sea water circulation pump was switched on and simulated sea water was pumped into the specimen tank. Correct circulation rate was confirmed by monitoring the outflow from the specimen tank, via the twin overflow pipes. Water temperature was continuously monitored by means of a mercury thermometer, suitably positioned inside the specimen tank.

(d) Prior to the commencement of fatigue loading, the test specimen was connected in circuit with a Potentiostat, via the insulated flying lead , in accordance with the circuit diagram shown schematically in Appendix 14.

In this application, the Potentiostat was considered to provide effective simulation of the Impressed Current Cathodic Protection technique commonly used offshore for the corrosion protection of sub-sea jacket structures. A carbon rod from a small dry-cell battery was used as the power electrode within the specimen tank.

A saturated Calomel reference electrode was used as the reference potential for control purposes. The saturated Calomel electrode was suspended from a retort stand positioned adjacent to the specimen tank. It was ¾ immersed and was arranged such that it sampled water from the immediate vicinity of the specimen, by means of an attached glass 'J' tube.

Following satisfactory connection in circuit, the Potentiostat was adjusted to provide a set specimen potential of - 780 mV_{SCE}. An independent digital voltmeter was bridged across the Potentiostat and was used to continuously monitor both the actual specimen potential and the set specimen potential, with respect to the saturated Calomel reference electrode.

As a result of continuous monitoring, minor periodic adjustments were made to the Potentiostat controls in order to compensate for electronic drift and satisfactorily maintain the desired specimen potential of nominally - 780 mV_{SCE}.

NOTE : Potential control for the simulated C.P. system was used throughout the project reported herein. In using potential as the control parameter, it was acknowledged that in practice, current density requirements form the basis of the design of C.P. systems offshore. However, the performance of offshore C.P. systems is commonly assessed on the basis of potential readings taken on the

protected structure. It was therefore considered to be valid to use potential as the control parameter in the laboratory simulation of C.P. reported herein.

Further, it should also be noted that in the design of sacrificial anode C.P. systems in particular, the principal reason for using current density is that it provides a means of calculating the required size and weight of anode material required, to achieve the specified service life.

(e) With the set potential of - 780 mV_{SCE} from the potentiostat satisfactorily established, the test specimen was allowed to stabilise its potential prior to the commencement of corrosion fatigue loading. Stabilisation of potential was arbitrarily considered to have been attained when a specimen potential of - 780 mV_{SCE} was satisfactorily maintained for a period of one hour. For all of the experiments at a C.P. potential of -780mV reported herein, stabilisation was usually attained after approximately 6 hours and was accompanied by the development of a uniform grey coloured calcareous coating on all exposed metal surfaces.

(f) Following stabilisation of the test specimen potential at - 780 mV_{SCE} the mean load control was adjusted to increase slowly the static load on the specimen, up to the calculated experimental mean load level. When the required mean load level was attained, adjustment of the mean load control ceased.

(g) With the required mean load applied to the test specimen, the frequency and amplitude controls were simultaneously adjusted to apply the required fatigue load to the specimen at a frequency of 0.5 Hz ± 1% and R ratio of nominally 0.1.

(h) Throughout each corrosion fatigue experiment at a C.P. potential of - 780 mV_{SCE}, the fatigue load applied to the test specimen was continuously monitored by regular observation of the peak and trough meters on the test machine load control panel. As a consequence, minor adjustments were made as necessary to the amplitude and mean load controls, to compensate for electronic drift in the associated control circuits. By this means the required experimental fatigue load on the specimen was consistently maintained to within ± 0.55% at the maximum load and ± 5.5% at the minimum load.

NOTE : The peak and trough meter readings were in volts. Actual load applied was determined by referring these voltages to the appropriate load cell calibration curve.

(i) For all corrosion fatigue experiments at a C.P. potential of - 780 mV_{SCE}, the crack length was first measured at nominally 0 fatigue cycles and thereafter at regular intervals of 2000 fatigue cycles, over the life of the test specimen.

All measurements of crack length were made optically in accordance with the procedure given in sub-section 4.5.4.3.

NOTE : All corrosion fatigue experiments at a C.P. potential of - 780 mV_{SCE} were terminated when the calculated crack length at the specimen mid thickness (B/2) attained a nominal value of 18.00mm.

(j) When the crack length of nominally 18.00mm was attained at (i) above, the experiment was terminated in accordance with the procedure given in sub-section 4.5.12.

4.5.8 Experimental Procedure for Corrosion Fatigue Experiments at a Cathodic Protection Potential of - 1100 mV_{SCE} in an Environment of Simulated Sea Water

All corrosion fatigue experiments at a notional cathodic 'over-protection' potential of - 1100 mV_{SCE} were conducted in accordance with the following procedure.

(a) A test specimen having the required microstructure was selected and was prepared for use in accordance with the procedure given in sub-section 4.5.1. In addition, an insulated flying lead with a soldered eyelet and termination was fixed to the top edge of the specimen, using a pre-drilled and threaded hole in the position shown in Appendix 4.

(b) The test specimen was then loaded into the test machine in accordance with the procedure given in sub-section 4.5.2. Care was exercised to ensure that the insulated flying lead was not trapped.

(c) With the test specimen held in position in the test machine under the action of a small pinch load, the sea water circulation pump was switched on and simulated sea water was pumped into the specimen tank. Correct circulation rate was confirmed by monitoring the outflow from the specimen tank via the twin overflow pipes. Water temperature was continuously monitored by means of a mercury thermometer, suitable positioned inside the specimen tank.

(d) Prior to the commencement of fatigue loading, the test specimen was connected in circuit with a potentiostat via the insulated flying lead in accordance with the circuit diagram shown schematically in Appendix 14.

In this application, the potentiostat was considered to provide effective simulation of the Impressed Current Cathodic Protection technique commonly used offshore for the corrosion protection of sub-sea jacket structures. A carbon rod that was removed from a small dry-cell battery was used as the power electrode within the specimen tank.

A saturated Calomel reference electrode was used as the reference potential for control purposes. The saturated Calomel electrode was suspended from a retort stand positioned adjacent to the specimen tank. It was ¾ immersed and was arranged such that it sampled water from the immediate vicinity of the specimen, by means of an attached glass 'J' tube.

Following satisfactory connection in circuit, the potentiostat was adjusted to provide a 'set' specimen potential of - 1100mV_{SCE}. An independent digital voltmeter was 'bridged' across the potentiostat and was used to monitor continuously both the actual specimen potential and the 'set' specimen potential, with respect to the saturated Calomel reference electrode.

As a result of continuous monitoring, minor periodic adjustments were made to the potentiostat controls in order to compensate for electronic drift and satisfactorily maintain the desired specimen potential of nominally - 1100 mV_{SCE}.

(e) With the set potential of - 1100 mV_{SCE} from the potentiostat satisfactorily established, the test specimen was allowed to stabilise its potential prior to the commencement of corrosion fatigue loading. Stabilisation of potential was arbitrarily considered to have been attained when a specimen potential of - 1100 mV_{SCE} was satisfactorily maintained for a period of one hour. For all of the experiments at a C.P. potential of - 1100 mV_{SCE} for this project, stabilisation was usually attained after approximately 3 - 4 hours lapsed time and was accompanied by the development of a uniform grey coloured calcareous coating on all exposed metal surfaces with an extensive covering of small attached bubbles which were assumed to contain molecular Hydrogen.

(f) Following stabilisation of the test specimen potential at - 1100 mV_{SEC}, the mean load control was adjusted to increase slowly the static load on the specimen, up to the calculated experimental mean load level. When the required mean load level was attained, adjustment of the mean load control ceased.

(g) With the required mean load applied to the test specimen, the frequency and amplitude controls were simultaneously adjusted to apply the required fatigue load to the specimen at a frequency of 0.5 Hz ± 1% and R ratio of nominally 0.1.

(h) Throughout each corrosion fatigue experiment at a C.P. potential of - 1100 mV_{SCE}, the fatigue load applied to the test specimen was continuously monitored by regular observation of the peak and trough meters on the test machine load control panel. As a consequence, minor adjustments were made as necessary to the amplitude and mean load controls to compensate for electronic drift in the associated control circuits. By this means, the required experimental fatigue load on the specimen was consistently maintained to within ± 0.55% at the maximum load and ± 5.5% at the minimum load.

NOTE : The peak and trough meter readings were in volts. Actual load applied was determined by referring these voltages to the appropriate load cell calibration curve.

(i) For all corrosion fatigue experiments at a C.P. potential of - 1100 mV_{SCE}, the crack length was first measured at nominally 0 fatigue cycles and thereafter at regular intervals of 2000 fatigue cycles, over the life of the test specimen.

All measurements of crack length were made optically in accordance with the procedure given in sub-section 4.5.4.3.

NOTE : All corrosion fatigue experiments at a C.P. potential of - 1100 mV_{SCE} were terminated when the calculated crack length at the specimen mid thickness (B/2) attained a nominal value of 18.00 mm.

(j) When a crack length of nominally 18.00mm was attained at (i) above, the experiment was terminated in accordance with the procedure given in sub-section 4.5.12.

4.5.9 *Experimental Procedure for Crack Propagation Experiments in an Environment of Simulated Tidal Immersion*

All crack propagation experiments in an environment of simulated tidal immersion were conducted in accordance with the following procedure.

(a) A test specimen having the required microstructure was selected and was prepared for use in accordance with the procedure given in sub-section 4.5.1.

(b) The test specimen was then loaded into the test machine in accordance with the procedure given in sub-section 4.5.2.

(c) With the test specimen held in position in the test machine under the action of a small pinch load, the mean load control was adjusted to increase slowly the static load acting on the specimen, up to the calculated nominal mean experimental load level. When this load level was attained, adjustment of the mean load control ceased.

(d) With the calculated mean experimental load applied to the specimen, the frequency and amplitude controls were simultaneously adjusted, to apply the required experimental fatigue load to the specimen at a frequency of 0.5 Hz ± 1% and R ratio of nominally 0.1.

(e) Throughout each fatigue experiment in an environment of simulated tidal immersion, the fatigue load applied to the specimen was continuously monitored by regular observation of the peak and trough meters on the test machine load control panel. As a consequence, minor adjustments were made as necessary to the amplitude and mean load controls, to compensate for electronic drift in the associated control circuits. By this means the required experimental fatigue load on the specimen was consistently maintained to within ± 0.55% at the maximum load and ± 5.5% at the minimum load.

NOTE : The peak and trough meter readings were in volts. Actual load applied was determined by referring these voltages to the appropriate load cell calibration curve.

(f) For all fatigue experiments in an environment of simulated tidal

immersion, the initial environment was laboratory air for the first 11000 fatigue cycles. Consequently, the fatigue crack length was first measured at nominally 0 fatigue cycles and thereafter at regular intervals of 2000 fatigue cycles, up to a total of 11000 cycles in air, in accordance with the procedure given in sub-section 4.5.4.2.

(g) At 11,000 cycles, the sea water circulation pump was switched on and simulated sea water was pumped into the specimen tank. Correct circulation rate was confirmed by monitoring the outflow from the specimen tank via the twin overflow pipes. Water temperature was continuously monitored by means of a mercury thermometer, suitably positioned inside the specimen tank.

(h) For the subsequent 11,000 cycles period of crack growth in an environment of free corrosion potential, all measurements of fatigue crack length were made at intervals of 2000 fatigue cycles, in accordance with the procedure given in sub-section 4.5.4.3.

(i) When the 11,000 cycles of crack growth in an environment of free corrosion potential were completed, the sea water circulation pump was switched off and the specimen tank was allowed to drain.

(j) For the subsequent 11,000 cycles period of crack growth in an environment of laboratory air, all measurements of fatigue crack length were made at intervals of 2000 fatigue cycles, in accordance with the procedure given in sub-section 4.5.4.2.

(k) The technique of applying alternate crack growth periods of 11,000 cycles in laboratory air, followed by 11,000 cycles in an environment of free corrosion potential was then regularly repeated for the duration of the experiment. The experiment was continued until either the calculated crack length at the specimen mid-thickness (B/2) attained a nominal value of 18.00 mm or the crack stopped propagating. Crack arrest , i.e. zero crack propagation, was considered to have occurred when no growth was detected for an unbroken period of at least 50,000 fatigue cycles.

(l) When either a crack length of nominally 18.00 mm was attained or crack arrest was considered to have occurred, as detailed in paragraph (k) above, the experiment was terminated in accordance with the procedure agreed in sub-section 4.5.12.

4.5.10 Experimental Procedure for Corrosion Fatigue Crack Propagation Experiments in an Environment of Simulated Splash Zone

All corrosion fatigue crack propagation experiments in an environment of simulated splash zone conditions were conducted in accordance with the following.

(a) A test specimen having the required microstructure was selected and was prepared for use in accordance with the procedure given in sub-section 4.5.1.

(b) The test specimen was then loaded into the test machine in accordance with the procedure given in sub-section 4.5.2.

(c) With the specimen held in position in the test machine under the action of a small pinch load, the sea water circulation pump was switched on and the specimen tank was allowed to fill to a depth of approximately 100mm. When this depth was attained, the circulation pump was switched off and the flow valve adjacent to the circulation pump was closed, to prevent back-draining of the specimen tank through the circulation pump.

(d) A low pressure compressed air supply was then introduced in accordance with the arrangements shown schematically in Appendix 13.

NOTE : For these experiments, a perspex lid was fitted to the specimen tank, to contain the effects of splashing, etc.

(e) The compressed air flow rate was regulated to provide the desired simulation of splash zone conditions. When the simulated splash zone conditions had been satisfactorily established, the mean load control was adjusted to increase slowly the static load acting on the specimen, up to the calculated nominal mean experimental load level. When this load level was attained, adjustment of the mean load control ceased.

(f) With the calculated experimental mean load applied to the specimen, the frequency and amplitude controls were simultaneously adjusted to apply the required experimental fatigue load at a nominal frequency of 0.5 Hz ± 1% and R ratio of nominally 0.1.

(g) Throughout the experiment, the fatigue load applied to the specimen was continuously monitored by regular observation of the peak and trough meters on the test machine load control panel. As a consequence, minor adjustments were made as necessary to the amplitude and mean load controls, to compensate for electronic drift in the associated control circuits. By this means the required experimental fatigue load on the specimen was consistently maintained to within ± 0.55% at the maximum load and ± 5.5% at the minimum load.

NOTE : The peak and trough meter readings were in volts. Actual load applied was determined by referring these voltages to the appropriate load cell calibration curve.

(h) For all corrosion fatigue experiments in an environment of simulater splash zone conditions, the crack length was first measured at nominally 0 fatigue cycles and thereafter at regular intervals of 2000 fatigue cycles, over the life of the test specimen. All measurements of crack length were made optically in accordance with the procedure given in sub-section 4.5.4.3.

NOTE : All corrosion fatigue experiments in an environment of simulated splash zone, were terminated when the calculated crack length of the specimen mid thickness (B/2) attained a nominal value of 18.00 mm.

(i) When the crack length of nominally 18.0 mm was attained at (h) above, the low pressure compressed air supply was switched off and the flow valve was opened to allow the specimen tank to drain. The experiment was then terminated in accordance with the procedure given in sub-section 4.5.12.

4.5.11 *Experimental Procedure for the Termination of Fatique Experiments in Air*

For all fatigue experiments in air, when the calculated crack length at the specimen mid-thickness (B/2) attained a nominal value of 18.00mm, the experiment was terminated as follows :-

(a) The amplitude and frequency controls were simultaneously adjusted to reduce the fatigue load and frequency of loading to zero.

(b) The mean load control was then adjusted to reduce slowly the static load on the specimen down to zero. During down-loading, the specimen was steaded in position by hand and was removed from the test machine at zero load.

(c) The test specimen was then clamped in a soft-jawed engineering vice and was manually sawn in half using a fine-bladed hacksaw. The saw cut was made from the bottom specimen edge towards the crack tip, along the projected line of crack advance.

(d) The presence of hand-stamped specimen identification marks was confirmed for both halves and they were placed in a dedicated dessicator for storage, pending preparation for examination in accordance with the procedure given in sub-section 4.5.13.

(e) Throughout all post-experimental work on the specimen, extreme care was exercised to avoid accidental damage to the exposed fracture surfaces. Also the Silica Gel crystals in the dessicator were regularly changed/dried, at two weekly intervals, throughout the project to ensure that satisfactory moisture free storage conditions were maintained.

4.5.12 *Experimental Procedure for the Termination of Corrosion Fatique Experiments in Simulated Sea Water*

For all corrosion fatigue experiments, when the calculated crack length at the specimen mid-thickness (B/2) attained a nominal value of 18.00mm, the experiment was terminated as follows :-

(a) The load amplitude and frequency controls were simultaneously adjusted to reduce the fatigue load and frequency of loading to zero.

(b) The mean load control was then adjusted to increase slowly the static load on the specimen. During this load application, the specimen was continuously monitored/observed until the crack was seen to 'open-out'. At this stage loading was stopped.

(c) With the crack opened-out , the mean load control was adjusted to reduce slowly the static load on the specimen down to zero. During down-loading, the specimen was steadied in position by hand and was removed from the test machine at no load. Simultaneously, the water circulator pump was switched off and the specimen tank was allowed to empty by back-flow through the circulation pump.

(d) The opened-out specimen was then immediately washed in Methanol, rinsed in Gramasol and thoroughly dried by use of a hand held hot air blower.

(e) When completely dry, the specimen was placed in a soft-jawed engineer's vice and was cut in half by manually sawing from the bottom specimen edge towards the crack tip, along the projected line of crack advance.

(f) The presence of hard-stamped specimen identification marks was confirmed and both halves of the specimen were placed in a dedicated dessicator for storage, pending preparation for further examination in accordance with the procedure given in sub-section 4.5.13.

NOTE : The specimens were opened-out , prior to washing and drying. In order to ensure that no post experimentation crevice corrosion reactions occurred within the fatigue crack, due to inadequate penetration of the hot air blast used for drying.

(g) Throughout all post-experiment activity, extreme care was exercised to avoid accidental damage to the exposed fracture surfaces.

4.5.13 Experimental Procedure for the Preparation of Specimens for Examination in a Scanning Electron Microscope

Throughout the project reported herein, all test specimen fracture surfaces were prepared for examination in the scanning electron microscope in accordance with the following procedure.

4.5.13.1 In air fatigue fracture surfaces

(a) The required ex fatigue in-air test specimen was removed, in two halves, from the storage dessicator and was positively identified against the master specimen Index List contained in the experimental log.

(b) One specimen half was then returned to the dessicator for continued safe storage. The remaining specimen half was secured in a soft-jawed engineer's vice in such a position that the fracture face could be manually cut away. A fine hacksaw was used and the cut was made nominally 3.00mm to the rear of the fracture face. The specimen was sawn from the top edge towards the bottom edge.

(c) The saw cut at (b) above was stopped at a nominal distance of 10.00mm from the bottom specimen edge. The specimen half was then rotated in the vice such that the fracture face was uppermost and horizontal.

(d) With the fracture face horizontal, a scribed reference line was marked across the fracture face 10.00mm above and parallel to the specimen bottom edge. A cut was then made on this line, to intersect the cut made at (c) above and the fracture surface was removed from the body of the specimen half. This produced a fracture surface specimen that measured nominally 20 x 15 x 3.00mm. Extreme care was exercised during all cutting-out operations, to ensure that the fracture surface was not accidentally damaged.

NOTE : A specimen size of 20 x 15 was nominally the maximum size that could be successfully accommodated in the working section of the scanning electron microscope.

(e) A scanning electron microscope specimen mounting stub was selected and the appropriate specimen identification marks were vibro-etched onto the stub under surface.

(f) The mounting stub top surface was then coated with a special conductive paint, which was used to permanently fix the fracture specimen in position. The fracture surface specimen produced at (d) above was then mounted at the stub and centrally positioned. The mounted specimen was then stored in a separate dessicator cupboard, to allow the fixative paint to finally set.

(g) When the fixative paint had firmly set, the mounted specimen was handed to a laboratory technician for vacuum coating with Carbon.

(h) When satisfactorily coated with Carbon, the specimen was stored in a dedicated dessicator cupboard, pending examination in the scanning electron microscope (S.E.M.),

(i) All examination of fracture surface specimens using the scanning electron microscope (S.E.M.) was carried out in accordance with standing departmental procedures for use of the S.E.M.

4.5.13.2 *Corrosion fatique fracture surfaces (cleaned)*

(a) The required ex-corrosion fatigue test specimen was removed, in two halves, from the storage dessicator and was positively identified against the Master Specimen Index List contained in the experimental log.

(b) One specimen half was then returned to the dessicator for continued safe storage. The remaining specimen half was secured in a soft-jawed engineer's vice in such a position that the fracture face could be manually cut away. A fine hacksaw was used and the cut was made nominally 3.00m m to the rear of the fracture face. The specimen was sawn from the top edge towards the bottom edge.

(c) The saw cut at (b) above was stopped at a nominal distance of 10.00mm from the specimen bottom edge. The specimen half was then rotated in the vice, such that the fracture face was uppermost and horizontal.

(d) With the fracture face horizontal, a scribed reference line was marked across the fracture face nominally 10.00mm above and parallel to the specimen bottom edge. A cut was then made on this line, to intersect the cut made at (c) above and the fracture surface was removed from the body of the specimen half. This produced a fracture surface specimen that measured nominally 20 x 15 x 3.00mm. Extreme care was exercised during all cutting-out operations, to ensure that the fracture surface was not accidentally damaged.

(e) The specimen fracture surface was then immersed in a 50% solution of Hydrochloric Acid and Distilled Water, buffered with Stannous Chloride. While immersed in the buffered H.Cl solution, the specimen was continuously observed and was withdrawn when all calcareous deposits, corrosion products etc. were seen to have been removed. At this stage the specimen was immediately washed in flowing water, thoroughly and repeatedly rinsed in Methanol and was finally dried in a hot air blast.

(f) A scanning electron microscope specimen mounting stub was selected and the appropriate specimen identification marks were vibro-etched onto the stub under the surface.

(g) The mounting stub top surface was then coated with a special conductive paint, which was used to fix permanently the fracture specimen in position. The cleaned fracture surface specimen produced at (e) above was then mounted onto the stub and centrally positioned. The mounted specimen was then stored in a separate dessicator cupboard, to allow the fixative paint to set firmly.

(h) When the fixative paint had set, the mounted specimen was handed to a laboratory technician for vacuum coating with Carbon.

(i) When satisfactorily coated with Carbon, the specimen was stored in a dedicated dessicator cupboard, pending examination in the scanning electron microscope (S.E.M.).

(j) All examination of fracture surface specimens using the scanning electron microscope was carried out in accordance with standing departmental procedures for use of the S.E.M.

4.5.13.3 Corrosion fatigue fracture surfaces (un-cleaned)

For all corrosion fatigue experiments reported herein, where S.E.M. examination of calcareous deposits or of corrosion products present on corrosion fatigue fracture surfaces was required, the appropriate specimen was prepared for examination in accordance with the procedure given in sub-section 4.5.13.1.

4.6. ASSESSMENT OF ERRORS IN da/dN AND ΔK DATA

Throughout this project, the values of da/dN and ΔK used to describe crack growth behaviour, are derived by graphical and conventional calculation methods respectively. This data is graphically presented in a Paris type format, from which the associated values of Paris parameters C and m have been derived. The level of error inherent in

the derivation of the fundamental da/dN and ΔK data, was assessed as follows :

4.6.1. Calculation of ΔK Values

Throughout this project, a constant load amplitude of the same magnitude, was applied in all experiments. For a given crack length, the associated value of ΔK was calculated from the relationship :

$$\Delta K = \frac{6.\Delta P.Y}{B.W^{\frac{1}{2}}} \quad \text{where } Y = f(\frac{a}{W})$$

and $f(\frac{a}{W})$ is a series expansion given by

$$f(\frac{a}{W}) = 1.93(\frac{a}{W})^{0.5} - 3.07(\frac{a}{W})^{1.5} + 14.53(\frac{a}{W})^{2.5} - 25.11(\frac{a}{W})^{3.5} + 25.8(\frac{a}{W})^{4.5}$$

The effect of an error in the measurement of crack length, was assessed at a nominal minimum/initial crack length of 10.4mm and at a maximum/final crack length of 18.0mm, for a given microscope resolution of ± 5 μm.

By substitution of the appropriate crack length values in $f(\frac{a}{W})$, it was determined that at the minimum crack length of nominally 10.4mm, the potential error in ΔK was of the order of ± 0.23%. Whereas, at the maximum crack length of nominally 18.0mm, the error was virtually nil.

The significance of this result is, that for this project, the values of ΔK presented are valid and the error across the experimental span can be ignored.

4.6.2. Graphical Determination of da/dN Values

Throughout this project the value of da/dN at any given crack length was determined by fitting a tangent to the associated curve of a Vs N data at the point of interest and measuring the angle subtended with the horizontal. The angle was measured using a 360° Draughtsman's protractor with a resolution of ± ½° of arc and the value of da/dN was derived by calculation of the value of the associated tangent function which was then multiplied by the scale factor for tan 45° associated with the particular a Vs N curve. Therefore the error present in a given value of da/dN is represented by the error present in the associated value of the tangent function.

The potential errors in this technique were assessed, for the minimum and maximum values of subtended angle that were anticipated experimentally. These were assigned notional values of 16.5° and 79.5° respectively, based on data obtained from the pre-commissioning tests.

At a minimum angle of notionally 16.5°, which corresponds to a growth rate at an initial crack length of 10.4mm, the error in the

tangent function was determined to be ± 1.62%. Whereas at a maximum angle of notionally 79.5°, which corresponds to a growth rate at the final crack length of 18.0mm, the error in the tangent function was found to be in the range + 2.5% to - 2.38%. This feature is considered to reflect the sensitivity of the tangent function to errors in angular measurement at angles close to 90°. For practical purposes, the above error can be restated as being ± 2.5%. Given the value of the tangent function between angles of 0° and 90°, the above trend in errors was not unexpected.

This project is phenomenologically biased and in this context the low level of errors derived above are considered to be insignificant and can be ignored in the graphical presentation of data.

The practical significance of this is summarised as follows :

1. The derivation of da/dN by graphical means is justified and has no adverse effect upon the quality of crack growth rate data produced.

2. For the presentation of da/dN Vs ΔK data in a log-log scale Paris type format, the fitting of a mean line through the data points and the absence of specific data detail is justified. Furthermore, each Paris curve so plotted, is a valid illustration of material crack growth behaviour.

3. On log-log scale presentations of data, the addition of error bands for very low levels of error is unnecessary.

The range of quality present in the crack growth rate data produced during this project is illustrated in Figures 39 and 40 respectively. Where Figure 39 illustrates the maximum level of data scatter and Figure 40 illustrates the minimum level of data scatter. The associated graphs of a Vs N data are presented in Figures 41 and 42 respectively.

CHAPTER 5

RESULTS AND DISCUSSION

The results from the project are presented and discussed in the following groups :

5.1 Overload effects

5.2 Fatigue crack propagation in -air

5.3 Corrosion-fatigue crack propagation

5.1 DISCUSSION OF OVERLOAD EFFECTS

The effect of single cycle overload on fatigue and corrosion fatigue crack propagation behaviour in BS 4360 50D type structural steel, was investigated by reference to simulated storm loading conditions. Each specimen was subjected to more than one single overload with the safeguard that for avoidance of interactive influences from previous overloads, the fatigue or corrosion fatigue crack was allowed to propagate out of 'overload-effect' for a nominal distance of approximately 1.00mm before a further single cycle of overload was applied.

Graphs of crack length against endurance in cycles of fatigue loading are presented in Figures 2 and 3 respectively, where Figure 2 refers to the effect of overload on fatigue crack propagation behaviour in air and Figure 3 refers to the effect of overload on corrosion fatigue crack propagation behaviour in simulated sea water at free corrosion potential. A significant feature in both graphs is that following overload, fatigue and corrosion fatigue crack propagation is shown to be retarded, where degree of induced retardation can be correlated with the level of overload applied. In this context it will be recalled from the literature survey that level or degree of overload can be expressed as a percentage by reference to the identity :-

$$\% \text{ OVERLOAD} = \frac{K_{OVERLOAD} - K_{MAX.}}{K_{MAX.}} \times 100$$

For overload of the order of 67%, Figures 2 and 3 show that crack growth was retarded with clearly defined limits of affected crack length. Subsequent overload at a level of the order of 34% was found to promote retarded crack propagation, but to a reduced degree with less well defined limits of affected crack length. In this context it will be recalled from the literature survey that for steels in general, Bernard et al (59) have proposed that a threshold overload level in the range 40 - 60% is required for retardation of crack growth. In general the data presented in Figures 2 and 3 is considered to be consistent with the concept of 'overload threshold',

but indicates that for BS 4360 50D type steel overload threshold level is outside the general range proposed.

A particularly noticeable feature of the data presented in Figures 2 and 3 respectively, is the difference in form of the respective graphs, at first application of overload. For fatigue crack propagation in -air, overload to 67% was found to promote a defined period of retarded crack growth which terminated in 'nil-growth' or apparent 'crack-arrest'. In contrast, for corrosion fatigue crack propagation at free corrosion potential, overload to 67% was found to promote delayed retardation but no 'crack-arrest',as shown in Figure 3.

The phenomenon of retarded fatigue and corrosion fatigue crack propagation in BS 4360 50D type structural steels, following overload was considered to be significant and worthy of more detailed investigation. To this end, for conditions of both fatigue and corrosion fatigue crack propagation, local crack propagation rate was plotted against position relative to point of overload, as shown in Figure 4. The significant feature of the data presented in Figure 4 is that fatigue and corrosion fatigue crack propagation rates are shown to attain minimum values after the crack front had propagated a determinable distance from the point of overload. Thereafter crack propagation rates were found to increase and ultimately attain pre-overload levels. It will be recalled from the literature survey that this effect has been described as 'delayed-retardation'. Within the overload affected crack length, the following trends were identified in the data :-

(a) an abrupt increase in propagation rate to a value greater than the previous steady state pre-overload rate,

(b) a rapid decrease in propagation rate to a minimum value over a small distance ahead of the crack tip,

and (c) subsequent gradual increase in propagation rate to the pre-overload value.

It should be noted, however, that effect (a) above was not detected by analysis of data presented in Figures 2 and 3 but was found from analysis of 'secant' data recorded during performance of the respective overload experiments. This data has been incorporated in Figure 4 as appropriate.

It will further be recalled from the literature survey, that a number of mechanisms have been proposed to describe the phenomenon of retarded fatigue crack propagation. These proposals include the effects of crack tip blunting, residual compressive stress ahead of the crack tip, crack closure effects and crack tip strain hardening. In view of the complex mechanistic nature of fatigue crack propagation phenomena, it is considered reasonable to assume that no simple mechanism is solely responsible for the phenomenon of retardation following overload. Such an assumption does not, however, preclude the possible existence of a single dominant mechanism.

For the investigation reported herein, it was considered that effects of crack closure and crack tip strain hardening were insignificant and could be ignored. Lack of crack closure effects was attributed to the influence of positive R ratio which was considered to result in a minimum value of crack tip opening displacement, CTOD, in excess of twice the depth of overload residual plastic zone. This assumption was based on fractographic examination of overload fracture surfaces which revealed no evidence of surface abrasion or 'fretting contact'. The only unusual surface fracture found was a faint discoloured line type marking on the in-air fracture surface, which was found to correlate with the position of first overload.

From the data presented in Figures 2, 3 and 4 and Table 1, it was considered that for BS 4360 50D type structural steel, retardation of fatigue crack propagation following overload was due to the combined influence of crack tip blunting and enhanced residual compressive stress in the material ahead of the crack tip. Crack tip blunting was considered to increase the radius of curvature at the crack tip and thereby promote a reduction in the value of crack tip stress intensity factor responsible for crack propagation. Whereas residual compressive stress in the crack tip region was considered to oppose crack tip opening displacement through enhanced local constraint.

From a relationship of the form $\delta = 0.22\ K_1^2/E.\sigma_y$ (93), a dependency of CTOD, δ, upon crack tip stress intensity factor K_1 and thereby on the overload level of K_1 also, can be established. Further, the influence of residual stress ahead of the crack tip can be related to the size of the crack tip plastic zone and is therefore also dependent upon the appropriate value of K_1. For the specimens used in this project, predominantly plane strain conditions were assumed at the crack tip, because the specimen width (B) satisfied the criteria for essentially plane strain conditions, as established in sub-section 4.3. The radius of the crack tip plastic zone for plane strain conditions is given by $\Gamma_y = 1/6\pi\ (K_1/\sigma_y)^2$.

On this basis it was considered significant that the overall overload affected zone size or crack length, corresponded with the calculated monotonic plane stress plastic zone size associated with the overload stress intensity factor, given by $\Gamma_s = 1/2\pi\ (K_1/\sigma_y)^2$. Further, the associated delayed retardation zone size was found to be given by the monotonic plane stress plastic zone size associated with the baseline K_{max} value, as shown in Table 1. A particularly interesting feature of the data presented in Table 1, is that overload affected crack length and delayed retardation zone size, appear to be independent of test environment. However, as calculation of respective plastic zone sizes was based upon mechanical considerations only, lack of environmental influence was not unexpected.

In terms of a phenomenological model, the behaviour discussed above was interpreted in terms of growth of a fatigue or corrosion fatigue crack through a region in the material that had been subjected to enhanced residual compressive stresses. Application of overload was considered to enhance local residual compressive stresses at the crack tip region, to the limit given by the previous plane stress monotonic plastic zone size. Therefore this region of

plastically deformed material was subjected to enhanced levels of residual compressive stress in comparison to that present in the remainder of the overload plastic zone size. This proposed model was considered to be consistent with the observed phenomenon that apparent minimum growth rate following overload was found to occur at a distance ahead of the point of overload, given by the pre-overload monotonic plane stress plastic zone size, as shown in Figure 4. This general model can be illustrated schematically as shown below :-

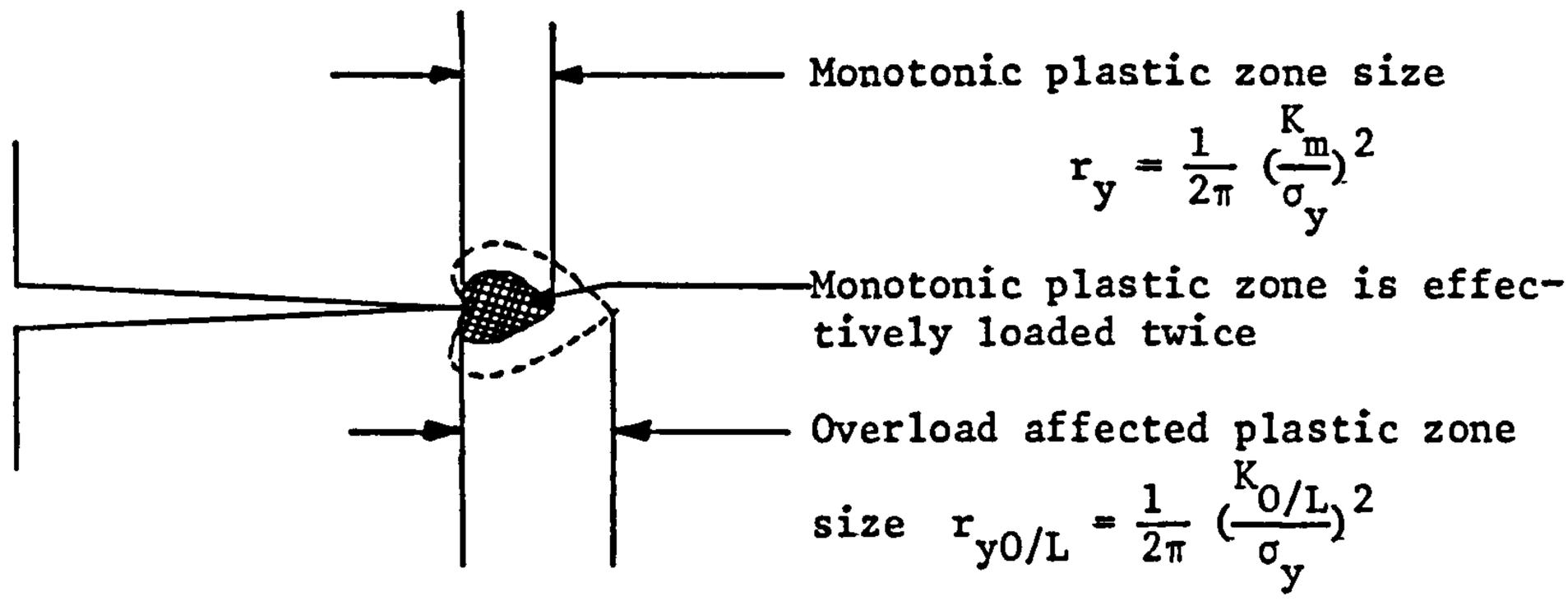

Schematic to illustrate residual stress arising from crack tip plasticity

In practical terms, the period of retarded crack propagation represents the number of fatigue cycles required to extend the crack through the overall overload affected zone. This can be expressed as shown below :-

Let $r_{y_{O/L}}$ = radius of overload affected plastic zone

Let $da/dN_{O/L}$ = average fatigue crack propagation rate following overload.

In this context, a significant feature of the data presented in Table 1 is that, contrary to the above prediction, the duration of retarded corrosion fatigue crack growth is shown to be in excess of the equivalent in-air value. This unexpected feature of the result is attributed to the beneficial influence of increased crack tip blunting, promoted by strain enhanced anodic dissolution activity, at the point of overload. In general, however, anodic dissolution activity in BS 4360 50D type structural steel, is not considered to be strain sensitive to any significant degree.

Let $N_{O/L}$ = number of fatigue load cycles required for propagation through the overload affected zone.

Hence $N_{O/L} = \frac{r_{y_{O/L}}}{da/dN_{O/L}}$ cycles

$$N_{O/L} \alpha \Gamma s_{O/L} \text{ or } \alpha(da/dN_{O/L})^{-1}$$

The interesting feature of this result is that the number of fatigue cycles required for the fatigue or corrosion fatigue crack to propagate out of overload effect is shown to be proportional to the overload plastic zone size and inversely proportional to the associated local average rate of crack propagation. Therefore, the expectation is created that delay produced by overload in an aggressive environment, such as sea water at free corrosion potential, would be shorter than that for an identical overload level, under conditions of fatigue crack propagation in air. The fact that data in Table 1 shows that this is not the case, is probably due to the beneficial influence of changes in crack tip geometry caused by electrochemical corrosion reactions.

Lastly, a particularly interesting feature of the data presented in Figures 2 and 3 was that the degree of retardation in crack growth promoted by overload was found to decrease with corresponding increase in crack length at which the overload was applied. This effect was attributed to increase in steady state crack tip stress intensity factor with crack length, which was considered to result in a reduced differential between steady state and overload plastic zone sizes. In this context it will be recalled that for all overload applications reported herein, the level of applied overload was arbitrarily fixed at the calculated storm case value, irrespective of crack length. Thus in circumstances where the pre-overload crack tip plastic zone size was large there was a small retardation effect which was not considered to be significant.

5.2 *DISCUSSION OF FATIGUE CRACK PROPAGATION BEHAVIOUR IN AIR*

For parent plate, weld metal, heat affected zone and fusion line microstructures, fatigue crack propagation rate data for in-air conditions is presented graphically in the form log da/dN against log ΔK, as shown in Figure 5. The data presented in Figure 5 has two notable features, first for values of ΔK less than approximately 37 M.Pa.$\sqrt{n}$, the fatigue crack propagation rate in weld metal was found to be less than for the other microstructures tested. Second, for each microstructure, the appropriate fatigue crack propagation rate data was found to be 'bi-modal' in form with a clearly defined 'transition point'.

In respect of the low fatigue crack propagation rates exhibited by weld metal, it will be recalled from the literature survey that the fatigue crack propagation rate da/dN can be expressed in terms of calculated crack tip opening displacement, δ, by a relationship of the form :

$$da/dN = A \frac{\Delta\delta - \Delta\delta_{TH}}{\delta_c - \delta_{max}} \qquad |43|$$

where $\Delta\delta = \delta_{max} - \delta_{min}$, δ_{max} and δ_{min} are the maximum and minimum values of δ in the loading cycles, $\Delta\delta_{TH}$ is the value of $\Delta\delta$ at the threshold, δ_c is the critical value of δ for unstable fracture and A and α are material dependent parameters analogous to those developed by Paris. For the microstructures tested, appropriate cal-

culated values of δ are presented in Table 2 and associated values of material yield stress are given in Appendix 5B. In general, this data is considered to demonstrate that the mechanical properties of weld metal are superior to those of the other microstructures tested and that reduced fatigue crack propagation rate in weld metal is therefore not unexpected.

The bi-modal form exhibited by the graphs presented in Figure 5, arose from attempts to describe each set of data points by a single Paris crack propagation rate relationship. This was found to produce considerable inaccuracy of data-fit at low values of ΔK, which was unacceptable. As a consequence, bi-modal presentation of data points was adopted, based on Paris format associated values of constant 'C' and exponent 'm' are presented in Table 3 and show that above transition, experimental fatigue crack propagation rate data was adequately described by a Paris crack propagation rate relationship, whereas below transition it was not.

Not withstanding this particular feature of the results, the fitting of a best straight line to below transition point data was found to provide a means of assessment of microstructural influence on ΔK_{TH} values. This was achieved by back-extrapolation of below transition-point data, to an arbitrary fatigue crack propagation rate of $da/dN = 1.00 \times 10^{-10}$ m/cycle. On this basis, the data presented in Table 5 was derived from the bi-modal graphs presented in Figure 5. A particularly interesting feature of the results presented in Table 5, was that ΔK (threshold) for Parent Plate material was found to be approximately 9.40 M.Pa.$\sqrt{m}$ which compared with a theoretical value of 10.05 M.Pa.$\sqrt{m}$, given by a relationship of the form $\Delta K_{TH} = K^{o}_{TH}(1-R)^{\gamma}$, proposed by Austen (10). For BS 4360 50D type structural steel $K^{o}_{TH} = 10.76$ and $\gamma = 0.637$. The closeness of this result was considered sufficient encouragement for the use of extrapolation techniques in assessment of microstructural influences on general threshold performance.

A particularly interesting result from back-extrapolation of this kind, was that ΔK (threshold) for heat affected zone microstructure was found to be less than 50% of the corresponding value for both parent plate material and weld metal. For heat affected zone microstructure, crack initiation at an arbitrary distance of 1.00mm from the fusion line was deliberately selected to promote fatigue crack propagation in the most unfavourable local microstructure, as illustrated schematically below :-

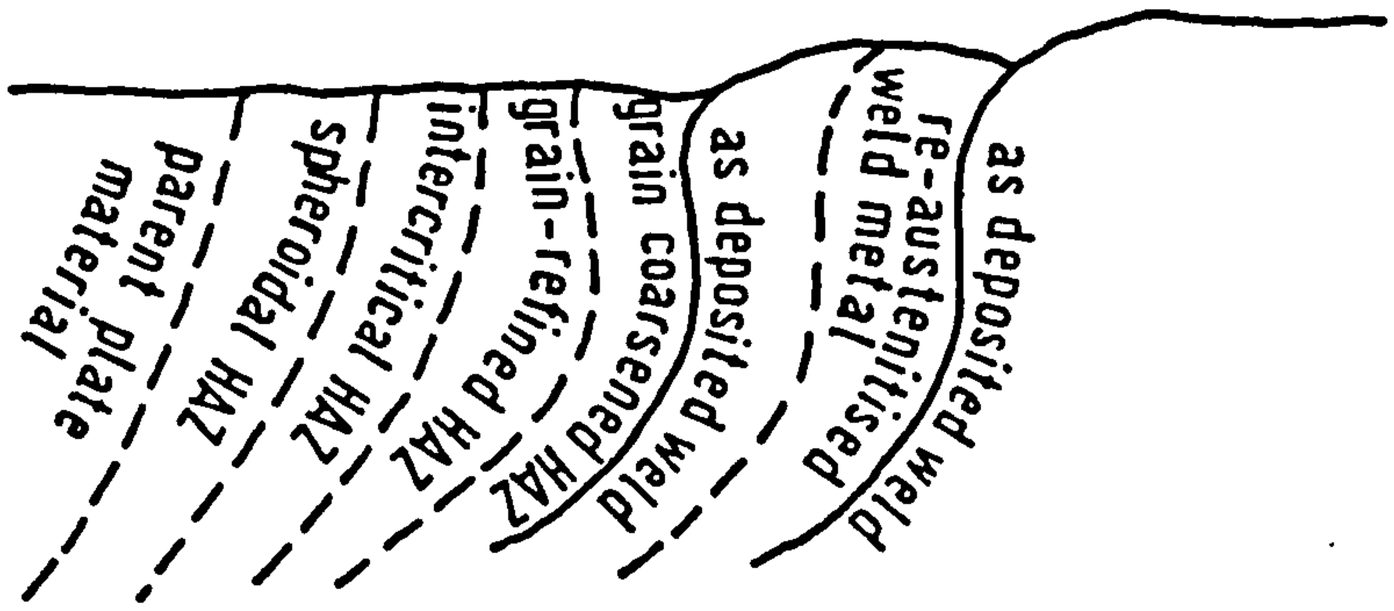

Schematic of the microstructure associated with a multi-pass weld

In general, the influence of microstructure on ΔK (threshold) values, as shown by the values presented in Table 5, was considered to be significant for the following reasons :-

(1) The greatly reduced ΔK_{TH} value for grain coarsened heat affected zone microstructure, identified this region as a major potential source of fatigue or corrosion fatigue fracture initiation, particularly as low inherent fatigue resistance would be enhanced by the presence of weld or fabrication defects. It should be noted, however, that the absolute values of extrapolated ΔK_{TH} presented in Table 5 are regarded as being of less importance, in comparison to the trend in behaviour indicated.

(2) It will be recalled from the literature survey that the level of heat input during welding has been identified as a major influence on local sensitivity of weldment microstructure to aqueous corrosion attack (60). Therefore for weldments in BS 4360 50D type structural steel, weld procedures should be arranged such that heat affected zone microstructure is established as cathodic with respect to its surroundings.

It must be remembered, however, that the values of extrapolated ΔK_{TH} presented in Table 5 were derived for a single value of stress ratio R, load amplitude and frequency of loading .

A notable feature of bi-modal presentation of data was that transition in fatigue crack propagation rate was generally found to occur in a narrow band of ΔK values and associated values of da/dN, as shown in Table 4 and associated graphs in Figure 5. For the graphs presented in Figure 5, approximate redrawn values of ΔK and da/dN at transition are 24 M.Pa.$\sqrt{m}$ and 1.00×10^{-7} m/cycle respectively, irrespective of microstructure.

Initially it was thought possible that the phenomenon of transition in fatigue crack propagation rate, was caused by a fundamental change in fatigue crack propagation mechanism; such as, a change from inhomogeneous to homogeneous plastic flow at the crack tip where the plastic zone was initially contained wholly within one grain. This would have encouraged assymetric shear decohesion in the manner proposed by Tomkins (26), for stage I crack propagation. However, for BS 4360 50D type structural steel, comparison of calculated crack tip plastic zone size and measured grain size demonstrated that at transition, crack tip plastic zone size was much larger than the local grain size. Therefore, transition in fatigue crack propagation rate could not be attributed to a fundamental change in crack propagation mechanism.

Metallographic and fractographic examination of fracture surfaces, revealed that irrespective of microstructure, a major change in extent and size of secondary or branched cracks occurred in the vicinity of the transition point. Below transition, branched cracks were few in number and of relatively small throat opening, whereas above transition point, the number of cracks and size of throat

opening were both found to have increase. For BS 436) 50D type plate material, the approximate degree of change in extent of branched crack activity in relation to the transition point is shown in Figure 6.

In this context it will be recalled from the literature survey that crack branching causes a reduction in the effective level of ΔK operative at the main crack front. As a consequence, the expectation is that change in degree of branched crack activity would be reflected by a change in average fatigue crack propagation rate. The overall trend in data presented in Figure 5, is considered to be consistent with this proposal. Further, from metallographic examination of fracture surface sections, which numbered approximately 20 per fracture surface, it was noted that branched cracks had a generally elliptical or thumbnail form and were mainly orientated at approximately 45^{o} to the plane of crack advance. The elliptical nature of branched cracks could possibly be attributed to local attainment of minimum strain energy conditions, for a given length of crack front. However, in current literature, the mechanism of branched crack initiation and propagation in a preferred orientation, has received little attention. It is therefore considered that this feature of the results could usefully be made the subject of further research.

Overall, the significance of transition in fatigue crack propagation rate was considered to be that it marked the end of near-threshold crack growth and the start of Paris type crack propagation. Especially as for the microstructures tested, calculated values of crack tip opening displacement associated with transition point were found to be in the range 1 to 2 μm, values which are often attributed to structural steels in the near threshold region.

Above transition point fatigue crack propagation rate data was found to obey Paris type crack propagation rate relationships of the form $da/dN = C.\Delta K^{m}$. Associated values of constant C and exponent m, derived from Figure 5, are presented in Table 3 as values C_2 and m_2. It must be noted that for all fatigue crack propagation rate tests in -air, mechanical test parameters were fixed. Namely, stress ratio R, load amplitude and frequency of loading. Therefore values of parameters C_2 and m_2 presented in Table 3 are regarded as being representative of mean fatigue crack propagation rate behaviour only. As a consequence, test data reported herein is only comparable with data from the United Kingdom Offshore Steels Research Programme. U.K.O.S.R.P., in circumstances where mean fatigue crack propagation rate data are quoted for comparable mechanical test parameters. On this basis, for BS 4360 50D type structural steel, U.K.O.S.R.P. literature was found to quote a mean fatigue crack propagation rate of the order of $da/dN = 5.32 \times 10^{-11} (\Delta K)^{2.53}$ m/cycle. Whereas from data presented in Table 3, the equivalent rate is given by $da/dN = 5.40 \times 10^{-11} (\Delta K)^{2.36}$. In view of the differences in experimental and data analysis techniques, the closeness of these results is particularly encouraging and provides general confidence in the quality of the experimental data reported herein.

For fatigue crack propagation behaviour in -air, data in Table 3 indicates that a gross change in microstructure morphology has a major

influence on values of the Paris experiment m, reflected in values of 2.36 and 3.25 for parent plate material and weld metal respectively. In contrast, associated values of constant C were generally found to exhibit relatively little change with microstructure. A notable exception was data associated with heat affected zone microstructure where value of constant C was found to be enhanced by an order of magnitude.

Fatigue endurance in cycles of loading, for crack growth between an initial crack length of 15.00mm and a final crack length of 18.00mm was calculated for each of the microstructures tested, by numerical integration of the approximate Paris fatigue crack propagation rate relationship derived from data presented in Table 3. Endurance data derived in this way is presented in Table 6, where overall predictive accuracy was found to be of the order of ± 8%. It should be noted that measured endurance was recorded directly from an electro-mechanical cycle counting device attached to the test machine.

The high level of accuracy demonstrated, vindicates integration of appropriate Paris type crack propagation rate relationships for prediction of fatigue endurance in structural steel. An interesting feature of the data presented in Table 6, is that parent plate material has the lowest value of fatigue endurance and weld metal has the highest. Further, in general terms, correlation can be made between relative level of fatigue endurance and value of exponent m. For in-air data, associated with fatigue crack propagation in parent plate and weld metal, values of constant C were found to be of similar magnitude but with variation of the order of square to cubic respectively, in value of associated exponent m. As a generalisation, this result indicates that the value of exponent m is the more significant element within a given Paris crack propagation rate relationship. Further, the trend in values of C and m corroborates the view that microstructural considerations have a significant influence on the value of exponent m, whereas environmental considerationshave a significant influence on the value of constant C.

In this context, a particular feature of the data presented in Table 3 is that a linear relationship of the form $m = A.\ln C + D$ was found to exist between exponent m and constant C, as shown in Figure 38. It was noted with interest, that this feature of the results supported similar data reported by Bathias (96), for fatigue of steel in air, which for comparison is also shown in Figure 38. This combined data has two significant features. Firstly, the curves for in-air and an environment of aqueous corrosion, are shown to be essentially parallel with a lesser value of constant D associated with an environment of aqueous corrosion. Secondly, for an environment of corrosion fatigue, the relationship between exponent m and constant C is shown to be independent of both microstructure and applied cathodic protection protential. This feature of the results is particularly significant, as it can be inferred that the constants A and D in the above relationship are not material dependent.

A particular feature of fatigue and corrosion fatigue crack propagation in heat affected zone microstructure was that in all tests, the direction of crack propagation was found to be towards the softer parent plate material, as represented by the in-air case shown in Figure 7. This

phenomenon was regarded as being of considerable importance to fatigue and corrosion fatigue endurance of structural steel weldments and was investigated in more detail, by means of hardness measurements. Survey of hardness values for a typical welded specimen, showed maximum hardness at the fusion line interface with the heat affected zone microstructure and a decrease in hardness across the width of the heat affected zone down to values associated with parent plate material. Hardness data is presented in Appendix 11.

The yield strength of the grain coarsened heat affected zone microstructure was estimated by reference to an empirical relationship of the form $\sigma_y = 3.25H_v - 349$ (94), where H_v is the average hardness value for the area of interest. Estimated yield strength derived in this way was found to have a value between the respective measured values for parent plate material and weld metal, as shown in Appendix 5B The significance of this result, is that a gradient in material yield strength is present at the fusion line which might reasonably be expected to influence the size and shape of crack tip plastic zones associated with a growing fatigue crack, through interference in the formation of plastic flow bands.

It will be recalled that for the test specimens used throughout this project, fatigue crack propagation was considered to occur under predominantly plane strain conditions, with yielding confined to a narrow zone, immediately ahead of the crack point, whose radius is given by $r_y = 1/2\pi\ (K_m/\sigma_y)^2$. The concept of inhibited development of plastic flow bands and consequent modification to plastic zone shape, is illustrated schematically below :-

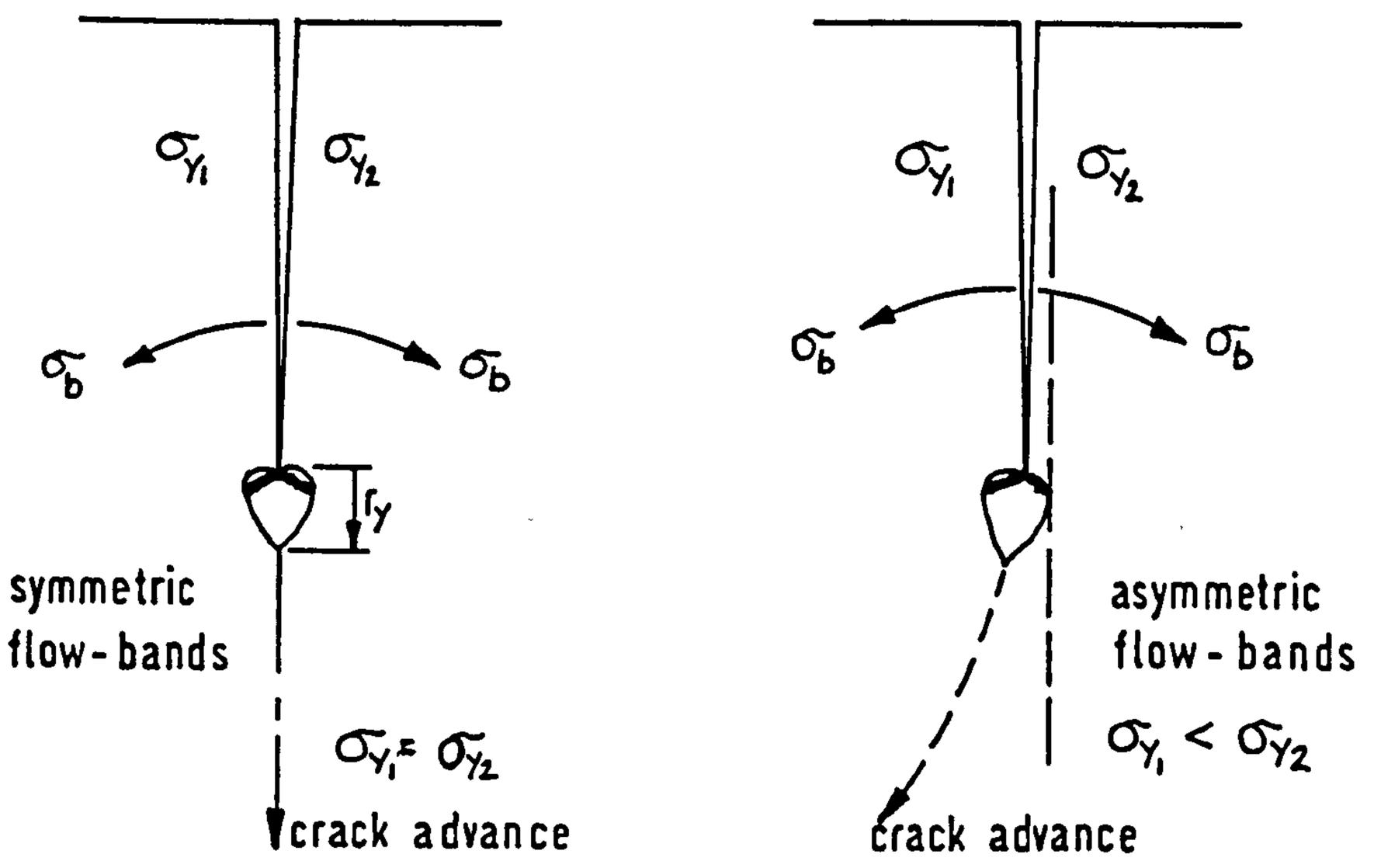

Schematic illustration of the influence of asymmetric plastic flow bands

The important feature of the proposed mechanism, is that asymmetric development of plastic zone shape is considered to establish a preferred direction of crack propagation, in the direction of lowest constraint. Away from the influence of yield strength gradient, the symmetry of the plastic zone shape is considered to be gradually re-established with associated fatigue crack propagation in the direction of lowest constraint. Further limited investigation of the proposed concept of asymmetric plastic flow bands was carried out using specimens of configuration 4.3(B). In this investigation, fatigue cracks at constant load amplitude were propagated from weld metal, through heat affected zone into parent plate and from parent plate material, through heat affected zone into weld metal. In all cases, fusion line boundary was at an angle of approximately 30^{o} to the lind of crack advance. An unexpected result from these tests, was that fatigue crack propagation rate and direction of crack advance were found to be unaffected by local changes in material yield strength. This feature of the results prompted a change in experimental design, in which fatigue crack propagation was arranged to occur from weld metal into parent plate material under conditions of constant ΔK and K_{max}.

Data from this experiment is presented in the form of a graph of fatigue crack propagation rate da/dN against crack length 'a', as shown in Figure 8. The notable feature in Figure 8 is that fatigue crack propagation rate was found to decrease sharply in the region of the weld fusion line and subsequently increase across the width of the heat affected zone, to a sensibly constant value in parent plate material.

During conduct of the tests, observation of the crack-tip showed that at the fusion line, the crack deviated from its plane of 'projected advance' and propagated parallel to the fusion line for a distance of approximately 1.50mm. After which, direction of fatigue crack propagation returned to the 'normal plane' and the crack propagated out of the heat affected zone into the parent plate material. In a repeat test under identical conditions, fatigue crack propagagion rate was found to be retarded at the fusion line boundary, as before, but direction of crack propagation remained in the projected plane of crack advance. Lack of repeatability in this respect was considered to indicate that the phenomena could usefully be made the subject of more detailed research with a view to definition of critical parameter required for deviation of crack growth out of the projected plane of initial crack growth.

Not withstanding the lack of repeatability demonstrated, the occurrence of deviation in direction of crack growth was considered to have a potentially significant influence upon fatigue and corrosion fatigue endurance of structural steel weldments. For a given weldment, the toughness of each constituent microstructure is reflected by associated values of crack tip opening displacement, δ, given by empirical formulae of the form $\delta = 0.22\ K_{max}^{2}/E.\sigma_{y}$. Hence it can be shown that $\delta \alpha 1/\sigma_{y}$, material toughness is inversely proportional to yield strength. The significance of this result is that for a structural steel weldment, the overall fatigue endurance of the joint may be determined by the toughness of the lowest strength constituent

microstructure. As a consequence, the use of high strength weld consumables in fabrication of offshore structures can be considered to be unwarranted where fatigue or corrosion fatigue endurance is a major design consideration.

For fatigue crack propagation in ferrite-pearlite type steels, it will be recalled from the literature survey that pearlite is considered to act as reinforcement within the bulk ferrite matrix and locally providesa mechanical barrier to crack advance. As a consequence,fatigue crack propagation in BS 4360 50D type structural steel, could be expected to occur preferentially in the ferrite phase. Metallographic examination of fracture surface sections, for the in-air tests reported herein, was found to corroborate this proposal. A typical example of crack detour around a pearlite colony is shown in Figure 9. Preferential fatigue crack propagation through the ferrite phase was found to be clearly illustrated in macrographs of the crack tip region, as shown in Figure 10. It is particularly noticeable in Figure 10, that crack tip plasticity had induced bending of adjacent pearlite bands ahead of the crack tip, with shear displacement of pearlite at the fracture location accommodated by means of the interspersed ferrite phase.

A particularly interesting feature of the metallographic examination in general, was that orientation ofiron carbide platelets within a given pearlite colony was found to determine the capacity of the pearlite colony to mechanically interfere with the direction of crack advance. Near parallel orientation of platelets was found not to interfere with the direction of crack advance and to accommodate crack propagation across the pearlite colony; this type of behaviour is illustrated in Figure 11. Conversely, less favourable orientations were found to promote interference in direction of crack advance and occasionally crack arrest as illustrated in Figure 12. It should be noted, that the behaviour illustrated in Figures 11 and 12 respectively was observed for branched crack propagation and not that associated with the main crack point.

Lastly, it will be recalled from the literature survey that the theoretical maximum fatigue crack propagation rate in air, can be given by $\delta/2$. In this context, a notable feature of the data reported herein was that the trend in relation to the theoretical maximum was found to be influenced by microstructure, in the manner illustrated in Figure 13. The significant feature in Figure 13 is that for increase in value of ΔK, fatigue crack propagation rates in weld metal tend towards the theoretical maximum given by $\delta/2$, whereas propagation rates in parent plate and heat affected zone microstructure, are shown to be approximately parallel to the theoretical $\delta/2$ bound, but an order of magnitude lower.

The trend in data associated with parent plate and heat affected zone microstructure was attributed to work hardening in the crack tip region, which was considered to increase local toughness with increase in K. Conversely, for weld metal, it was considered unlikely that work hardening was a significant influence. The likely cause of the trend in data shown in Figure 13, was considered

to be reduction in effective weld metal toughness with increase in crack length, promoted by the combined influence of single groove weld preparation and single sided multi-pass weld procedure without back-gauging.

It will be recalled from the literature survey that ductile striations can be considered to reflect the amount of shear displacement at the crack tip per cycle of fatigue and therefore represent the amount of crack advance per cycle of loading. During the course of fractographic examination of fatigue and corrosion fatigue fracture surfaces, in both parent plate material and weld metal, an attempt was made to correlate measured striation spacing with both local derived fatigue crack propagation rate and calculated crack tip opening displacement. Typical fractographs featuring ductile striations in both weld metal and parent plate material are presented in Figures 14 and 15 respectively. For both materials it was found that correlation was not possible in the manner predicted from assessment of current literature.

For parent plate material, the striation spacing measured in Figure 15 was found to be of the order of 1μm at a level of ΔK associated with a derived fatigue crack propagation rate of the order of 0.18μ/cycle as shown in Figure 5. Similarly for weld metal, striation spacing measured in Figure 14 was found to be of the order of 0.73μ at a level of ΔK associated with a derived fatigue crack propagation rate of the order of 0.086μ/cycle. It was a particular feature of striation markings in weld metal, that large well-defined striations were often found to have much finer, regular striation type markings contained within, as illustrated in Figure 14. This feature of the results was considered to show that possibly more than a single cycle of fatigue loading was required to form a ductile striation type marking. Such a mechanism would also be consistent with the noted lack of correlation between striation spacing and calculated crack tip opening displacement.
The significance of striation type surface markings was considered to be that they represent a permanent record of localised shear decohesion at the crack tip. A possible explanation of the finer striation type markings featured in Figure 14, is that they are plastic flow lines, which are in some way associated with a minimum dislocation spacing in the bulk matrix.

5.3 DISCUSSION OF CORROSION FATIGUE CRACK PROPAGATION

5.3.1 Corrosion Fatigue Crack Propagation Rate Behaviour in BS 4360 50D Type Structural Steel

Corrosion fatigue crack propagation rate data for stress relieved BS 4360 50D type structural steel plate, associated with conditions of free corrosion, cathodic protection potential of - 780 m $V_{S.C.E.}$ and cathodic protection potential of - 1100 m $V_{S.C.E.}$, is presented graphically in the form log da/dN against log ΔK as shown in Figure 16.
The graphs presented in Figure 16 exhibit three significant features :-

(1) Lack of correlation between experimental corrosion fatigue crack propagation rate data and theoretical crack propagation rate given by δ/2.

(2) The influence of notionally correct cathodic protection potential of - 780 mV_{SCE} is shown to reverse with increase in ΔK.

(3) The graph associated with notional cathodic 'overprotection' potential of - 1100 mV_{SCE} was found to have a form characteristic of stress corrosion dominated crack propagation behaviour. Further, at high values of ΔK, conditions of cathodic 'overprotection' are shown to promote closest approach of corrosion fatigue crack propagation rates to equivalent in-air values.

Lack of correlation between experimentally derived corrosion fatigue crack propagation rate and theoretical fatigue crack propagation rate given by δ/2 was not unexpected. The original proposal made by Tomkins that dissolution related mechanisms of corrosion fatigue are limited to da/dN maximum values of $\delta_{max}/2$ is subject to certain limitations. Firstly, the $\delta_{max}/2$ criterion only applies to transgranular cracking where the basic fatigue mechanism is by an alternate shear process. It would therefore not be applicable where crack penetration or propagation occurs by preferential dissolution down a specific path, such as a grain-boundary. Under these particular conditions, the da/dN value might be greater than $\delta_{max}/2$, since the crack tip dissolution is not confined to the work hardened region on the immediate flanks of the crack tip. Secondly, an upper limit to dissolution controlled crack growth rate (da/dt) may well be associated with bare surface dissolution. The significance of this would depend upon whether the bare surface dissolution rate was liquid diffusion controlled or activation controlled.

The apparent adverse change in influence of 'correct' cathodic protection potential, - 780 mV_{SCE}, on corrosion fatigue crack propagation rates with increase in ΔK, was investigated in more detail. In this context it will be recalled from the literature survey that overall corrosion fatigue crack propagation rate can be considered to reflect the sum influence of environmental and mechanistic components. As an attempt to isolate and assess the influence of the environmental component, an Environmental Enhancement Factor was defined as :-

$da/dN_{ENV} - da/dN_{AIR}/da/dN_{AIR}$ and was plotted against ΔK for each of the test environments, as shown in Figure 17. The data presented in Figure 17 has four significant features :-

(1) For values of ΔK less than approximately 30 M.Pa.$\sqrt{m}$ a cathodic protection potential of - 780mV_{SCE} was found to promote minimum values of environmental enhancement factor, in the range 0.2 - 0.3. Whilst a cathodic protection potential of - 1100 mV_{SCE} was found to promote higher values in the range 0.3 - 3.0+.
(2) Conditions of free corrosion were found to promote a sensibly constant value of environmental enhancement factor of 0.35, down to a value of ΔK of 26 M.Pa.$\sqrt{m}$. Below this value, there was a significant rise in the factor.
(3) For values of ΔK in excess of approximately 30 M.Pa.$\sqrt{m}$ a cathodic protection potential of - 780 mV_{SCE} was found to promote increasing values of environmental enhancement factor in the range 0.3 - 0.6 with increase in ΔK. Whilse for the same range of ΔK values, a cathodic protection potential of - 1100 mV_{SCE} was found to promote a sensibly constant values between 0.2 and 0.3.
(4) The extremes in value of environmental enhancement factor were

found to be confined to comparatively low values of ΔK, in the range 22 - 30 M.Pa.√m. This feature of the results was considered to be particularly significant as it implied that a critical relationship existed between the influence of cathodic protection potential and either corrosion fatigue crack propagation rate or crack depth.

To assess the significance of this feature, the experimental corrosion fatigue crack propagation rate data were re-plotted, in the form of da/dN against crack depth a , as shown in Figure 34. The significant feature of the curves presented in Figure 34, was that crack lengths in the range 14 - 16mm were found to correlate with the apparent reversal in influence of cathodic protection potential.

In this context, it is important to note that the overall crack length of 14.8mm, encompassed an actual fatigue fracture length of approximately 5mm, the remainder of the crack length was composed of machined starter notch. The significance of this result is that for an un-notched specimen, it implies that the capacity of nominally correct cathodic protection potential, $-780mV_{SCE}$, to favourably influence corrosion fatigue crack propagation rates, is limited to crack depths of 5mm or less.

The nature of the relationship between the influence of cathodic protection potential and crack depth was assessed by examination of associated fracture surfaces, using a scanning electron microscope. Two groups of fracture surfaces were examined, those which had been chemically cleaned to remove corrosion products and associated surface deposits, and those direct from the test environment, complete with surface deposits. Of the specimens examined direct from the test environment, those associated with conditions of cathodic protection potential were found to have a common, significant feature. Namely, that irrespective of applied cathodic protection potential, the fracture surfaces were found to be coated with calcareous deposits, whose density was found to reduce with crack depth. Sides of the starter notch, pre-fatigue fracture surfaces and external specimen surfaces were found to have a uniform and relatively dense calcareous coating. Away from the pre-fatigue fracture area, calcareous deposits were found to rapidly decrease in density and terminate in virtually no coating in the region of the crack tip. This particular feature of the results was considered to indicate that a pH gradient was present within the crack and that access of cathodic protection current was possibly limited by a critical value of crack opening displacement. Relevance of pH gradient is discussed further in Section 5.3.1 (A).

Results from examination of cleaned fracture surfaces are presented in summary form in Table 7, with associated fractographic evidence presented in Figures 18 to 20 respectively. The following features were considered to be significant :-

(1) Hydrogen embrittlement indicated by many quasi-cleavage facets was found to be a common feature in the fracture surfaces. For conditions of free corrosion potential, it was found that quasi-cleavage facets at high ΔK and long

crack lengths were larger than those associated with low ΔK and short crack length. This feature of the results was considered to imply that BS 4360 50D type structural steel was behaving in a more brittle manner than might have been expected.

(2) Formation of corrosion pits was found to be a common feature in all fracture surfaces, irrespective of crack depth and applied environment. For fracture surfaces associated with cathodic protection, it was found that the severity of corrosion pitting was greatest for a potential of - 780 mV_{SCE}, and crack length > 14.8mm and least for a potential of - 1100 mV_{sce}. This result implied that nominally correct cathodic protection potential of $-780mV_{SCE}$ was ineffective in suppressing electrochemical corrosion reactions at crack lengths > 14.8mm whereas a potential of - 1100 mV_{SCE} was at least partially effective.

(3) Initial high values of environmental enhancement factor shown in Figure 17, were correlated with enhanced hydrogen embrittlement in all fracture surfaces for a < 14.8mm. This feature was attributed to the establishment of equilibrium conditions, prior to commencement of individual corrosion fatigue crack propagation rate tests. Conditions of cathodic overprotection potential of $-1100mV_{SCE}$ were considered to have promoted forced hydrogen charging of the steel, whereas conditions of free corrosion potential promoted natural hydrogen charging and nominal correct cathodic protection potential of - 780 mV promoted suppressed natural hydrogen charging. Notwithstanding the artificial nature of this effect, it was nevertheless considered to be valid in relation to(in-service)offshore fracture environments.

Overall, the results of fractographic examination were found to confirm the proposal that favourable influence of correct cathodic protection potential of $-780mV_{SCE}$ was limited to relatively shallow cracks, less than~5mm deep. As a consequence, cathodic protection was categorised as a surface related, 'line-of-sight' phenomena. It was therefore considered to be particularly significant that cathodic overprotection potential of - 1100 mV, was found to promote minimum values of corrosion fatigue crack propagation rate in cracks deeper than 5mm. This effect was attributed to partial suppression of anodic dissolution reactions at the crack tip with associated reduced levels of effective hydrogen embrittlement. It should be noted, that detrimental influence of excessive cathodic protection potential was found in the threshold region, where enhanced hydrogen embrittlement could be expected to promote significant reductions in the value of ΔK_{TH}, particularly as it has been shown in Figure 16, that initial crack propagation promoted by cathodic overprotection potential had a form characteristic of stress-corrosion dominated fracture behaviour. Environments of free corrosion and nominally correct cathodic protection potential of $-780mV_{SCE}$ were found to promote normal corrosion fatigue crack propagation in initial stages of crack growth with no influence of stress corrosion.

For these environments, values of ΔK_{TH} derived by extrapolation

of data presented in Figure 16, are presented in Table 5. The interesting feature of this data, is that ΔK_{TH} level associated with cathodic protection potential of - 780 mV_{SCE}, was found to be sensibly the same as that promoted by conditions of free corrosion. In relation to the data reported herein, this result was attributed to the effects of natural hydrogen changing associated with the establishment of equilibrium conditions. The significance of the data presented in Table 5, is that the value of ΔK_{TH} is shown to be only slightly reduced by approximately 15% under conditions of aqueous corrosion fatigue, compared to the in air value. This minor reduction in the ΔK_{TH} value is possibly due to embrittlement effects.

The foregoing results have shown that hydrogen embrittlement has a significant influence upon overall corrosion fatigue crack propagation behaviour in BS 4360 50D type structural steel. It is therefore considered to be a significant feature of the data presented in Figure 16, that associated values of Paris parameter C and m presented in Table 3 appear to be generally insensitive to influence of embrittlement. Aqueous environment at free corrosion potential was found to promote a small increase in value of constant C and no change in value of exponent m, in relation to comparable in-air data. Whereas an environment of cathodic protection potential of - 1100 mV_{SCE} was found to promote no change in value of constant C and a small increase in value of exponent m, in relation to comparable data for free corrosion potential. Conversely, an environment of nominally correct cathodic protection potential of - 780 mV_{SCE}, was found to promote a reduced value of constant C and an increased value of exponent m. This feature of the results was considered to demonstrate that a threshold level for sensitivity of Paris parameters to hydrogen embrittlement was probably present, below which the exponent m reflected the influence of microstructure and the constant C reflected the influence of environment.

In relation to prediction of corrosion fatigue endurance by integration of an appropriate, Paris crack propagation rate relationship, data presented in Table 3 promoted the expectation that endurance under conditions of free corrosion and cathodic overprotection potential, would be of similar magnitude, whereas endurance under conditions of nominally correct cathodic protection potential would be reduced. For the corrosion fatigue crack propagation rate tests reported herein, values of endurance calculated by numerical integration of appropriate Paric crack propagation rate relationships, for crack growth between crack lengths of 15.00mm and 18.00mm, are presented in Table 6. The significant features of this data are considered to be :-

(1) The overall level of predictive accuracy achieved by numerical integration, was found to be of the order of ± 8%.

(2) The trend in both measured and calculated values of endurance was found to reflect the bias exhibited by the curves presented in Figure 34.

(3) Endurance associated with conditions of nominal correct cathodic protection potential,-780mV$_{SCE}$, was found to be markedly lower than that associated with environments of free corrosion and cathodic overprotection potential.

It was also noted that for environments of free corrosion and cathodic overprotection potential, measured values of endurance recorded direct from the test machine, were found to be in close agreement. Whereas a sizeable difference was present in the predicted values, derived by integration. Close agreement of measured values was not unexpected, in view of the influence of lack of penetration of cathodic protection current discussed previously. Variation in predicted values of endurance was attributed to the influence of arithmetical errors in integration of the appropriate Paris relationship and experimental errors present in derivating the Paris parameters C and m.

Lack of penetration of cathodic protection current into cracks or crevices deeper than nominally 5mm, was considered to be a critical effect in relation to attainment of structural corrosion fatigue endurance offshore. Especially as a specific crack depth of 5mm can be considered to have particular relevance to in-service offshore structures, through correlation with reported structural defects. In many instances, surface breaking cracks, particularly in welded node joints, are frequencly found to be less than 5mm deep, but to be more than 5mm in surface length. The combination of in-service experience and critical crack depth reported herein, prompted a critical appraisal of test specimen geometries, to determine an optimum geometry for simulation of offshore corrosion fatigue fracture. As a result, it was considered that conventional CTS and SEN. type specimens, which simulate through thickness crack propagation, were generally unrepresentative of the majority of offshore corrosion fatigue fracture. A suitable alternative test specimen was considered to be a modified SEN type, to the design illustrated schematically below :-

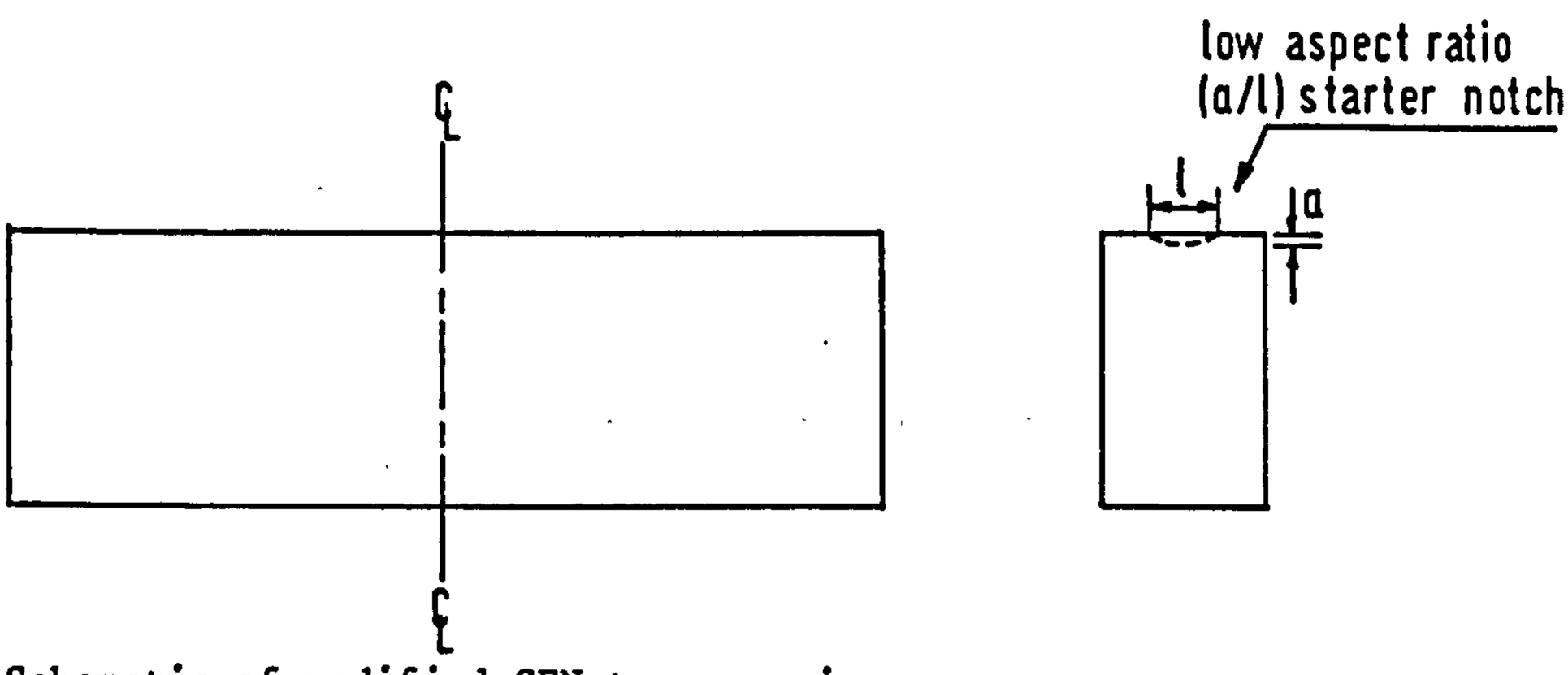

Schematic of modified SEN type specimen

Specific advantages of this type of specimen are considered to be :-

(1) More realistic simulation of initial in-service corrosion fatigue fracture behaviour.

(2) Improved assessment of the influence of cathodic protection current, with particular regard to degree of penetration into surface breaking defects.

(3) Improved cost-effectiveness, as the nature of corrosion fatigue crack development, particularly change in crack aspect ratio, a/ℓ, with time could be investigated concurrently with fundamental corrosion fatigue crack propagation rate behaviour, though an electrical method of crack length measurement would probably be necessary.

(4) Improved understanding of the influence, if any, of crack blocking by calcareous deposits. This is considered to have particular importance, as Scott and Silvester (12) have proposed that physical blockage of a corrosion fatigue crack by calcareous deposits mechanically interferes with crack closure and thereby promotes reduced values of ΔK with an increased R ratio and associated reduction in rate of corrosion fatigue crack propagation. In this context, it is considered that Scott and Silvester have possibly misinterpreted the significance of reduced corrosion fatigue crack propagation rates under conditions of nominally correct cathodic protection potential, at low values of ΔK. Especially as data reported herein has indicated that initial corrosion fatigue crack propagation rates are artifically enhanced through the influence of pre-test equilibrium conditions. Away from this region of influence, data reported herein is considered to indicate, that for BS 4360 50D type structural steel plate, corrosion fatigue crack propagation rates are enhanced by nominal correct cathodic protection potential and that calcareous deposits do not significantly interfere with crack closure.

5.3.1 (A) Electrochemical Corrosion Processes and Corrosion Protection in Relation to Corrosion Fatigue Crack Propagation in BS 4360 50D Type Structural Steel

Significant electrochemical corrosion reactions associated with both corrosion fatigue crack propagation and corrosion prevention by means of cathodic protection, are summarised in Table 8. In the summary, two reactions are of particular importance :-

(1) Cathodic reactions initiated in the occluded region which result in the production of molecular hydrogen in conjunction with corrosion activity that can become self-sustaining and need not necessarily rely on an external cathode.

(2) The action of applied cathodic protection current can encourage the development of alkalinity away from the occluded region where the crack opening is sufficient to allow the formation of calcareous deposits.

The significance of the above reactions is that under conditions of both no protection, i.e. free corrosion and corrosion protection current, potentially damaging hydrogen is produced. Therefore, under all conditions of aqueous corrosion fatigue, irrespective of applied cathodic protection, evidence of embrittlement can be expected.

In respect of anodic dissolution reactions, summarised in Table 8, it must be noted that electrochemical reactions are assumed to occur at both the crack tip and on the crack walls, where rates of reduction relevant to the production of hydrogen are given by :-

(1) Reduction or ionization of water :

$$i_{H_2O} = k(H^+) \exp.\{ \frac{-\beta(H^+).F.E.}{R.T.} \}$$

where k is a rate constant dependent upon the hydrogen ion concentration (H^+)
β is a transfer coefficient also dependent upon hydro-ion concentration,
F is Faraday's constant,
V is electrode potential,
R is the gas constant,
and T is temperature.

Similarly for reduction of oxygen :

(2) $$i_{O_2} = k'(O_2) \exp.\{ \frac{-\beta'.F.V.}{R.T.} \}$$

where k' is a rate constant
and β' is a transfer coefficient (95).

The important feature of the above relationships is that rate of reduction is shown to be dependent upon the parameters pH and electrical potential, both of which are unlikely to be in equilibrium within a growing corrosion fatigue crack due to the effects of mass transport.

In corrosion fatigue, mass transport of a dissolved species such as hydrogen ions is assumed to occur through the combined influence of advection, diffusion and ion migration. Where advection is defined as fluid flow resulting from cyclic displacement of the crack walls, diffusion and ion migration are a consequence of electrode reactions on the crack walls and at the crack tip, which by generation or removal of ionic species creates concentration and potential gradients. For a given species, the relevant mass transport equation can be expressed mathematically in the form :-

$$(3) \qquad J = K_1 V - D_1 \frac{\partial K_1}{\partial x} - \frac{D_1 F . K_1}{R.T} \cdot \frac{\partial \phi}{\partial x} \qquad (95)$$

where $K_1 V$ is the component due to advection.

$D_1 \frac{\partial K_1}{\partial x}$ is the component due to diffusion of species

$\frac{D_1 . F . K_1}{R.T} \cdot \frac{\partial \phi}{\partial x}$ is the component due to ion migration.

K_1 is concentration of relevant species

D_1 is diffusion coefficient of relevant species

$\frac{\partial \phi}{\partial x}$ is defined as the gradient in potential between the external surface and any point along the crack at a distance x.

To accurately model corrosion fatigue crack propagation under conditions of cathodic protection, mass transport and continuity equations would be required for each of the dissolved species in the crack (H^+, OH^-, O_2), in addition to sodium and chloride ions which although not consumed or produced, are assumed to undergo ionic migration to maintain electrical neutrality. As a consequence, mathematical description of electrochemical processes associated with corrosion fatigue would necessarily require the solution of complex differential equations.

In the context of phenomenological understanding of the significance of pH and potential gradients, within a corrosion fatigue crack, it is considered that appropriate experimental data could be obtained by use of a suitably instrumented, simulated corrosion fatigue crack, of the kind illustrated schematically below :-

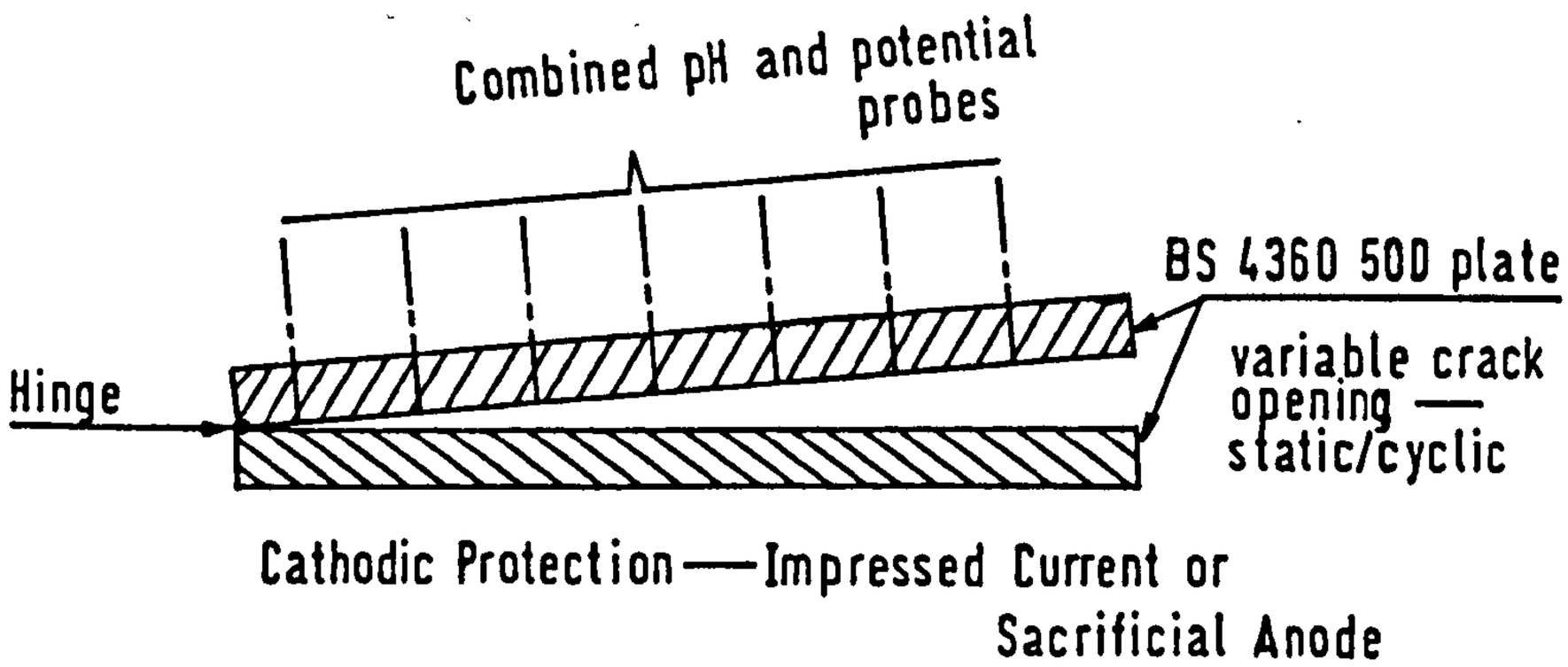

Schematic of an instrumented, simulated corrosion fatigue crack

A device of the kind illustrated on the previous page would be particularly valuable in determining the true extent of penetration of cathodic protection current into a corrosion fatigue crack together with assessment of the critical parameters. Research of this kind is considered to be vital to the scientific understanding of the fundamental processes of cathodic protection in relation to corrosion fatigue and is therefore a suitable subject for future research programmes.

5.3.2 *Corrosion Fatigue Crack Propagation Rate Behaviour in Weld Metal*

Corrosion fatigue crack propagation rate data for stress relieved weld metal, associated with conditions of free corrosion, nominal correct cathodic protection potential of - 780 mV_{SCE} and cathodic overprotection potential of - 1100 mV_{SCE} is presented graphically in the form log da/dN against log ΔK, in Figure 21. The graphs presented in Figure 21 were found to exhibit the following significant features :-

(1) A general trend in corrosion fatigue crack propagation rate data towards the theoretical maximum fatigue crack propagation rate, given by $\delta/2$.

(2) The graph associated with conditions of cathodic overprotection potential was found to have a form characteristic of stress corrosion dominated crack propagation behaviour.

(3) Environments of nominally correct cathodic protection potential and cathodic overprotection potential were found to promote below, equivalent, in-air rates of crack propagation, at high values of ΔK.

(4) The graph associated with conditions of free corrosion potential was found to provide the closest approach of corrosion fatigue crack propagation rate to the theoretical maximum rate given by $\delta/2$.

With the exception of the in-air data, which was sensibly parallel to the $\delta/2$ curve, the general convergent trend in data noted above was attributed to the sensitivity of weld metal to environmental influences in respect of corrosion fatigue crack propagation behaviour. Compared to plate material, weld metal contains a smaller crack tip plastic zone size for the same load and also has a lower K_{1c} value. Because the plastic zone size is smaller, the associated strain gradient is by implication steeper and as a consequence the potential hydrogen diffusion path is shorter. Therefore, the convergent trend in data, compared to that of parent plate material, is not unexpected.

In common with previous discussion of parent plate data in Section 5.3.1, Environment Enhancement Factor for weld metal was plotted against ΔK for each test environment, as shown in Figure 22. The significant features of the curves presented in Figure 22 are considered to be :-

(1) Cathodic protection potential in general, was found to promote negative values of environmental enhancement factor at high values of ΔK, where the value of environmental enhancement factor was found to be independent of level of applied cathodic protection potential.

(2) Cathodic overprotection potential, - 1100 mV_{SCE}, in particular was found to promote high initial values of environmental enhancement factor, in excess of 4.0, whereas environments of nominal correct cathodic protection potential, - 780 mV_{SCE} and free corrosion potential were both found to promote comparatively low values of environmental enhancement factor in the range 1.0 to 1.3, for the same range of K values. This result is not readily explicable.

(3) The general trend in data exhibited by weld metal, namely high initial values of environmental enhancement factor at low values of ΔK and low final values of environmental enhancement factor at high values of ΔK, was found to be identical to the general trend exhibited by data for parent plate material. To assess the significance of this feature, experimental corrosion fatigue crack propagation rate data for weld metal, was replotted in the form da/dN against crack length a, as shown in Figure 35.

The important feature of the curves presented in Figure 35 is that a unique value of crack length, approximately 15.0mm, was found to correlate with the beneficial influence of nominally correct cathodic protection potential, noted in Figure 21. The significance of this feature is that the crack length of approximately 15.0mm is nominally the same as the equivalent measurement for parent plate material. In common with previous discussion in Section 5.3.1, change in influence of cathodic protection potential with crack length, is attributed to lack of penetration of cathodic protection current into cracks deeper than nominally 5.00mm. An interesting general feature is that restricted crack tip opening displacement present in weld metal, appears not to influence significantly crack tip electrochemical corrosion reactions. As a result, the influence of restricted environmental access at the crack tip, often discussed in literature, is considered to be an influence associated with threshold conditions and not stage II growth in the Paris region.

The nature of the relationship between influence of cathodic protection potential and crack depth was assessed by examination of associated fracture surfaces, using a scanning electron microscope. Two groups of fracture surfaces were examined, those which had been

chemically cleaned to remove corrosion products and associated surface deposits and those direct from the test environment, complete with surface deposits. Of the specimens examined direct from the test environment, those associated with conditions of cathodic protection potential were found to have a common, significant feature. Namely, that irrespective of applied cathodic protection potential, the fracture surfaces were found to be coated with calcareous deposits, whose density was found to reduce with crack length. Sides of the starter notch, pre-fatigue fracture surfaces and external specimen surfaces were found to have a uniform and relatively dense calcareous coating. Away from the pre-fatigue fracture area, calcareous deposits were found to decrease in density and terminate in virtually no coating in the region of the crack tip. This particular feature of the results was considered to indicate that a pH gradient was present within the crack and that access of cathodic protection current was possibly limited by a critical value of crack opening displacement.

Results from examination of 'cleaned' fracture surfaces are presented in summary form in Table 9, with associated fractographic evidence presented in Figures 23 to 25 respectively. The following features were considered to be significant :-

(1) Hydrogen embrittlement, witnessed by way of quasi-cleavage facets was found to be a common feature in all fracture surfaces. It was, however, noted with interest that for conditions of applied cathodic protection potential, quasi-cleavage facets were most clearly defined for crack lengths less than approximately 15.0mm.

(2) Formation of corrosion pits was found to be a common feature in all fracture surfaces. However, it was particularly noticeable that corrosion pitting attack was most severe under conditions of nominal correct cathodic protection potential of $-780mV_{SCE}$ and associated crack length > 15.0mm. Whereas it was less severe under conditions of cathodic overprotection potential of $-1100mV_{SCE}$. It was also noted that compared to equivalent data for parent plate material, weld metal fracture surfaces generally exhibited more severe corrosion pitting attack, especially at crack lengths in excess of 15.00mm, irrespective of applied cathodic protection potential. This feature of the results was considered to indicate that possibly, anodic dissolution reactions in weld metal are particularly sensitive to the level of plastic strain, in a manner that parent plate material is not. This effect could also be associated with the size of the plastic zone.

(3) Initial high values of environmental enhancement factor shown in Figure 22, were correlated with enhanced hydrogen embrittlement in all fracture surfaces for crack lengths less than approximately 15.0mm. This feature was attributed to the establishment of equilibrium conditions, prior to the commencement of individual corrosion fatigue crack propagation rate tests. Relative differences in level of initial hydrogen embrittlement were attributed to the manner in which embrittlement was induced. Conditions of cathodic overprotection potential were considered to have promoted

forced hydrogen charging of the weld metal. In comparison, conditions of free corrosion potential were considered to have promoted natural hydrogen charging and nominal correct cathodic protection potential was considered to have promoted suppressed natural hydrogen charging. Notwithstanding the artificial nature of this effect, it was nevertheless considered to be valid in relation to offshore environments.

In general, the results of fractographic examination were found to confirm that, in common with data for parent plate material discussed previously, effectiveness of cathodic protection current in weld metal was limited to relatively shallow cracks, less than approximately 5.0mm deep. However, a difference in behaviour between parent plate material and weld metal of major significance was also considered to be present. Namely, that applied cathodic protection potential in weld metal, irrespective of penetration of cathodic protection current, appeared to enhance the strain sensitivity of anodic dissolution reactions. As a consequence, for crack lengths in excess of approximately 15.0mm for which cathodic protection current was considered to be ineffective. Enhanced anodic dissolution reactions were considered to result in severe crack tip blunting with rates of corrosion fatigue crack propagation, below equivalent in -air levels. In this context, degree of reduction in corrosion fatigue crack propagation rate is sensibly independent of applied cathodic protection potential. A further important feature of this result is that crack tip blunting has a dominent influence upon overall corrosion fatigue crack propagation behaviour, to the detriment of possible hydrogen embrittlement.

For weld metal, values of ΔK_{TH}, derived by extrapolation of data presented in Figure 21, are presented in Table 5 and are considered to exhibit the following significant features :-

(1) An environment of aqueous corrosion, in the absence of cathodic protection, was found to reduce the value of ΔK_{TH} to below in -air levels.

(2) An environment of nominally correct cathodic protection potential of - 780 mV, was found to increase the value of ΔK_{TH}, to above in -air levels.

(3) Values of ΔK_{TH} for both weld metal and parent plate material were found to be the same, for an environment of free corrosion, i.e. aqueous corrosion in the absence of cathodic protection.

It should be noted, however, that the values of ΔK_{TH} given in Table 5 are considered to be of less significance in comparison to the overall trend in data indicated. Assignment of significance to absolute values of ΔK_{TH}, was considered to be outside the scope of the project reported herein.

For corrosion fatigue crack propagation in weld metal, values of

Paris parameters C and m derived from graphs presented in Figure 22 are given in Table 3, where the following features were considered to be significant :-

(1) Change in corrosion fatigue crack propagation environment, from laboratory air to simulated sea water was found to promote reduction of constant C, of two orders of magnitude in conjunction with a relatively small increase in exponent m of approximately 20%.

(2) Magnitude of exponents m for environments of free corrosion potential and cathodic protection potential of - 780 mV_{SCE} were found to be the same, whereas respective values of constant C were reduced by a factor of approximately 20%.

(3) An environment of cathodic overprotection potential of - 1100 mV_{SCE} was found to promote an increase in magnitude of constant C by approximately 20% and negligible reduction in exponent m, compared to an environment of free corrosion. Overall, the trend in weld metal data present in Table 3, was considered to be consistent with the proposal discussed previously in Section 5.3.1. Namely, that exponent m reflected the influence of microstructure and constant C reflected the influence of environment. This is not, however, consistent with the change in plastic zone size in relation to parent plate material.

The trends in data discussed above, promoted the expectation that magnitude of corrosion fatigue endurance in weld metal would exhibit dependence upon applied cathodic protection potential in general, but be independent of precise level of protection applied. For the corrosion fatigue crack propagation rate tests reported herein, endurance data calculated by numerical integration of appropriate Paris crack propagation rate relationships for crack growth between crack lengths of 15.0mm and 18.0mm, are presented in Table 6. The significant features of this data are considered to be :-

(1) The overall level of predictive accuracy achieved by numerical integration was found to be of the order of ± 8%.

(2) The trend in both measured and calculated values of endurance was found to reflect the bias exhibited by the curves presented in Figure 35, for crack lengths in excess of 15.0mm.

(3) Corrosion fatigue endurance associated with conditions of cathodic overprotection potential, was found to be in excess of the in-air value. It was also noted that for environments of cathodic protection potential in general, measured values of endurance recorded direct from the test machine were found to be in close agreement whereas a sizeable difference was present in the respective, predicted values derived by integration.

Close agreement of measured values was not unexpected, in view of the noted lack of penetration of cathodic protection current and

the virtual error free method of cycles counting employed in the test machine. Variation in predicted values was attributed to the combined influence of arithmetical errors present in integration of appropriate Paris relationships and general experimental errors present in derivation of the Paris parameters C and m.

Overall, the results for corrosion fatigue crack propagation rate tests in weld metal were considered to have two features of major significance :-

(1) Critical crack length for effective penetration of cathodic protection current, was found to be approximately 15.0mm, the same as previously discussed for parent plate material in Section 5.3.1. This feature was considered to confirm that corrosion protection by means of applied cathodic protection current was a surface related phenomenon.

(2) In contrast to the behaviour exhibited by parent plate material, as previously discussed in section 5.3.1, weld metal was considered to be particularly sensitive to environmental influences in respect of corrosion fatigue crack propagation behaviour. This sensitivity was attributed to the combined influence of a smaller crack tip plastic zone size with an associated steeper strain gradient in a material with a lower K_{1c} value. From photographic evidence it is apparent that the result is enhanced corrosion attack on the fracture surface. However, the mechanism by which enhanced corrosion attack occurs is undetermined at present and could usefully be made the subject of future research.

5.3.3. *Corrosion Fatigue Crack Propagation Rate Behaviour in Heat Affected Zone Microstructures*

For stress relieved heat affected zone microstructure, corrosion fatigue crack propagation rate data associated with environments of free corrosion, nominal correct cathodic protection potential, - 780 mV, and cathodic overprotection potential, - 1100 mV, is presented in Figure 26 in the form of graphs of log da/dan against log ΔK. The principal features of the curves presented in Figure 26 were considered to be :-

(1) Trend in data associated with conditions of cathodic overprotection potential, was found to have a form characteristic of stress corrosion dominated crack propagation behaviour

(2) For values of ΔK less than approximately 24 M.Pa.$\sqrt{m}$, correct cathodic protection potential was found to promote closest approach of crack propagation rates to in-air values. Whereas for values of ΔK in excess of 24 M.Pa.$\sqrt{m}$, correct cathodic protection potential was associated with maximum rates of corrosion fatigue crack propagation.

(3) For values of ΔK in the range, approximately, 30 M.Pa.$\sqrt{m}$ to 44 M.Pa.$\sqrt{m}$, cathodic overprotection potential was found to promote below in-air rates of corrosion fatigue crack propagation. This particular feature of the results contrasts with the trend exhibited by equivalent data for parent plate material, presented in Figure 16, in which propagation rates were shown to be generally in excess of associated in-air values.

In general, the significance of the data presented in Figure 26 was considered to be that influence of cathodic protection potential on corrosion fatigue crack propagation behaviour in heat affected zone microstructure was essentially the same as previously discussed in respect of parent plate material, with one notable excaption. Namely, that an environment of cathodic overprotection potential was found to promote below in-air rates of corrosion fatigue crack propagation, whereas in parent plate material, it did not. This particular feature of the results was attributed to limited enhancement of anodic dissolution activity in the region of the crack tip which was considered to cause crack tip blunting and associated reduced rates of corrosion fatigue crack propagation. In this context, enhanced anodic dissolution was considered to be responsible due to the combined influence of high hardness, coarse grain structure, material strain sensitivity and lack of penetration of applied cathodic protection current into the occluded region at the crack tip.

In common with previous discussion, for parent plate material and weld metal, environmental enhancement factor was plotted against ΔK as shown in Figure 27, for corrosion fatigue crack propagation in each of the test environments. The principal features of the curves presented in Figure 27 were considered to be :-

(1) Environments of free corrosion and correct cathodic protection potential were found to promote positive values of environmental enhancement factor at all values of ΔK. It was, however, noted that insignificant values of environmental enhancement factor were associated with values of ΔK in the range 26 to 32 M.Pa.$\sqrt{m}$. A feature, that was clearly reflected in Figure 36. Also for values of ΔK in excess of approximately 32 M.Pa.$\sqrt{m}$, both curves were found to exhibit a divergent trend with increase in ΔK.

(2) Cathodic overprotection potential was found to promote maximum, initial, values of environmental enhancement factor, whereas for ΔK less than approximately 30 M.Pa.$\sqrt{m}$, minimum values were found to be associated with correct cathodic protection potential.

(3) The general trend in environmental enhancement factor data for heat affected zone microstructure, was considered to be the same as that exhibited for parent plate material in Figure 17, with a significant exception, namely, that for an environment of cathodic overprotection potential and ΔK in excess of 30 M.Pa.$\sqrt{m}$, associated values of environmental enhancement factor were found to be negative.

In common with previous discussion of data associated with parent plate material and weld metal, corrosion fatigue crack propagation

rate in heat affected zone microstructure was plotted against crack length, for each of the test environments, as shown in Figure 36. The following features were considered to be significant :-

(1) An environment of nominal correct cathodic protection potential was found to promote maximum rates of corrosion fatigue crack propagation for crack lengths in excess of approximately 14.5mm and minimum rates, i.e. closest approach to in-air values, for crack lengths less than 14.5mm.

(2) For crack lengths in excess of 14.5mm, trends in data associated with environments of free corrosion and correct cathodic protection potential, were found to be sensibly coincident. This feature was considered to be consistent with the proposal discussed previously in Section 5.3.1., namely that cathodic protection current at correct cathodic protection potential, did not penetrate into cracks deeper than approximately 5.0mm.

(3) For crack lengths in excess of 14.5mm, trend in data associated with an environment of cathodic overprotection potential was found to be sensibly coincident with data associated with in-air conditions. This feature of the result was in marked contrast to the trend in data for crack lengths less than 14.5mm, where cathodic overprotection potential was found to promote maximum rates of corrosion fatigue crack propagation.

The proposal that in general, behaviour of heat affected zone microstructure was essentially the same as that of parent plate material, was confirmed by fractographic examination of relevant heat affected zone fracture surfaces. Overall, results from fractographic examination were not found to differ significantly from those previously reported for parent plate material, in Table 7, with one important exception, namely that heat affected zone fracture surfaces associated with cathodic overprotection potential, were found to exhibit similar detail to that found in equivalent weld metal fracture surfaces, reported in Table 9 and previously discussed in Section 5.3.2. This result was considered to be consistent with the proposal discussed previously, that the heat affected zone microstructure was susceptible to the effects of strain enhanced anodic dissolution under the influence of excessive cathodic protection potential.

For heat affected zone microstructures values of ΔK_{TH} derived by extrapolation of data presented in Figure 26, are presented in Table 5, where the following features were considered to be significant :-

(1) General values of ΔK_{TH} associated with heat affected zone microstructure, irrespective of environment, were found to be lower than comparable data for both parent plate material and weld metal.

(2) An environment of nominal correct cathodic protection potenial was found to increase the value of ΔK_{TH} to above in-air

levels.

(3) An environment of free corrosion was found to reduce the value of ΔK_{TH}, to below in-air levels.

It should be noted, however, that absolute values of ΔK_{TH} given in Table 5 were considered to be of less significance, in comparison with the overall trend in data indicated. Namely, that in common with previous discussion, in respect of a proposed critical crack depth for effective penetration of cathodic protection current. Data presented in Table 5 was considered to indicate that nominal correct cathodic protection potential, has a potentially beneficial influence in the threshold region, where it can be assumed that an initial defect is likely to be less than 5mm deep. In this respect a significant general feature of the data presented in Table 5, is that an environment of nominal correct cathodic protection potential was shown to promote an increase in value of ΔK_{TH}, for all microstructures tested.

For corrosion fatigue crack propagation in heat affected zone microstructures, values of Paris parameters C and m , derived from graphs presented in Figure 26, are given in Table 3 where the following features are considered to be particularly significant :-

(1) Change in crack propagation environment from laboratory air to simulated sea water was found to promote an increase in exponent m of approximately 50% with an associated reduction in constant C.

This feature of the results was in marked contrast to the close agreement exhibited by equivalent data for parent plate material.

(2) Values of constant C and exponent m for heat affected zone microstructure were found to be influenced by environment in a manner not exhibited in equivalent data for parent plate material.

(3) For both heat affected zone microstructure and parent plate material, close agreement was found between respective values of exponent m , associated with environments of free corrosion and cathodic overprotection potential.

(4) The general trend in influence of nominal correct cathodic protection potential, on the values of constant C and exponent m for heat affected zone microstructure was found to be opposite to that exhibited by parent plate material.

(5) Not withstanding the general similarity of behaviour exhibited by heat affected zone microstructure and parent plate material, specific differences in value of constant C and exponent m,presented in Table 3, were considered to promote the expectation that corrosion fatigue endurance in heat affected zone microstructure, would be in excess of that for parent plate material, in a given environment.

(6) For heat affected zone microstructure, the relative influence

of environment and microstructure on the magnitude of Paris parameters C and m , previously proposed in respect of parent plate material, was found to be not as clearly defined. Apparent lack of definition was attributed to the combined influence of general experimental errors, inhomogeneous microstructure, variation in material hardness in the line of crack advance and deviation in direction of crack advance, away from the high hardness region of the heat affected zone towards the softer parent plate.

Endurance data, for corrosion fatigue crack propagation in heat affected zone microstructure, is presented in Table 6 in way of measured and calculated and predicted values. Measured values were obtained from the test machine, predicted values were obtained by numerical integration of appropriate Paris crack propagation rate relationships, given by the parameters in Table 3, for a fixed interval of crack growth 15.0 - 18.0mm. The principal features of this data were considered to be :-

(1) Irrespective of environment, both measured and predicted endurance was found to be in excess of that for parent plate.

(2) Trends in both measured and predicted values of endurance, were found to reflect the bias exhibited by the curves presented in Figure 36, for crack lengths in excess of approximately 14.5mm.

(3) Endurance associated with an environment of cathodic overprotection potential, was found to be in excess of the equivalent in-air value.

(4) Minimum value of endurance was found to be associated with an environment of nominal correct cathodic protection potential.

(5) Overall accuracy of predicted endurance values relative to measured values, was found to be in the range - 3 to + 12%. The unusually large error, + 12%, associated with an environment of cathodic overprotection potential, was attributed to the combined influence of poor data fit , and associated accumulative errors present in derivation of Paris parameters C and m . In general, however, the high level of predictive accuracy demonstrated was considered to vindicate the technique of prediction of corrosion fatigue endurance by integration of appropriate Paris corrosion fatigue crack propagation rate relationships.

Overall, the results from corrosion fatigue crack propagation rate tests in heat affected zone microstructure were considered to exhibit the following major features :-

(1) Critical crack length for effective penetration of cathodic protection current was found to be approximately 14.5mm.

This result compared favourably with equivalent values of critical crack length, derived from parent plate material and weld metal, previously discussed in Sections 5.3.1 and 5.3.2 respectively.

(2) Except for an environment of cathodic overprotection potential, heat affected zone microstructure was generally found to behave in the same manner as BS 4360 50D type structural steel, but with enhanced levels of corrosion fatigue endurance for a given environment.

5.3.4 *Corrosion Fatigue Crack Propagation Rate Behaviour in Fusion Line Microstructure*

For stress relieved fusion line microstructure, corrosion fatigue crack propagation rate data associated with environments of free corrosion, nominal correct cathodic protection potential and cathodic overprotection potential is presented in Figure 28, in the form of graphs of log da/dN against log ΔK. The principal features of these graphs were considered to be :-

(1) Data associated with an environment of cathodic overprotection potential was found to have a form characteristic of stress corrosion dominated crack propagation behaviour.

(2) The trend in data associated with an environment of correct cathodic protection potential was found not to exhibit reversal with increase in level of ΔK, in the manner previously discussed for parent plate, weld metal and heat affected zone microstructures.

(3) For values of ΔK less than approximately 31 M.Pa.$\sqrt{m}$, an environment of correct cathodic protection potential was found to promote closest approach of corrosion fatigue crack propagation rates to in-air values. Whereas, for values of ΔK in excess of 31 M.Pa.$\sqrt{m}$, below in-air rates of crack propagation were promoted by an environment of cathodic overprotection potential.

(4) For above transition crack growth, the near-parallel trend in data present in Figure 28, was considered to create the expectation that irrespective of environment, close agreement would be exhibited by associated values of Paris exponent m .

The significance of the above features was considered to be that cathodic protection potential in general was shown to have a particularly favourable influence on corrosion fatigue crack propagation behaviour, especially as an environment of cathodic overprotection potential was found to promote below equivalent in-air rates of corrosion fatigue crack propagation, for levels of K in excess of approximately 31 M.Pa.$\sqrt{m}$.

In common with previous discussion for parent plate, weld metal and heat affected zone microstructures, environmental enhancement

factor was plotted against ΔK, as shown in Figure 29, for corrosion fatigue crack propagation in each of the test environments. The principal features of the curves presented in Figure 29, were considered to be :-

(1) Environments of free corrosion and nominal correct cathodic protection potential were found to promote positive values of environmental enhancement factor, at all values of ΔK. It was noted in particular that for both curves, the trend in data was convergent with in-air performance.

(2) For values of ΔK in excess of approximately 34 M.Pa.√m, an environment of cathodic overprotection potential was found to promote negative values of environmental enhancement factor.

(3) For all environments, maximum values of environmental enhancement factor were found to be associated with minimum values of ΔK. It was noted in particular, that maximum initial values of environmental enhancement factor were associated with an environment of cathodic overprotection potential. Whereas for the same value of ΔK, minimum initial values were found to be associated with an environment of nominal correct cathodic protection potential. In common with previous discussion for parent plate, weld metal and heat affected zone microstructures, high initial values of environmental enhancement factor, were attributed to the influence of hydrogen charging , associated with the establishment of equilibrium conditions, prior to commencement of corrosion fatigue testing.

The overall significance of the features noted above,was considered to be that response of fusion line microstructure to cathodic protection potential in general was found to exhibit a combination of parent plate and weld metal behaviour. In view of the inhomogeneous nature of microstructure in the region of the fusion line, due to the influences of thermal cycle and chemical dilution of parent plate material into weld metal, this trend in behaviour was not unexpected.

Combined parent plate and weld metal behaviour was also considered to be reflected in the graphs of corrosion fatigue crack propagation rate against crack length, presented in Figure 37. The principal features of this data were considered to be :-

(1) For crack lengths less than approximately 14.6mm, an environment of nominal correct cathodic protection potential was found to promote rates of corrosion fatigue crack propagation, closest to associated in-air values.

(2) For crack lengths in excess of 14.6mm, the curve associated with an environment of correct cathodic protection potential was located almost centrally between the respective curves for environments of free corrosion and cathodic overprotection potential. Further, at high values of ΔK, the curve for

correct cathodic protection was found to converge with the curve associated with in-air data.

(3) For crack lengths in excess of 14.6mm, an environment of cathodic overprotection potential was found to promote corrosion fatigue crack propagation rates at below equivalent in-air levels.

The overall significance of the data presented in Figure 37 was considered to be that in common with previous discussion for parent plate, weld metal and heat affected zone microstructures. Cathodic protection current was considered not to penetrate into cracks deeper than approximately 5.0mm. In this context it was noted from fractographic examination of associated fracture surfaces that surface detail for fusion line microstructure was similar in nature to that previously discussed for weld metal, as summarised in Table 9.

Values of ΔK_{TH} by extrapolation of data presented in Figure 28, are presented in Table 5, where the following features were considered to be particularly noteworthy :-

(1) An environment of nominal correct cathodic protection potential, was found to increase the value of ΔK_{TH} to above in-air levels. Further, value of ΔK_{TH} in fusion line microstructure was shown to be comparable to that recorded for parent plate material, under identical environmental conditions.

(2) Notwithstanding the result noted above in general,values of ΔK_{TH} for fusion line microstructure were found to be in excess of those for heat affected zone but less than equivalent values for parent plate material.

As discussed in previous sections, absolute values of ΔK_{TH} given in Table 5, were considered to be of less significance in comparison to the overall trend in data indicated, namely that an environment of nominal correct cathodic protection potential was likely to have a beneficial effect upon overall corrosion fatigue endurance, through enhancement of the threshold level for corrosion fatigue crack propagation. More detailed discussion of the significance of absolute values of ΔK_{TH} was not pursued, as it was considered to be beyond the scope of the project reported herein.

Values of Paris parameters constant C and exponent m , derived from the graphs presented in Figure 28, are given in Table 3. The principal features of this data were considered to be :-

(1) Change in crack propagation environment from laboratory-air to simulated seawater in the absence of cathodic protection potential, was shown to promote a relatively minor decrease in magnitude of exponent m , with an associated increase in constant C of an order of magnitude. In this context, it was noted that the trend in mechanical behaviour of fusion line microstructure was comparable to that of parent plate material, whereas electrochemical behaviour was comparable to that of weld metal.

(2) Environments of free corrosion and applied cathodic protection potential, were shown to promote comparatively minor changes in value of constant C in the range 2.70 to 1.80 and a sensibly constant value of exponent m of the order of 2.20.

The overall significance of the data presented in Table 3 was considered to be that it related corrosion fatigue crack propagation rate in fusion line microstructure, to that of the major constituent microstructures present in a structural steel weldment. Namely, parent plate, heat affected zone and weld metal. As a consequence, therefore, by reference to data presented in Table 3, relative significance of corrosion fatigue crack propagation at a given location within a structural steel weldment, can be assessed in relation to its likely influence on attainment of the desired level of corrosion fatigue endurance.

Endurance data for corrosion fatigue crack propagation in fusion line microstructure, is presented in Table 6 by way of measured and calculated or predicted values. Measured values were obtained from the test machine, predicted values were obtained by numerical integration of appropriate Paris crack propagation rate relationships, given by the parameters in Table 3, for a fixed interval of crack growth 15.0 - 18.0mm. The principal features of this data were considered to be :-

(1) Irrespective of environment, both measured and predicted endurance was found to be in excess of that for parent plate material, but generally less than that of weld metal.

(2) Trends in both measured and predicted values of endurance, were found to reflect the bias exhibited by the curves presented in Figure 37, for crack lengths in excess of approximately 14.6mm.

(3) Maximum endurance was found to be associated with an environment of cathodic overprotection potential and was equal to the equivalent in-air value.

(4) In common with endurance data for weld metal, minimum value of endurance was found to be associated with an environment of free corrosion.

(5) Overall accuracy of predicted endurance values was found to be in the range - 4 to + 3%.

The overall significance of the foregoing results and discussion contained in Sections 5.3.1 to 5.3.4 inclusive was considered to be that cathodic protection current did not penetrate into cracks deeper than approximately 5.0mm and could therefore be regarded as a surface related phenomenon. Whereas applied cathodic potential was considered to be effective in cracks deeper than approximately 5.0mm, through enhancement of anodic dissolution reactions at the crack tip, which was found to promote below equivalent in-air rates of corrosion fatigue crack propagation.

Hydrogen embrittlement promoted by natural electrochemical corrosion reactions, was identified as a major adverse influence upon corrosion fatigue crack propagation rates, in all microstructures tested, especially at minimum values of ΔK with associated crack lengths, less than approximately 14.5mm. Hydrogen embrittlement in cracks larger than approximately 14.5mm, was considered to be of secondary importance in comparison to the influence of gross crack tip blunting, promoted by enhanced anodic dissolution reactions in the region of the crack tip. Gross crack tip blunting was considered to result in reduced levels of crack tip stress intensity factor which were ultimately found to promote below in-air rates of corrosion fatigue crack propagation. This effect was particularly severe in relatively 'hard' microstructures such as weld metal, heat affected zone and fusion line.

5.3.5 *Corrosion Fatigue Crack Propagation Rate Behaviour in Parent Plate Material in an Environment of Simulated Tidal Immersion*

The trend in corrosion fatigue crack propagation behaviour in stress relieved parent plate material, is shown in a typical graph of crack length a against number of fatigue cycles N , presented in Figure 30. The principal feature of this graph was, that for crack lengths in excess of approximately 11.5mm, the amount of crack growth associated with an environment of free corrosion was found to be in excess of that associated with an environment of laboratory air, in a ratio of approximately 2 : 1.

A particularly interesting feature of this result, was that correlation between trend in crack growth behaviour and environment was not present for crack lengths in excess of approximately 15.0mm. Further, from consideration of the associated Paris crack propagation rate relationships, for equilibrium environments derived from data given in Table 3, approximate equivalent ratio of crack growth rate was found to be 1.3 : 1. This apparent contradiction was attributed to the following factors :-

(1) Corrosion fatigue crack propagation rate tests reported herein, were conducted under conditions of constant load-amplitude. As a consequence, increase in K with crack length could be expected to promote an inherent increase in crack propagation rate, irrespective of environment.

(2) An environment of simulated tidal immersion is non-equilibrium in nature. Therefore associated corrosion fatigue crack propagation rate data is not comparable with equivalent data associated with single environment, equilibrium conditions. As a consequence of the factors noted above, lack of correlation between respective crack growth ratios was not considered to be unexpected.

In general, the significance of the data presented in Figure 30, was considered to be that it demonstrated the marked influence of non-equilibrium environmental conditions, on corrosion fatigue crack propagation rate behaviour in structural steel.
Assessment of the growth mechanism responsible for the trend in growth

behaviour, exhibited in Figure 30, was attempted by fractographic examination of associated fracture surfaces. This examination was unsuccessful as all fracture surfaces were found to be severely corroded with total destruction of surface detail. As a consequence, assessment of the likely growth mechanism was based on consideration of data presented in Figure 30 only.

From previous discussion, it will be recalled that hydrogen embrittlement was considered to generally enhance corrosion fatigue crack propagation rates, particularly in BS 4360 50D type structural steel. Enhanced crack growth exhibited in Figure 30, during periods of free corrosion environment, was considered to be consistent with the influence of embrittlement. It should be noted, however, that an environment of free corrosion could also be expected to promote anodic dissolution reaction reactions at the crack tip with an associated tendency for crack-tip blunting to occur. For early stages of crack development, i.e. short crack length, adverse influence of embrittlement could be expected to outweigh possible beneficial influence of crack tip blunting, provided that an environment of excess hydrogen was maintained.

However, if aqueous environment was abruptly removed and not reinstated, it was considered that limited influence of embrittlement would be maintained, pending final exhaustion of the aqueous medium from the crack tip region. Thereafter it could be expected that in-air conditions of fatigue crack propagation would be established by re-sharpening of the crack tip in conjunction with reduced rates of crack propagation. The combined influence of which was considered to result in the trend in data, exhibited in Figure 30.

It was also noted with particular interest, that measured endurance for crack growth in the interval 15.0 - 18.0mm, was found to be of the order of 9750 cycles. Whereas from data in Table 6, maximum endurance associated with equilibrium conditions was given as 9400 cycles, for an environment of laboratory air. As a consequence, it was considered that influence of intermittent or tidal immersion or corrosion fatigue crack propagation behaviour in BS 4360 50D type structural steel was favourable, with a tendency to exceed equivalent in-air levels of endurance.

5.3.6 *Corrosion Fatigue Crack Propagation Rate Behaviour in Weld Metal Material in an Environment of Simulated Tidal Immersion*

The trend in corrosion fatigue crack propagation behaviour in stress relieved weld metal, is shown in a typical graph of crack length a against number of fatigue cycles N, presented in Figure 31. The principal feature of this data, together with data from two repeat tests, was that 'crack arrest' was found to consistently occur at a crack length of approximately 14.5mm.

It was noted with interest, that for initial phases of crack growth presented in Figure 31, the relative growth ratio, of free corrosion to in-air rates, was found to be approximately 2 : 1, comparable to the value discussed previously in Section 5.3.5, for parent plate material. However, subsequent to the initial growth phase, the crack growth rate

was found to progressively reduce and ultimately attain a zero level, for crack lengths in excess of approximately 14.5mm.

The significance of the trend in data, shown in Figure 31, was considered to be that intermittent or tidal immersion was shown to inhibit corrosion fatigue crack propagation in weld metal, by the mechanism of crack arrest , especially as the phenomenon of crack arrest was absent in equivalent data for parent plate material, previously discussed in Section 5.3.5.

Assessment of the crack propagation mechanism responsible for growth in an environment of tidal immersion, was attempted by examination of associated fracture surfaces, using a scanning electron microscope. However, as previously noted in Section 5.3.5, all fracture surfaces were found to be severely corroded with total destruction of surface detail. As a consequence, assessment of a possible growth mechanism was limited to consideration of data presented in Figure 31 only.

The trend in initial corrosion fatigue crack growth data, associated with the first phase of immersion, at free corrosion potential, was considered to be consistent with an embrittlement dominated crack propagation mechanism, of the kind previously discussed in Section 5.3, for an environment of free corrosion. The trend in data associated with the subsequent phase of in-air growth, was considered to reflect the influence of residual embrittlement , in the manner previously discussed in Section 5.3.5. Namely that initial growth in the in-air phase, was dominated by embrittlement influences promoted by residual aqueous environment at the crack tip. Following exhaustion of residual aqueous environment, from the crack-tip region, mechanical resharpening of the crack tip was considered to occur, in association with reduced rates of crack propagation, as reflected in the initial stage of the retarded phase of crack growth, exhibited in Figure 31.

However, the significant difference in behaviour of weld metal, compared to that of parent plate, was considered to occur on subsequent reinstatement of aqueous conditions at free corrosion potential. In this context it should be recalled from previous discussion, that anodic dissolution in weld metal can be considered to be strain sensitive. As a consequence, it is proposed that for the particular phase of corrosion fatigue crack propagation in question, strain enhanced anodic dissolution, possibly resulted in gross blunting of the crack tip region, with associated reduced levels of crack tip stress intensity factor. In this context, the beneficial influence of reduced crack tip stress intensity factor, was considered to outweigh the adverse influence of embrittlement, promoted by natural electrochemical corrosion reactions. As a consequence, progressive reduction in corrosion fatigue crack propagation rate was continued from the previous in-air phase of growth, as reflected in Figure 31.

During the following in-air phase of crack growth, limited resharpening of the crack tip was considered to occur, but to an insignificant degree. Subsequent re-instatement of the aqueous environment, at free corrosion potential with increased crack length

was considered to promote further enhancement of anodic dissolution at the crack tip with associated increased crack tip blunting. As a consequence, associated corrosion fatigue crack propagation rate was considered to be further retarded, in the manner reflected in Figure 31. Ultimately, the combined influence of gross crack tip-blunting and limited mechanical re-sharpening, was considered to promote crack arrest , as shown in Figure 31.

5.3.7 *Corrosion Fatigue Crack Propagation Rate Behaviour in Parent Plate Material, in an Environment of Simulated Splash Zone*

Corrosion fatigue crack propagation rate data for stress relieved BS 4360 50D type parent plate material in a simulated splash zone environment is presented graphically in Figure 32, in the form log da/dN against log ΔK. The principal features of this data were considered to be :-

(1) For values of ΔK less than approximately 27 M.Pa.$\sqrt{m}$, crack propagation rates were shown to coincide, initially, with equivalent data for an environment of free corrosion. Thereafter, propagation rates were shown to progressively exceed free corrosion values and to tend towards data associated with an environment of cathodic overprotection potential.

(2) For values of ΔK in the range 27 to 35 M.Pa.$\sqrt{m}$, crack propagation rates were shown to be the highest of any environment.

(3) For values of ΔK in excess of 35 M.Pa.$\sqrt{m}$, crack propagation rates were found to rapidly approach equivalent in-air values.

The significance of the features noted above was considered to be that, influence of splash zone environment was shown to change with level of ΔK. At relatively low values of ΔK, less than approximately 35 M.Pa.$\sqrt{m}$, influence was shown to be generally unfavourable and to have promoted enhanced rates of crack propagation. Conversely, for values of ΔK in excess of approximately 35 M.Pa.$\sqrt{m}$, influence was shown to be generally favourable and to have promoted progressive reduction in crack propagation rates. As a consequence, it was inferred that maximum adverse influence on corrosion fatigue crack propagation rates was likely to occur at short crack lengths, i.e. in the near threshold region.

In common with previous discussion, Environmental Enhancement Factor was plotted against ΔK, as shown in Figure 17. The principal features of the data associated in the splash zone environment were considered to be :-

(1) Initial values of environmental enhancement factor were shown to be equivalent to data for an environment of free corrosion.

(2) For values of ΔK in the range 22 to 27 M.Pa.$\sqrt{m}$, level of environmental enhancement was found to be closest to that associated with an environment of cathodic overprotection potential.

(3) For values of ΔK in the range 27 to 35 M.Pa.$\sqrt{m}$, level of environmental enhancement was found to be maintained at levels in excess of those associated with all other test environments.

(4) For values of ΔK in excess of 35 M.Pa.$\sqrt{m}$, value of environment enhancement factor was found to progressively reduce with increase in ΔK and to ultimately attain minimum value for any test environment.

The significance of the features noted above was considered to be that they reflected the propagation behaviour exhibited in Figure 32. Further, the expectation was created that corrosion fatigue endurance in a splash zone environment would be of similar magnitude to that associated with environments of free corrosion and cathodic overprotection potential. This expectation was vindicated by associated endurance data, given in Table 6, where endurance in splash zone environment was given as 6750 cycles, compared to 7000 and 7250 respectively, for environments of free corrosion and cathodic overprotection.

In this context it was noted with interest in Table 3, that the Paris parameters C and m associated with splash zone environment, were found to exhibit significant differences in comparison to the remainder of data associated with parent plate material.The value of the constant C was found to be in excess of that for equivalent data in-air and free corrosion environments, by an order of magnitude. In contrast, value of exponent m was found to be reduced by a factor of 0.78. The significance of this feature was considered to be that exponent m was shown not to be solely dependent upon microstructural considerations, in the manner proposed in foregoing sections. However, the value of constant C was considered to remain dependent upon environment, as previously proposed.

During conduct of corrosion fatigue crack propagation rate tests, in splash zone environment. It was noted that extensive formation of corrosion products occurred on all specimen surfaces, in conjunction with severe corrosion pitting attack. Comparable degradation was also found to be present on associated fracture surfaces which was considered to preclude examination of fracture surface detail by use of a scanning electron microscope. As a consequence, overall assessment of corrosion fatigue crack propagation behaviour was based on appraisal of derived data only. The increased level of environmental enhancement associated with splash zone environment, was attributed to enhanced anodic dissolution, promoted by increased oxygenation of the aqueous environment in conjunction with turbulent fluid flow. Extensive formation of corrosion products was also attributed to increased level of oxygenation through its influence on enhanced production of hydroxyl irons in the manner summarised in Table 8. Subsequent reduction in level of environmental enhancement factor with increasing ΔK was considered to be consistent with progressive increase in beneficial influence of anodic dissolution at the crack tip, in way of crack tip blunting combined with reduction in the influence of hydrogen embrittlement.

The significance of the foregoing results was considered to be

that splash zone environment was shown to have an unexpected and particularly favourable influence on corrosion fatigue crack propagation behaviour, particularly at relatively long crack lengths. Further, in common with the majority of previous data, irrespective of microstructure or environment, the maximum degree of adverse influence was shown to occur at relatively short crack lengths and associated low values of ΔK, where the critical crack length was found to be of the order of 16.5mm.

5.3.8 *Corrosion Fatigue Crack Propagation Rate Behaviour in Weld Metal Material, in an Environment of Simulated Splash Zone*

Corrosion fatigue crack propagation rate data for stress relieved weld metal in a simulated splash zone environment is present graphically in Figure 33, in the form log da/dN against log ΔK. The principal features of this data were considered to be :-

(1) For values of ΔK less than approximately 29 M.Pa.$\sqrt{m}$, trend in crack propagation rate data was considered to exhibit a high degree of enhancement, which resulted in the following significant effects :-

(A) Initial levels of crack propagation rate were found to be in excess of and divergent from those associated with other test environments, with the exception of cathodic overprotection potential. The divergent trend noted above, was particularly noticeable in relation to data associated with an environment of free corrosion.

(B) Rapid rise in crack propagation rate to levels in excess of those associated with stress-corrosion dominated behaviour, promoted by an environment of cathodic overprotection potential.

(2) For values of ΔK in excess of 29 M.Pa.$\sqrt{m}$, enhancement of crack propagation rates was shown to rapidly decay with increase in ΔK. This was shown to promote a high degree of retardation and ultimately resulted in rates of corrosion fatigue crack propagation, noticeably below equivalent in-air levels.

The significance of the features noted above was considered to be that splash zone environment was shown to have an inconsistent influence upon corrosion fatigue crack propagation behaviour. In a general manner similar to that discussed previously for parent plate material, in Section 5.3.7. For weld metal in particular, the apparent increased degree of influence over that exhibited by equivalent data for parent plate material, was attributed to increased sensitivity of weld metal to anodic dissolution reactions, as previously discussed in Section 5.3.2, enhanced by particular environmental conditions of high oxygenation of the aqueous environment in conjunction with turbulent fluid flow. Enhanced sensitivity was considered to be particularly relevant to the trend in data at high values of ΔK, where 'excessive' crack tip-blunting could be expected to promote retardation in crack propagation rate, in a manner consistent with the trend in data exhibited in Figure 33.

In common with previous discussion, Environment Enhancement Factor was plotted against ΔK, for corrosion fatigue crack propagation in a splash zone environment, as shown in the associated graph presented in Figure 22. The principal features of this data were considered to be :-

(1) Initial values of environmental enhancement factor were found to be in excess of 4.0.

(2) For values of ΔK in the range 28 to 36 M.Pa.$\sqrt{m}$, environmental enhancement factor was found to be maintained at levels in excess of those associated with all other test environments.

(3) For values of ΔK in excess of 36 M.Pa.$\sqrt{m}$, environmental enhancement factors were found to be progressively reduced with increase in ΔK and to ultimately attain negative values. In this context, it was noted in particular that for values of ΔK in excess of approximately 39 M.Pa.$\sqrt{m}$, associated rates of corrosion fatigue crack propagation were below equivalent in-air values.

The overall significance of the features noted above was considered to be that trend in environmental enhancement factor data reflected the crack propagation rate behaviour, exhibited in Figure 33. Further, the adverse influence of hydrogen embrittlement in initial stages of crack growth was clearly identified by high values of environmental enhancement factor.

For crack growth in the range 15.0 to 18.0mm, the trend in the data present in Figure 22 was considered to create the expectation that endurance in splash zone environment would be in excess of the value associated with an environment of free corrosion, but would be less than that associated with environments of both cathodic protection potential in general and laboratory air. This expectation was considered to be vindicated by associated corrosion fatigue endurance data, given in Table 6. In this context, it was noted with interest in Table 3, that values of Paris parameters C and m associated with splash zone environment were found to exhibit major differences in comparison to the remainder of data related to corrosion fatigue crack propagation in weld metal. Value of constant C was found to be in excess of equivalent data for free corrosion environments by four orders of magnitude. In contrast, the value of exponent m was found to be reduced by approximately 70%. The significance of this feature of the data was considered to be, that in common with comparable data for parent plate material, discussed previously in Section 5.3.7, the exponent m was shown not to be solely dependent upon microstructural considerations, in circumstances where embrittlement ceased to have a significant influence upon corrosion fatigue crack propagation behaviour, due to dominance by the effects of crack tip blunting.

During conduct of corrosion fatigue crack propagation rate tests in splash zone environment, extensive corrosion attack of all specimen surfaces was found to have occurred in an identical manner to that discussed previously in Section 5.3.7 in respect of parent plate material. As a consequence, overall assessment of corrosion fatigue crack propagation behaviour was based, as before, on appraisal

of derived data only. Initial high values of environment enhancement factor, exhibited in Figure 22, were considered to reflect the adverse influence of hydrogen embrittlement, promoted by the establishment of equilibrium conditions prior to the commencement of testing. Subsequent rapid decrease in values of environmental enhancement factor with increase in ΔK, was considered to reflect the influence of enhanced anodic dissolution reactions at the crack tip, which were considered to increase progressively the degree of crack tip blunting with associated decrease in corrosion fatigue crack propagation rate. As a consequence, the influence of inherent embrittlement, promoted by natural electrochemical corrosion reactions, was considered to be progressively reduced and ultimately nullified by the effects of crack tip blunting.

5.4 DISCUSSION OF CRACK MONITORING AND DATA PROCESSING METHODS

It will be recalled from the literature survey, that for accurate measurement of crack length under conditions of corrosion fatigue, a number of authors (12, 25), have developed a crack monitoring technique that is based upon the change in specimen compliance with increase in crack length. It is apparent, however, that in terms of the accuracy to which this technique can measure actual crack lengths, it is doubtful whether this technique offers any significant improvement over more conventional optical methods. It is also important to note that the change in compliance technique does not provide a direct measurement of actual crack length. The actual crack length is derived by reference calibration data, which is often obtained by use of mathematical modelling techniques in conjunction with optical crack length monitoring of fatigue specimens in air. Notwithstanding the inherent reliance on the accuracy of prior-calibration of fatigue specimens in-air, advocates of the technique argue that under conditions of corrosion fatigue, it is the only feasible method of crack length monitoring, particularly as it can be considered to accommodate both crack-front curvature, which is popularly assumed to be present in all specimens, and the masking of specimen surfaces due to the formation of corrosion products or calcareous scales, etc.

In the context of the project reported herein, the above arguments are considered to be fallacious for the following reasons :-

(1) All specimens used in this project were manufactured with a nominal thickness of 15.00mm (B = 15). This thickness was derived from the relationship $B \geq 2.5 (K_{max}/\sigma_y)$, which defines the specimen thickness required for essentially plane strain conditions of the crack tip. This relationship was in turn developed from a standard expression $B \geq 2.5(K_{1c}/\sigma_y)^2$, which is used extensively to define the specimen thickness required for valid K_{1c} testing.

The practical significance of a thickness measurement of 15.00mm, is that a crack could be expected to grow under predominantly plane strain conditions with an associated lack of significant crack front curvature. For this project, the lack of significant crack front curvature was confirmed by direct observations, post test.

Therefore possible compensation for the influence of crack front curvature on the accurate measurement of crack length, was not a significant consideration for this project.

(2) By careful, localised cleaning of the specimen surfaces, using a mild abrasive and cotton wool swabs, it was found that in all experiments, the fatigue crack could be satisfactorily observed, irrespective of environmental conditions.

Further, it should be noted that the change in compliance technique has two particular limitations that are worthy of special consideration, namely :-

(1) The technique is not capable of satisfactorily monitoring the discontinuous nature of corrosion fatigue crack propagation.

(2) The technique will not discriminate between crack growth in the, normal, plane of fracture and out-of-plane growth, of the kind reported herein for growth in the heat affected zone region.

In view of the lack of any significant benefit associated with the use of change in compliance crack monitoring, the complexity and cost of such a system was not considered to be justified for the project reported herein. As a consequence, an optical crack monitoring technique was developed and was applied mose successfully throughout the project reported herein. The technique was based upon the use of a vernier type travelling microscope and was found to be reliable in operation and capable of producing very accurate measurements of crack length. In view of the success achieved using optical crack monitoring in this project, it is concluded that ease of automation and compatability with computer based data gathering systems is possibly the overriding but unstated motive for the apparent popularity of the change in compliance and electrical crack monitoring techniques, particularly the A.C.p.d. method.

For corrosion fatigue crack propagation rate studies in general, the accuracy of the growth rate data produced can be considered to be significantly influenced by the choice of method used to process basic crack length, against number of elapsed cycles data. In this context it will be recalled from the literature survey that data processing methods can be either graphical or computer based and can be considered to have a significant influence on the degree of data scatter, but to have essentially no influence on the central trend of data. It should be noted in particular, however, that in the literature survey, graphically based methods were considered to be inherently over-subjective and of no practical use. This proposal is, at best, considered to be an unsubstantiated overstatement, not supported by the results obtained from the project reported herein. It is also considered to be directly contradicted by the results obtained from a limited appraisal of the two, most popular computer-based data processing methods.

The Finite Difference method was found to exaggerate the discontinuous nature of corrosion fatigue crack growth and as a consequence tended to produce excessively high levels of data scatter. Variable levels of data scatter were found to be associated with curve fitting to a 2nd order polynomial expression over a limited range of 5 or 7 data points, the so-called splining method . Further, from back-plotting it was found that a 2nd order polynomial curve did not consistently reflect the original a versus N' data, to an acceptable degree of accuracy. As a consequence, gross smoothing of the original data was invariably introduced. A similar, more pronounced level of gross data smoothing, was found to be associated with continuous curve fitting to a higher order polynomial. For the project reported herein,

the data smoothing inherent in computer based data processing methods was considered to be wholly unacceptable. As a consequence, graphical data processing by the tangent to curve method (86) was adopted and applied to all data reported herein. It was, however, acknowledged, that errors arising from subjectivity were likely to be present in the finished data. To assess the general level of likely error, individual sets of da/dN data were randomly cross-checked and were found to be repeatable to within ± 10%. The high level of repeatability demonstrated, in conjunction with negligible levels of data scatter, was considered to be sufficient proof that errors arising from the effects of subjectivity were acceptable and that the use of graphical data processing methods was justified.

CHAPTER 6

6.1 CONCLUSIONS

6.1.1 Optical crack monitoring by use of a vernier-type travelling microscope is a simple, inexpensive, accurate and entirely satisfactory method of crack length monitoring under conditions of corrosion fatigue. The formation of either corrosion products or calcareous deposits on the specimen surfaces, is not a significant constraint upon the application of the technique and does not adversely influence the accuracy of crack length measurement.

6.1.2 Graphical data processing using the tangent to curve technique is a simple, reliable and particularly effective method for the determination of crack growth rate from experimental data of crack length against number of fatigue cycles. The use of graphical methods, results in an exceptionally low level of data scatter, which is insignificant when compared to the magnitude of scatter associated with alternative data processing techniques, such as finite difference or incremental polynomial. Moreover, the use of graphical data processing methods promotes a high degree of confidence that specific material behaviour will be accurately reflected in the derived growth rate data. Conversely, little confidence is associated with the use of finite difference or polynomial methods in general, where significant distortion of true material behaviour can occur.

6.1.3 Fatigue and corrosion fatigue crack growth rates, measured in BS 4360 50D type steel, under constant load-amplitude conditions, confirmed the existence of delayed retardation, following the application of a single cycle of overload.

6.1.4 The most likely cause of retardation in crack propagation rates following overload, is residual compressive stresses in the material ahead of the crack tip together with strain hardening, as might be expected in a ductile metal.

6.1.5 The length of crack which is subject to retarded growth behaviour following overload is independent of environment and even for relatively small specimen sizes, $B \leq 15.00$mm, can be correlated with the calculated value of the pre-overload plane-stress, monotonic plastic zone size.

6.1.6 Retarded crack growth does not occur under conditions, where the overload plastic zone is contained wholly within the pre-overload, plane-stress monotonic plastic zone.

6.1.7 For low values of $\Delta K << K_{1c}$, crack propagation rate data can be characterised in a multi-modal format with clearly defined transition. The phenomenon of transition is independent of microstructure and can be correlated with the formation of

branched cracks which reduce the effective level of stress intensity factor at the dominant crack front and result in reduced levels of crack propagation rate.

6.1.8 Back-extrapolation of crack propagation rate data is a satisfactory method for the estimation of ΔK_{TH} values of BS 4360 50D type structural steel and associated weldment microstructures. Use of this method has shown that the minimum value of ΔK_{TH} and hence the maximum probability of initiation of fatigue or corrosion fatigue fracture, occurs in the coarse-grained, super-critical region of the heat-affected-zone, irrespective of environment.

6.1.9 The Paris relationship $da/dN = C.\Delta K^m$ is applicable to corrosion fatigue crack propagation rate data for structural steel and associated weldments, under conditions of cathodic protection. Furthermore, it is confirmed that a relationship of the form $m = A.\ln C + D$, exists between Paris exponent m and constant C, where A and D are not material dependent quantities.

6.1.10 For crack propagation under conditions of corrosion fatigue, the specific influence of both environment and microstructure upon crack propagation rate, can be separately identified within the Paris relationship $da/dN = C.\Delta K^m$. The influence of environment is encompassed in the value of constant C, whereas the influence of microstructure is encompassed in the value of exponent m. The manner in which the respective influences are exercised is not clear and could usefully be made the subject of future research.

6.1.11 For structural steel weldments, the presence of a yield strength gradient in the heat-affected-zone, invariably causes significant deviation in the direction of crack propagation under pure mode 1 crack opening at low values of $\Delta K << K_{1c}$. As a consequence the majority of crack growth occurs in the 'softer' region of the h.a.z. which borders the parent plate material. This effect is attributed to the influence of material yield strength on the size and shape of the, predominantly, plane-stress crack tip plastic zone. The practical significance of this phenomena is that for mode 1 crack opening, fractures initiated in the region of the fusion line are unlikely to propagate along it. In this context, the 'fusion line' can be taken to include the super-critical region of the h.a.z., as in the majority of structural weldments offshore, this region is generally less than 0.5mm wide.

6.1.12 In ferritic-pearlitic steel, the ability of pearlite colonies to act as microstructural barriers to fatigue crack advance, is confirmed. The degree of influence is determined by the orientation of the iron-carbide platelets within the pearlite colonies, relative to the projected direction of crack advance. The degree of influence is a maximum, where individual platelets are orientated normal to the local crack front.

6.1.13 For fatigue and corrosion fatigue crack propagation in structural steel and associated weldments, the measured spacing of individual surface striation markings, is not equivalent to the derived value of crack propagation rate. Nor is striation spacing equivalent to the magnitude of associated crack tip opening displacements, per cycle of fatigue. The only significance of surface striation markings to fatigue and corrosion fatigue studies in general is considered to be that they provide a permanent record of the localised shear-decohesion processes, operative within the crack tip plastic zone, which results in crack advance during fatigue loading.

6.1.14 The influence of cathodic protection on corrosion fatigue crack propagation rates in BS 4360 50D type structural steel and associated weldments, is determined by the level of applied cathodic protection potential in conjunction with crack depth, which is an interesting factor in view of the open-sided nature of test specimens.

6.1.15 For shallow cracks less than approximately 5.0mm deep, which are loaded at a small positive R ratio $\leq$ 0.1, cathodic protection applied at the theoretical optimum potential of $-780mV_{S.C.E}$, is beneficial irrespective of microstructure and results in reduced corrosion-fatigue crack propagation rates, close to in-air values. The beneficial influence of cathodic protection under these conditions, is attributed to reduced anodic dissolution activity in the region of the crack tip with associated reduction in the level of hydrogen embrittlement within the crack-tip plastic zone. At positive values of R ratio, the beneficial influence of cathodic protection is not considered to arise from enhanced crack-closure effects, in the manner postulated in UKOSRP literature.

6.1.16 For cracks which are deeper than approximately 5.0mm, the influence of cathodic protection at the theoretical optimum potential of - 780 mV_{SCE} is material dependent. In BS 4360 50D type structural steel the influence is adverse and results in enhanced rates of corrosion fatigue crack propagation and reduced endurance. Conversely, in weld metal and heat affected zone material, the influence is beneficial and results in reduced rates of corrosion fatigue crack propagation and increased endurance. The apparent anomaly in the influence of cathodic protection is attributed to the physical effect of modified anodic dissolution activity in the region of the crack tip which is stimulated by an increased level of electrical potential in the absence of meaningful current flow. In BS 4360 50D steel, the dominant physical effect is increased hydrogen embrittlement which promotes enhanced rates of crack propagation. Conversely, in weld metal and heat affected zone material, the dominant physical effect is change in crack-tip geometry which results in crack blunting and reduced rates of crack propagation.

6.1.17 For shallow cracks less than approximately 5.0mm deep, which are loaded at a small positive R ratio $\leq$ 0.1, the influence of cathodic protection at a potential of - 1100 mV_{SCE}, is markedly detrimental, irrespective of microstructure and results in

enhanced rates of corrosion fatigue crack propagation and reduced endurance with stress corrosion dominated crack growth behaviour. The markedly adverse influence of cathodic protection at a high potential is attributed to the effect of enhanced hydrogen embrittlement which is caused by a significant increase in the level of uptake of ionic hydrogen, during the initial polarisation period. This result clearly demonstrates that the widespread industrial practice offshore, of deliberately 'overprotecting' structures in order to achieve rapid polarisation is foolhardy and must be actively discouraged. This feature of the results has considerable practical importance in view of the type of cracking which is often found in sub-sea nodal joints offshore. Namely, the cracks are surface breaking in the heat affected zone and are of comparatively short length in relation to the circumference of the member. The crack depth is generally small, frequently of the order of 5.00mm and associated values of crack tip opening displacement are very low.

6.1.18 For cracks which are deeper than approximately 5.00mm, the influence of cathodic protection at a potential of - 1100 mV_{SCE} is beneficial irrespective of microstructure and results in reduced rates of corrosion fatigue crack propagation and increased endurance. In BS 4360 50D type steel it is considered that the high level of cathodic protection potential applied externally is probably reduced within the crack and with adequate access of environment, results in satisfactory cathodic protection, in a manner comparable to that for shallow cracks at a potential of - 780 mV_{SCE}. Conversely, for weld metal and heat affected zone microstructure, the reduced levels of crack tip opening displacement present, are considered to restrict access of protection current into the crack. As a consequence, modified anodic dissolution activity occurs in the region of the crack tip stimulated by an increased level of electrical potential in the absence of meaningful current flow. The dominant physical effect is change in crack tip geometry which results in crack-tip blunting and reduced rates of crack propagation.

6.1.19 The influence of simulated tidal immersion, upon corrosion fatigue crack propagation behaviour, is dependent upon microstructure and is markedly different between parent plate and weld metal. In BS 4360 50D type structural steel, the mean rate of corrosion fatigue crack propagation is reduced with a corresponding increase in endurance. This effect is considered to be consistent with crack growth during alternating periods of crack-tip blunting and crack-tip re-sharpening. Conversely in weld metal, the average corrosion fatigue crack propagation rate is progressively reduced and terminates in zero growth rate or crack arrest. This phenomenon is attributed to the effect of cumulative residual crack-tip blunting, caused by ineffective crack-tip re-sharpening during successive periods of in-air crack growth.

6.1.20 An environment of simulated splash zone is non-equilibrium in nature and promotes severe corrosion attack within fatigue cracks, irrespective of microstructure. The Paris relationship can, however, be used to characterise associated corrosion fatigue crack propagation rate data, subject to the constraint that the values of constant C and exponent m obtained, are not compared to data obtained under equilibrium conditions.

6.2 *FUTURE WORK*

6.2.1 For corrosion fatigue crack propagation at low R values and low values of ΔK, in BS 4360 50D type structural steel and associated weldments. Investigation of the influence of crack depth, crack width and crack tip opening displacement, upon fundamental electrochemical parameters within the crack such as pH and solution electrical potential, relative to bulk environment values.

6.2.2 For BS 4360 50D type structural steel and associated weldment microstructures. Investigation of the influence of cathodic protection potential upon the corrosion fatigue threshold behaviour at low R values, in both un-cracked and pre-cracked specimens.

6.2.3 Investigation of the influence of cathodic protection upon the corrosion fatigue growth behaviour of low aspect ratio, surface-breaking cracks, in structural steels and associated weldments, without side access and subject to the inherent problems of measuring crack growth.

6.2.4 Determination of an optimum method for the monitoring of corrosion fatigue crack growth, together with subsequent processing and analysis of crack propagation rate data.

6.2.5 For corrosion fatigue crack propagation in structural steels and associated weldments, the determination of a numerical relationship which can be used to describe the influence of environment and microstructure, upon the values of Paris constant C and exponent m under conditions of cathodic protection.

6.2.6 Investigation of the influence of cathodic protection potential upon the density and depth of calcareous scales formed on protected surfaces, together with an assessment of their mechanical, electrical and chemical properties.

REFERENCES

1. OFFSHORE ENGINEER — March 1980.

2. DAILY TELEGRAPH — March 1982.

3. B.S. HOCKENHULL — Private Communication, Cranfield 1979.

4. OFFSHORE ENGINEER — Survey, March 1982.

5. P.C. PARIS and F. ERDOGAN — A critical analysis of crack propagation laws. Transactions of ASME. Basic Engineering Journal, Vol. 85, 1963.

6. STATUTORY INSTRUMENT NO. 289 AND ASSOCIATED DEPARTMENT OF ENERGY GUIDANCE NOTES

7. J.M. BARSOM — Effect of cyclic stress wave form on corrosion fatigue crack propagation below K_{ISCC} in a high-yield strength steel. Proceedings of International Conference on Corrosion Fatigue, University of Connecticut, (NACE), 1972.

9. A.T. STEWART — Engineering Fracture Mechanics, Vol. 13, 1980.

10. I.M. AUSTEN — Paper 14, European Offshore Steels Research, Select Seminar, Welding Institute, Cambridge. November 1978.

11. O. VOSIKOVSKY — Journal of Engineering Materials and Technology. Vol. 97, 1975.

12. P.M. SCOTT and D.R.V. SILVESTER — United Kingdom Offshore Steels Research Programme. Report 3/03, 1975.

13. T.C. LINDLEY and L.N. McCARTNEY — ASTM STP 513, P247, 1972.

14. J.M. BARSOM — Transactions of ASME, November 1971.

15. C.R. AITA and J. WEERTMAN — Metallurgical Transactions, Vol. 10A, May 1979.

16. M.R. KRISHNADEV, R. GOSH and A. GALIBOIS — Fatigue of Engineering Materials and Structures. Vol. 2, P107, 1979.

17. N.R. MOODY and W.W. GERBERICH — Metal Science, Vol. 14, P95, March 1980.

18.	H. SUZUKI and A.J. McEVILY	Metallurgical Transactions, Vol. 10A, P475, April 1975.
19.	J.A. RUPPEN and A.J. McEVILY	Fatigue of Engineering Materials and Structures, Vol. 2, P63, 1979.
20.	J.P. BENSON and D.V. EDMONDS	Metal Science, Vol. 12, P223, May 1978.
21.	K.R. DOWSE and C.E. RICHARDS	Metallurgical Transactions, Vol. 2, P599, February 1971.
22.	D. BENOIT et al	Paper 13, European Offshore Steels Research, Select Seminar, Welding Institute Cambridge, November 1978.
23.	A.M. SULLIVAN and T.W. CROOKER	NRL Report No. 7936, 1975.
24.	S.J. MADDOX	Metal Construction and British Welding Journal, P285, July 1970.
25.	T. MISAWA, N. RINGSHALL and J.F. KNOTT	Corrosion Science, Vol. 16, P805, 1976.
26.	B. TOMKINS	Metal Science, Vol. 13, P387, July 1979.
27.	P. SMITH and A.T. STEWART	Metal Science, Vol. 13, P429. July 1979.
28.	J.T. RYDER and J.P. GALLAGHER	Journal of Basic Engineering, Vol. 92, P121, March 1970.
29.	C. BATHIAS and J.P. BAILON	La Fatigue des Materiaux et des Structures. Collection Universite de Compiegne, P229.
30.	E. WALKER	ASTM, STP 462, 1970.
31.	R.E. FOREMAN, V.E. KEARNEY and R.M. ENGLE	Journal of Basic Engineering, Vol. 89D, P459, 1967.
32.	R. ROBERTS and J.J. KILBER	Journal of Basic Engineering, Vol. 93D, P671, 1971.
33.	J.F. KNOTT	Fundamentals of Fracture Mechanics, Butterworths, London. P109.
34.	R.N. PARKINS and B.S. GREENWELL	Metal Science, P405. Aug/Sept. 1977.
35.	J.D. ATKINSON and T.C. LINDLEY	I. Mech. E. London. P65. 1977

36.	J.M. BARSOM	Proceedings of International Conference on Corrosion Fatigue. University of Connecticut, NACE, P424. 1972.
37.	J.P. GALLAGHER and G.M. SINCLAIR	Journal of Basic Engineering. Vol. 91, P598, 1969.
38.	J.P. GALLAGHER and R.P. WEI	Proceedings of International Conference on Corrosion Fatigue. University of Connecticut, NACE, P409, 1972.
39.	J.M. BARSOM	International Journal of Fracture. Vol. 7, P163, 1971.
40.	O. VOSIKOVSKY	Corrosion NACE, Vol. 32, P472, 1976.
41.	P.M. SCOTT and D.R.V. SILVESTER	United Kingdom Offshore Steels, Research Programme, Report 3/02, 1977.
42.	K.J. MILLER	Metal Science, Vol. 11, P432, Aug/ Sept. 1977.
43.	C.M. BRANCO, J.C. RADON and L.E. CULVER	Metal Science, Vol. 10, P149, May 1976.
44.	W. ELBER	Engineering Fracture Mechanics, Vol. 2, P37, 1970.
45.	A. OHTA, M. KOSUGE and E. SASAKI	International Journal of Fracture, Vol. 14, P251, 1978.
46.	R.D. BROWN and J. WEERTMAN	Engineering Fracture Mechanics, Vol. 10, P757, 1978.
47.	T.C. LINDLEY and C.E. RICHARDS	Materials Science and Engineering, Vol. 14, P281, 1974.
48.	P.E. IRGING, J.L. ROBINSON and C.J. BEEVER	Engineering Fracture Mechanics, Vol. 7, P619, 1975.
49.	C.K. CLARKE and G.C. CASSATT	Engineering Fracture Mechanics, Vol. 9, P675, 1977.
50.	O. VOSIKOVSKY	International Journal of Fracture, Vol. 17, P301, 1981.
51.	C.M. HUDSON and KIN.RAJU	NASA TN D5702. March 1970.
52.	J. SCHIJVE and D. BROEK	Aircraft Engineer, Vol. 34, P314, 1962.
53.	O.E. WHEELER	Journal of Basic Engineering, Vol. 4 P181, 1972.

54.	W. ELBER	Engineering Fracture Mechanics Vol. 2, P37, 1970.
55.	W. ELBER	ASTM, STP 486, P230, 1971.
56.	E.F.J. VON EUW, R.W. HERTZBERG and P. ROBERTS	ASTM, STP 573, P230, 1972.
57.	R.M. CHRISTENSEN	Metal Fatigue, McGraw-Hill, New York. 1959.
58.	R.E. JONES	Engineering Fracture Mechanics. Vol. 5, P585, 1973.
59.	P.J. BERNARD, T.C. LINDSEY and C.E. RICHARDS	Metal Science, Vol. 11, P890, Aug/Sept. 1977.
60.	J.E. STRUTT and W.H. TURNER	Private Communication, Cranfield 1982.
61.	V. ASHWORTH	The theory of cathodic protection and its relation to the electrochemical theory of corrosion. NACE/I.Corr.ST. Conference on Cathodic Protection, Theory and Practice. Coventry, April 1982.
62.	H.J. ENGELL and P. FORCHAMMER	Corrosion Science, Vol. 5, P479, 1965.
63.	W.H. HARTT and S.L. WOOLFSON	Corrosion, Vol. 37, P70, 1981.
64.	I.B. ULANOVSKII	Prot. Met. Vol. 8, P191, 1972.
65.	V.P. GRIGOREV and S.Y. POPOV	Journal of Applied Chemistry (USSR), Vol. 35, P1555, 1962.
66.	V.P. GRIGOREV	Journal of Applied Chemistry (USSR) Vol. 34, P169, 1961.
67,	H. KLAS	Arch. Eisenhüttenwiss, Vol. 29, P321, 1958.
68.	A.A. FARKHADOV and R.N. KAREV	Azab. Neft. Khoz. Vol. 6, P161, 1971.
69.	C.M. HUDGINS	Paper OTC 1254. 2nd Offshore Technology Conference, Houston, 1970.
70.	M. WANATABE and Y. MUKAI	Proceedings of Conference on Welding in Offshore Constructions. Welding Institute, Newcastle, P46, 1974.

71.	G.S. BOOTH	Paper OTC 3420. 11th Offshore Technology Conference, Houston, 1979.
72.	O. SOLLI	Paper 10. European Offshore Steels Research, Select Seminar, Welding Institute Cambridge, November 1978.
73.	P.W. LOHNE	Norwegian Maritime Research Report No. 3, 1979.
74.	P.W. MARSHALL	Welding Research Council, Bulletin Number 193, April 1974.
75.	J.P. GALLAGHER	Journal of Materials, Vol. 6, P941, 1971.
76.	R.M. PROCTOR	'Detrimental effects of cathodic protection, embrittlement and cracking phenomena'. NACE/I.Corr.ST Conference on Cathodic Protection, Theory and Practice. Coventry, April 1982.
77.	E. BARDAL, J.M. SONDENFOR and P.O. GARTLAND	Paper 16, European Offshore Steels Research, Select Seminar, Welding Institute Cambridge, November 1978.
78.	R.P. WEI and R.L. BRAZILL	ASTM STP 738. 1979.
79.	G.H. ARONSON and R.O. RITCHIE	Journal of Testing and Evaluation, Vol. 7, Number 4, P208, 1979.
80.	R.P. GANELOFF and R.P. WEI	Metallurgical Transactions, Vol.8A, P1043, 1977.
81.	C.Y. LI and R.P. WEI	Material Research Standard, Vol. 6, Number 8, P892, 1966.
82.	R.O. RITCHIE and K.J. BATHE	International Journal of Fracture, Vol. 15, P47, 1979.
83.	H.H. JOHNSON	Material Research Standard, Vol. 5, Number 7, P442, 1965.
84.	G. CLARK and J.F. KNOTT	Journal of Mechanical and Physical Solutions. Vol. 23, P265, 1975.
85.	R.P. GANGLOFF	Fatigue of Engineering Materials and Structures, Vol. 4, Number 1, P15, 1981.
86.	J.F. KNOTT	Fundamentals of Fracture Mechanics, Butterworths, London. P244.
87.		Course Notes, Cranfield, 1980.

88. T. JACKSON — Private Communication, Cranfield 1979.

89. W.G. CLARK and S.J. HUDAK — Journal of Test and Evaluation. Vol. 3, P454, 1975.

90. W.G. CLARK and S.J. HUDAK — 'The analysis of fatigue crack growth rate data'. Mechanics Department, Westinghouse Research Laboratories, Pittsburgh, Pennsylvania, 1975.

91. C. KIRK — Course Notes, Cranfield 1979.

92. B. TOMKINS — Short Course Notes, Cranfield 1981.

93. A. McMINN — Fatigue of Engineering Materials and Structures, Vol. 4. Number 3, P235, 1981.

94. P.H.M. HART — 'Yield strengths from hardness data', Welding Institute Research Bulletin, June 1975.

95. A. TURNBULL — Corrosion Science, Vol. 22, Number 9, P877, 1982.

96. C. BATHIAS and J.P. BAILON — 'La Fatigue des Materiaux et des Structures'. Collection Universite de Compiegne, P218.

97. J.F. KNOTT — 'Fundamentals of Fracture Mechanics', Butterworths, London. P136.

98. W. DOVER — OTC Houston, 79/80.

99. T. MORAD — PhD Thesis, Cranfield 1982.

Figure 1A - General view of the fatigue testing machine used for the project

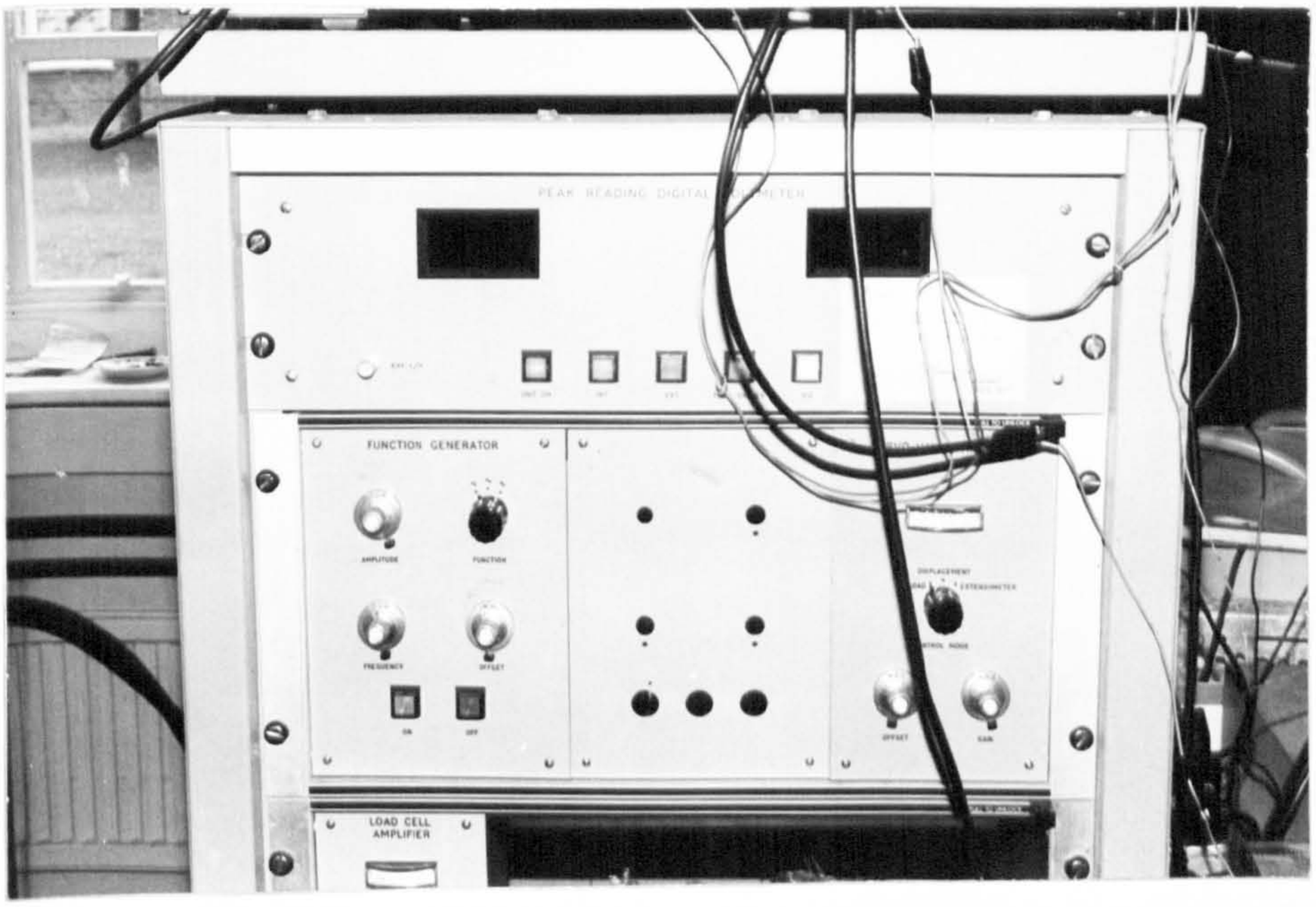

Figure 1B - Close-up view of the load control panel and function generator

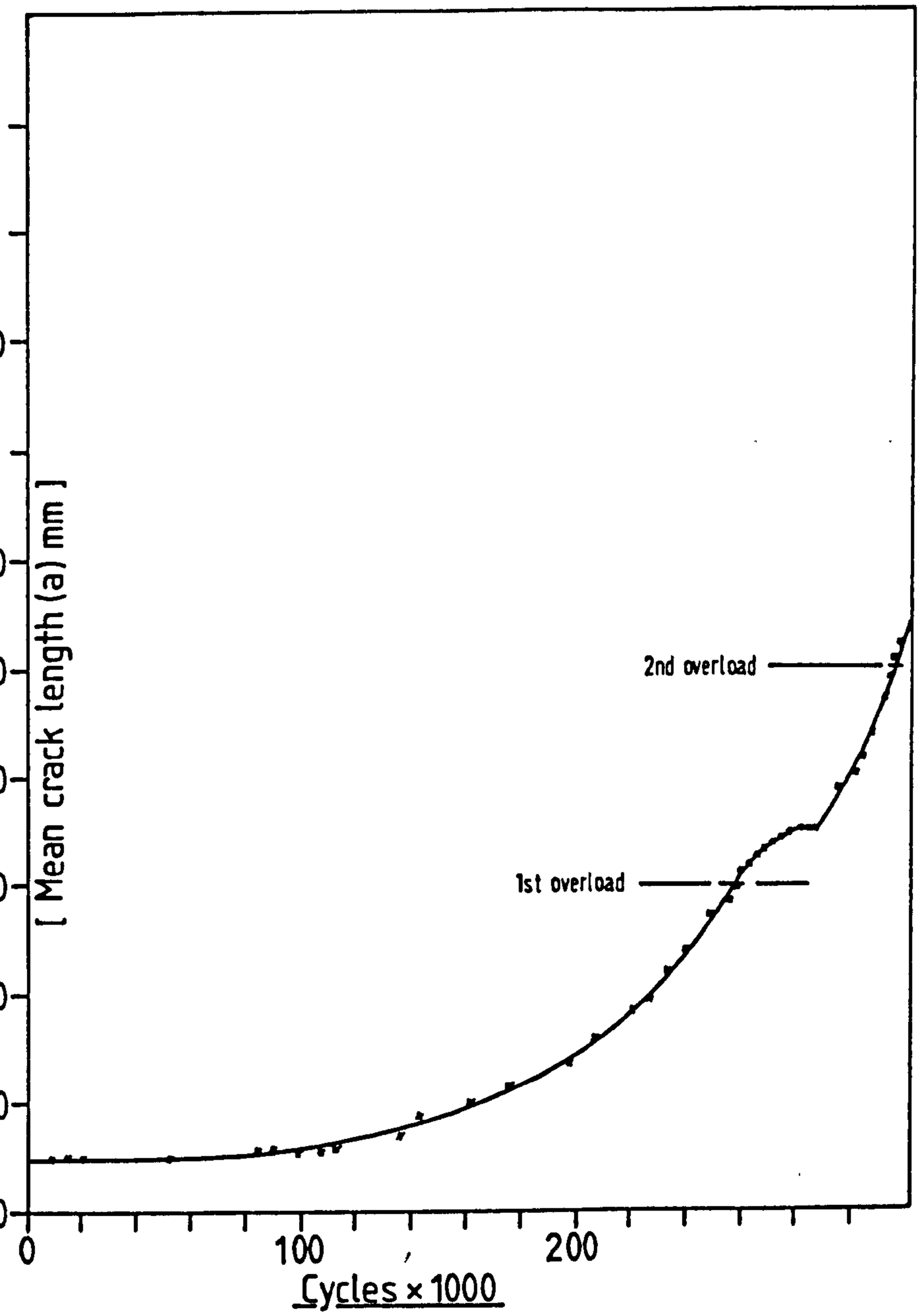

Figure 2 - Graph of a Vs N for crack growth in BS 4360 50D plate material, overloaded in air.

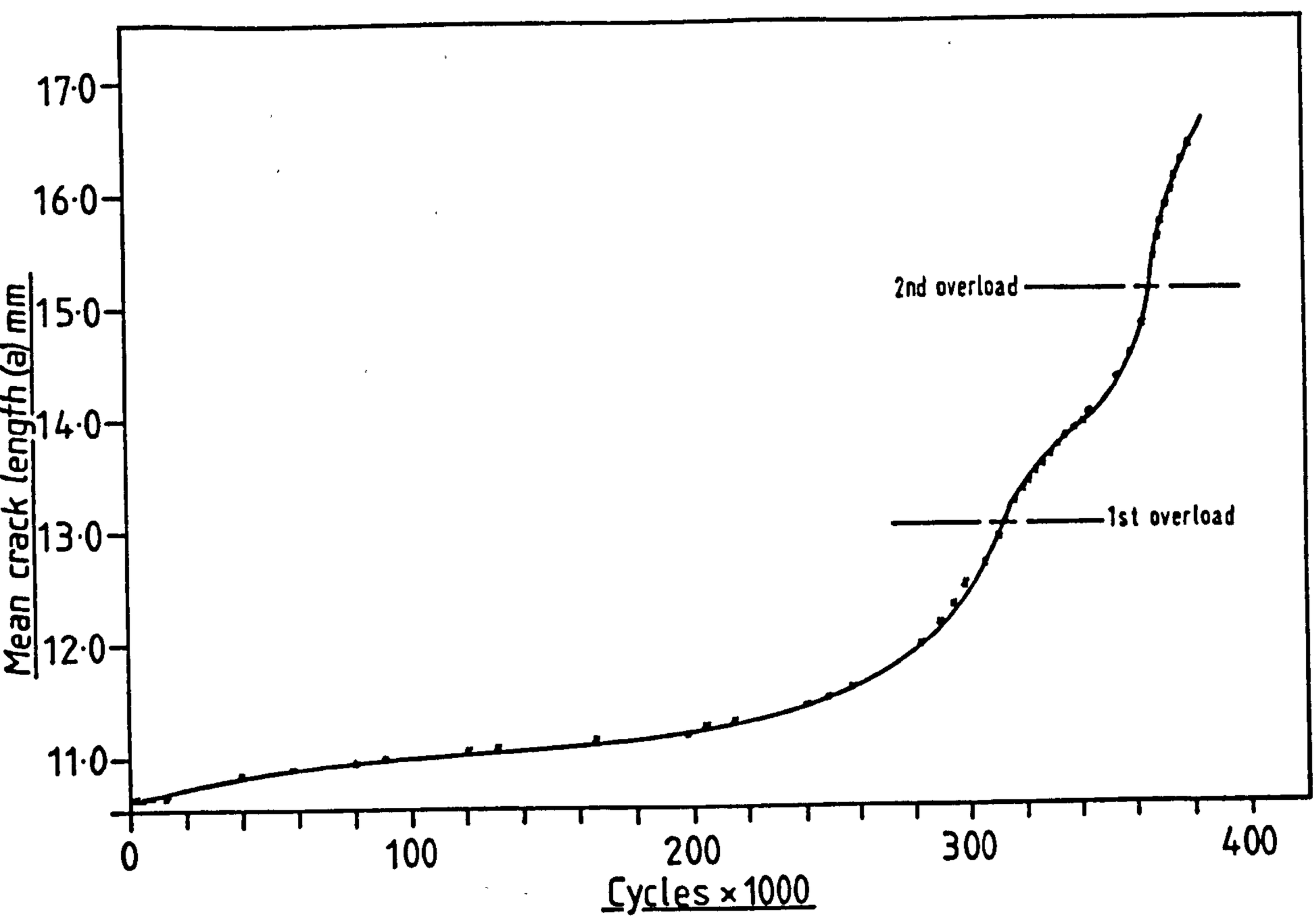

Figure 3 - Graph of a Vs N for crack growth in BS 4360 50D plate material, overloaded in an environment of synthetic seawater.

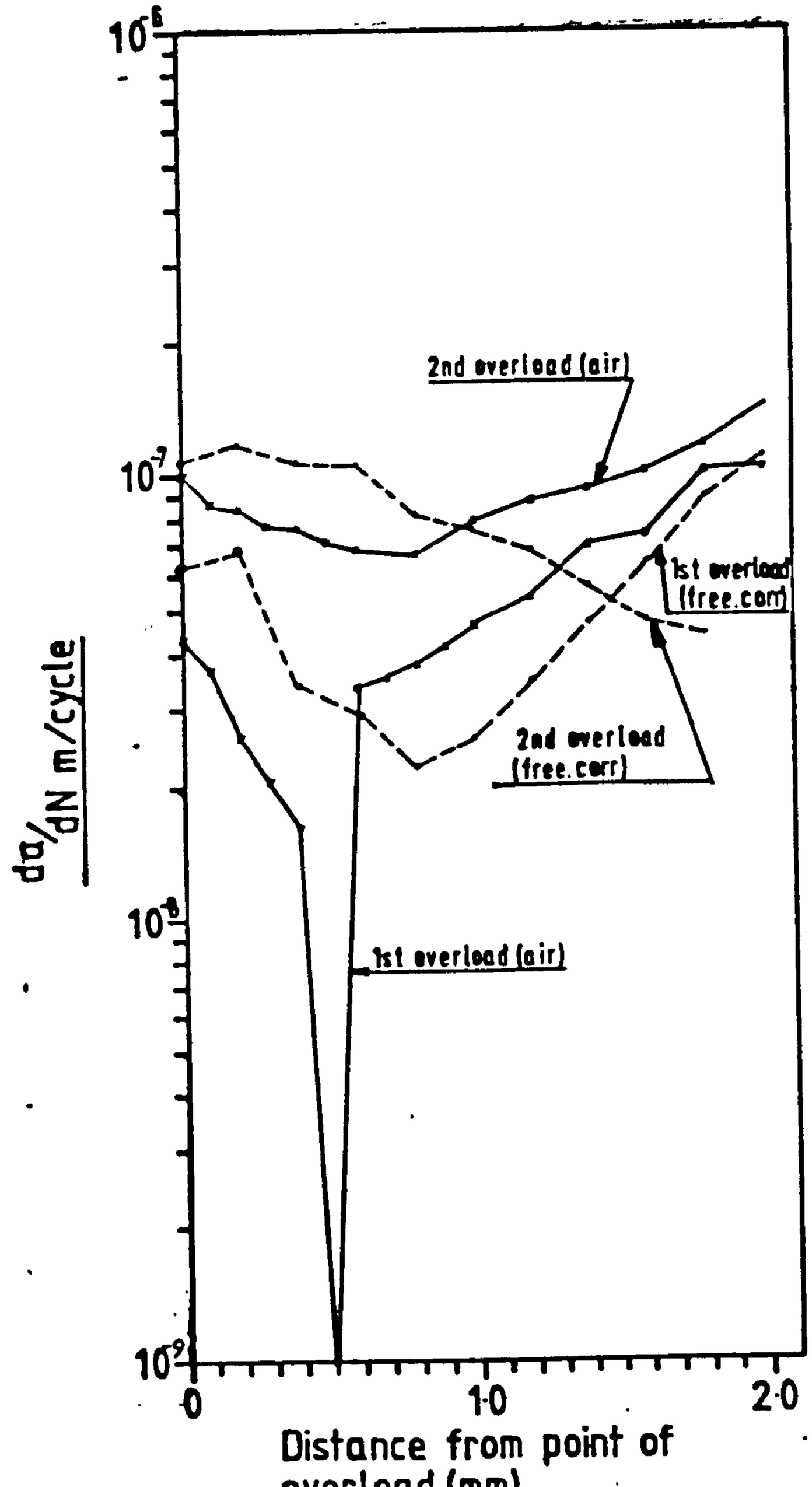

Figure 4 - Graph of log da/dN Vs 'Distance from point of overload' for crack growth in BS 4360 50D plate material, overloaded in air and simulated sea water

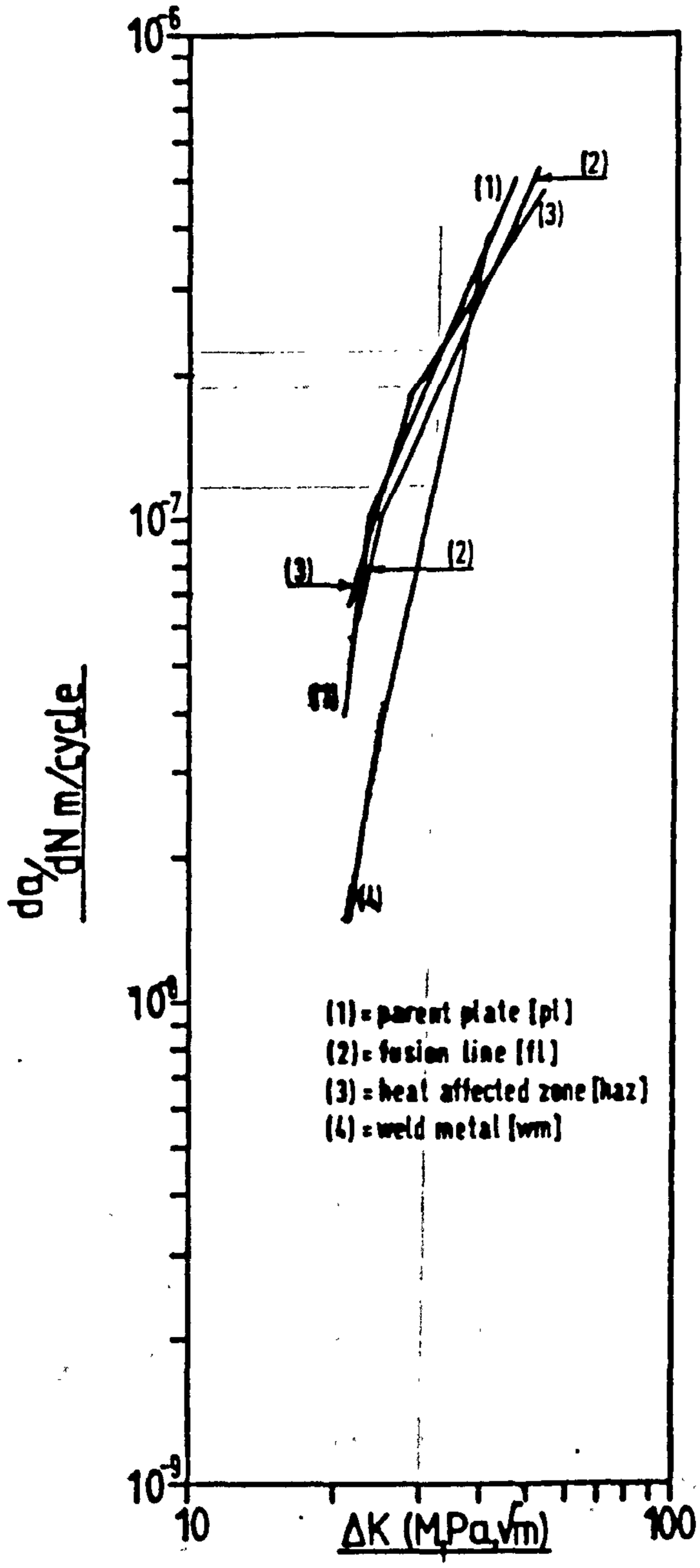

Figure 5 - Graphs of Log da/dN Vs log ΔK for crack growth in BS 4360 50D plate material, weld metal and heat affected zone microstructures in laboratory air at ambient temperature and relative humidity.

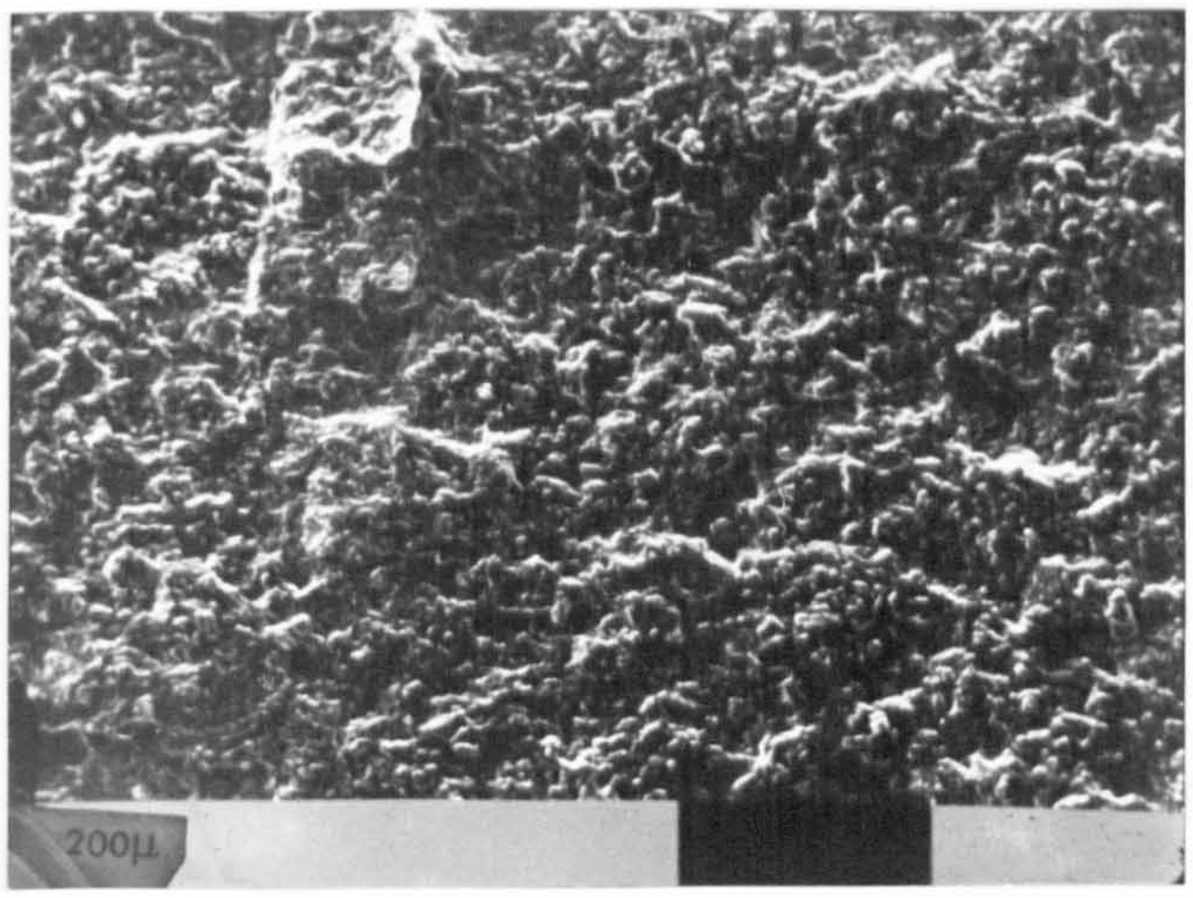

Crack growth direction

→

Figure 6A - Secondary cracking in BS 4360 50D plate material in air at $\Delta K \simeq 26$ M.Pa$\sqrt{m}$

Magnification x 100

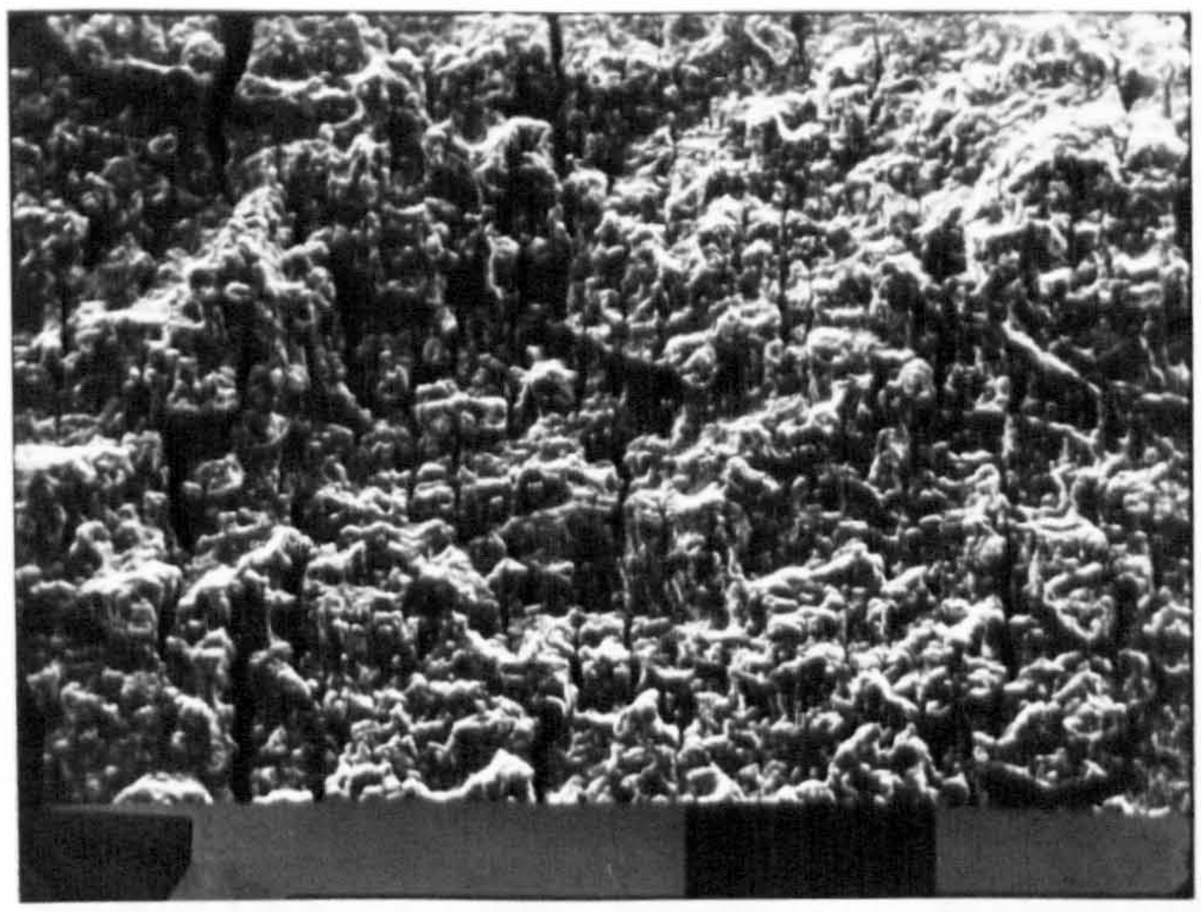

Crack growth direction

→

Figure 6B - Secondary cracking in BS 4360 50D plate material in air at $\Delta K \simeq 42$ M.Pa$\sqrt{m}$.

Magnification x 100

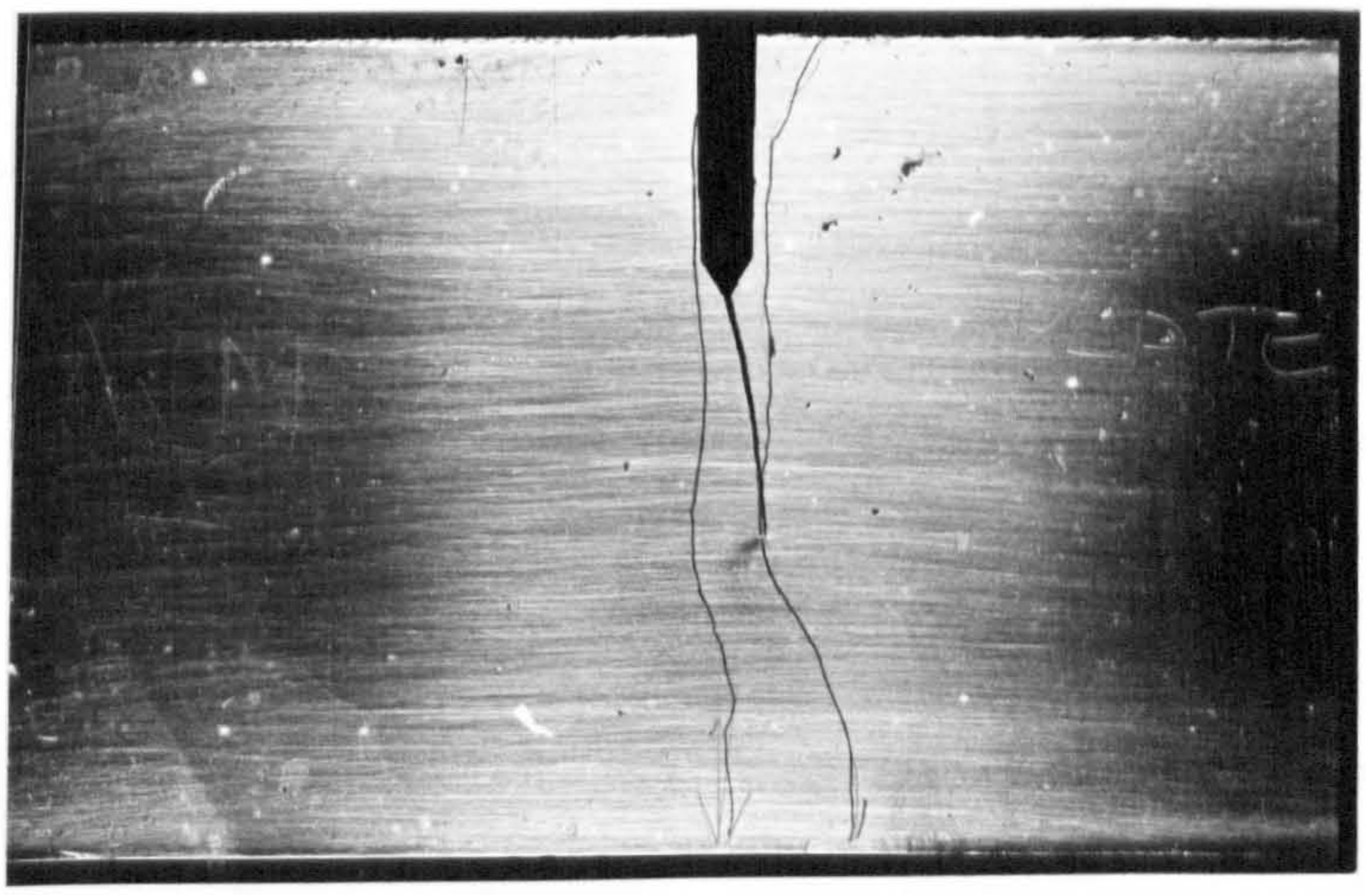

Figure 7 - Fracture in heat affected zone microstructure, exhibiting a preferred direction of crack growth

Magnification x 2

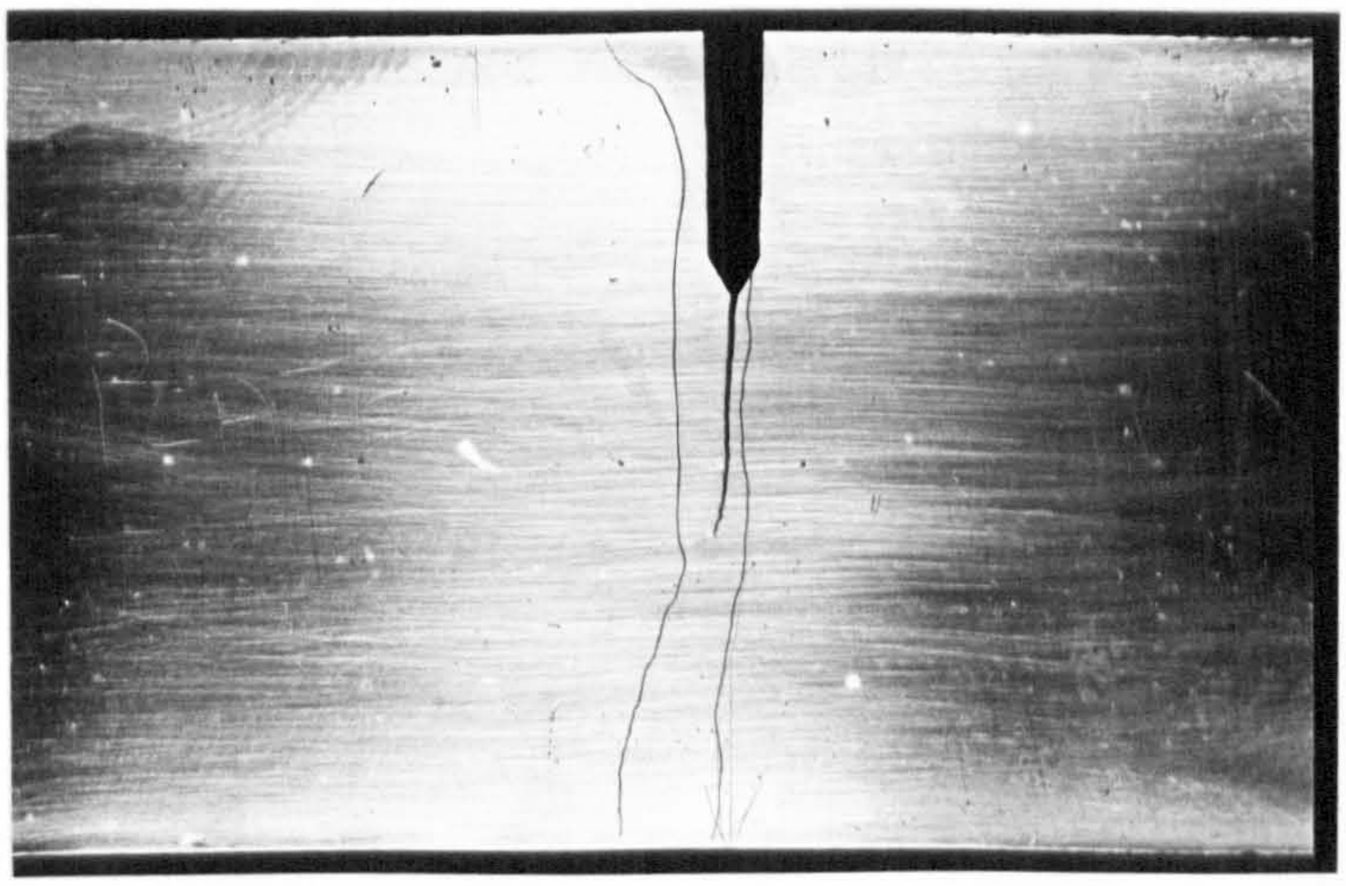

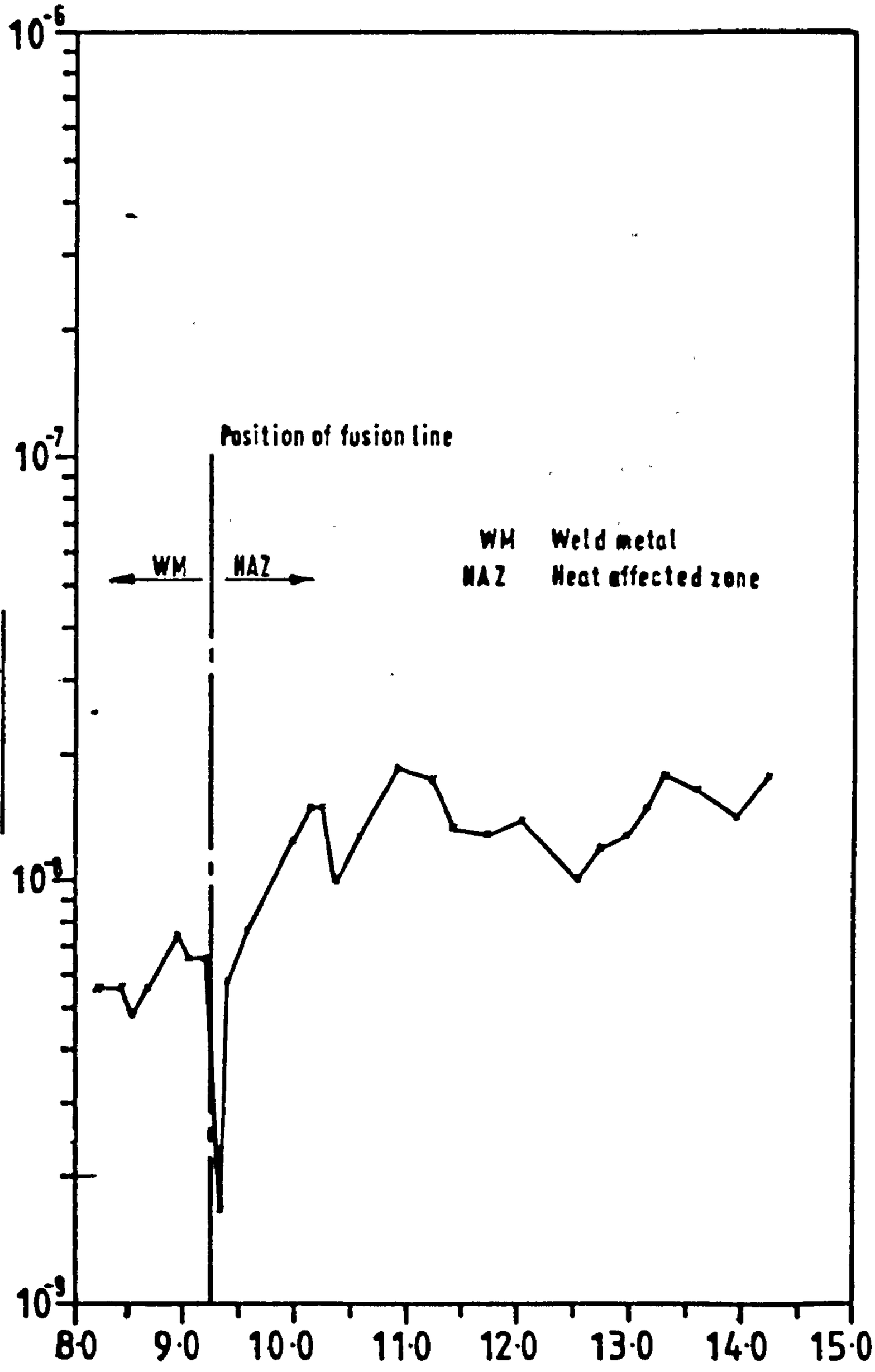

Figure 8 - Graph of log da/dN Vs crack length, for crack growth at constant ΔK and K_{max} in a weld metal specimen type 4.3(E)

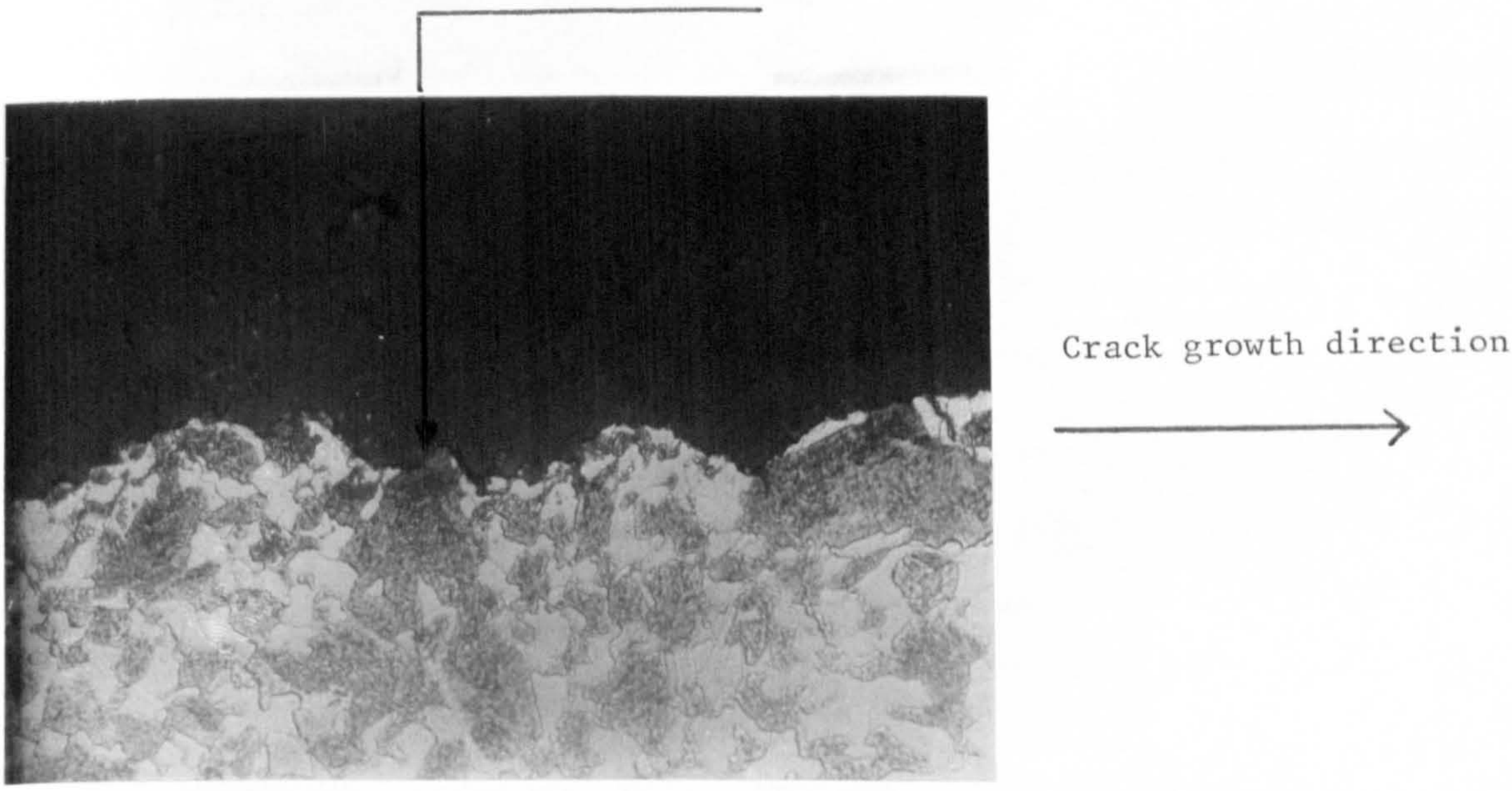

Figure 9 - Fracture in BS 4360 50D plate material, exhibiting deviation in the direction of crack propagation around a Pearlite colony Magnification x 200

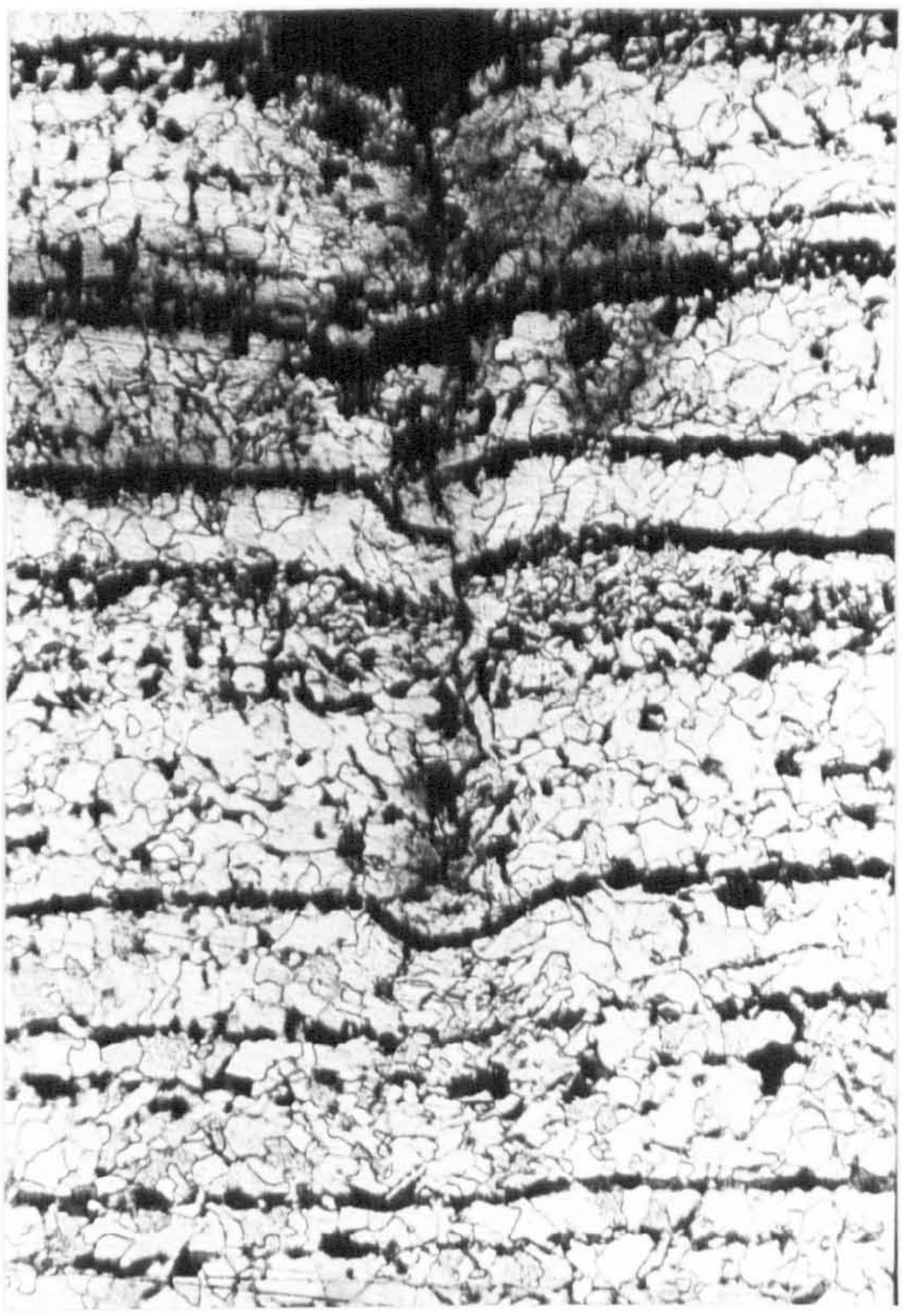

Figure 10 - Fracture in BS 4360 50D plate material, exhibiting plasticity induced bending of pearlite-bands at the crack tip

Polished and etched after crack growth

Magnification x 50

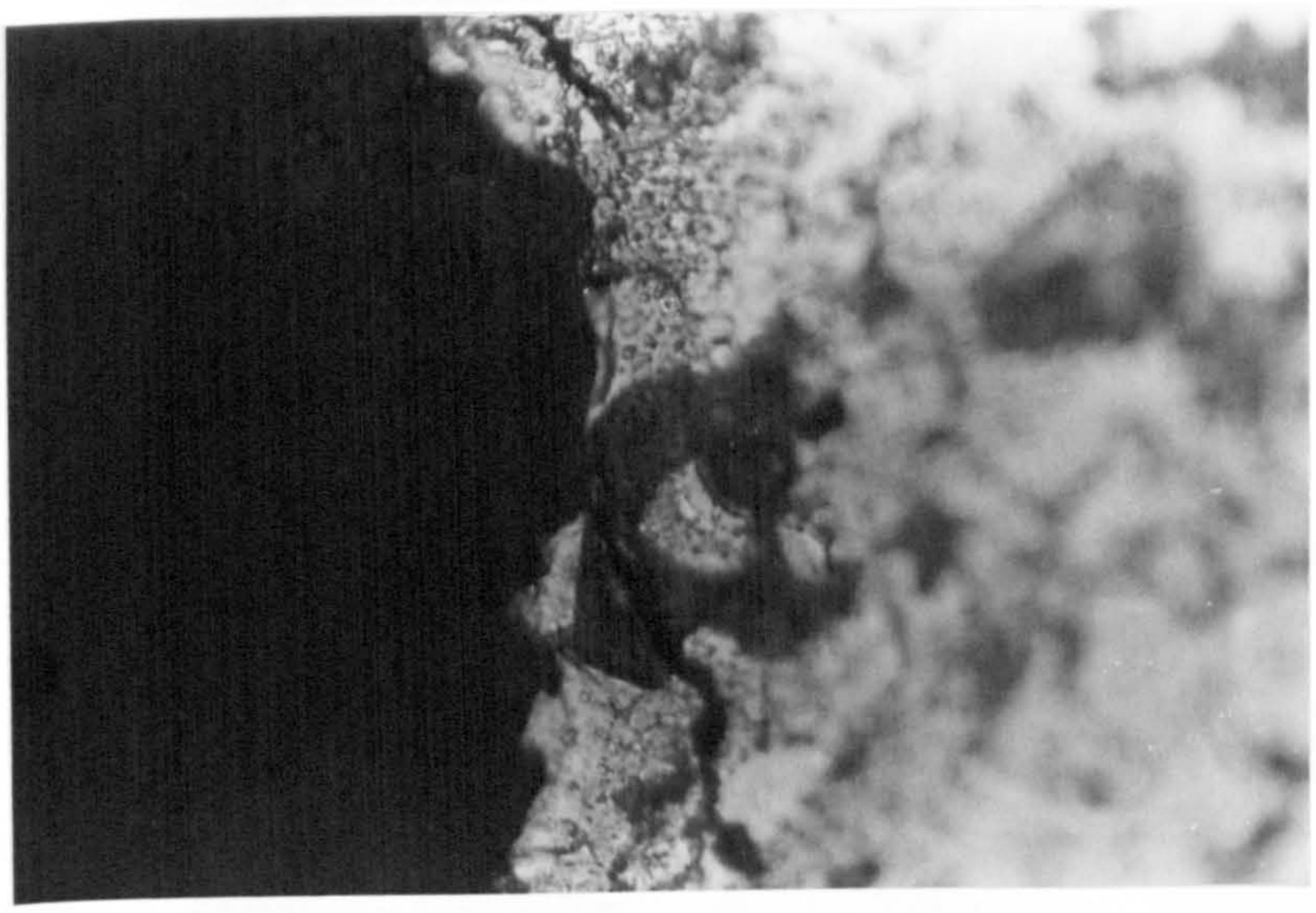

Figure 11 - Fracture in BS 4360 50D plate material, exhibiting propagation of a secondary crack across a pearlite colony.

Magnification x 320

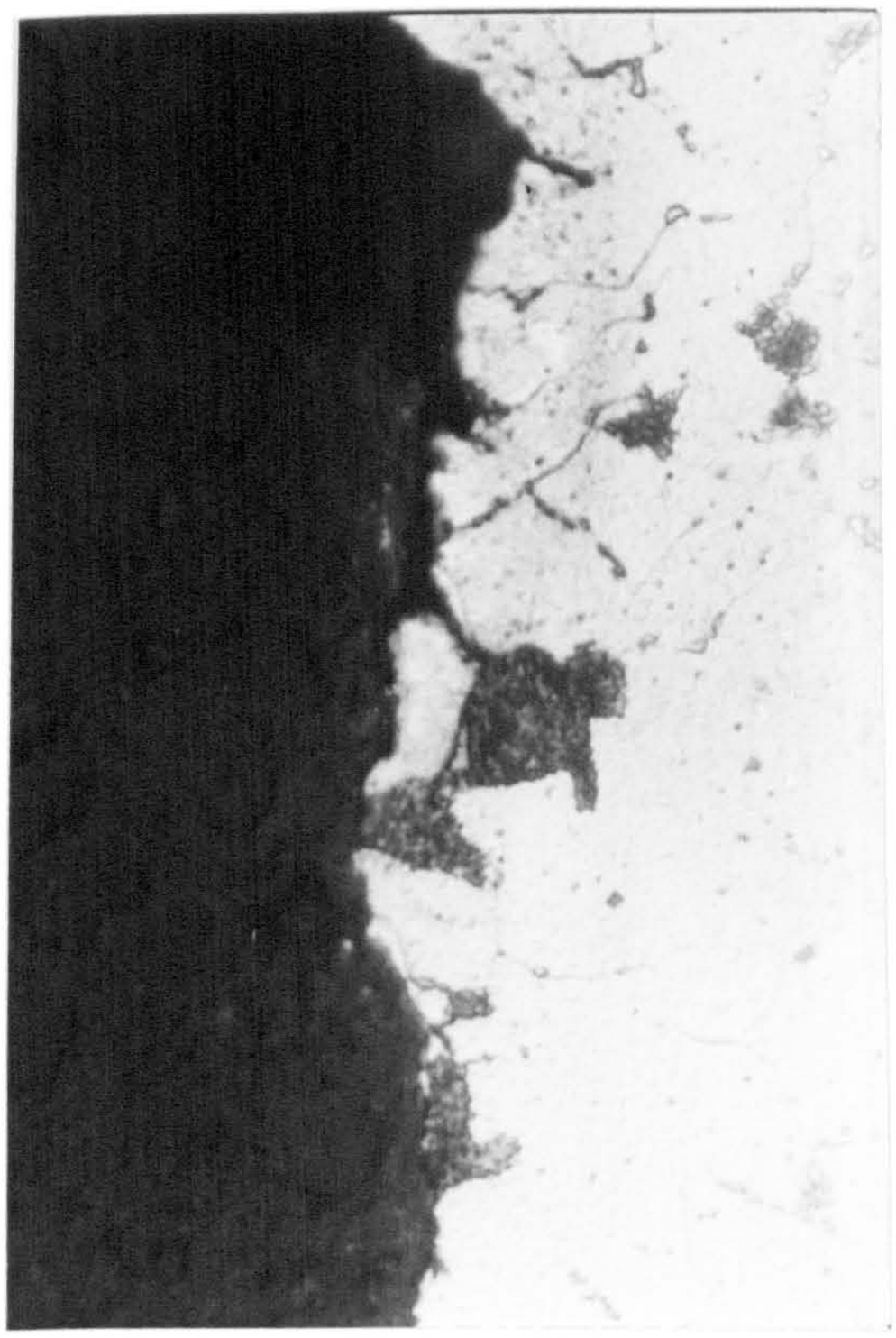

Figure 12 - Fracture in BS 4360 50D plate material, exhibiting 'arrested' growth of a secondary crack by a pearlite-colony

Magnification x 400

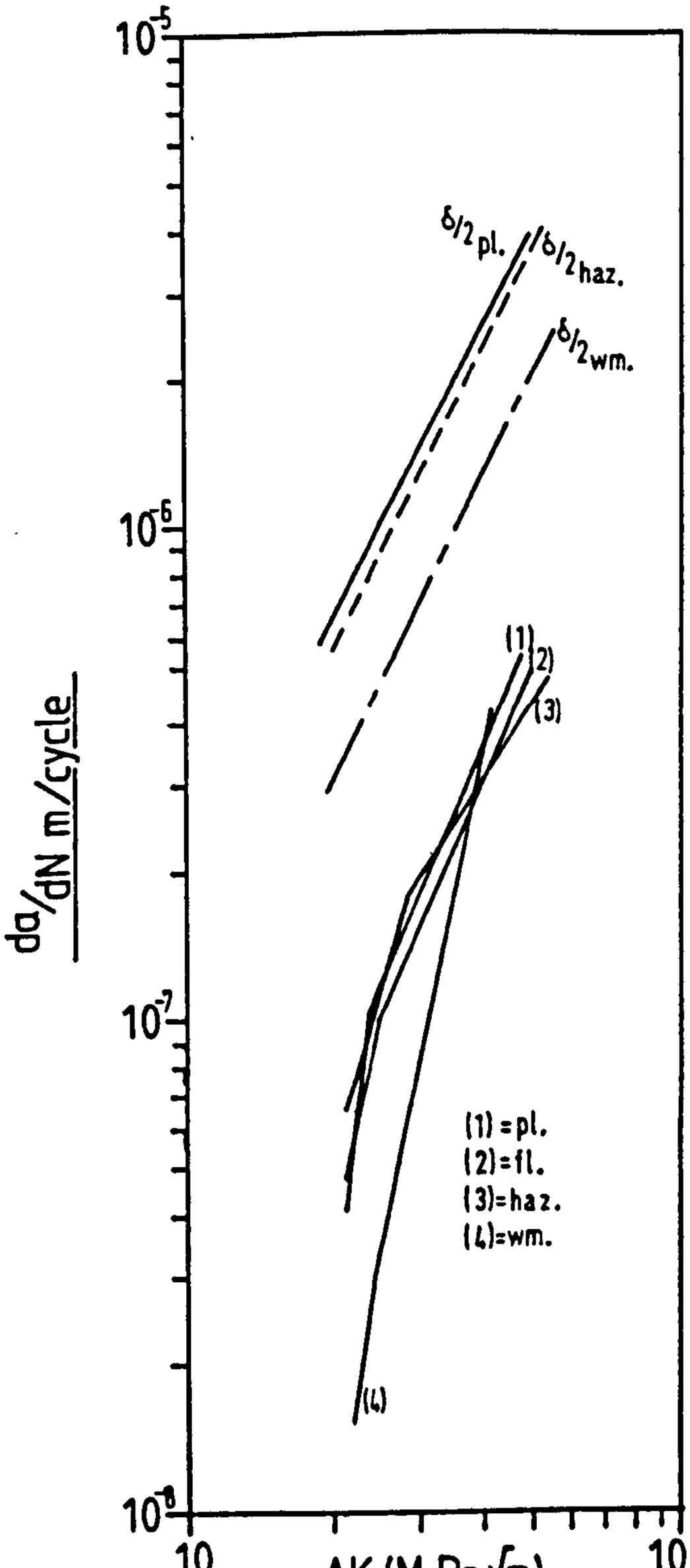

Figure 13 - Graphs of log da/dN Vs log ΔK, for data in Figure 5, compared to the theoretical maximum crack growth rate, given by δ/2.

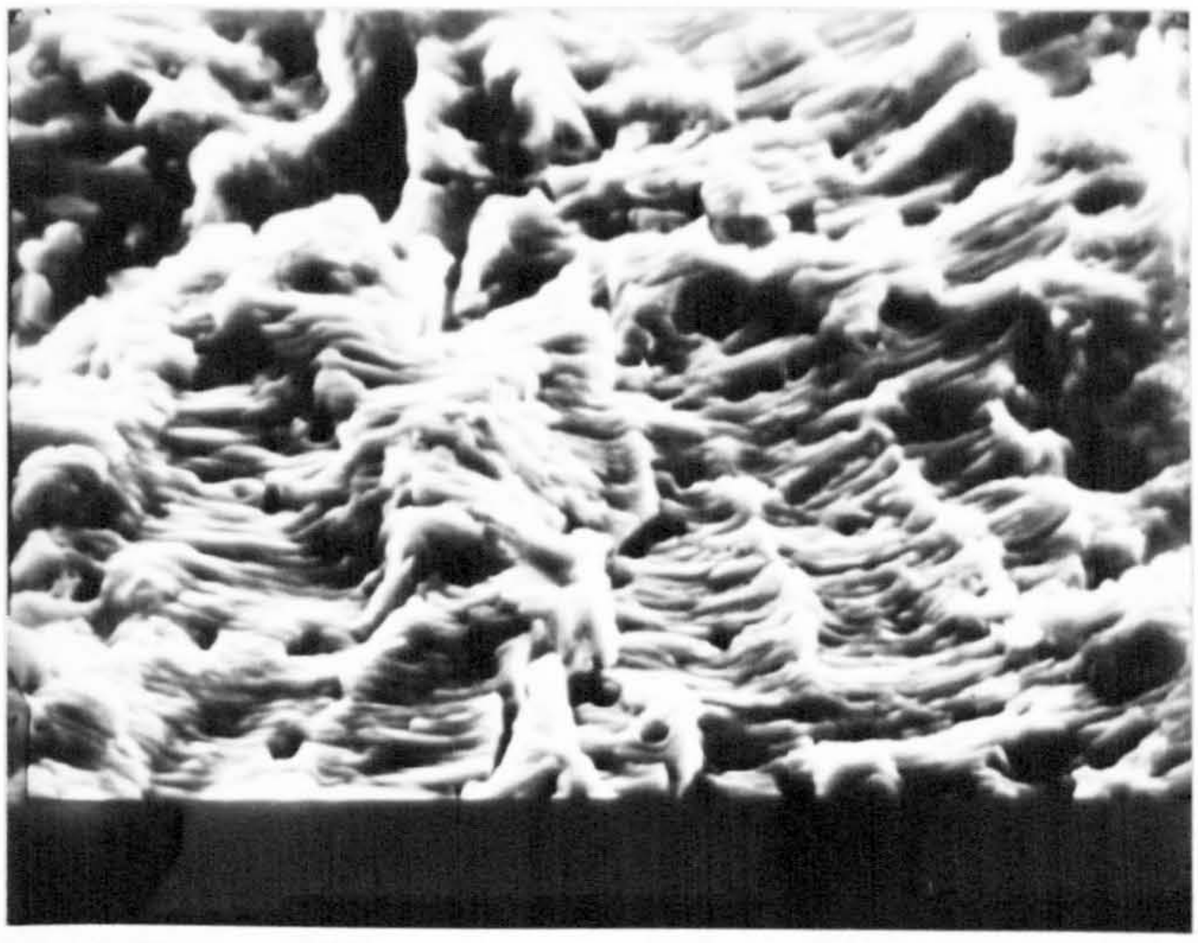

Crack growth direction

Figure 14 - Fracture surfaces in weld metal in air, exhibiting ductile striation-type surface markings

Magnification x 5000

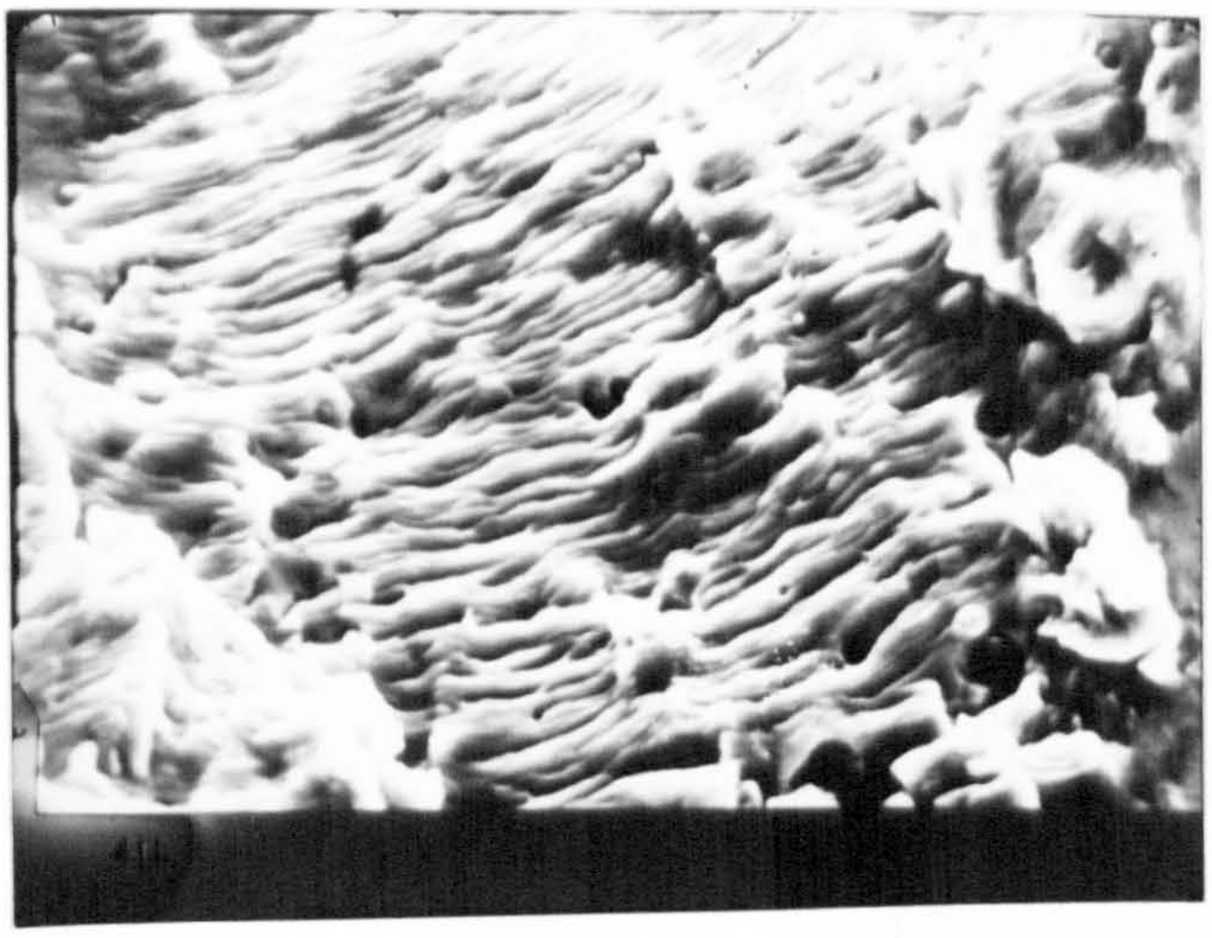

Crack growth direction

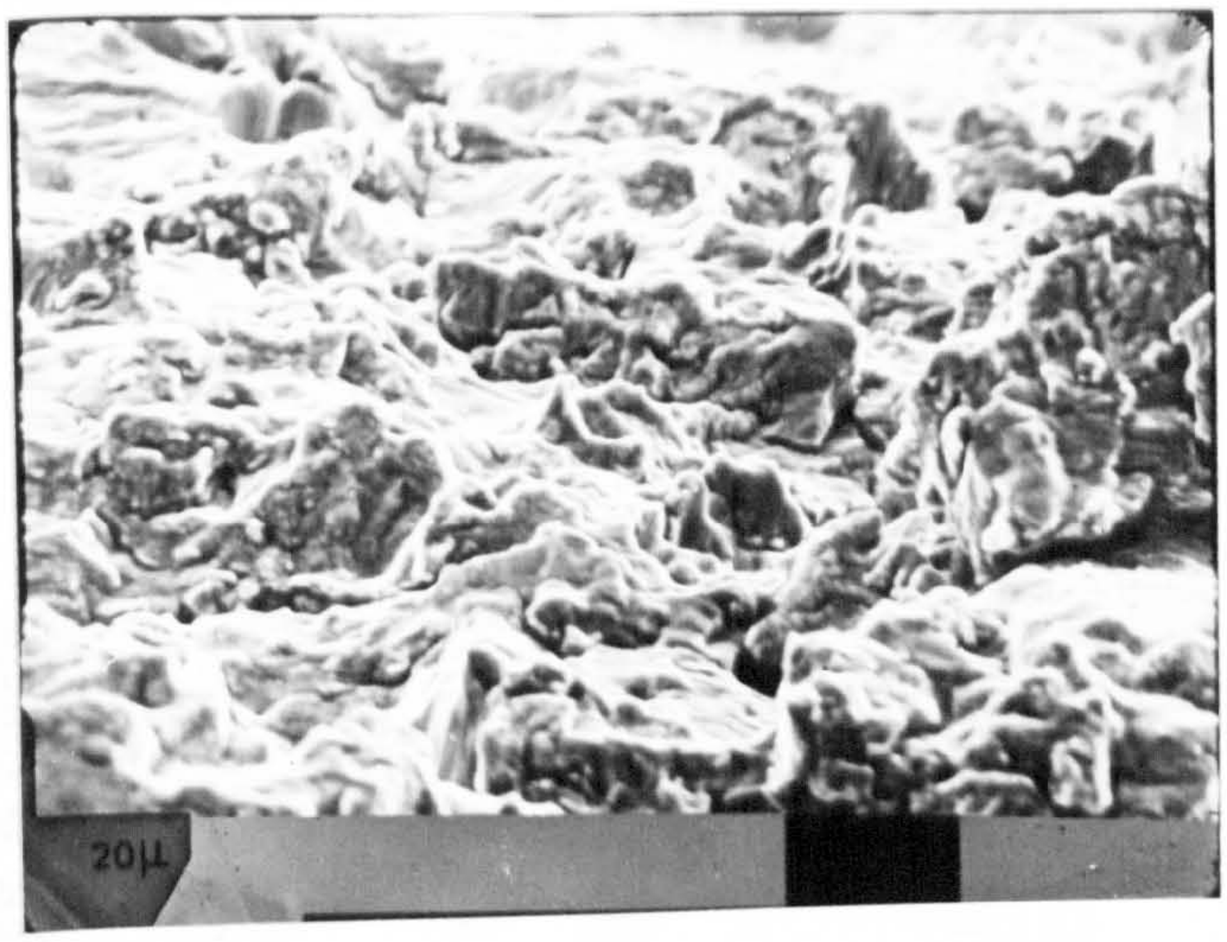

Crack growth direction

Figure 15 - Fracture surface in BS 4360 50D parent plate material in air, exhibiting ductile striation-type surface markings

Magnification x 1000

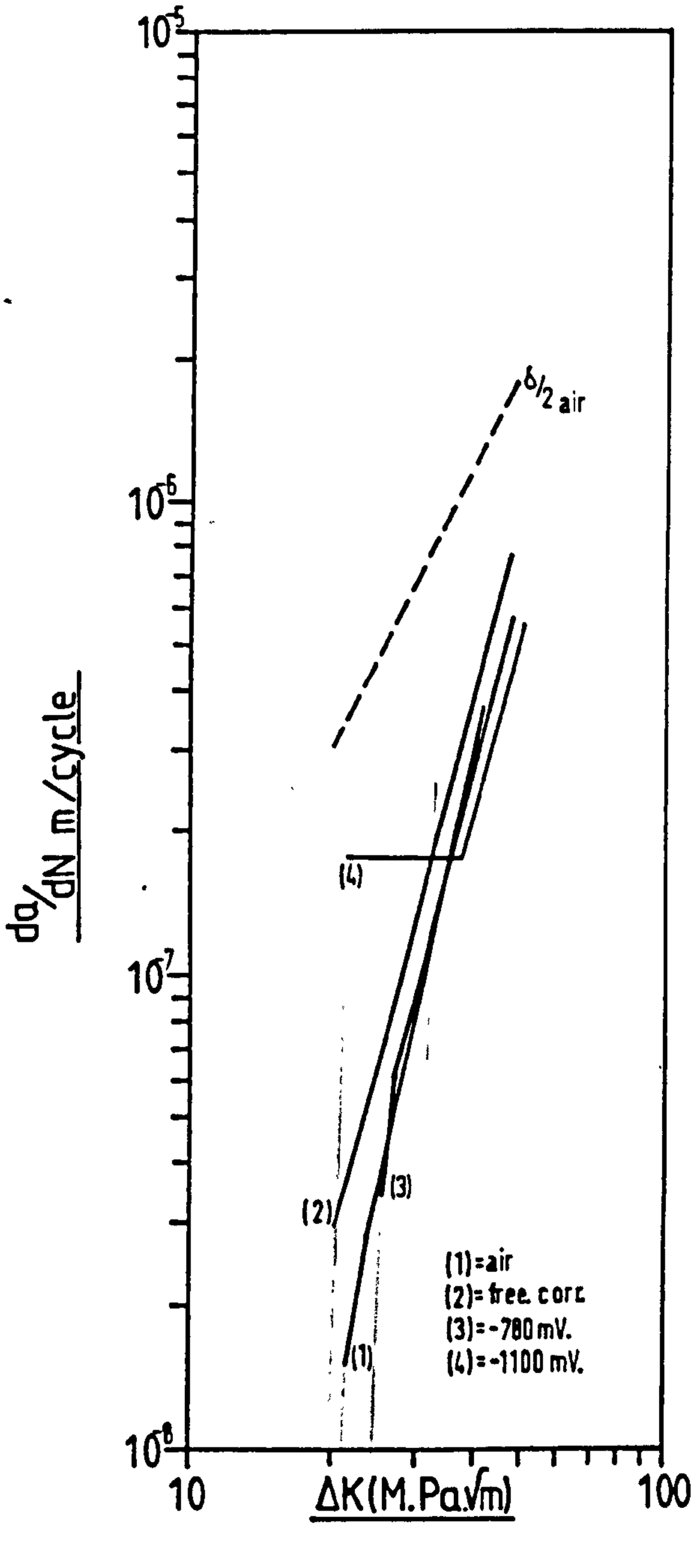

Figure 16 - Graphs of log da/dN Vs log ΔK, for crack growth in BS 4360 50D plate material in environments of laboratory air, nominal correct cathodic protection, nominal cathodic overprotection and free corrosion.

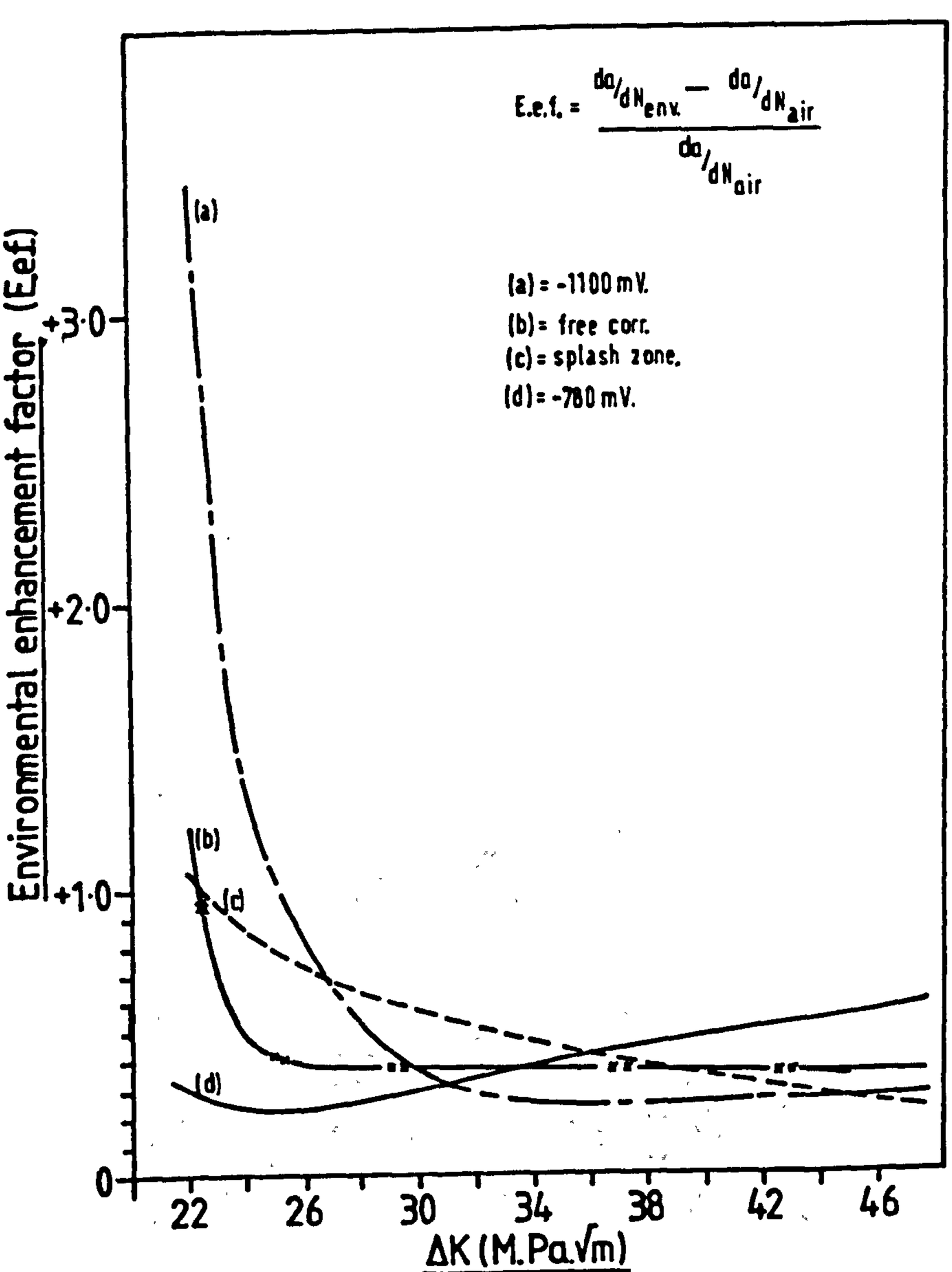

Figure 17 - Graphs of Environmental Enhancement Factor Vs ΔK, for crack growth in BS 4360 50D plate material

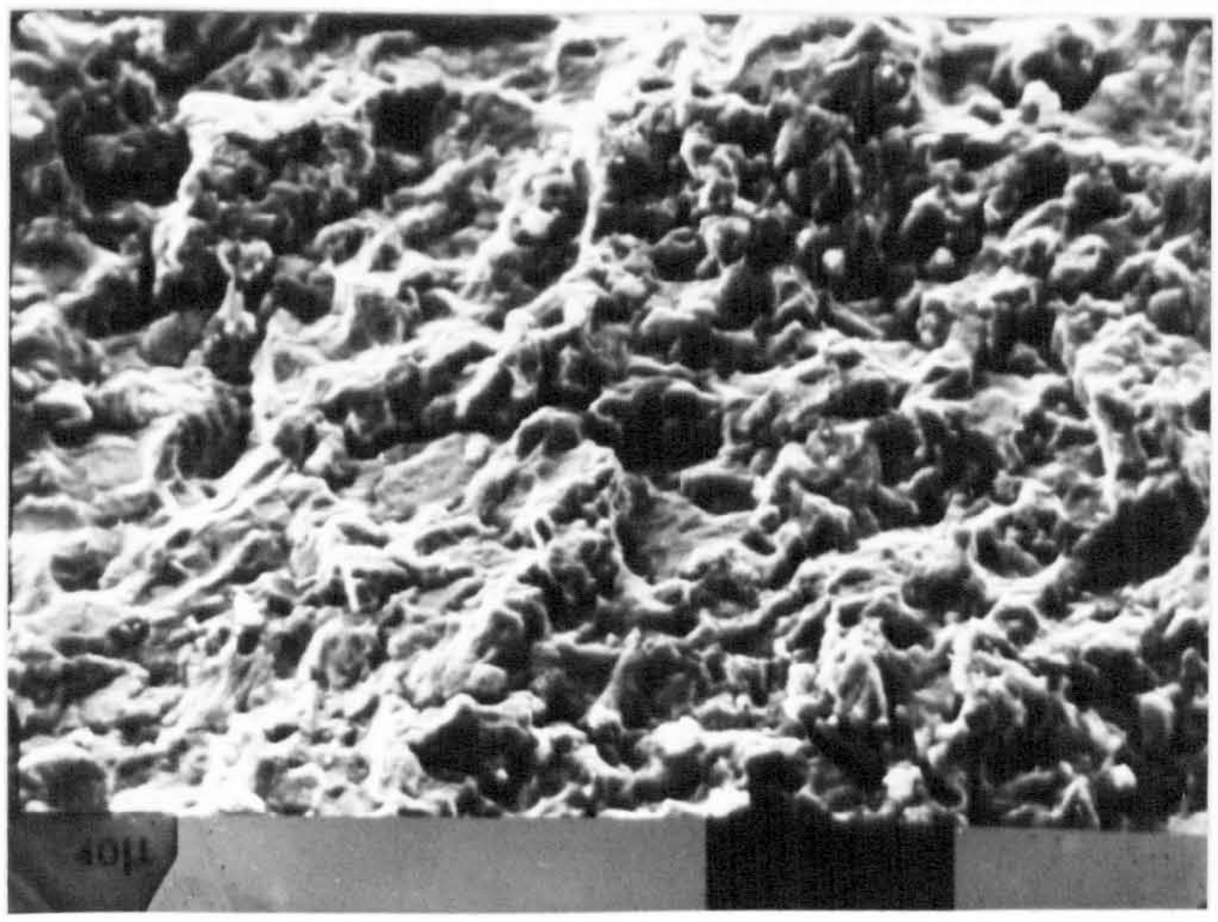

Crack growth direction

Figure 18A - Fracture surface in BS 4360 50D parent plate material, in an environment of free corrosion at $\Delta K \simeq 26$ M.Pa$\sqrt{m}$

Magnification x 500

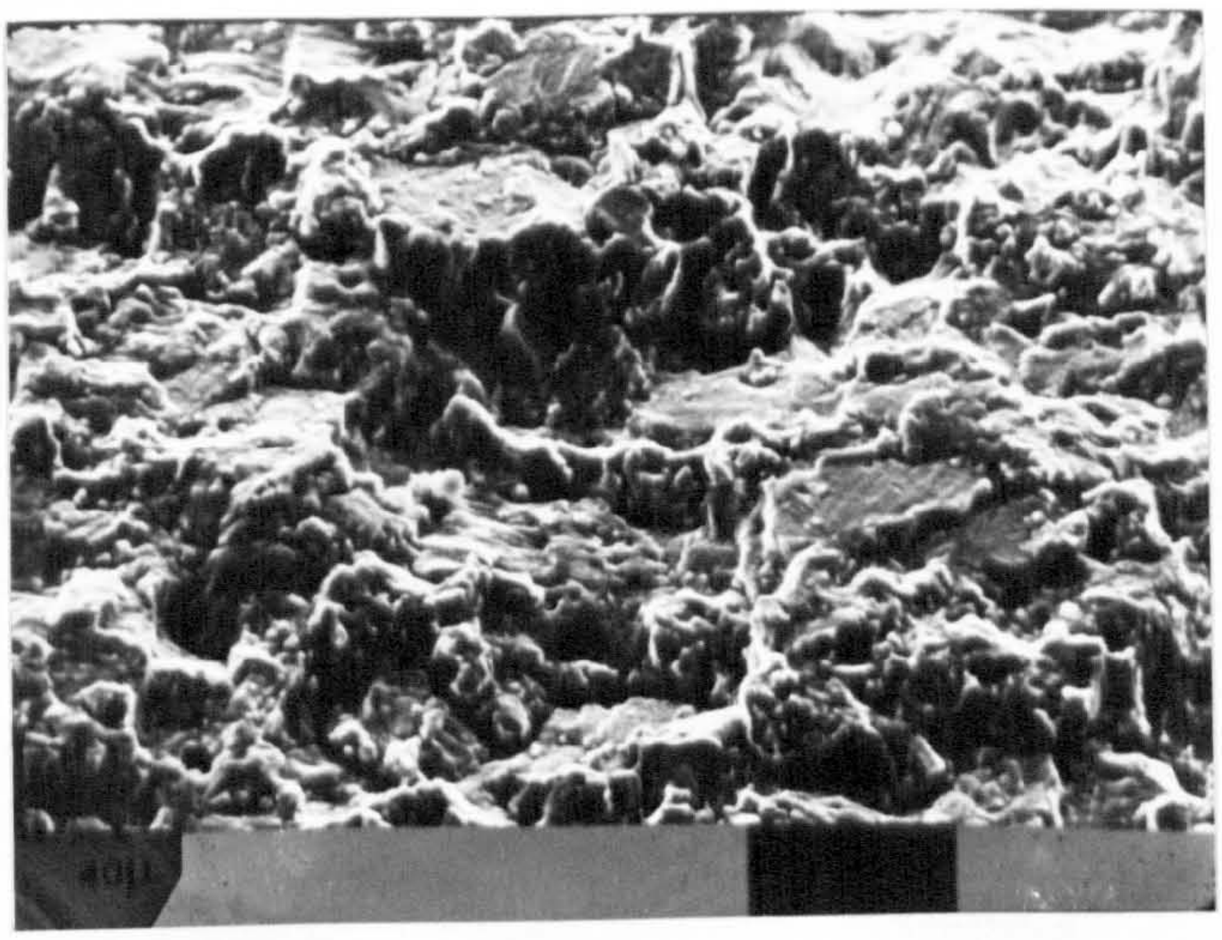

Crack growth direction

Figure 18B - Fracture surface in BS 4360 50D parent plate material, in an environment of free corrosion at $\Delta K \simeq 42$ M.Pa$\sqrt{m}$

Magnification x 500

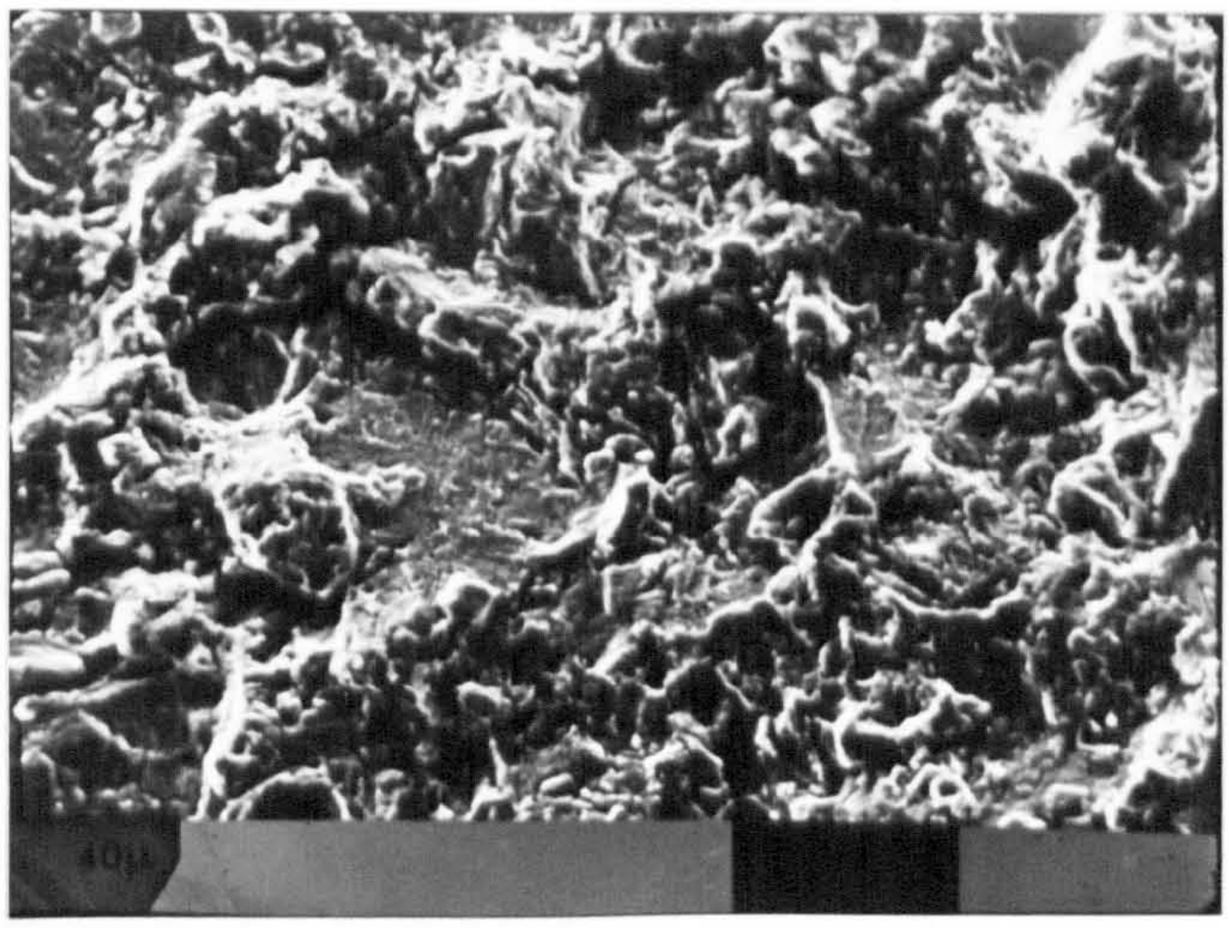

Crack growth direction

Figure 19A - Fracture surface in BS 4360 50D parent plate material, in an environment of nominal correct cathodic protection at $\Delta K \simeq 26$ M.Pa$\sqrt{m}$

Magnification x 500

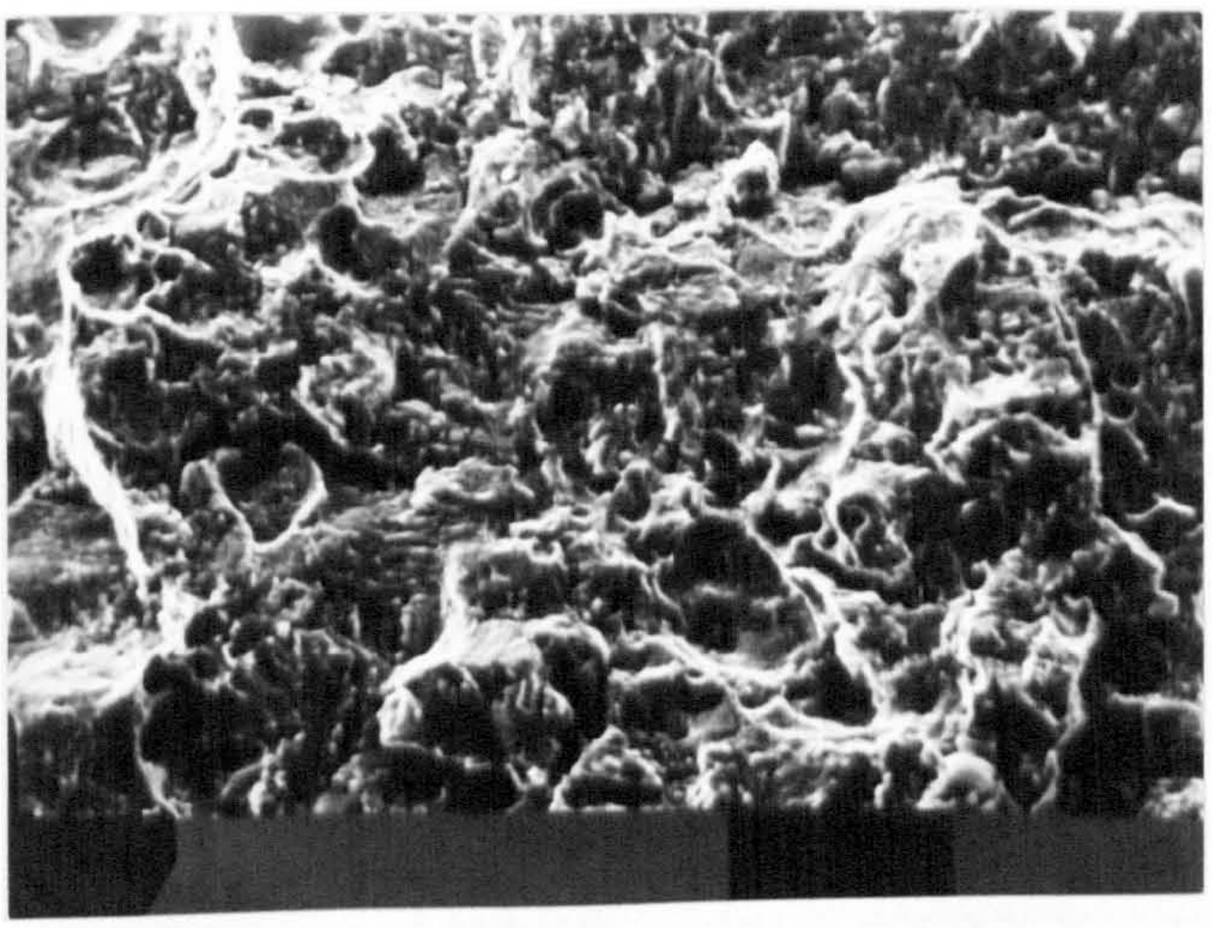

Crack growth direction

Figure 19B - Fracture surface in BS 4360 50D parent plate material, in an environment of nominal correct cathodic protection at $\Delta K \simeq 42$ M.Pa$\sqrt{m}$

Magnification x 500

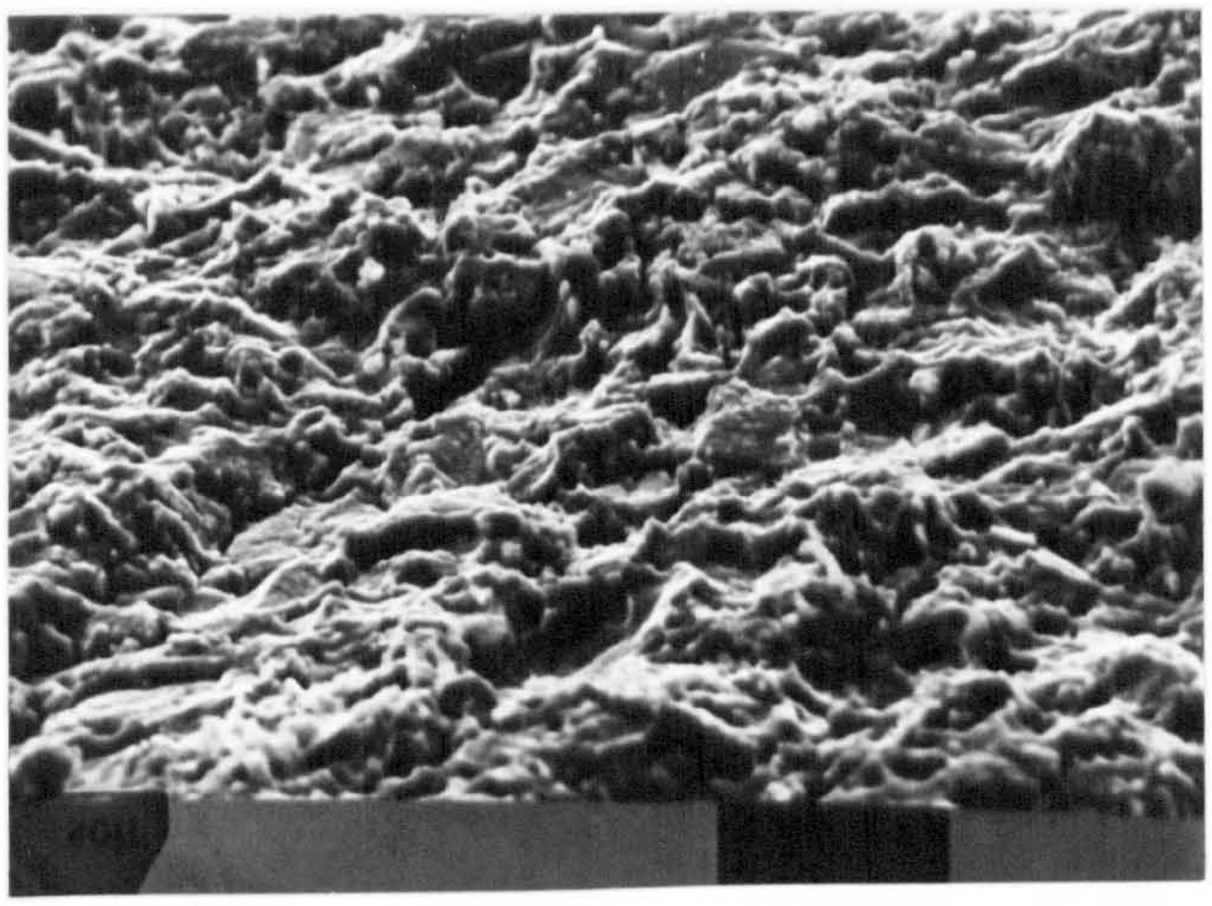

Crack growth direction

Figure 20A - Fracture surface in BS 4360 50D parent plate material, in an environment of nominal cathodic overprotection at $\Delta K \simeq 26$ M.Pa$\sqrt{m}$

Magnification x 500

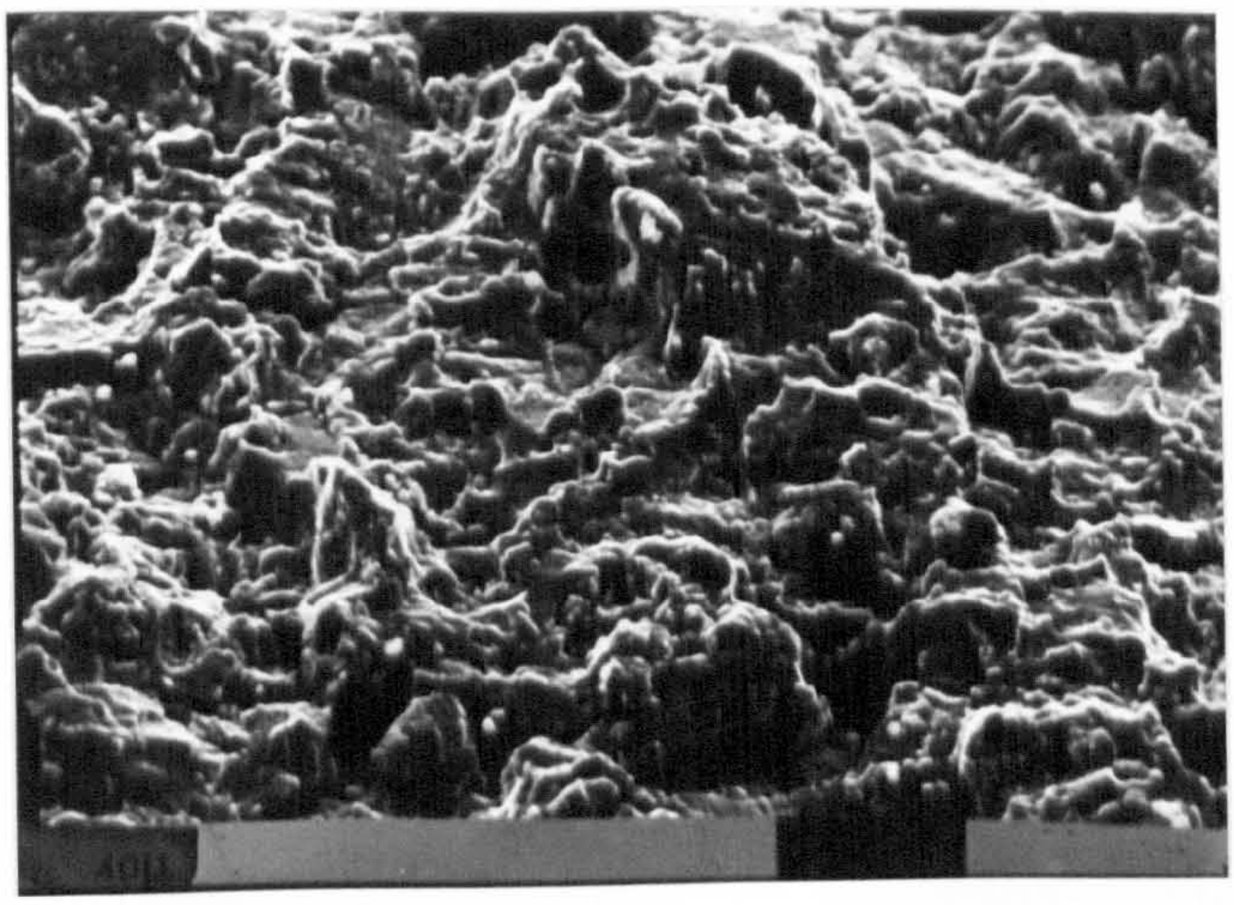

Crack growth direction

Figure 20B - Fracture surface in BS 4360 50D parent plate material, in an environment of nominal cathodic overprotection at $\Delta K \simeq 42$ M.Pa$\sqrt{m}$

Magnification x 500

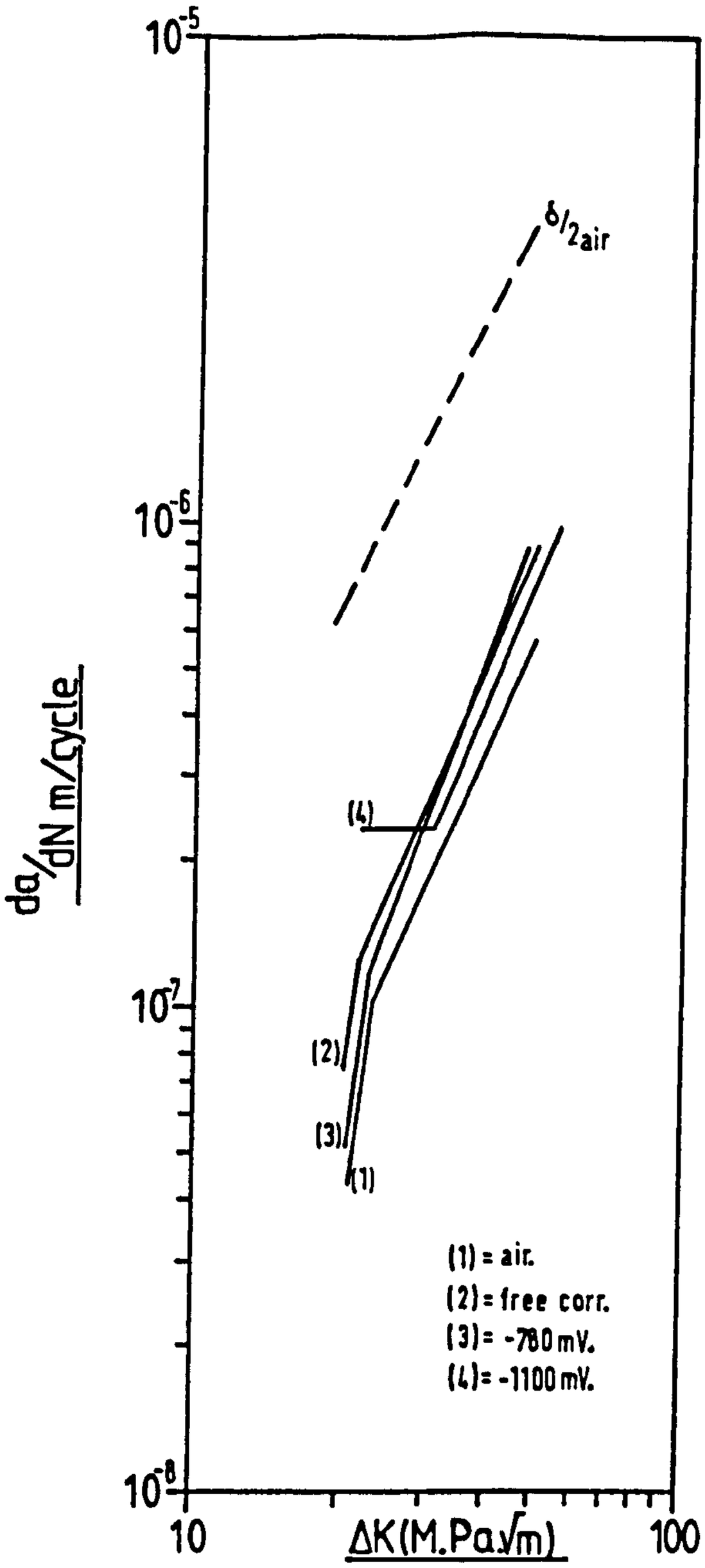

Figure 21 - Graphs of Log da/dN Vs Log ΔK, for crack growth in weld metal in environments of laboratory air, nominal correct cathodic protection, nominal cathodic overprotection and free corrosion.

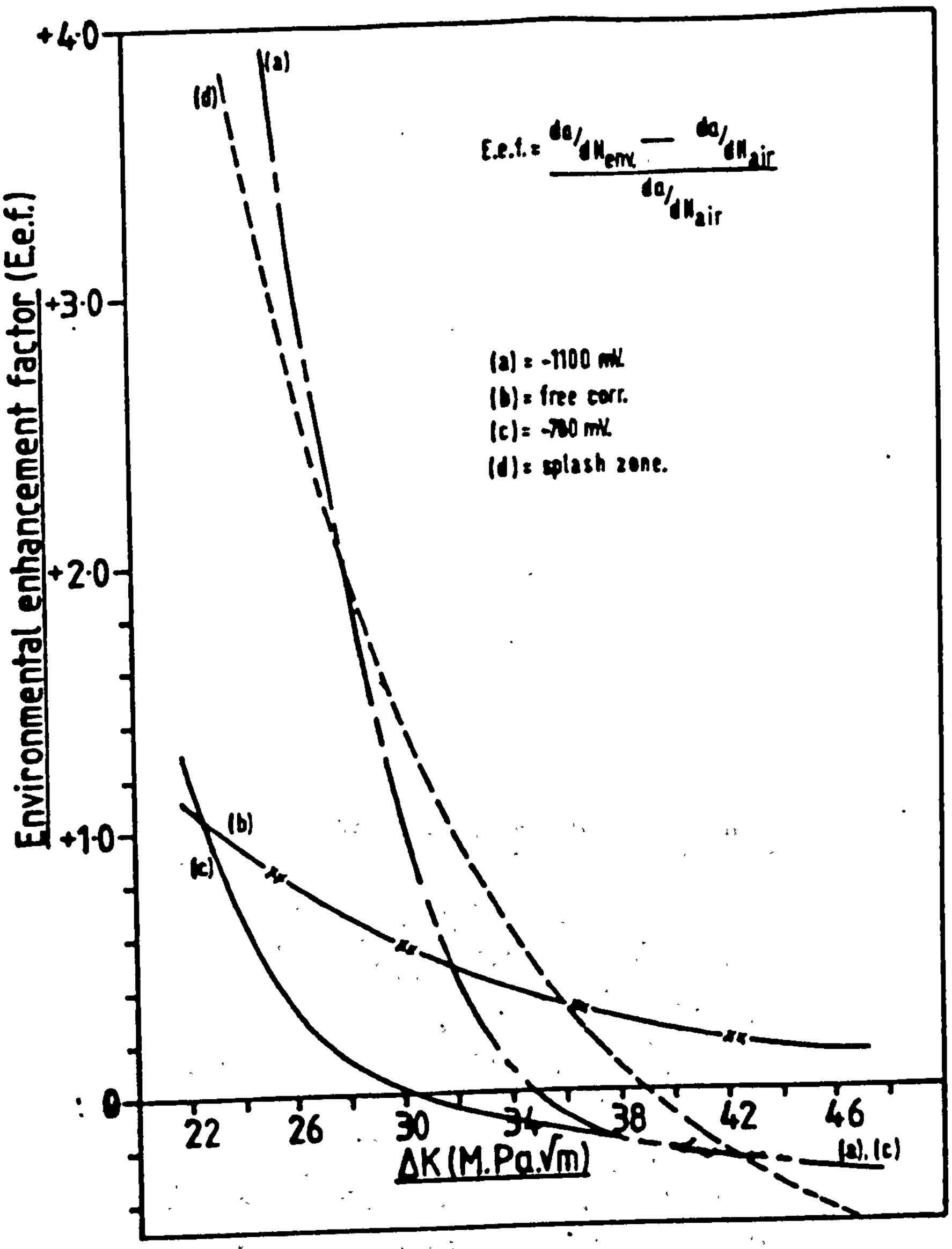

Figure 22 – Graphs of Environmental Enhancement Factor Vs ΔK, for crack growth in weld metal.

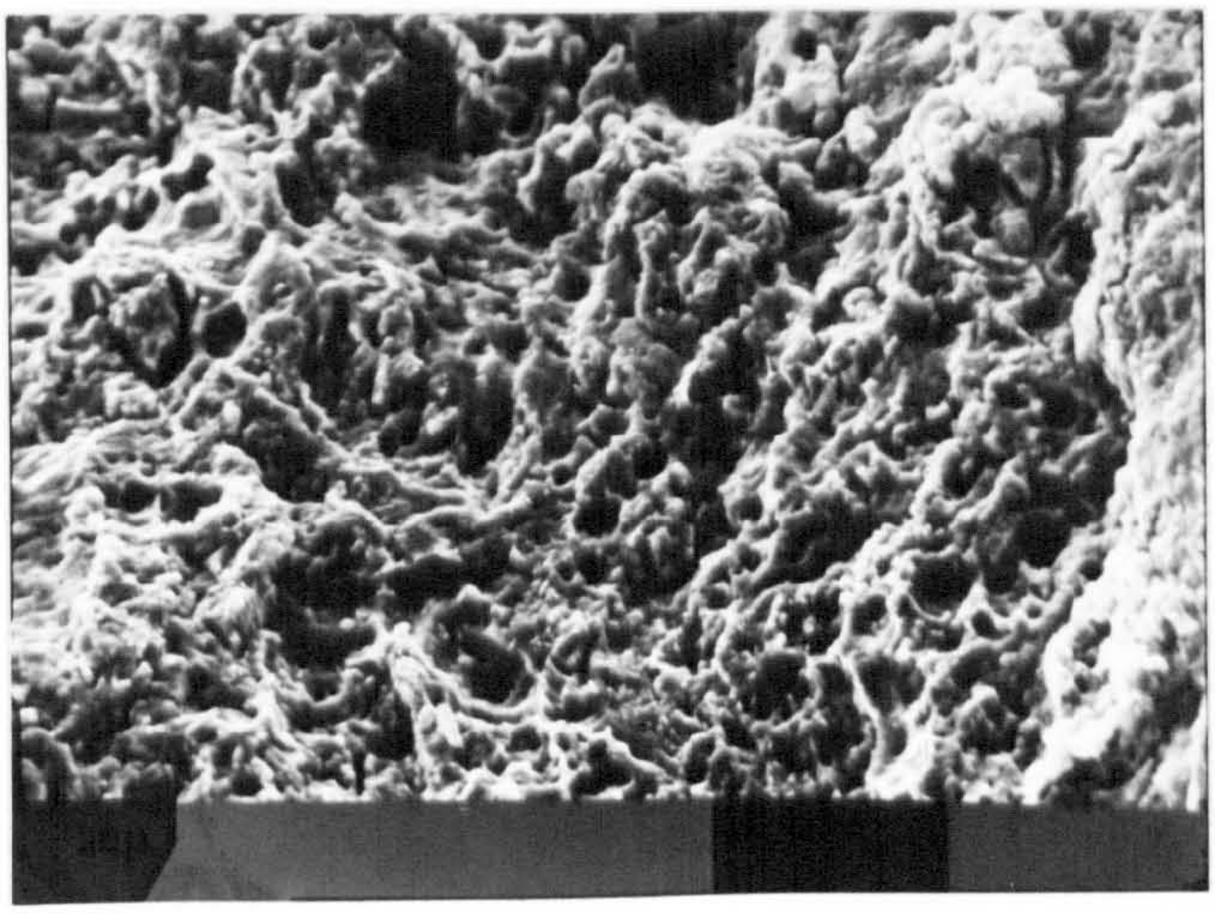

Crack growth direction

Figure 23A - Fracture surface in weld metal, in an environment of free corrosion at $\Delta K \simeq 26$ M.Pa$\sqrt{m}$

Magnification x 1000

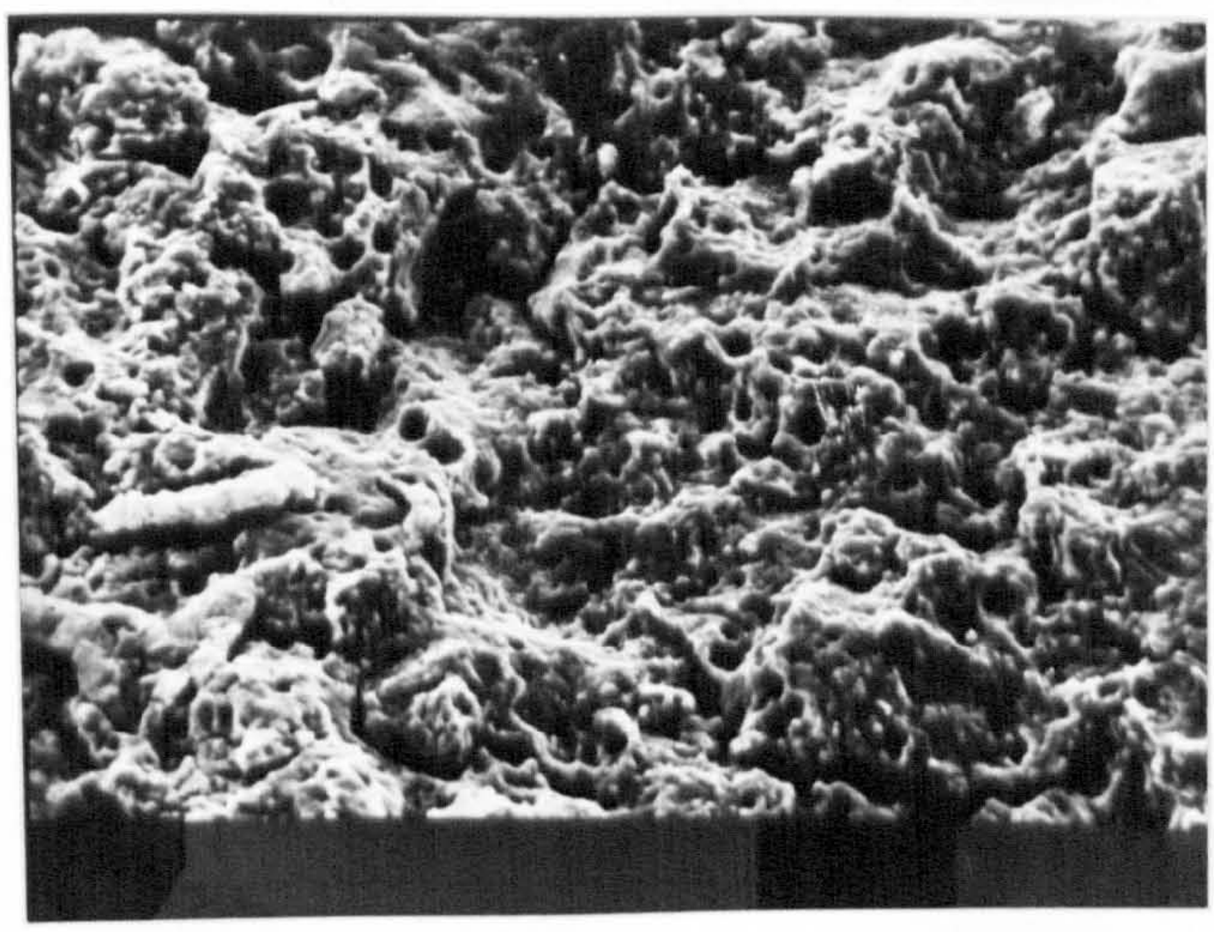

Crack growth direction

Figure 23B - Fracture surface in weld metal, in an environment of free corrosion at $\Delta K \simeq 42$ M.Pa$\sqrt{m}$

Magnification x 1000

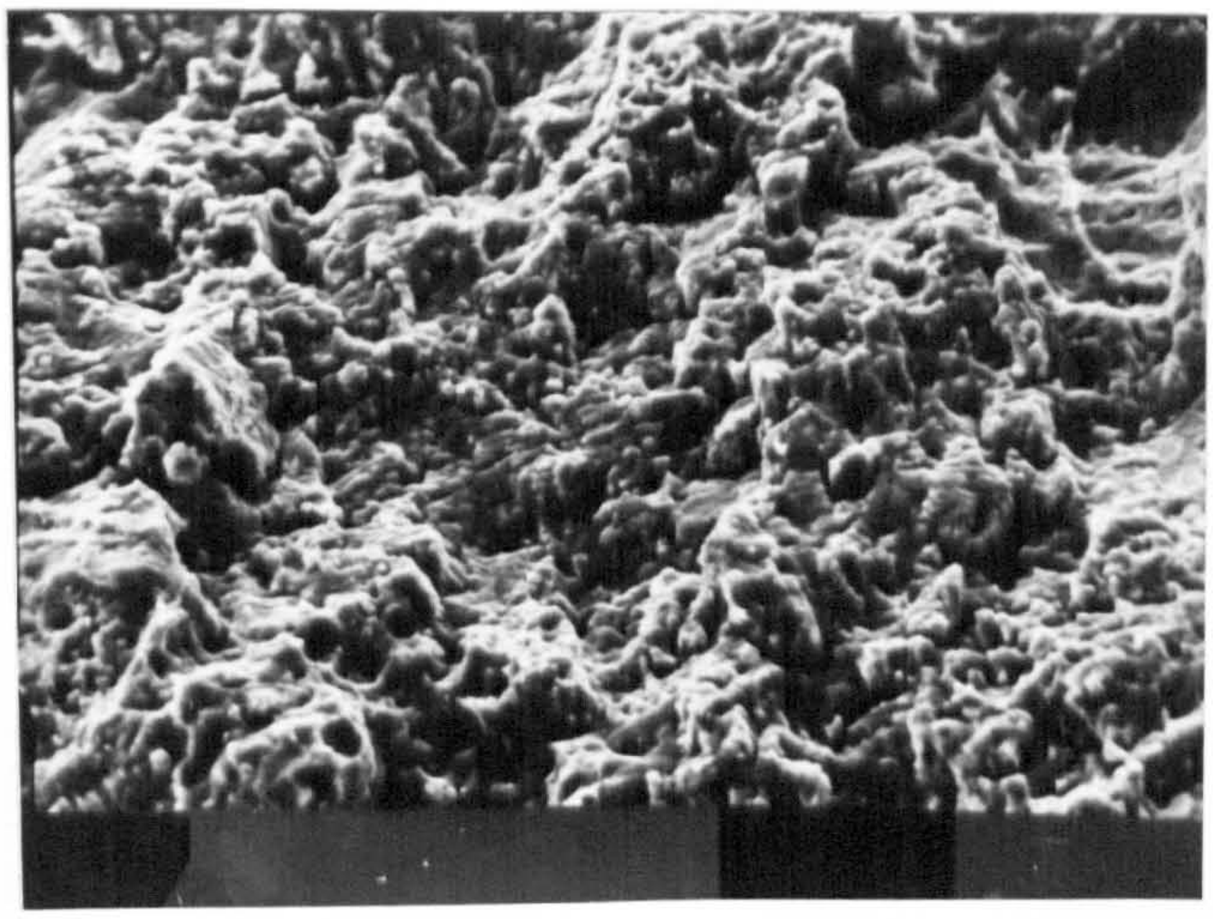

Crack growth direction

Figure 24A - Fracture surface in weld metal, in an environment of nominal correct cathodic protection at $\Delta K \simeq 26$ M.Pa$\sqrt{m}$

Magnification x 1000

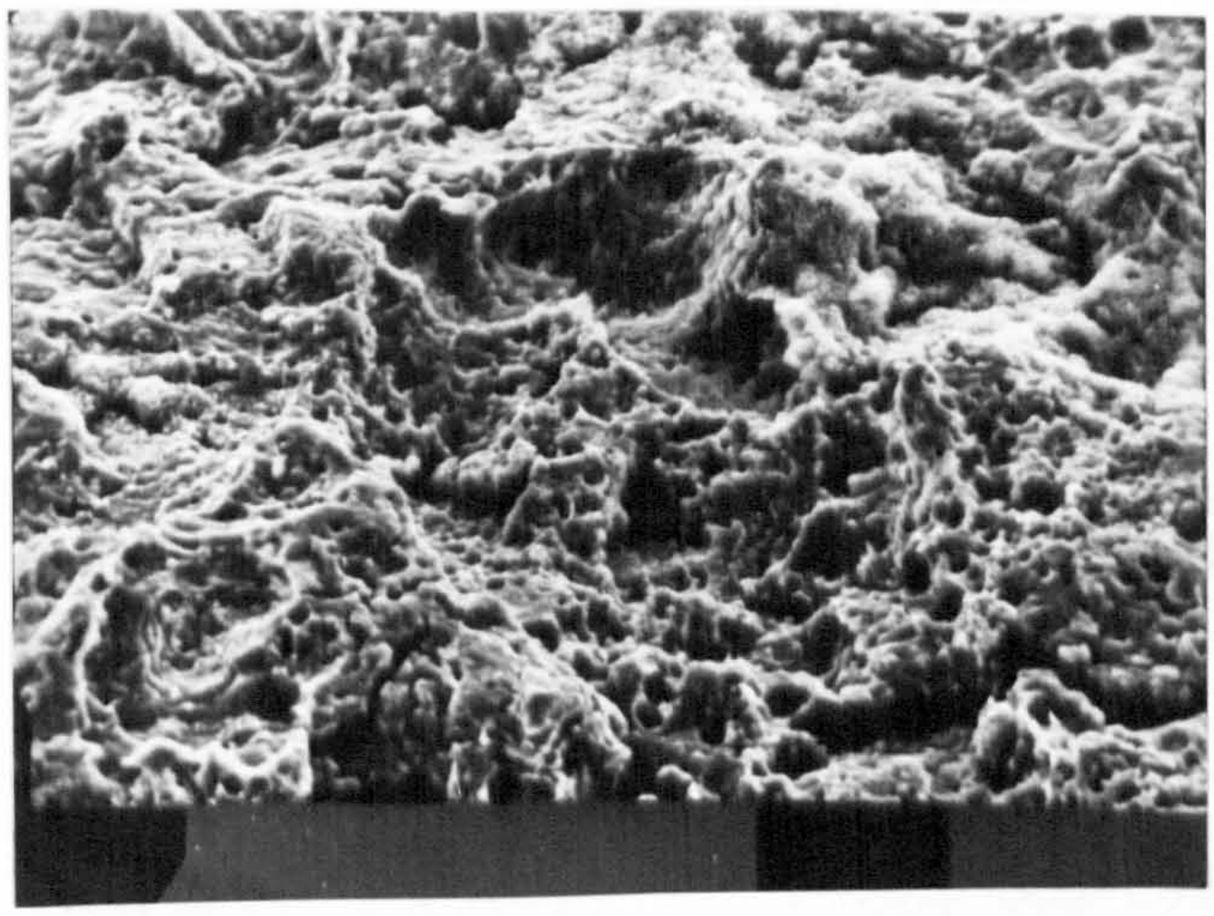

Crack growth direction

Figure 24B - Fracture surface in weld metal, in an environment of nominal correct cathodic protection at $\Delta K \simeq 42$ M.Pa$\sqrt{m}$

Magnification x 1000

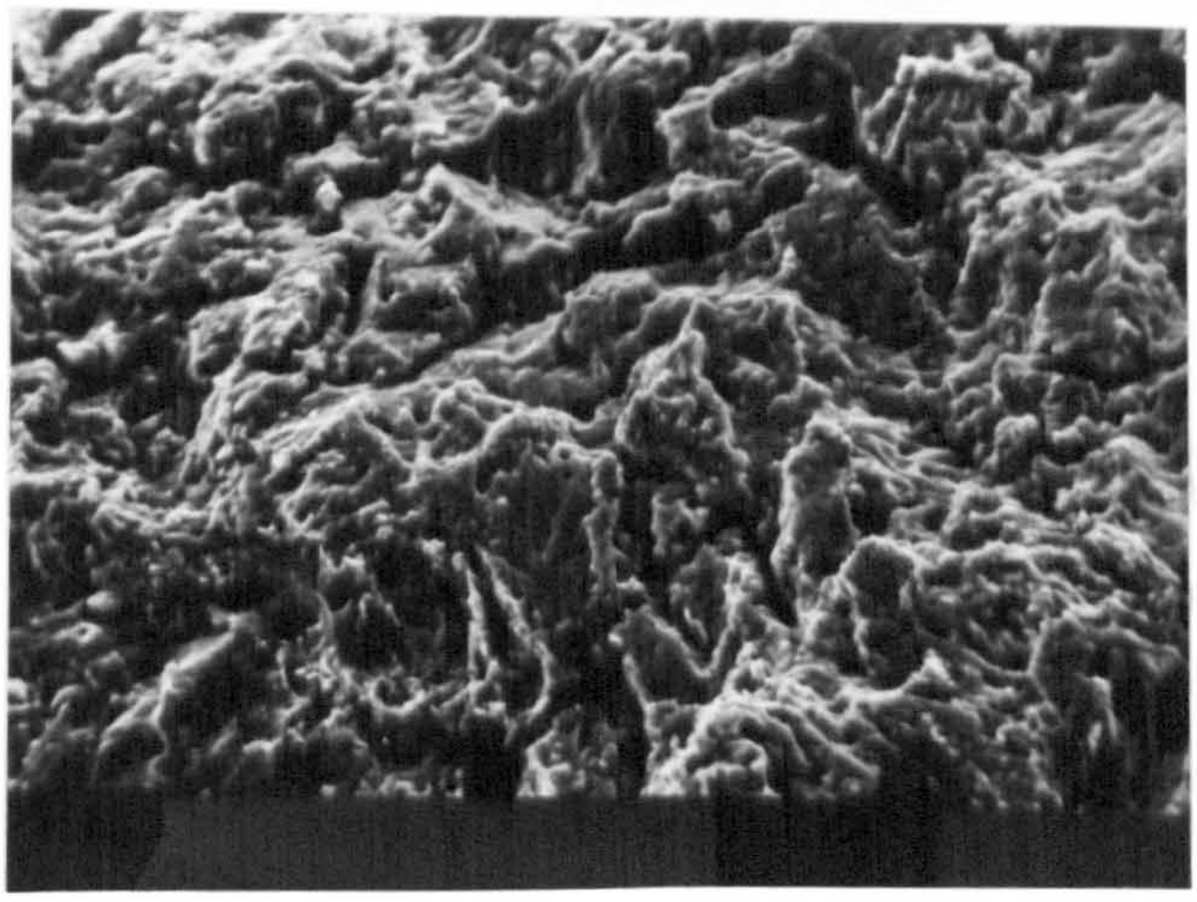

Crack growth direction

Figure 25A - Fracture surface in weld metal, in an environment of nominal cathodic overprotection at $\Delta K \simeq 26$ M.Pa$\sqrt{m}$

Magnification x 1000

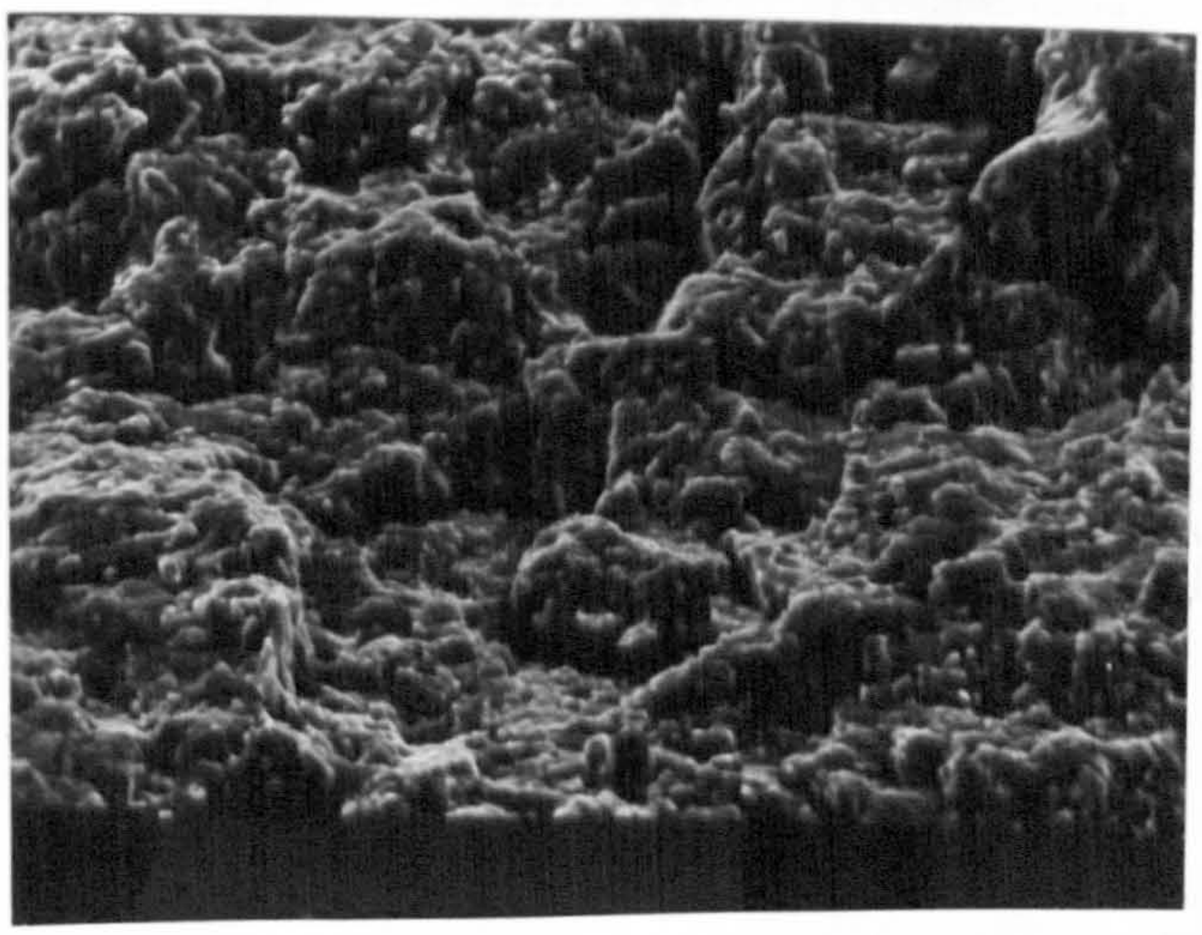

Crack growth direction

Figure 25B - Fracture surface in weld metal, in an environment of nominal cathodic overprotection at $\Delta K \simeq 42$ M.Pa$\sqrt{m}$

Magnification x 1000

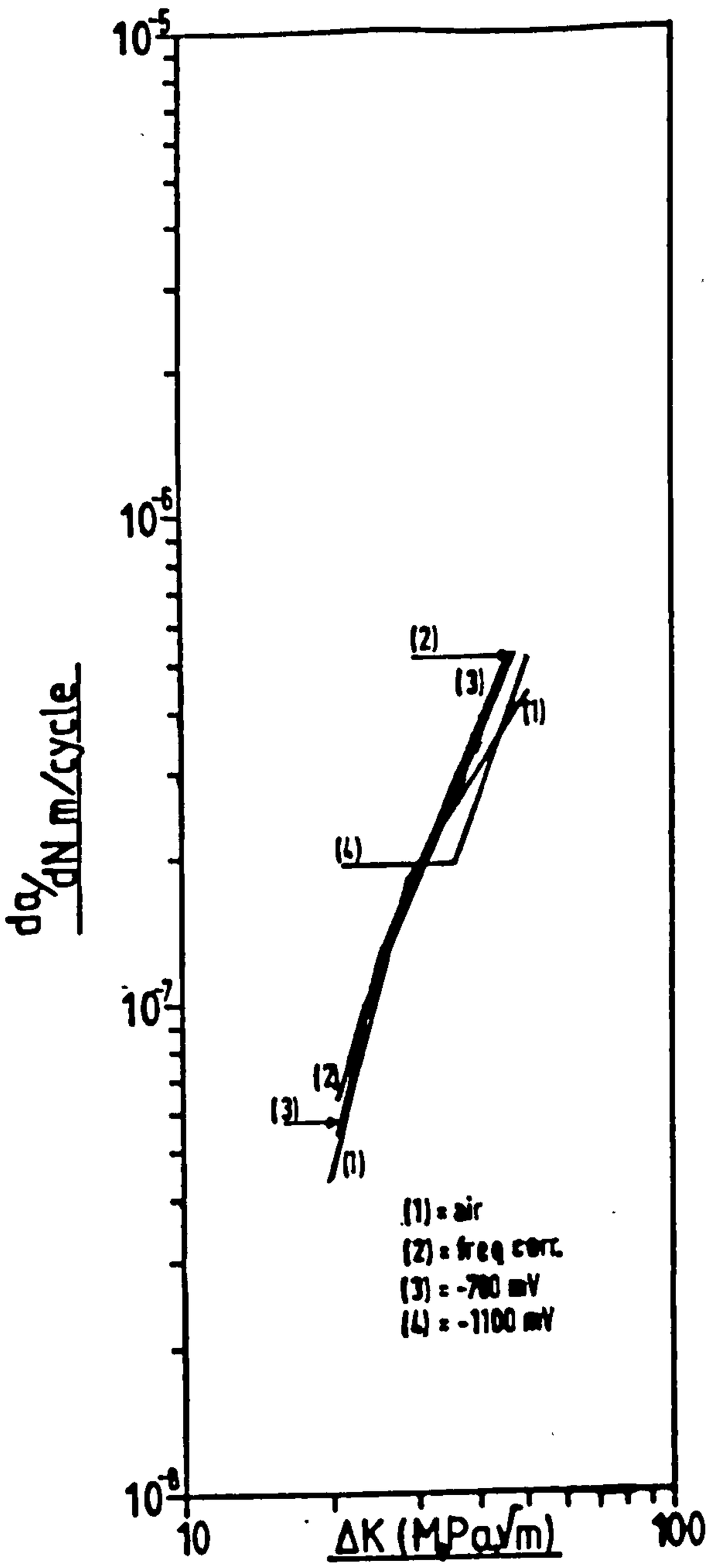

Figure 26 - Graphs of Log da/dN Vs Log ΔK for crack growth in heat affected zone microstructure in environments of laboratory air, nominal correct cathodic protection, nominal cathodic overprotection and free corrosion.

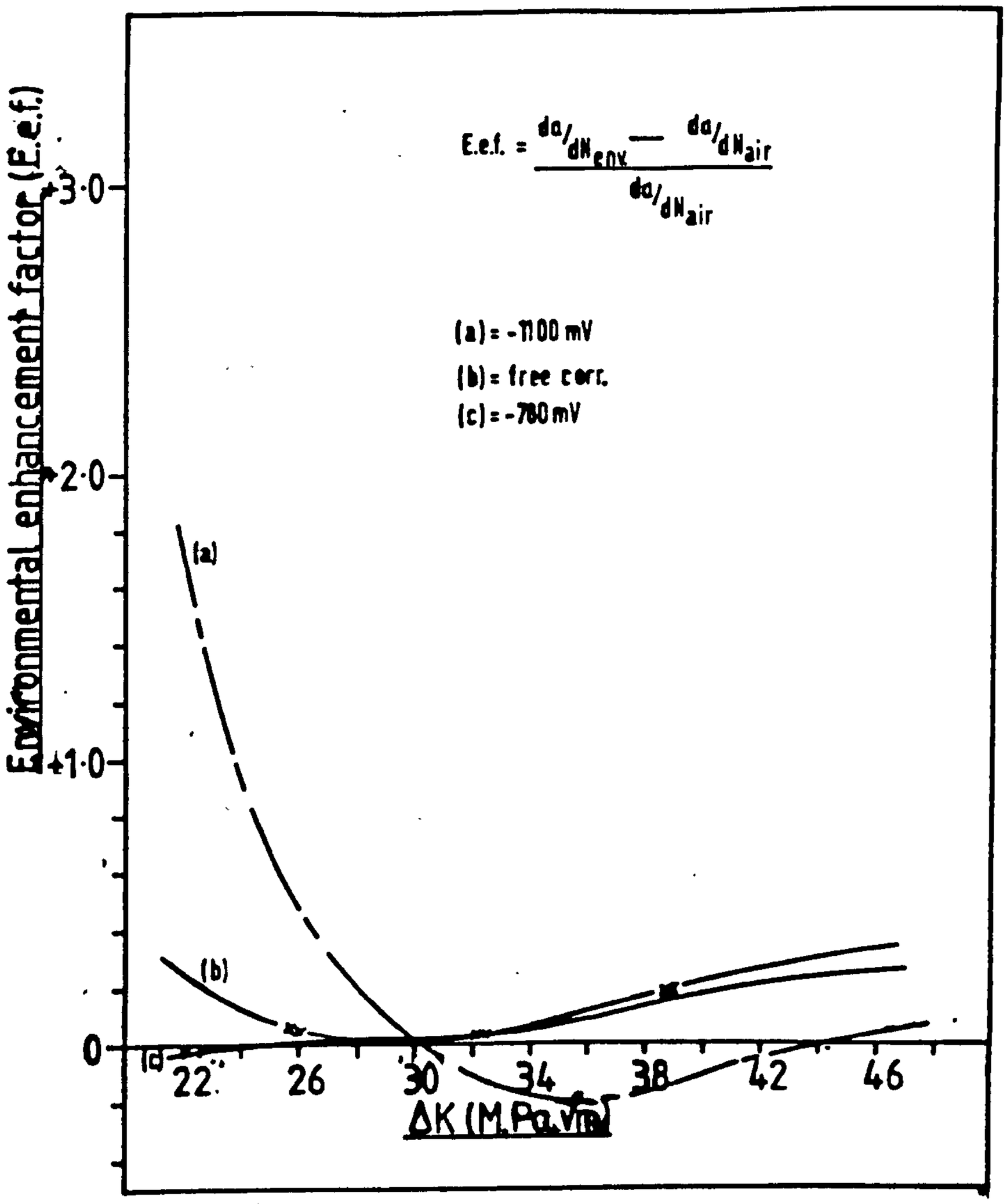

Figure 27 - Graphs of Environmental Enhancement Factor Vs ΔK, for crack growth in heat affected zone microstructure

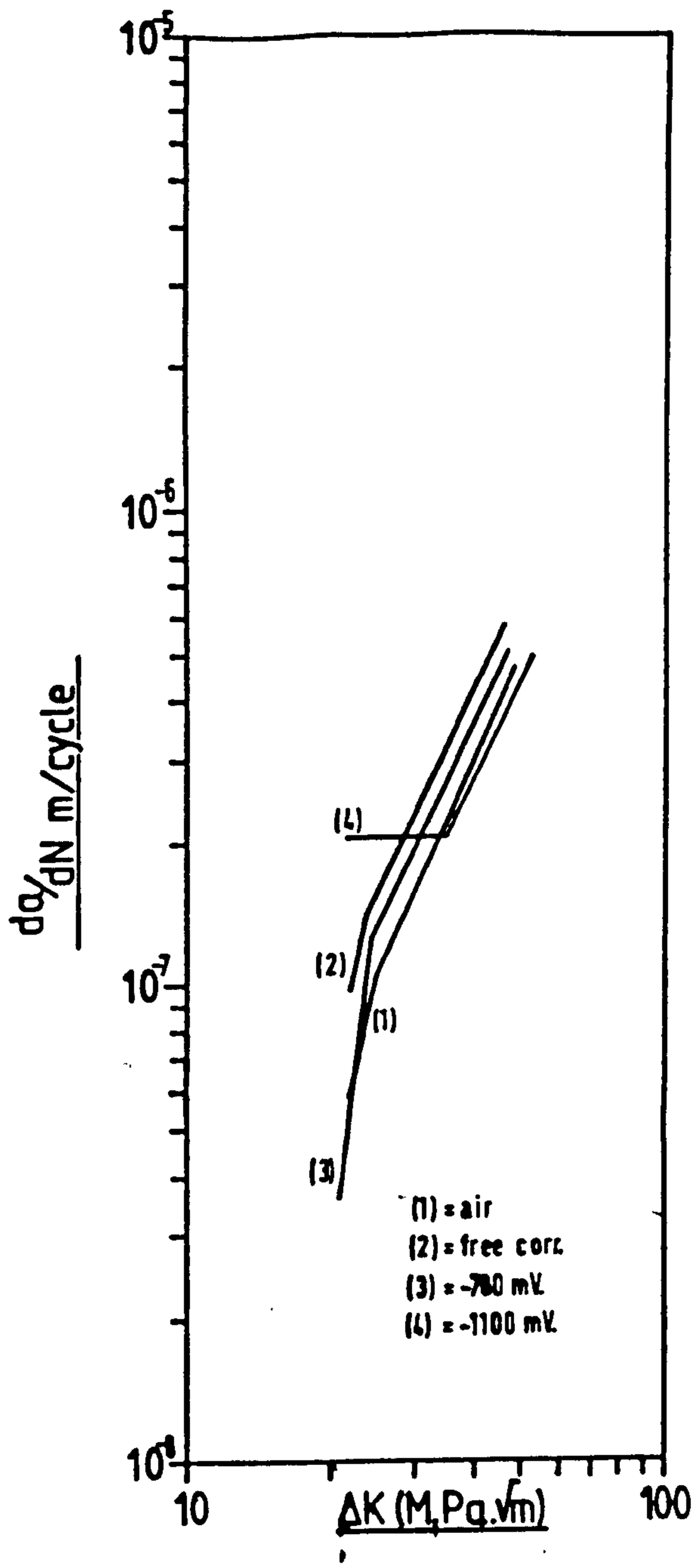

Figure 28 – Graphs of Log da/dN Vs Log ΔK, for crack growth in weld fusion-line microstructure, in environments of laboratory air, nominal correct cathodic protection, nominal cathodic overprotection and free corrosion.

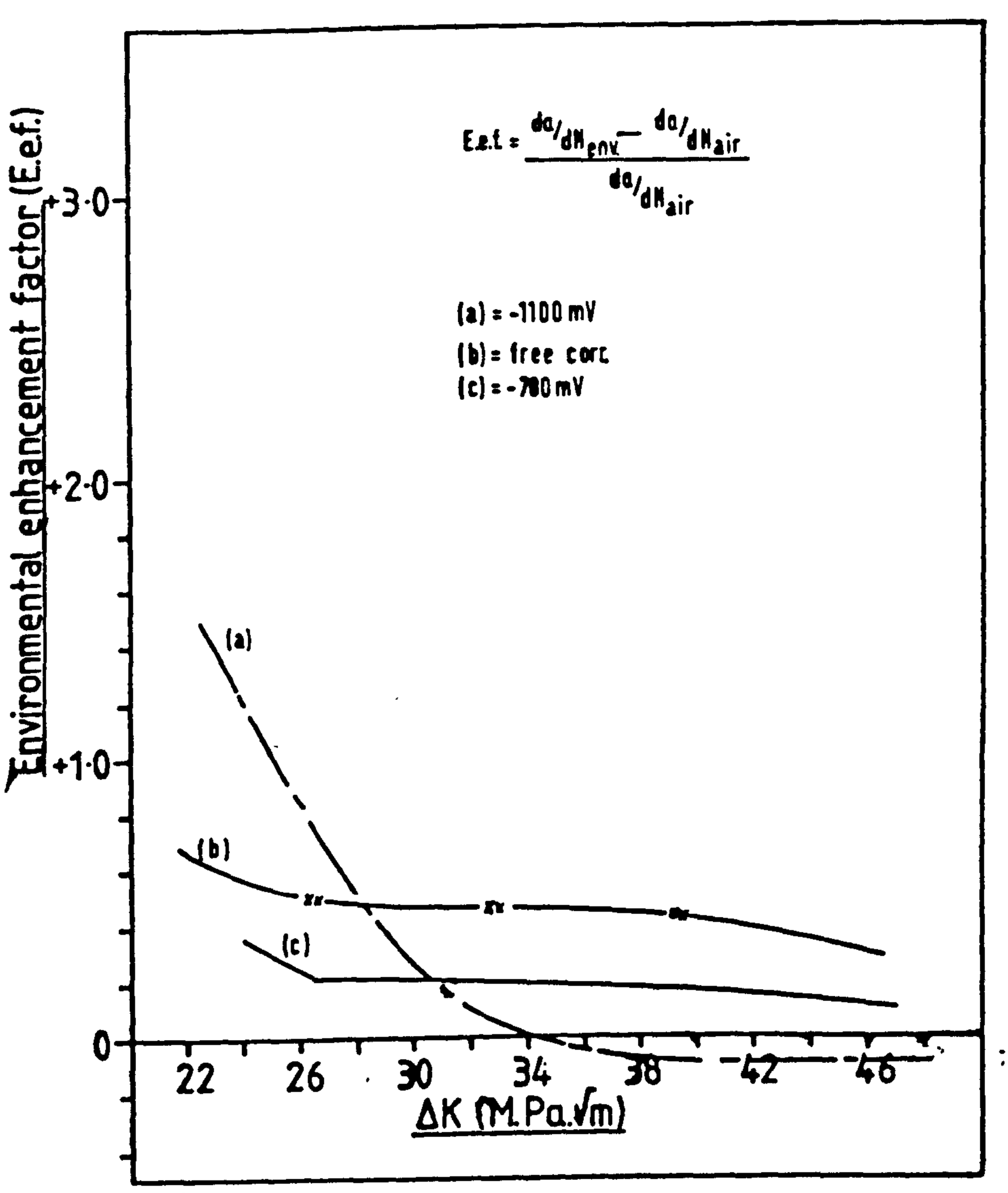

Figure 29 - Graphs of Environmental Enhancement Factor Vs ΔK for crack growth in weld fusion-line microstructure.

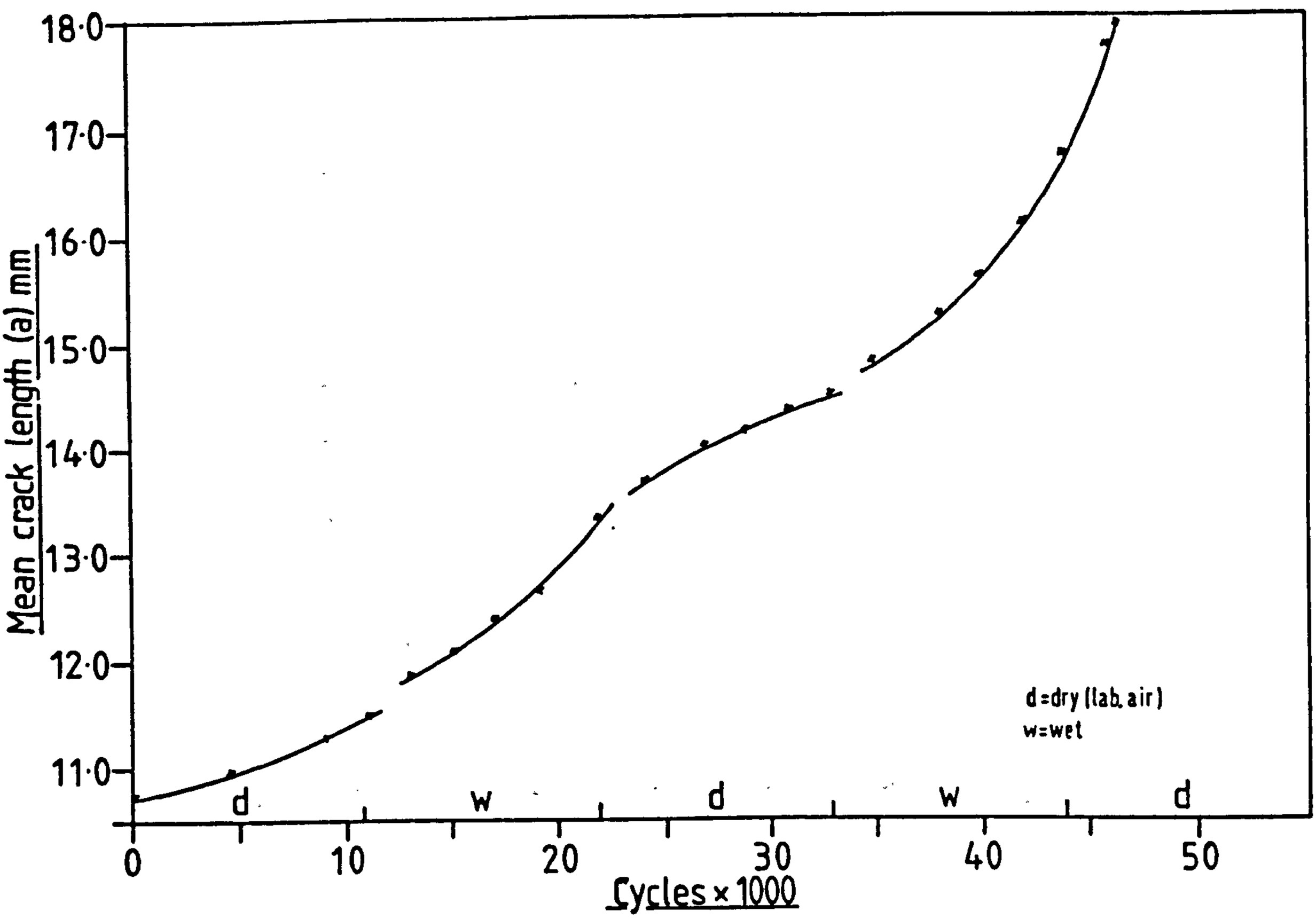

Figure 30 - Graph of a Vs N for crack growth in BS 4360 50D plate material in an environment of simulated tidal immersion.

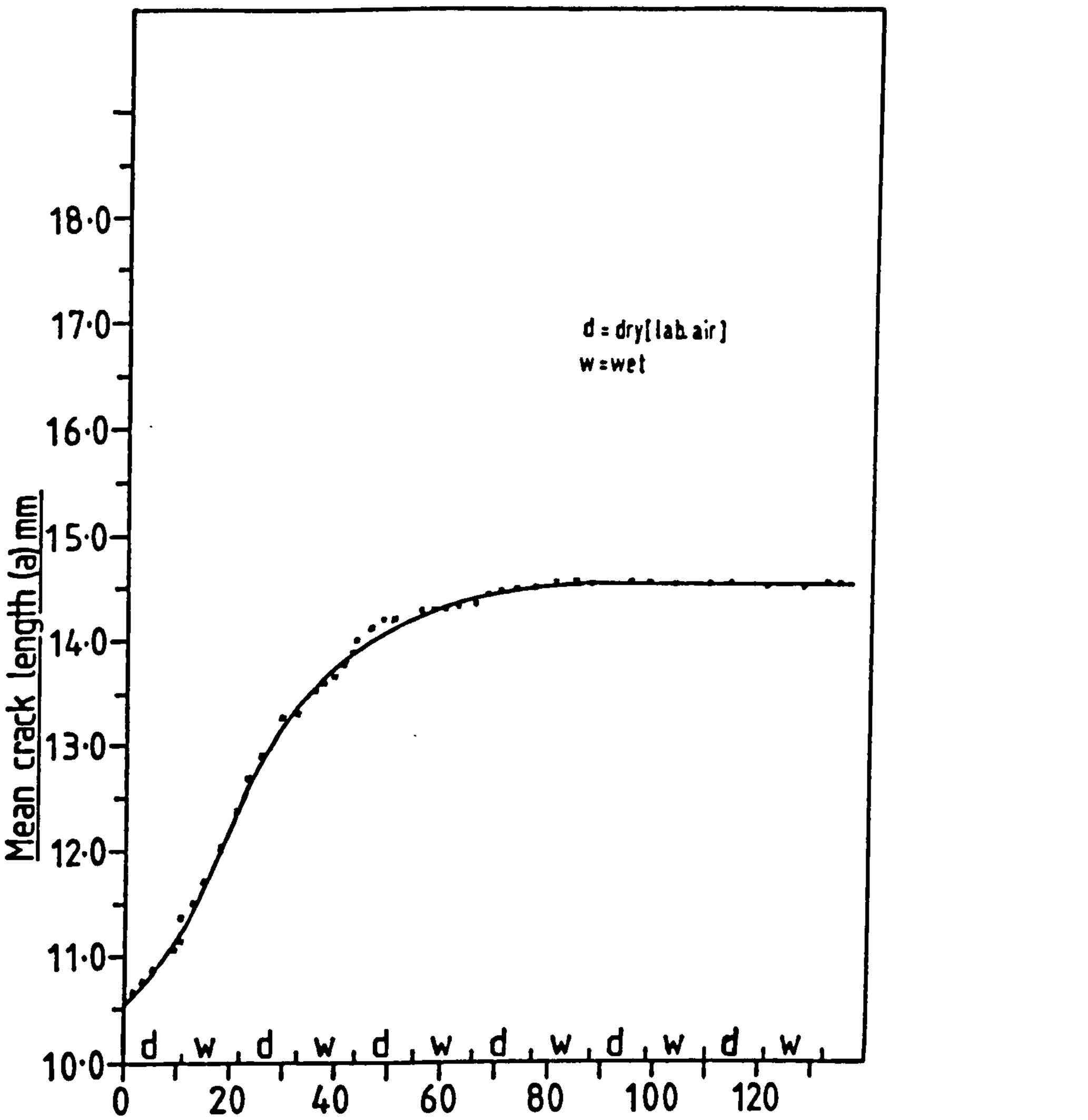

Figure 31 - Graph of a Vs N for crack growth in weld metal in an environment of simulated tidal immersion.

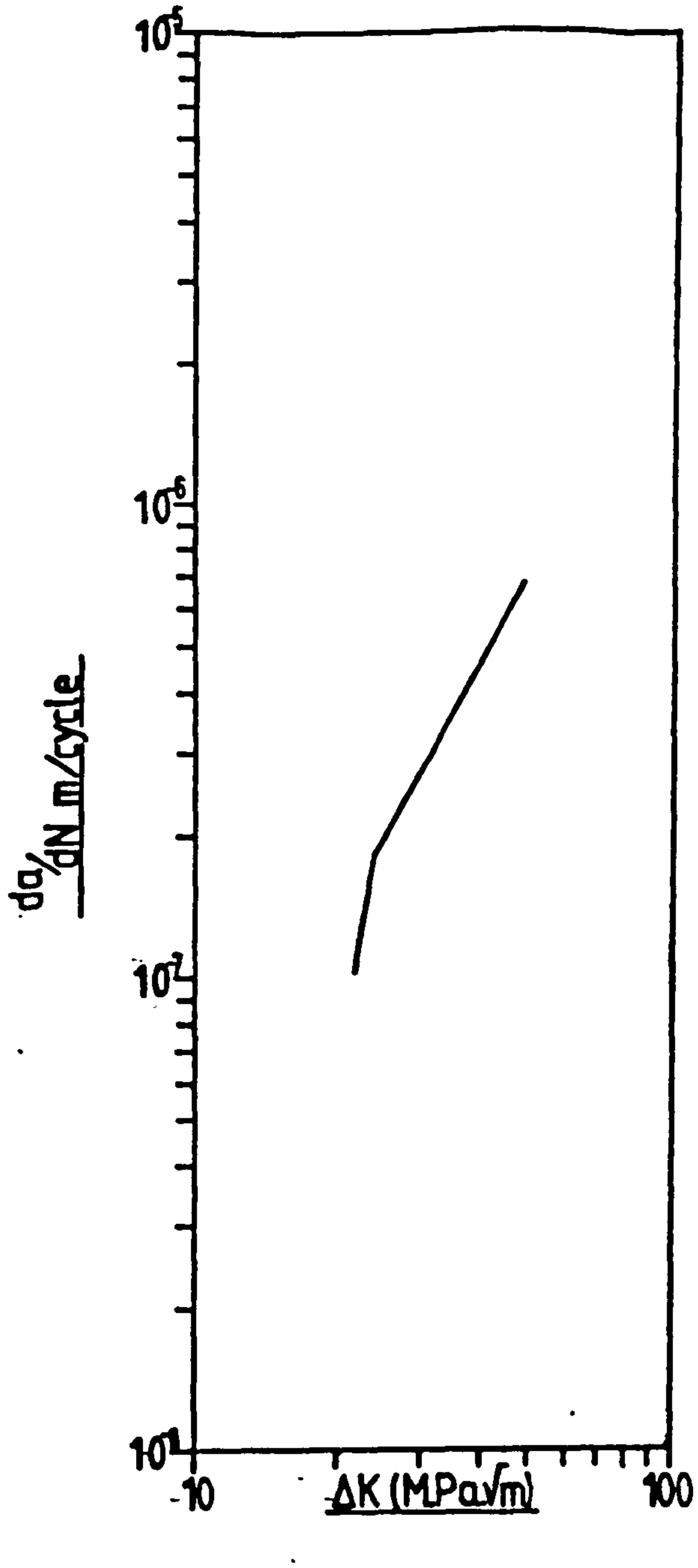

Figure 32 - Graph of log da/dN Vs log ΔK for crack growth in BS 4360 50D plate material, in an environment of simulated splash-zone.

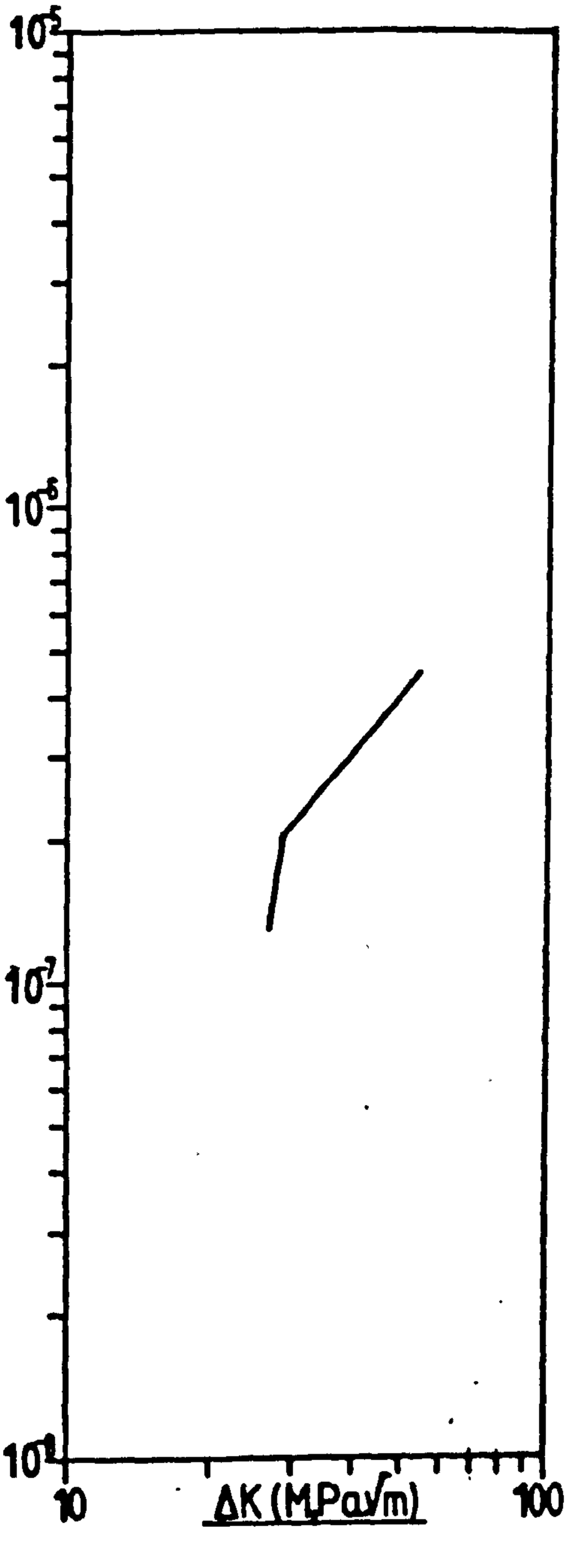

Figure 33 - Graph of log da/dN Vs log ΔK for crack growth in weld metal, in an environment of simulated splash-zone -

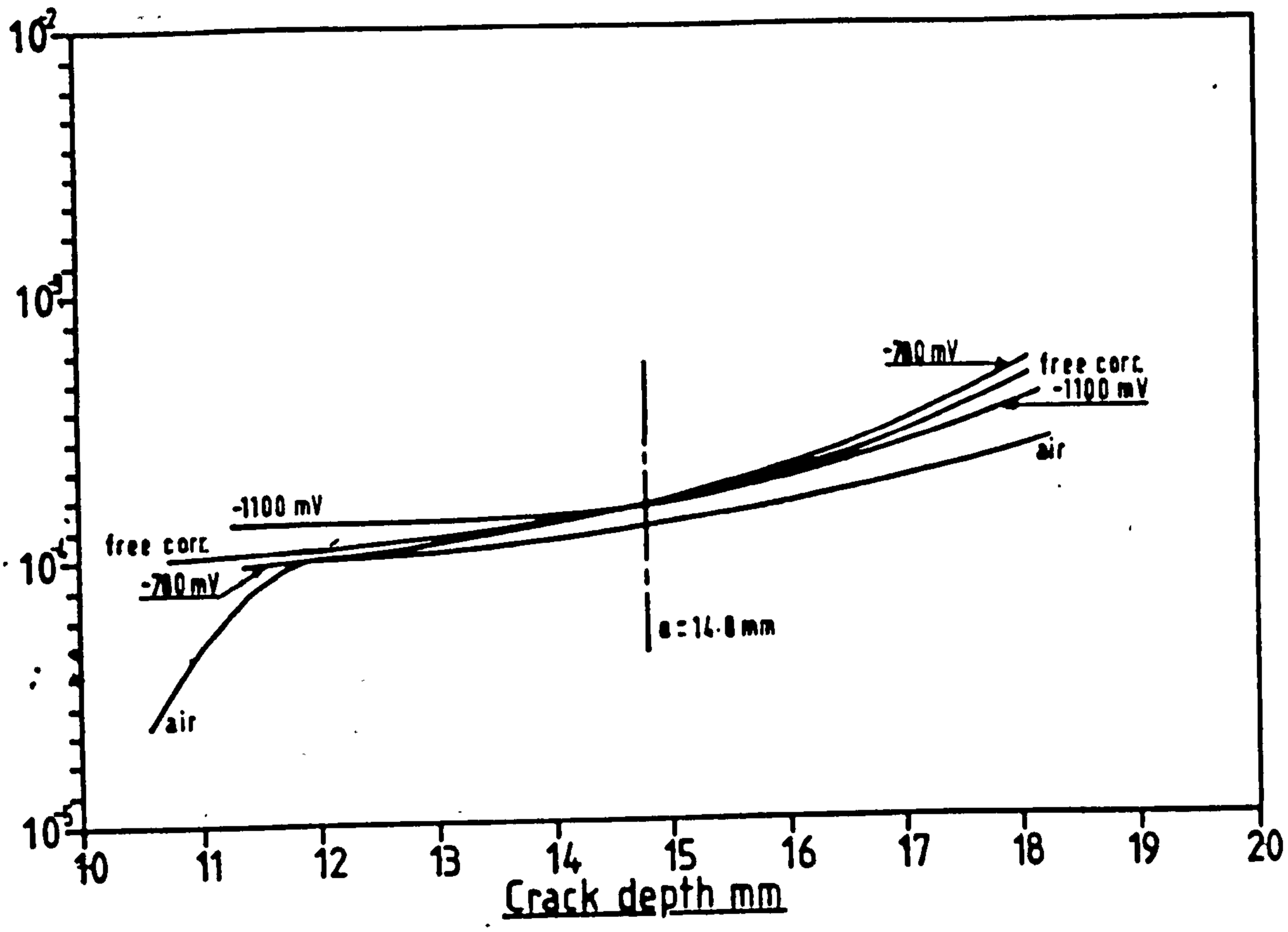

Figure 34 - Graphs of da/dN Vs a, for crack growth in BS 4360 50D parent plate material in environments of laboratory air, nominal correct cathodic protection, nominal cathodic overprotection and free corrosion.

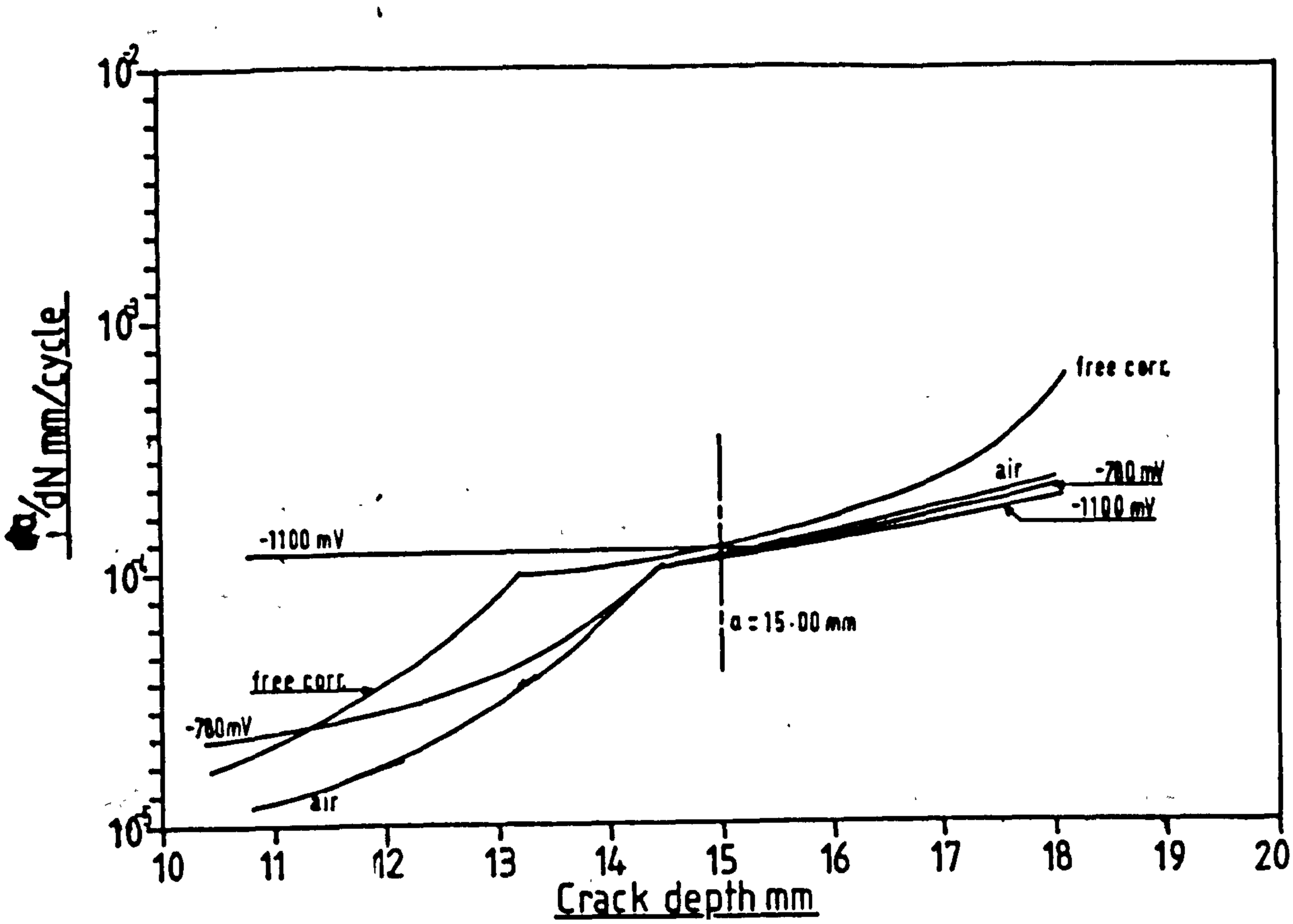

Figure 35 - Graphs of da/dN Vs a , for crack growth in weld metal in environments of laboratory air, nominal correct cathodic protection, nominal cathodic overprotection and free corrosion.

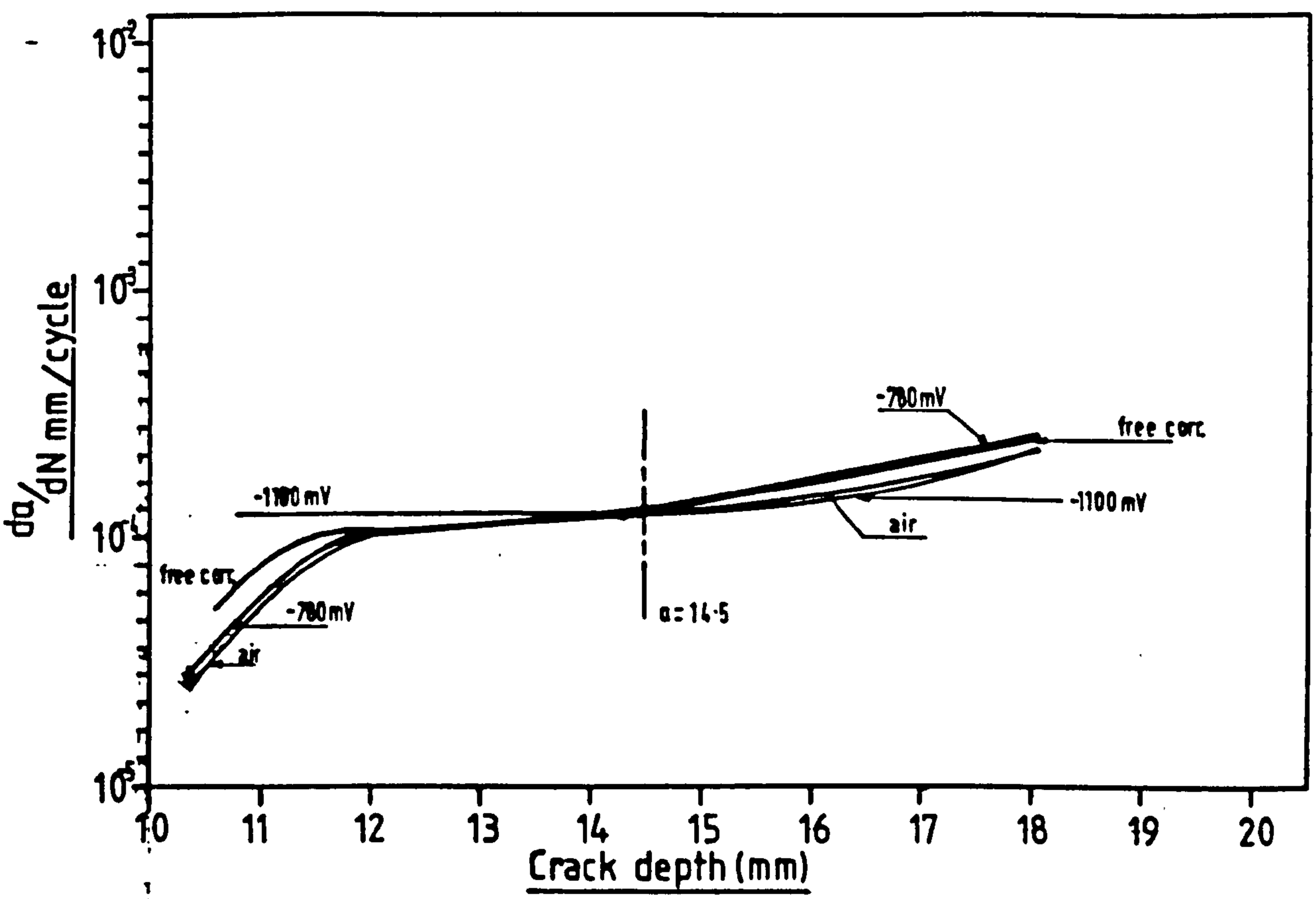

Figure 36 – Graphs of da/dN Vs a for crack growth in heat affected zone microstructure in environments of laboratory air, nominal correct cathodic protection, nominal cathodic overprotection and free corrosion.

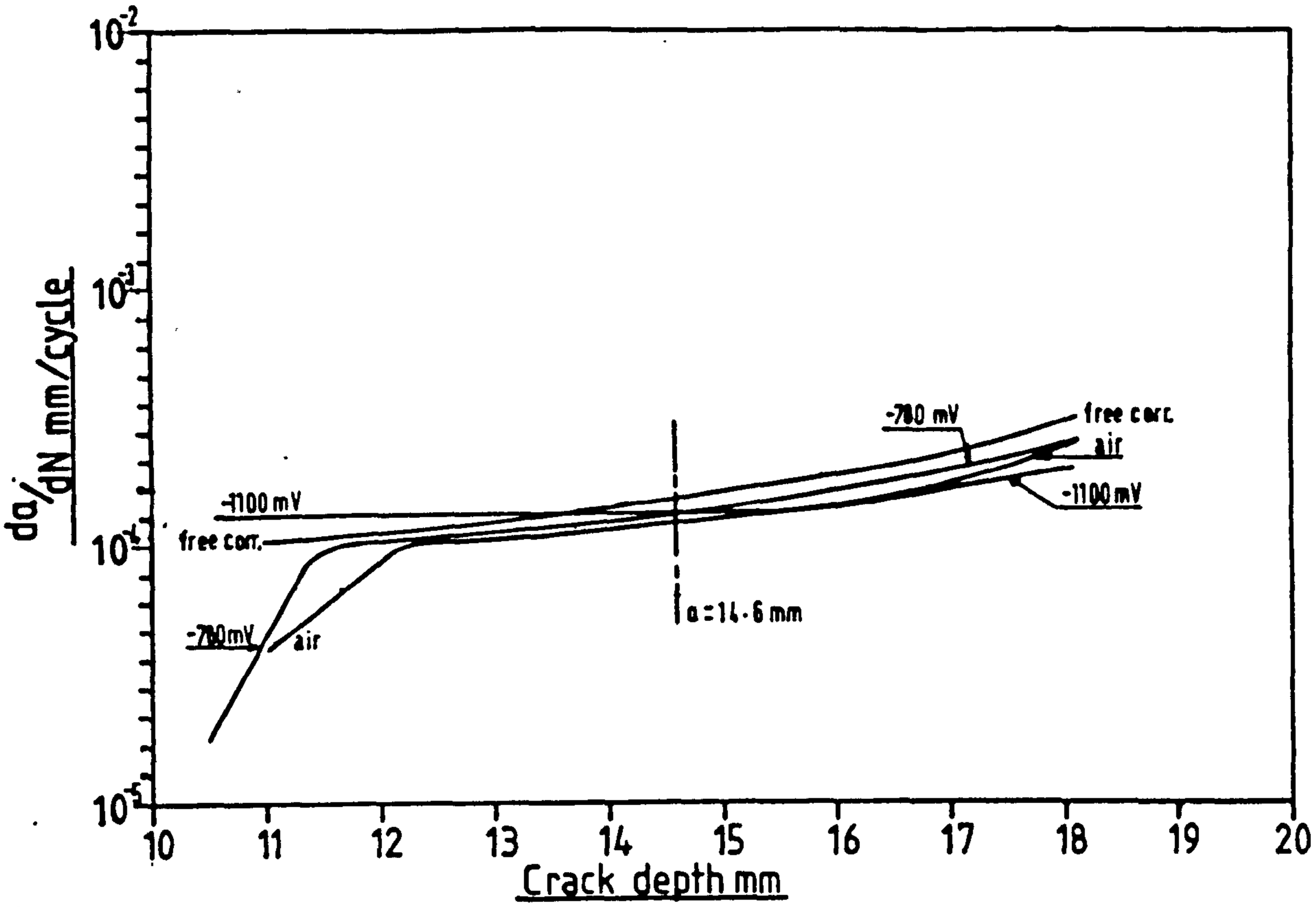

Figure 37 - Graphs of da/dN Vs a , for crack growth in weld fusion-line microstructure in environments of laboratory air, nominal correct cathodic protection, nominal cathodic overprotection and free corrosion.

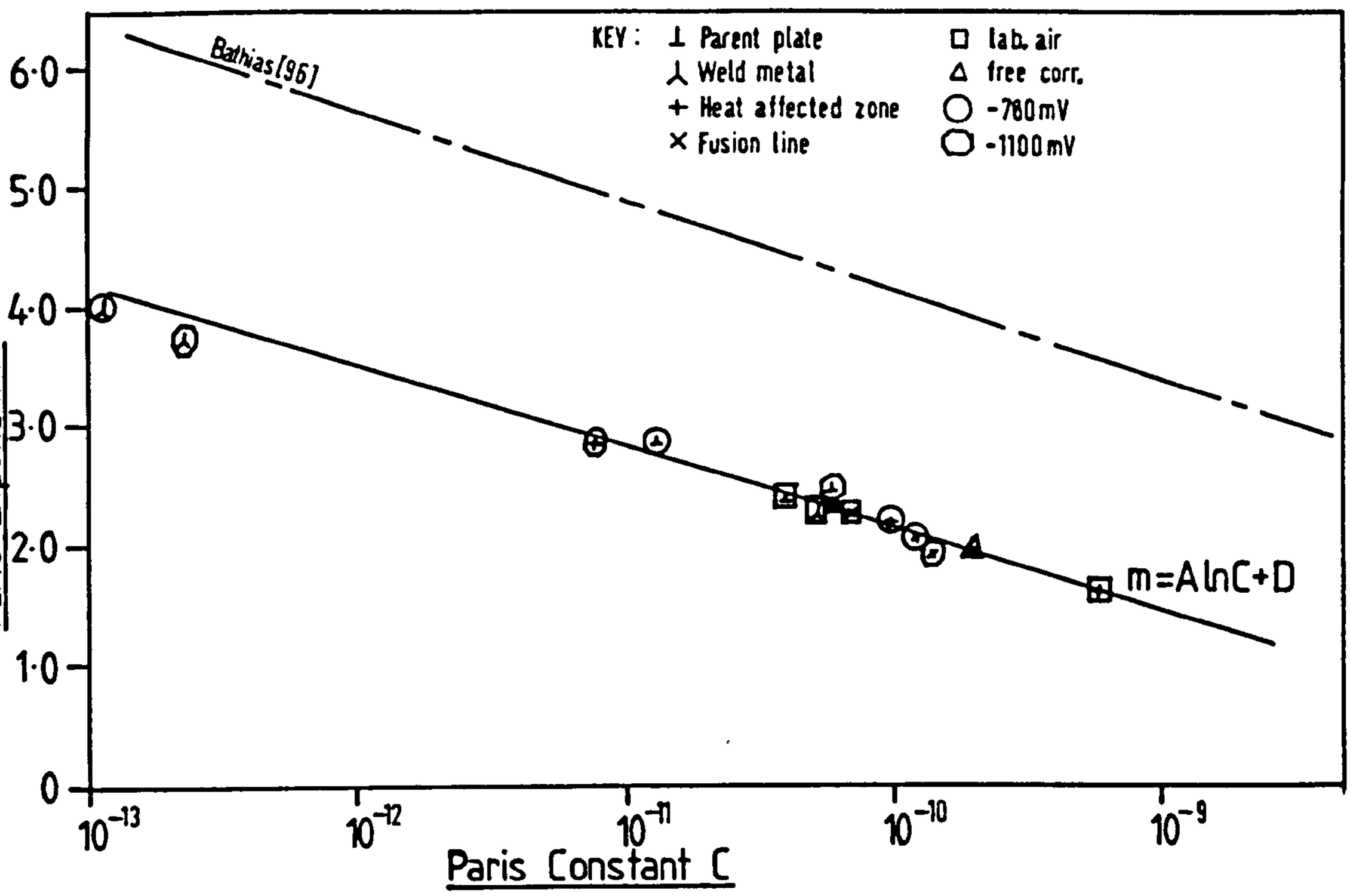

Figure 38 - Graph of Paris exponent m Vs Paris constant C.

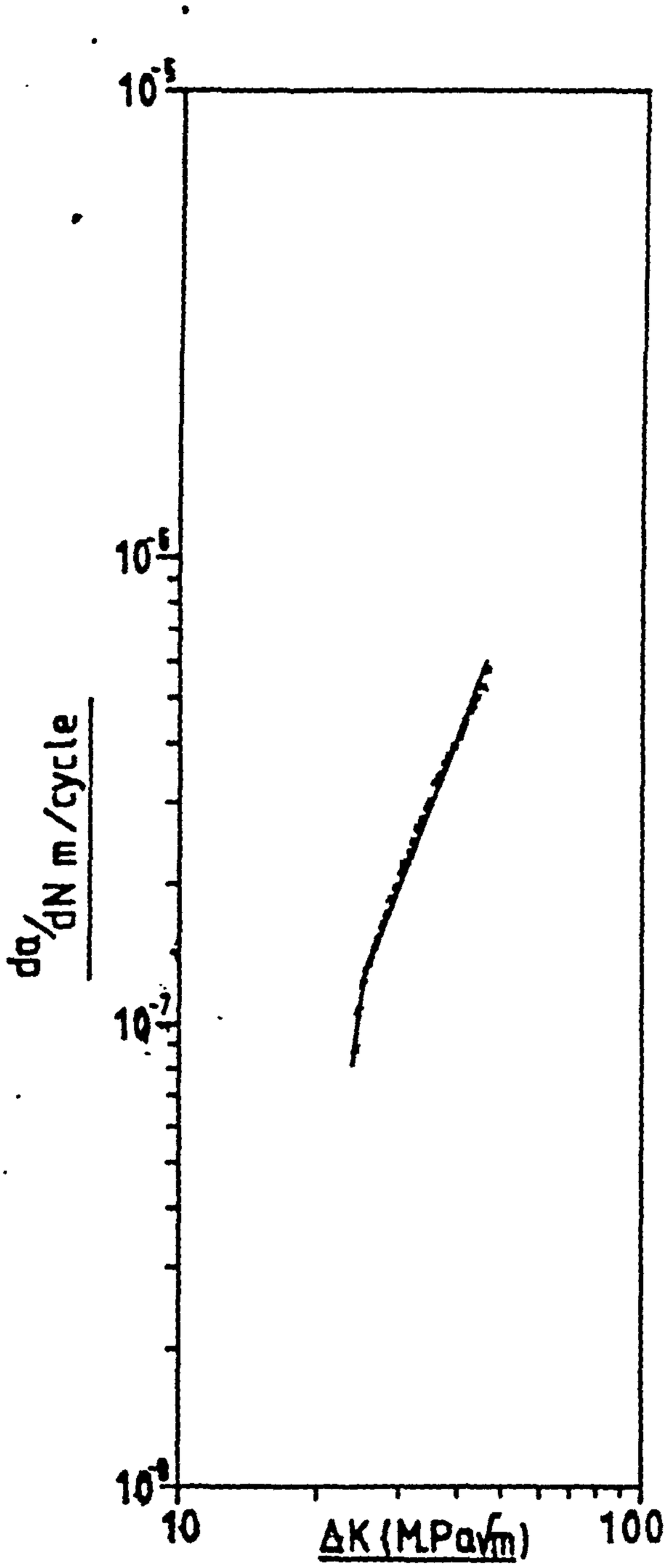

Figure 39 - Maximum level of scatter in da/dN Vs ΔK data
(after Experiment 10)

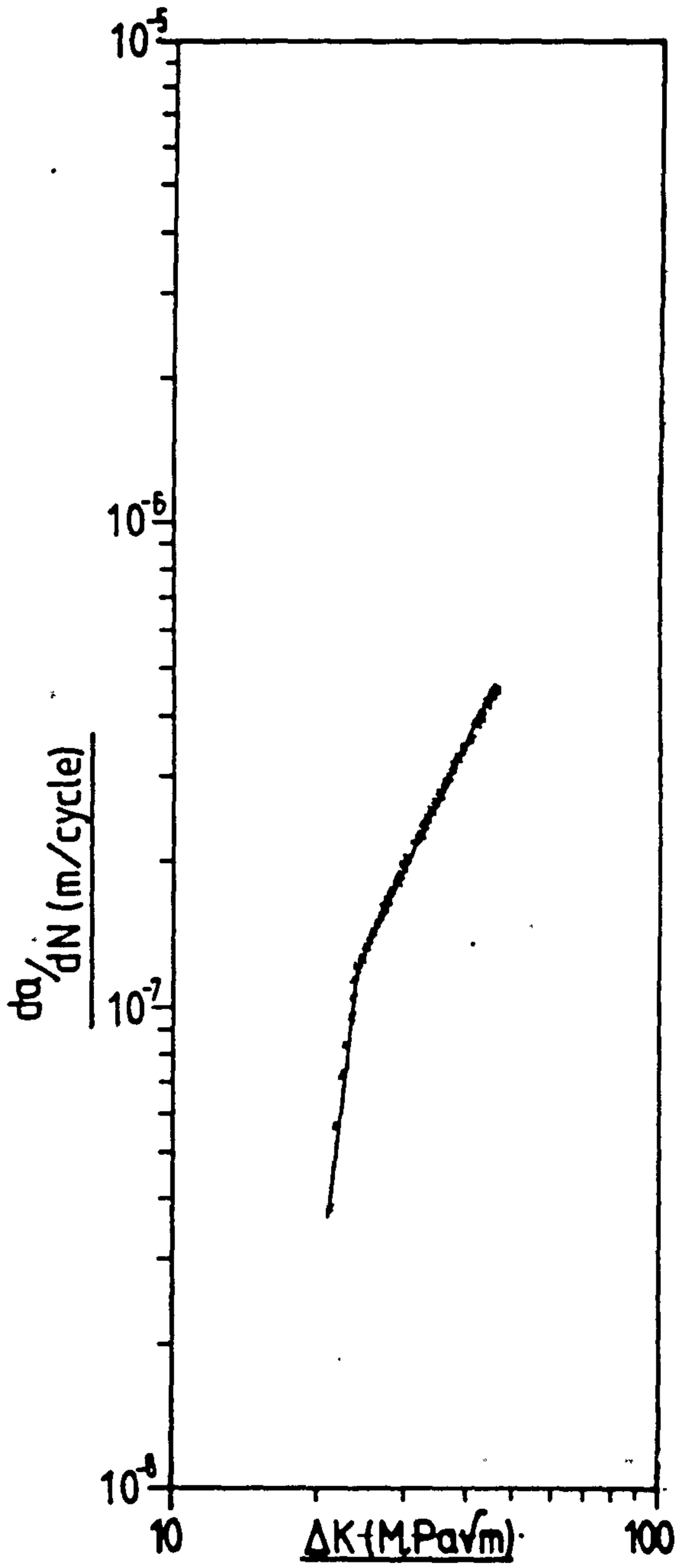

Figure 40 - Minimum level of scatter in da/dN Vs ΔK data, after Experiment 24

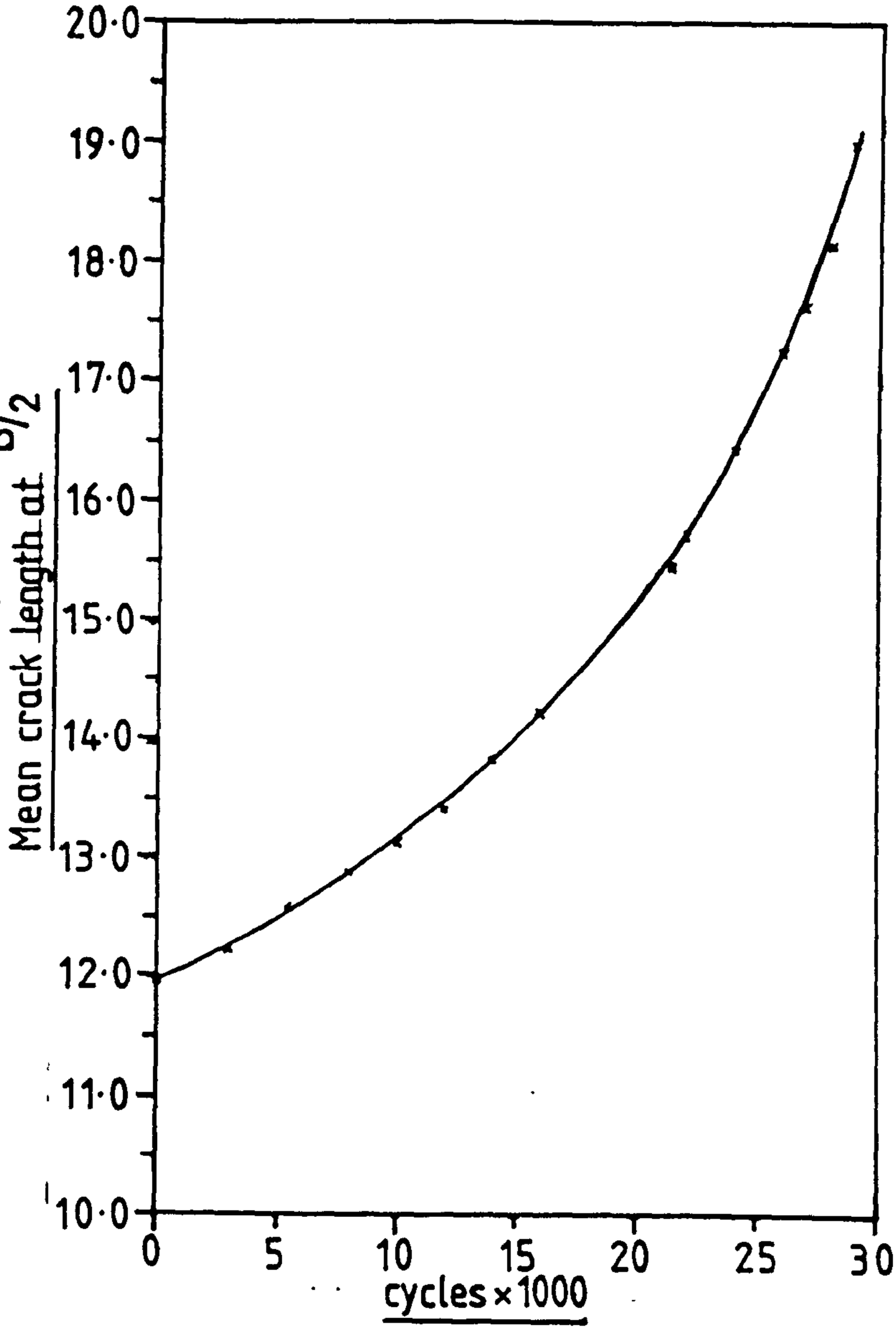

Figure 41 – a Vs N data associated with Figure 39
(after experiment 13)

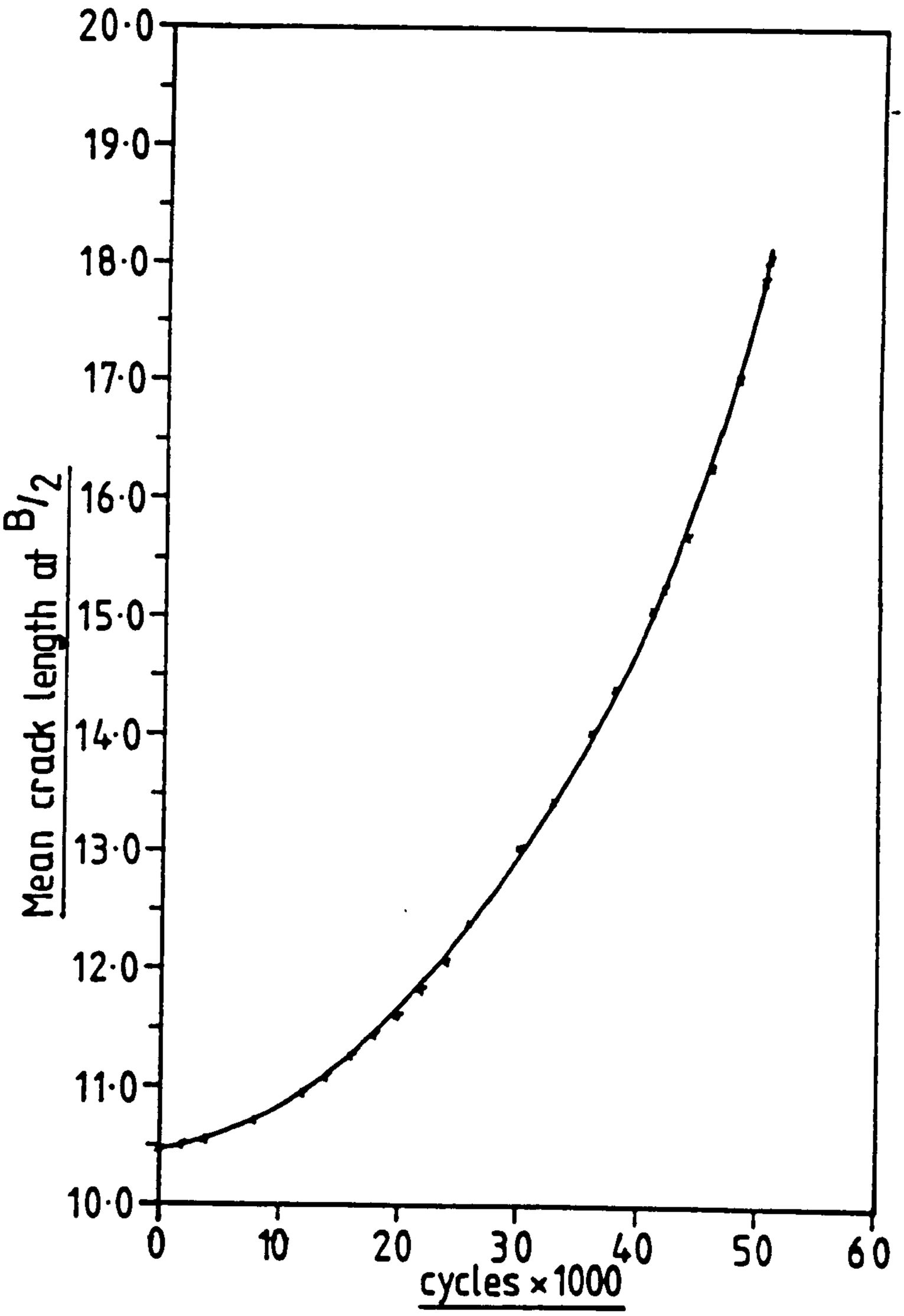

Figure 42 - a Vs N data associated with Figure 40
(after experiment 24)

Table 1 - Calculated values of plastic zone size associated with 'overload' in BS 4360 50D parent plate material

ENVIRONMENT	K_{max} (M.Pa.$\sqrt{m}$)	$K_{OVERLOAD}$ (M.Pa.$\sqrt{m}$)	CYCLES OF RETARDATION EFFECTS	CRACK GROWTH TO MINIMUM da/dN * (mm)	OVERALL AFFECTED CRACK LENGTH (mm)	PLANE STRESS		PLANE STRAIN	
						MONOTONIC FATIGUE $\frac{1\pi}{2}(\frac{K_{max}}{\sigma_y})^2$ (mm)	MONOTONIC OVERLOAD $\frac{1}{2\pi}(\frac{K_{OVERLOAD}}{\sigma_y})^2$ (mm)	MONOTONIC FATIGUE $\frac{1}{6\pi}(\frac{K_{max}}{\sigma_y})^2$ (mm)	MONOTONIC OVERLOAD $\frac{1}{6\pi}(\frac{K_{OVERLOAD}}{\sigma_y})^2$ (mm)
AIR	23.2	38.80	42,000	0.5	1.0	0.54	1.53	0.18	0.51
	28.45	38.80	20,000	0.8	1.6	0.82	1.53	0.27	0.51
FREE CORR.	23.2	38.80	49,000	0.8	1.6	0.54	1.53	0.18	0.51
	28.45	38.80	>18,000	POWER FAILURE TO RIG CAUSED OVERLOAD THEREFORE TEST STOPPED!					

(*) refers to secant data from experimental records. Data presented was obtained from tangent to curve technique.

Table 2 - CALCULATED VALUES OF CRACK-TIP-OPENING DISPLACEMENT

ΔK (M.Pa.$\sqrt{m}$)	K_{max} (M.Pa m)	δ_{PLATE} μ	$\delta_{WELD\ METAL}$ μ	δ_{HAZ} μ
20	22.22	1.33	0.64	1.18
22	24.44	1.61	0.77	1.43
24	26.67	1.91	0.92	1.71
26	28.89	2.25	1.08	2.00
28	31.11	2.60	1.25	2.32
30	33.33	2.99	1.44	2.67
32	35.56	3.40	1.64	3.03
34	37.78	3.84	1.85	3.43
36	40.00	4.30	2.07	3.84
38	42.22	4.80	2.31	4.30
40	44.44	5.31	2.56	4.74
42	46.67	5.90	2.82	5.23
44	48.89	6.43	3.10	5.74
46	51.11	7.03	3.40	6.27

$$\delta = 0.22 \frac{K_{max}^{2}}{E.\sigma_y}$$

Table 3 - PARIS RELATIONSHIPS DERIVED FROM EXPERIMENTAL DATA

ENVIRONMENT / MICROSTRUCTURE		LABORATORY AIR	m	FREE CORROSION POTENTIAL	m	CATHODIC PROTECTION - 780 mV_{SCE}	m	CATHODIC PROTECTION - 1100 mV_{SCE}	m	TIDAL IMMERSION	m	SIMULATED SPLASH ZONE	m
BS4360 50D PLATE MATERIAL (S/R)	C_1	1.70×10^{-18}	7.6	$> 10^{-23}$	14.3	7.40×10^{-19}	6.90	-	-	1.60×10^{-23}	11.43	1.00×10^{-16}	6.31
	C_2	5.40×10^{-11}	2.36	7.00×10^{-11}	2.36	2.00×10^{-11}	2.82	7.00×10^{-11}	2.40	1.00×10^{-16} 2.85×10^{-5}	6.31 4.92	5.55×10^{-10}	1.84
WELD METAL (S/R)	C_1	6.20×10^{-18}	9.13	1.00×10^{-16}	6.69	2.00×10^{-20}	8.78	-	-	-	-	2.80×10^{-14}	4.70
	C_2	6.40×10^{-11}	3.25	1.43×10^{-13}	4.00	1.25×10^{-13}	4.00	3.10×10^{-13}	3.93	CRACK ARREST!	-	2.95×10^{-1}	1.26
HEAT AFFECTED ZONE (S/R)	C_1	8.90×10^{-13}	3.73	8.20×10^{-13}	3.49	1.65×10^{-13}	4.17	-	-	-	-	-	-
	C_2	1.25×10^{-9}	1.48	6.20×10^{-11}	2.33	9.00×10^{-11}	2.27	3.40×10^{-11}	2.41	-	-	-	-
WELD FUSION LINE (S/R)	C_1	7.80×10^{-14}	5.14	5.00×10^{-14}	4.92	1.10×10^{-19}	8.14	-	-	-	-	-	-
	C_2	7.60×10^{-11}	2.25	2.70×10^{-10}	2.22	1.80×10^{-10}	2.20	2.35×10^{-10}	2.20	-	-	-	-

$$da/dN = C\ (\Delta K)^m$$

Table 4 - DATA TABLE : ΔK VALUES AND CORRESPONDING da/dN VALUES FOR POINTS AT WHICH CHANGE OF SLOPE OCCURS

FATIGUE ENVIRONMENT / MATERIAL CONDITION	AIR		FREE CORROSION		$-0.780V_{S.C.E.}$		$-1.100V_{S.C.E.}$		SPLASH ZONE	
	ΔK	$\frac{da}{dn}$	ΔK	$\frac{da}{dn}$	ΔK	$\frac{da}{dn}$	ΔK	$\frac{da}{dn}$	ΔK	$\frac{da}{dn}$
PLATE	23.5	1.0×10^{-7}	23	1.10×10^{-7}	23	9.0×10^{-8}	30	2.35×10^{-7}	23.5	1.8×10^{-7}
WELD METAL	23.5	2.8×10^{-8}	23	4.5×10^{-8}	25.5	1.20×10^{-7}	36	1.80×10^{-7}	26.5 29	1.4×10^{-7} 2.05×10^{-7}
GRAIN COARSENED H.A.Z.	25	1.80×10^{-7}	23	1.0×10^{-7}	25	1.40×10^{-7}	35	1.92×10^{-7}	-	-
FUSION LINE	24.5	1.0×10^{-7}	24	1.40×10^{-7}	24	1.23×10^{-7}	35	2.05×10^{-7}	-	-

Table 5 - EXTRAPOLATED VALUES OF ΔK THRESHOLD AT 10^{-10} m/cycle (M.Pa.√m)

Environment / Microstructure	Laboratory Air	Free Corrosion Potential	Cathodic Protection to - $0.780V_{SCE}$
Parent Plate Material	9.40	8.00	8.80
As-Deposited Weld Metal	10.80	8.00	11.50
Heat Affected Zone	4.00	3.40	5.00
Weld Metal Fusion Line	6.70	5.20	9.00

Values obtained by extrapolation to propagation rate of 10^{-10} m/cycle - assumed to represent threshold conditions.

Table 6 - TABLE OF CALCULATED AND MEASURED CYCLES OF FATIGUE ENDURANCE BETWEEN CRACK LENGTHS OF 15.00mm AND 18.00mm

ENVIRONMENT / MATERIAL		LABORATORY AIR	ERROR %	FREE-CORROSION POTENTIAL	ERROR %	CATHODIC PROTECTION - 780mV	ERROR %	CATHODIC OVER-PROTECTION - 1100mV	ERROR %	SIMULATED SPLASH-ZONE	ERROR %
Parent Plate	Na_d	10,181	+8.0	6,549	-6.0	5,170	-6.0	7,853	+7.0	6,565	-3.0
	Na_i to Na_+	9,400		7,000		5,500		7,250		6,750	
Weld Metal	Na_d	11,820	+3.0	9,686	+8.0	11,081	-8.0	12,313	+1.0	10,213	-0.3
	Na_i to Na_+	11,500		9,000		12,000		12,250		10,250	
Heat Affected Zone	Na_d	10,811	+1.0	9,889	-1.0	8,472	-3.0	13,484	+12.0	-	-
	Na_i to Na_+	10,750		10,000		8,750		12,000		-	-
Weld Metal Fusion-Line	Na_d	10,789	-4.0	8,719	+3.0	9,427	-0.7	11,587	+3.0	-	-
	Na_i to Na_+	11,250		8,500		9,500		11,250		-	-

Na_d = Endurance derived by integration of appropriate Paris relationship = 15.00mm

Na_i to Na_+ = Endurance recorded direct from test machine = 18.00mm

$$\text{Error } \% = \frac{\text{Calculated} - \text{Measured}}{\text{Measured}} \times 100$$

Table 7 - CORROSION FATIGUE OF BS4360 50D TYPE STRUCTURAL STEEL

ENVIRONMENT	FIG. NO.	OBSERVATIONS	
		LOW ΔK/SHORT CRACK a < 14.8mm	HIGH ΔK/LONG CRACK a > 14.8mm
Free Corrosion Potential	18 (A & B)	18A: (1) Small quasi-cleavage facets. (2) General corrosion attack of fracture surface. (3) Formation of corrosion pits. (4) No evidence of ductile striations. (5) Secondary cracks.	18B: (1) Relatively large quasi-cleavage facets, well-defined. (2) No evidence of general corrosion attack. (3) Isolated 'patches' of ductile striations. (4) Secondary cracks, more numerous than for Figure 18A.
Cathodic Protection Potential - 780 mV.	19 (A & B)	19A: (1) Quasi-cleavage facets in evidence. (2) General corrosion attack of fracture surface. (3) Formation of corrosion pits - less than for a 14.8mm. (4) No evidence of ductile striations. (5) Secondary cracks less clearly defined. (6) Indications that quasi-cleavage facet sites may be preferential locations for anodic dissolution. (7) Dense coating of calcareous deposits on uncleaned fracture surfaces.	19B: (1) No evidence of quasi-cleavage facets. (2) Relatively severe general corrosion attack of fracture surface. (3) Formation of corrosion pits. (4) Secondary cracks clearly visible. (5) Calcareous deposits present but thinly spread on uncleaned fracture surfaces.
Cathodic Protection Potential - 1100 mV	20 (A & B)	20A: (1) Quasi-cleavage facets in evidence. (2) General corrosion attack of fracture surface. (3) Formation of corrosion pits. (4) Secondary cracks less clearly defined. (5) Isolated patches of ductile striation type surface markings. (6) Dense coating of calcareous deposits on uncleaned fracture surfaces.	20B: (1) Small, widely-dispersed quasi-cleavage facets in evidence. (2) Formation of corrosion pits - relatively small. (3) Good degree of fracture surface preservation, compared to C.P. of - 780 mV$_{SCE}$. (4) Even covering of calcareous deposits on uncleaned fracture surfaces.

Table 8 - CORROSION AND CORROSION PROTECTION PROCESSES IN CRACKS OR OCCLUDED REGIONS

CORROSION	CATHODIC PROTECTION	
NO CATHODIC PROTECTION APPLIED (FREE CORROSION)	CATHODIC PROTECTION CURRENT DOES NOT PENETRATE INTO CRACK OR OCCLUDED REGION	CATHODIC PROTECTION CURRENT PENETRATES INTO CRACK OR OCCLUDED REGION
1. ANODIC dissolution confined to occluded region e.g. $Fe \rightarrow Fe^{2+} + 2\bar{e}$ CATHODIC reaction at surrounding external surface $O_2 + 2H_2O + 4\bar{e} \rightarrow 4OH^-$ IONISATION of water $H_2O \rightleftarrows H^+ + OH^-$ 2. Hydrolysis of anodic dissolution product. Development of acidity in occluded region. $Fe + H_2O \rightarrow FeOH^+ + H^+$	Corrosion sequence as given by items 1 to 4A or alternatively 1 to 4B	1. CP. SUPPRESSION of anodic dissolution in occluded region. Metal is rendered immune to corrosion. 2. CP. Development of alkalinity and generation of hydrogen in occluded region. $2H_2O + 2\bar{e} \rightarrow 2OH^- + H_2$
3A. Initiation of Cathodic reaction in occluded region. $2H^+ + 2\bar{e} \rightarrow H_2$ 4A. Corrosion in occluded region becomes self-sustaining i.e. external cathode no longer necessary.	3B. Insufficient acidity to initiate cathodic reaction in occluded region. 4B. Corrosion in occluded region does not become self-sustaining and continues to depend on external cathodic reaction.	1CP[1]. No further reaction in occluded region.	2.CP[1]. Calcareous deposits and scales are formed in occluded region. $Ca^{2+} + HCO_3^- + OH^- \rightarrow CaCO_3 + H_2O$ (formation of calcium carbonates) $Mg^{2+} + 2OH^- \rightarrow Mg(OH)_2$ (formation of magnesium hydroxide)

Table 8 - CORROSION AND CORROSION PROTECTION PROCESSES IN CRACKS OR OCCLUDED REGIONS .. Continued

CORROSION		CATHODIC PROTECTION	
NO CATHODIC PROTECTION APPLIED (FREE CORROSION)		CATHODIC PROTECTION CURRENT DOES NOT PENETRATE INTO CRACK OR OCCLUDED REGION	CATHODIC PROTECTION CURRENT PENETRATES INTO CRACK OR OCCLUDED REGION
5A	CONSEQUENCES 5B	CONSEQUENCES 5CP.	CONSEQUENCES 5CP' / 5CP"
(i) Crack Blunting - increase in CTOD at crack tip - loss of geometric sharpness - reduction in magnitude of crack tip stress intensity factor (ii) Hydrogen Diffusion into Metal Potentially two opposing influences on corrosion fatigue crack propagation rate.	(i) Crack Blunting As for 5A (i) Either no influence or favourable influence i.e. reduction in corrosion fatigue crack propagation rate.	As for 5A or 5B opposite.	5CP' (i) No crack blunting. (ii) Hydrogen diffusion into metal. Unfavourable influence on corrosion fatigue crack propagation rate. i.e. rate is enhanced. 5CP" (i) No crack blunting. (ii) Hydrogen diffusion into metal. (iii) Possible wedging action in crack. Opposing influences on corrosion fatigue crack propagation rate. More favourable than 5CP'.

Table 9 - CORROSION FATIGUE OF WELD METAL

ENVIRONMENT	FIG.NO.	OBSERVATIONS	
		LOW K/SHORT CRACK a < 15.0mm	HIGH K/LONG CRACK a < 15.0mm
Free Corrosion Potential	23 (A & B)	23A: (1) Extensive and relatively severe general corrosion attack of the fracture surface. (2) Widespread formation of corrosion pits. (3) No evidence of ductile striation. (4) Secondary cracks present but not clearly defined.	23B: (1) Extensive and relatively severe general corrosion attack of the fracture surface. (2) Widespread formation of corrosion pits. (3) No evidence of ductile striations. (4) Secondary cracks clearly visible. (5) Evidence of quasi-cleavage facets - small in size and widely dispersed.
Cathodic Protection Potential - 780 mV	24 (A & B)	24A: (1) Quasi cleavage facets in evidence, small in size and widely dispersed. (2) General lack of corrosion attack, although isolated patches of corrosion pits are present. (3) Evidence of ductile striations. (4) Secondary cracks clearly visible. (5) Dense coating of calcareous deposits on uncleaned fracture surfaces.	24B: (1) Extensive and very severe general corrosion attack of the fracture surface. (2) Widespread formation of corrosion pits. (3) No evidence of ductile striations or quasi-cleavage facets. (4) Secondary cracks clearly visible. (5) Calcareous deposits present but very sparse on uncleaned fracture surfaces.
Cathodic Protection Potential - 1100 mV	25 (A & B)	25A: (1) Clearly defined quasi-cleavage facets - relatively large. (2) Lack of general corrosion attack. (3) Widespread formation of corrosion pits - relatively large. (4) Secondary cracks clearly visible. (5) Isolated patches of ductile striation type surface markings. (6) Dense coating of calcareous deposits present on uncleaned fracture surfaces.	25B: (1) Small widely dispersed quasi-cleavage facet type features. (2) Lack of general corrosion attack. (3) Widespread formation of corrosion pits - relatively small. (4) Secondary cracks clearly visible. (5) Ductile striations clearly visible. (6) Calcareous deposits present in a sparse coating on uncleaned fracture surfaces.

Table 10A - SUMMARY OF THE RELATIVE MERITS OF OPTICAL CRACK MONITORING BY USE OF A VERNIER-TYPE TRAVELLING MICROSCOPE

ADVANTAGES	DISADVANTAGES
1. Resolution of crack length to within ± 10μm	1. The technique is limited to the measurement of surface crack length for cracks which are accessible. Therefore it is not suitable for use where access is restricted or the crack is obscured.
2. The technique is readily adaptable for use in an environment of corrosion fatigue.	2. The technique is not compatible with computer-based applications and is labour-intensive.
3. Low unit cost in comparison to electrically based techniques.	3. Satisfactory performance is limited to thin specimens where appreciable 'crack-tunneling would not be anticipated.
4. The equipment is technically simple, robust, reliable and highly portable.	4. Is susceptible to errors arising from operator subjectively.
5. Average level of operator skill is required.	

Table 10B - SUMMARY OF THE RELATIVE MERITS OF ELECTRICAL POTENTIAL DROP CRACK MONITORING TECHNIQUE

ADVANTAGES	DISADVANTAGES
1. Accuracy of crack length measurement is of the order of ± 10μm .	1. The technique relies on prior-calibration, using analytical or empirical models.
2. Provides crack monitoring in circumstances where the fatigue crack cannot be directly viewed.	2. The equipment required demands a high level of capital expenditure and is technically complex.
3. The technique is not labour-intensive and is readily adaptable for integration with computerised data acquisition, processing and analysis systems.	3. The equipment is not 'physically robust' and requires care in handling.
	4. Currents of the order of 20A are required, except for the A.C. p.d. system. Therefore the technique is not suitable for application to corrosion fatigue studies.
	5. A high level of 'operator-skill' is required.
	6. Results are sensitive to probe separation and position.

Table 11 - MASTER INDEX LIST

Test No.	Test Group (4.4)	Specimen Type (4.3)	Initial Crack Length (mm)	Microstructure	Environment	Stress Relief Yes/No	Remarks
1	1	A	12.56	Parent Plate	Laboratory Air	Yes	
2	2	B	12.24	Weld Metal	Laboratory Air	Yes	
3	7	B	8.64	Weld Metal	Laboratory Air	No	
4	7	B	10.37	Weld Metal	Free Corrosion	No	
5	7	B	11.13	Weld Metal	Free Corrosion	No	Crack length measured post-test.
6	7	B	11.40	Weld Metal	Free Corrosion	Yes	Crack length measured post-test.
7	1	A	12.64	Parent Plate	Dry Air (0% RH)	Yes	Crack length measured post-test.
8	2	B	8.40	Weld Metal	Laboratory Air	Yes	Constant ΔK, K_{max}
9	1	A	10.52	Parent Plate	Laboratory Air	Yes	Single overload cycle applied
10	1	A	12.59	Parent Plate	Laboratory Air	No	Single overload cycle applied
11	1	A	10.61	Parent Plate	Free Corrosion	Yes	Single overload cycle applied
12	5	C	10.85	Weld Fusion Line	Laboratory Air	Yes	
13	3	C	10.24	Heat Affected Zone	Laboratory Air	Yes	Crack in supercritical region
14	6	C	10.23	Weld Fusion Line	Laboratory Air	No	
15	5	C	10.81	Weld Fusion Line	Free Corrosion	Yes	
16	6	C	10.52	Weld Fusion Line	C.P. - 780mV$_{SCE}$	Yes	

Table 11 continued

Test No.	Test Group (4.4)	Specimen Type (4.3)	Initial Crack Length (mm)	Microstructure	Environment	Stress Relief Yes/No	Remarks
17	1	A	10.49	Parent Plate	C.P. - 780 mV_{SCE}	Yes	
18	2	B	11.98	Weld Metal	C.P. - 780 mV_{SCE}	Yes	
19	2	B	11.56	Weld Metal	C.P. - 1100 mV_{SCE}	Yes	
20	1	A	11.24	Parent Plate	C.P. - 1100 mV_{SCE}	Yes	
21	3	C	10.43	Heat Affected Zone	C.P. - 780 mV_{SCE}	Yes	Crack in supercritical region
22	2	B	10.37	Weld Metal	Free Corrosion	Yes	
23	1	A	10.33	Parent Plate	Free Corrosion	Yes	
24	5	C	10.47	Weld Fusion Line	C.P. - 780 mV_{SCE}	Yes	
25	3	C	10.56	Heat Affected Zone	C.P. - 1100 mV_{SCE}	Yes	Crack in supercritical region
26	5	C	10.55	Weld Fusion Line	C.P. - 1100 mV_{SCE}	Yes	
27	2	B	10.68	Weld Metal	Laboratory Air	Yes	Crack length measured post-test
28	1	A	10.52	Parent Plate	Laboratory Air	Yes	
29	3	C	10.44	Heat Affected Zone	Free Corrosion	Yes	Crack in supercritical region
30	1	A	10.77	Parent Plate	Splash Zone	Yes	
31	1	A	10.72	Parent Plate	Tidal Immersion	Yes	6 hr. cycle wet : dry
32	2	B	10.50	Weld Metal	Tidal Immersion	Yes	6 hr. cycle wet : dry
33	2	B	10.95	Weld Metal	Splash Zone	Yes	
34	3	C	10.39	Heat Affected Zone	Tidal Immersion	Yes	Crack in supercritical region 6 hr. cycle wet : dry
35	1	A	10.28	Parent Plate	Splash & Tidal combined	Yes	6 hr. cycle

Table 11 continued

Test No.	Test Group (4.4)	Specimen Type (4.3)	Initial Crack Length (mm)	Microstructure	Environment	Stress Relief Yes/No	Remarks
36	4	C	10.99	Heat Affected Zone	Laboratory Air	No	Crack in supercritical region
37	4	C	10.77	Heat Affected Zone	Free Corrosion	No	Crack in supercritical region
38	4	C	10.66	Heat Affected Zone	C.P. - 780 mV_{SCE}	No	Crack in supercritical region
39	4	C	11.12	Heat Affected Zone	C.P. - 1100 mV_{SCE}	No	Crack in supercritical region
40	2	C	12.14	Heat Affected Zone	Tidal Immersion	No	Crack in supercritical region. 6 hr. cycle wet : dry

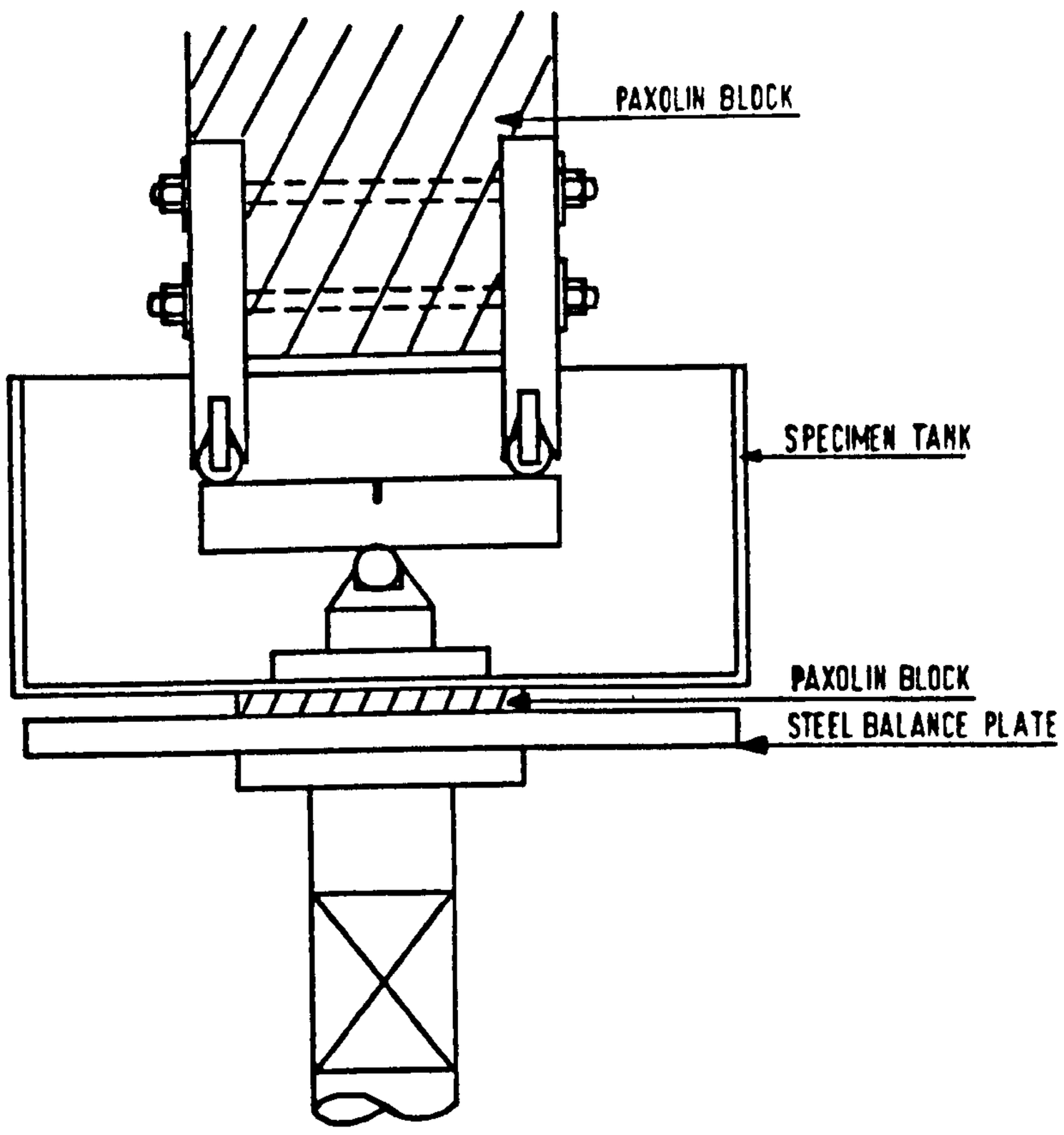

Appendix 1 - Schematic illustration of electrical isolation arrangements.

Sodium chloride	24.9 gram/litre
Calcium sulphide	1.50 gram/litre
Magnesium chloride	2.99 gram/litre
Magnesium sulphate	2.00 gram/litre

Any other elements present are incidental and exist only as trace elements

Appendix 2 - Chemical composition of sea water corrosion test mixture

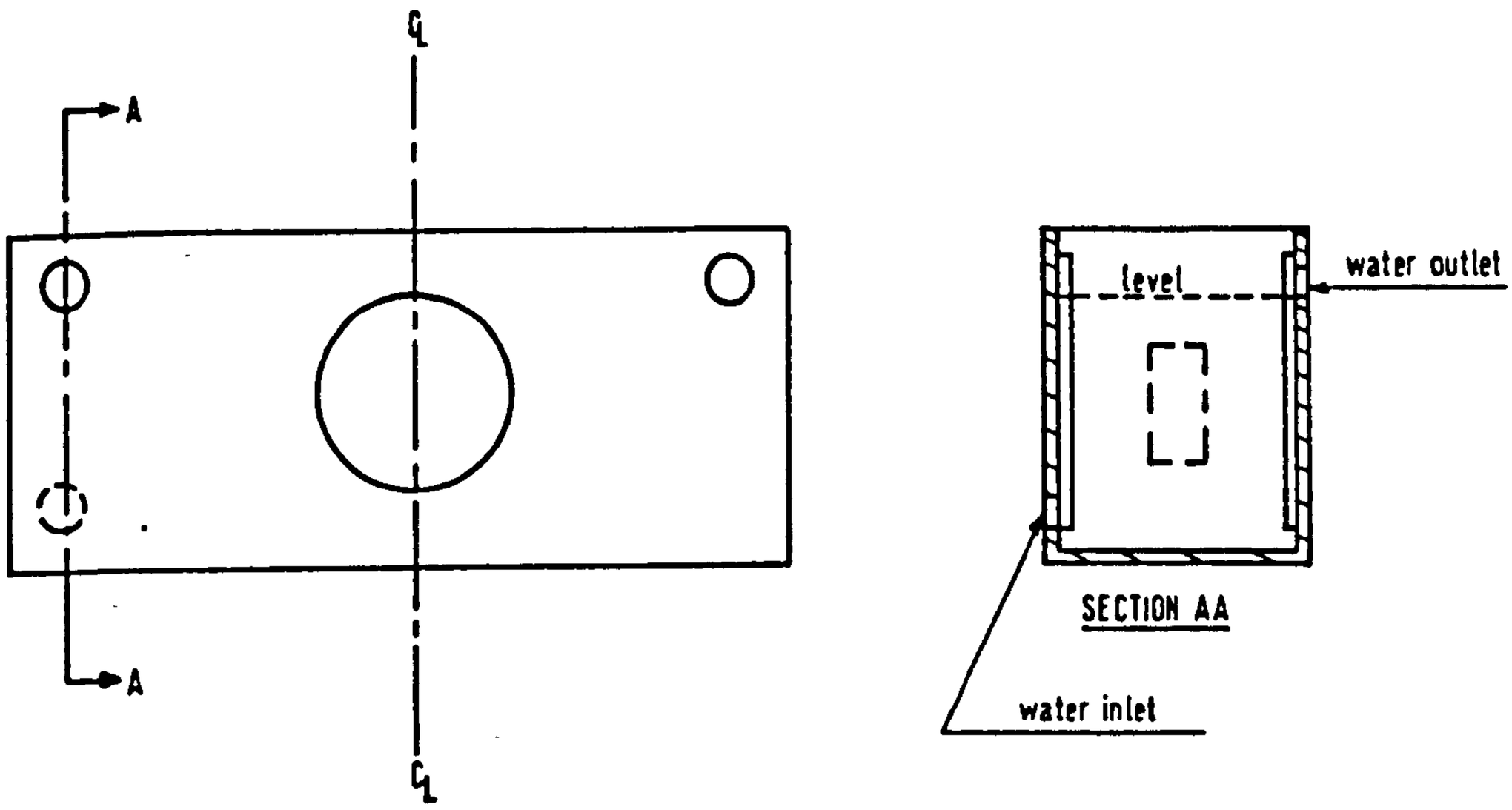

Appendix 3 - Schematic illustration of water-level control arrangements.

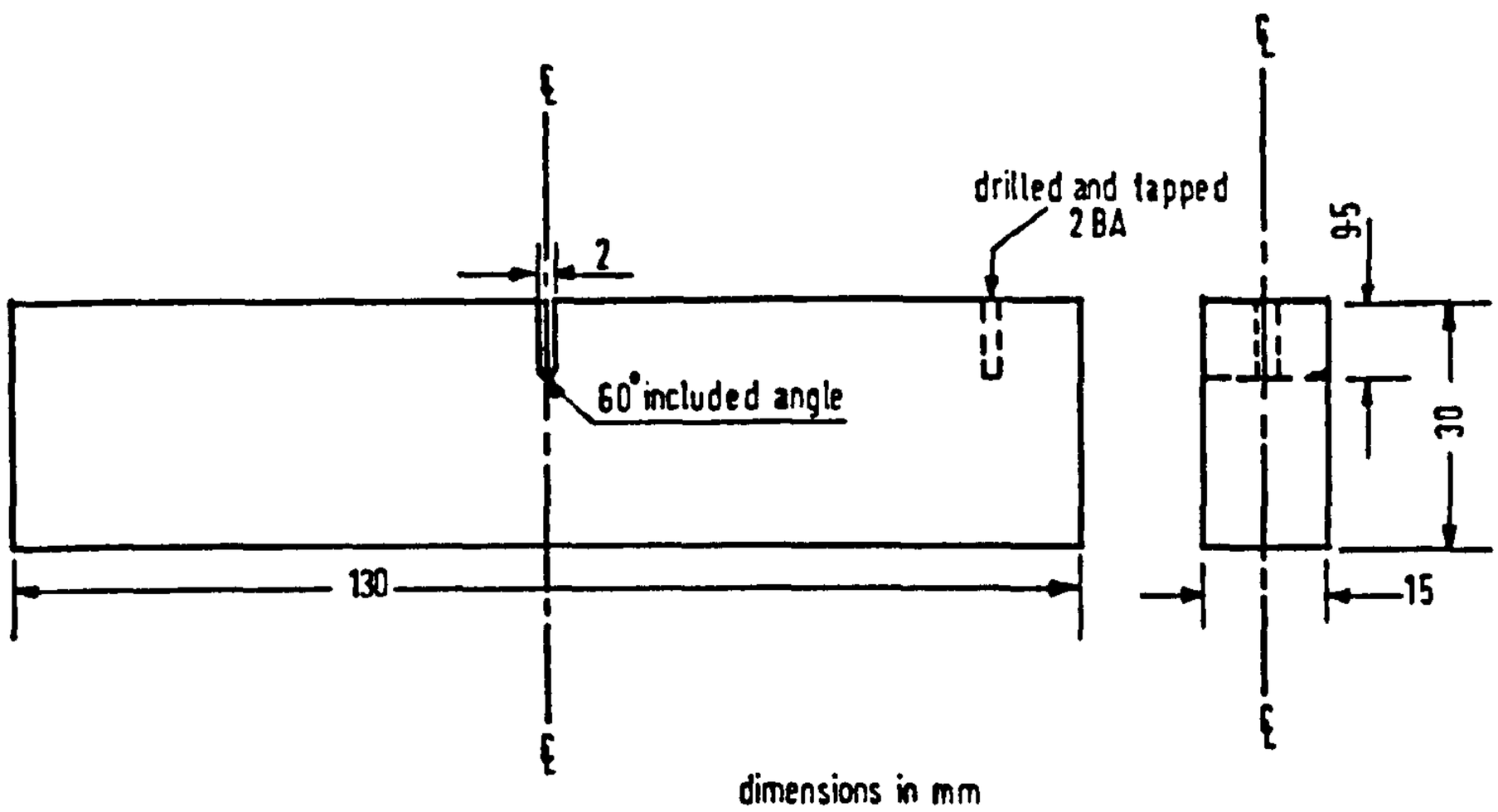

Appendix 4 - Three-point bend, single-edge-notched specimen design

Yield stress	386 MN/m^2
Tensile strength	536 MN/m^2
Charpy energy	33J at - 40 C

Appendix 5A - Mechanical properties of BS 4360 50D steel manufactured in Japan

MATERIAL	σ_y (N/mm^2)	U.T.S. (N/mm^2)	E (G.Pa)
BS 4360 50D plate	386	536	212
Weld Metal	611	653	277
Heat affected zone	434	-	

σ_y heat affected zone given by empirical relationship:

$\sigma_y = 3.25Hv - 349$ (94)

Appendix 5B - Mechanical properties of weld metal and heat affected zone materials.

Carbon	0.15%
Silicon	0.41%
Manganese	1.38%
Phosporus	0.005%
Sulphur	0.003%
Chromium	0.11%
Molybdenum	0.01%
Nickel	0.10%
Aluminium	0.03%
Boron	less than 0.001%
Cobalt	less than 0.01%
Copper	0.02%
	0.002%
Titanium	less than 0.01%
Vanadium	0.05%
Tungsten	less than 0.02%
Iron	Remainder

Appendix 6 - Chemical (product) analysis of BS 4360 50D plate material

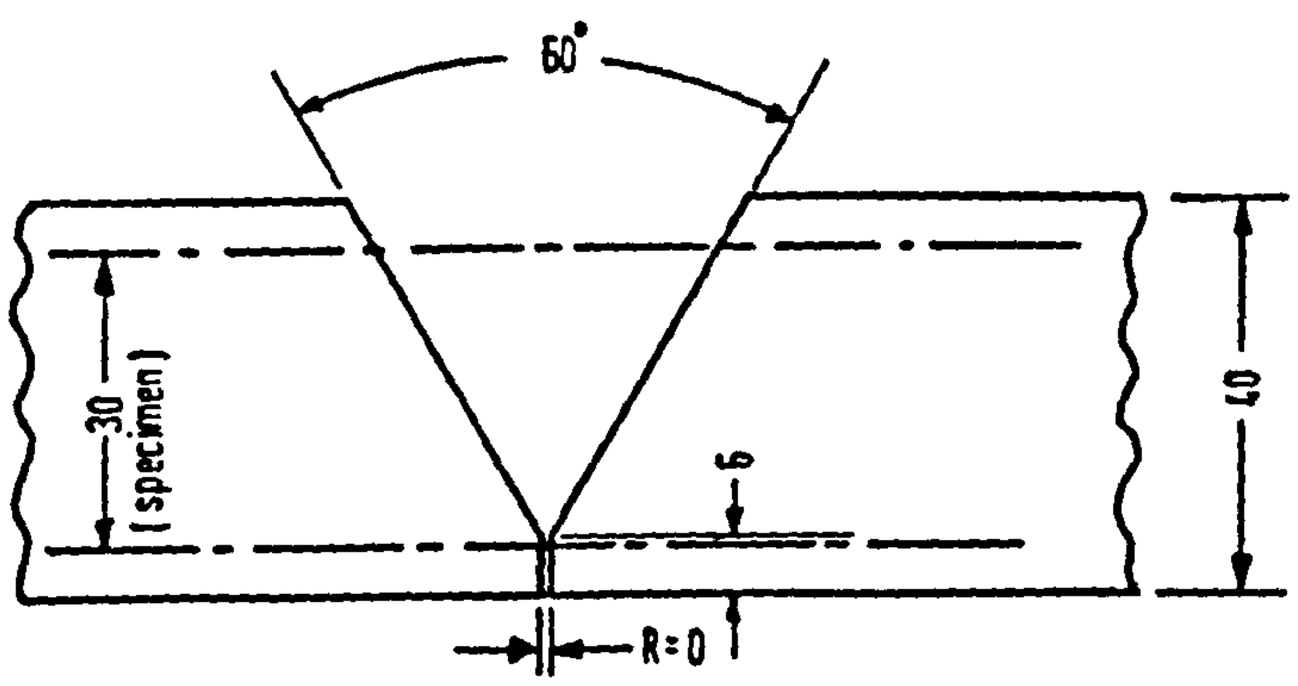

dimensions in mm

Appendix 7 - Single-vee groove weld preparation

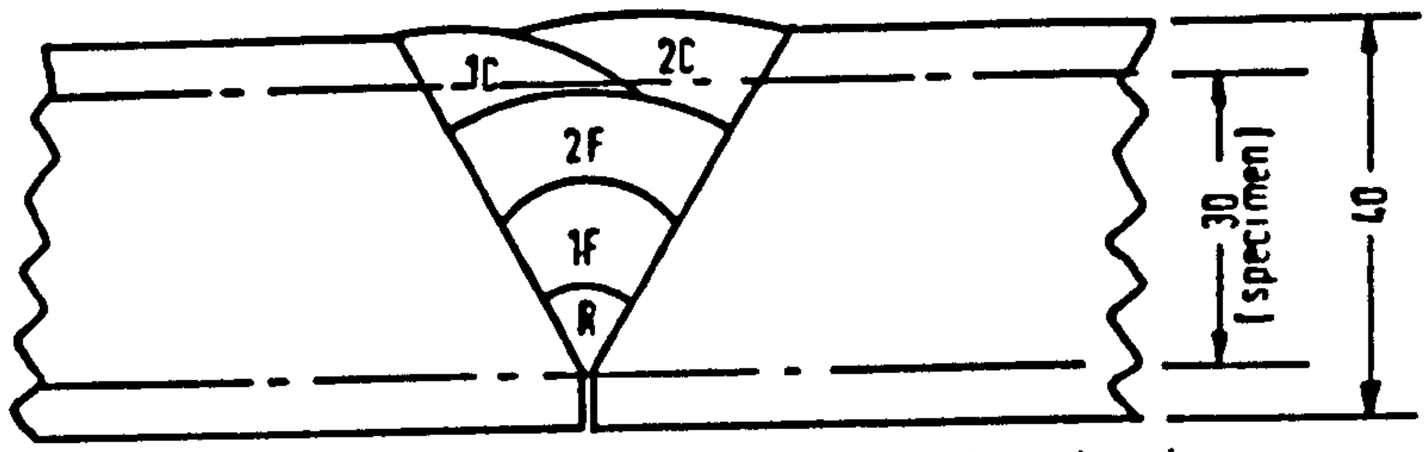

dimensions in mm

CONSUMABLES : Wire : 4mm 5D3Mo.

Flux : OP 41 TT

PROCEDURE :

AMPS	VOLTS	RATE mm/min.	INTERPASS TEMP., °C	PASS NO.
600	30	380	20	R
600	30	325	60	1F
600	30	250	60	2F
600	30	250	60	1C
600	30	250	60	2C

Appendix 8 : Single V-groove butt joint weld procedure

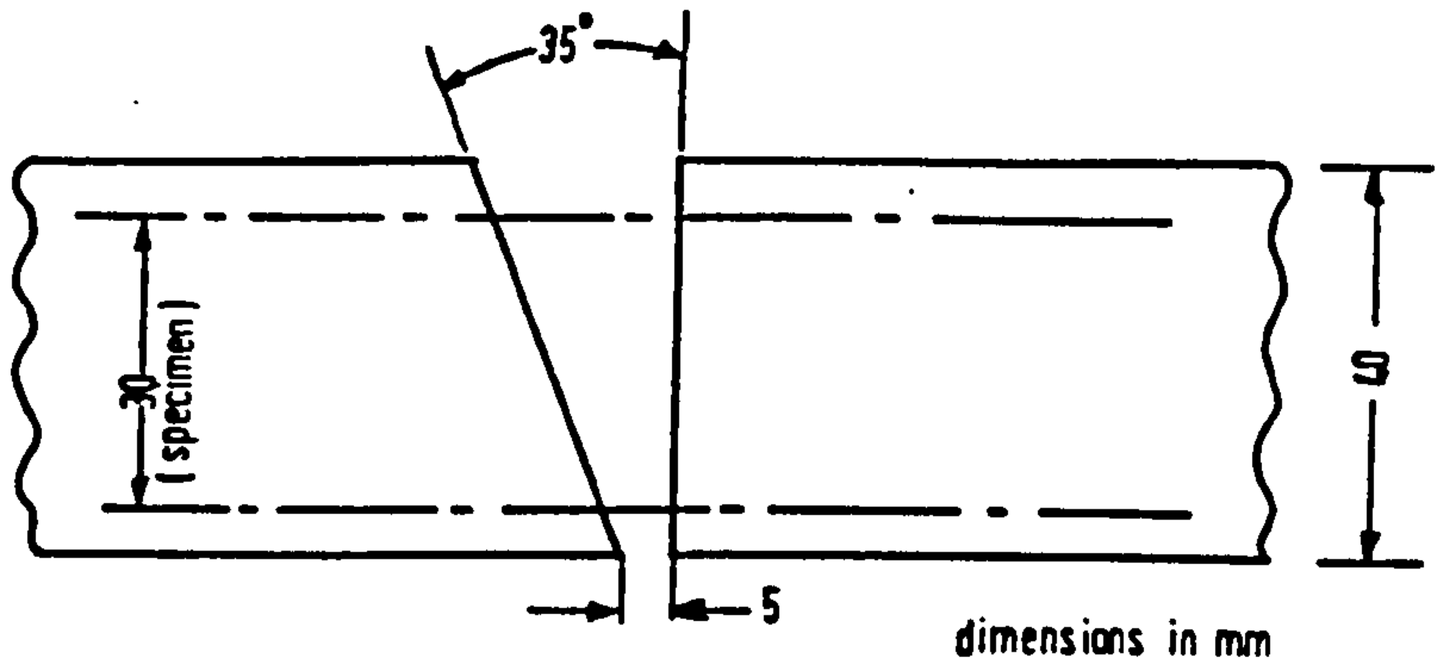

Appendix 9 - Single-bevel weld preparation

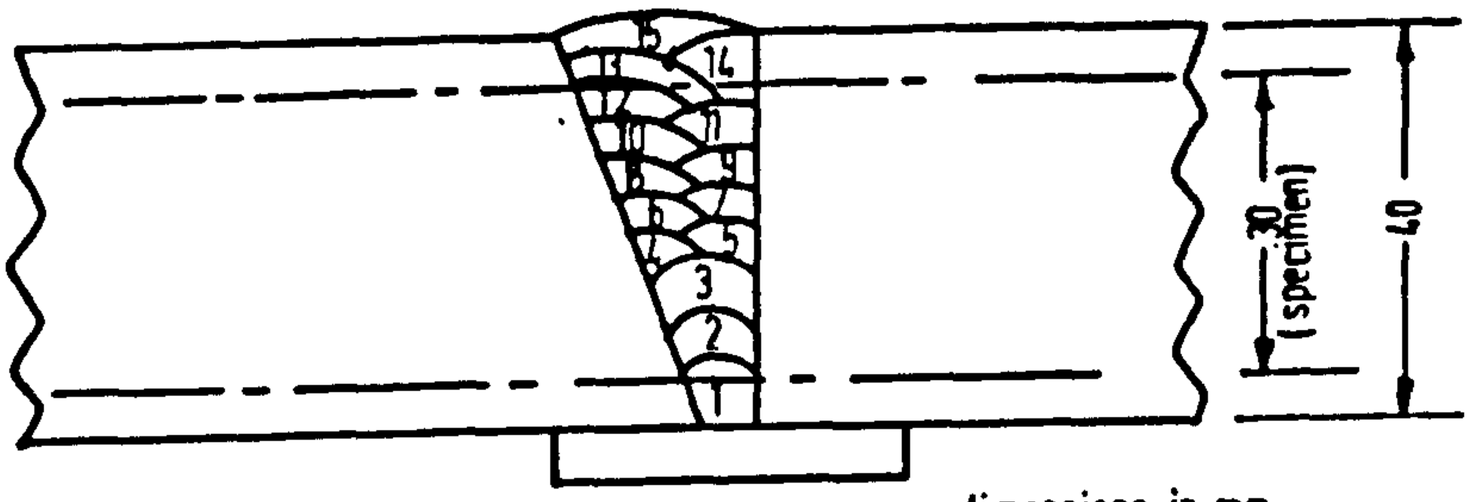

dimensions in mm

Backing strip

CONSUMABLES : Wire : 4mm 5D3 MO

PROCEDURE :

AMPS	VOLTS	RATE mm/min.	INTERPASS	PASS NO.
600	30	250	25	1
600	30	375	25	2
600	30	375	100	3
600	30	375	100	4
600	30	375	100	5
600	30	375	100	6
600	30	375	100	7
600	30	375	100	8
600	30	375	100	9
600	30	375	100	10
600	30	375	100	11
600	30	375	100	12
600	30	375	100	13
600	30	375	100	14
600	30	375	100	15

Pass numbers 1, 2, 3, 5, 7, 9, 11 and 14 set wire max. of 4.0mm from butt face.

Appendix 10 - Single-bevel-groove butt joint weld procedure

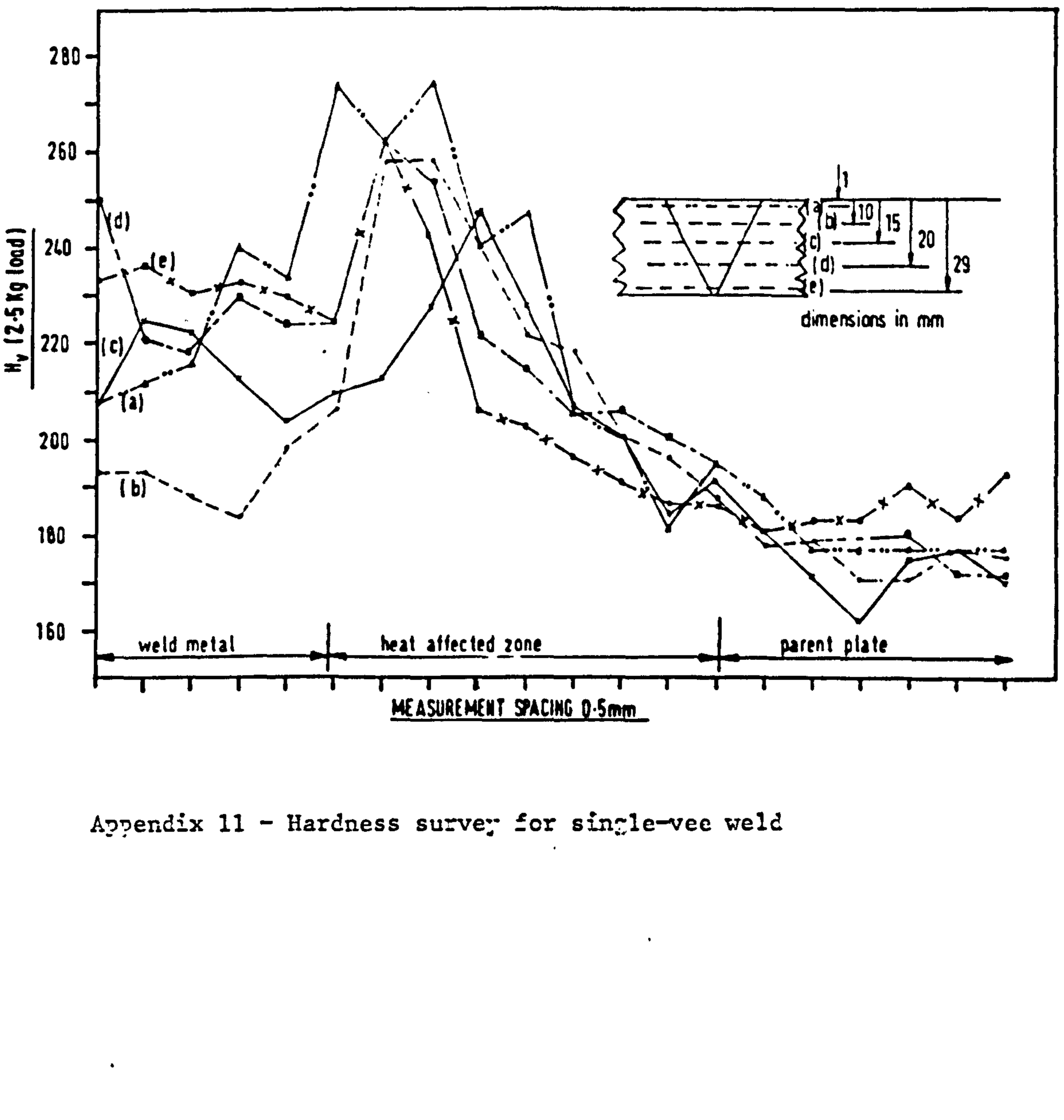

Appendix 11 - Hardness survey for single-vee weld

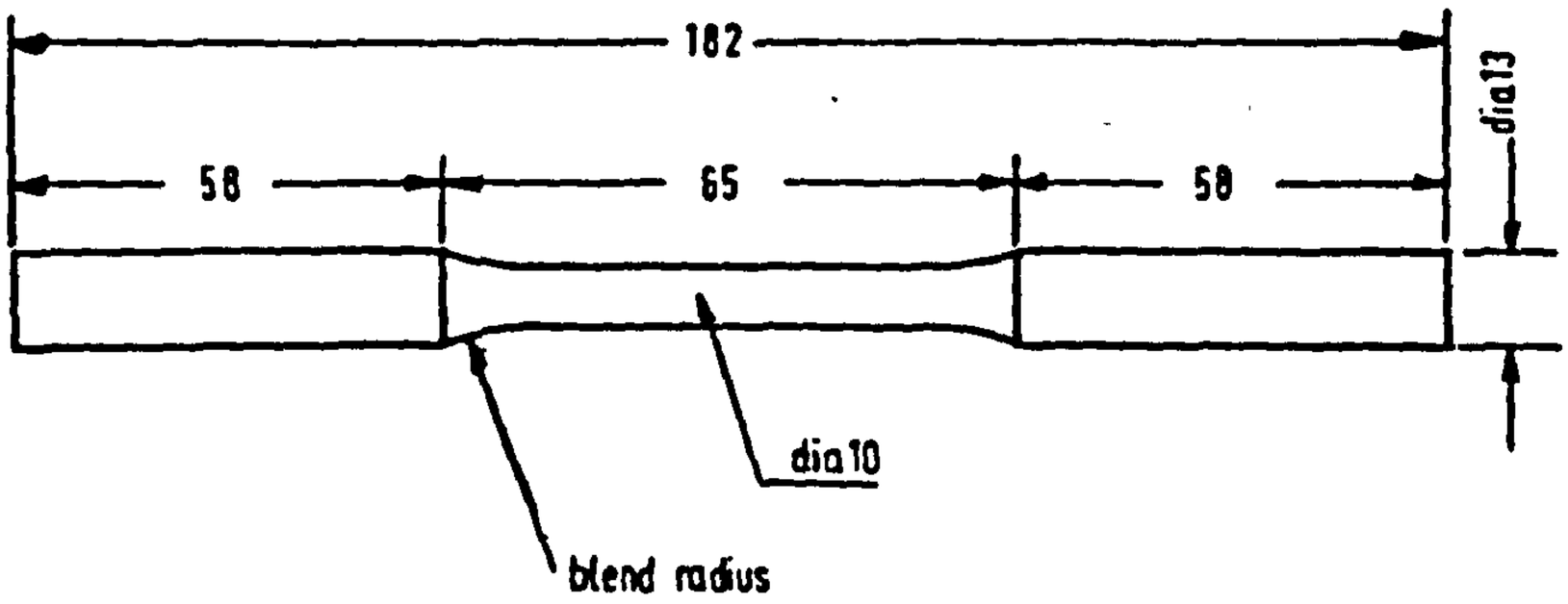

dimensions in mm

Appendix 12 - Tensile test specimen

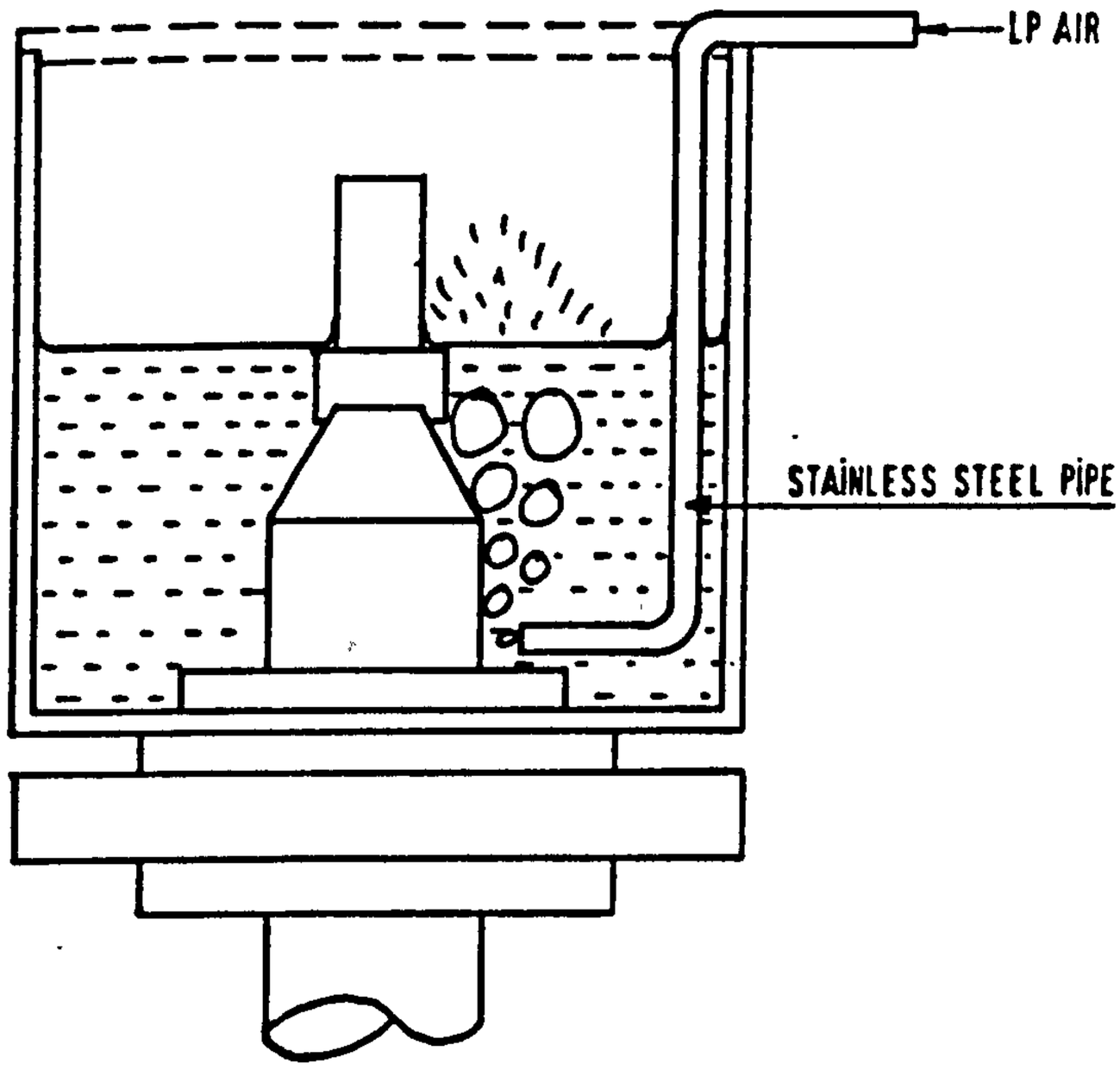

Appendix 13 - Schematic illustration of simulated splash-zone arrangements, using low-pressure compressed air.

KEY: AE = active electrode
RE = reference electrode
WE = working electrode

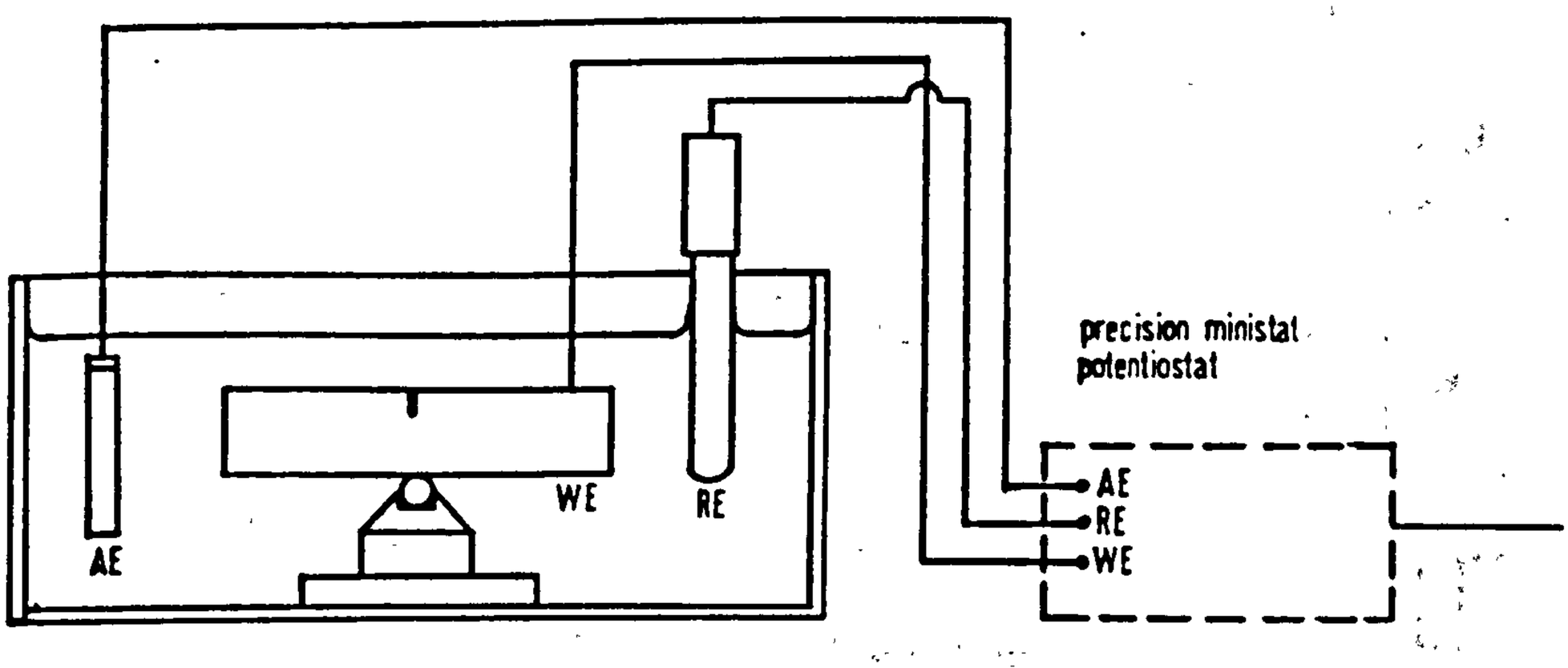

Appendix 14 - Circuit diagram for simulated impressed current cathodic protection system.

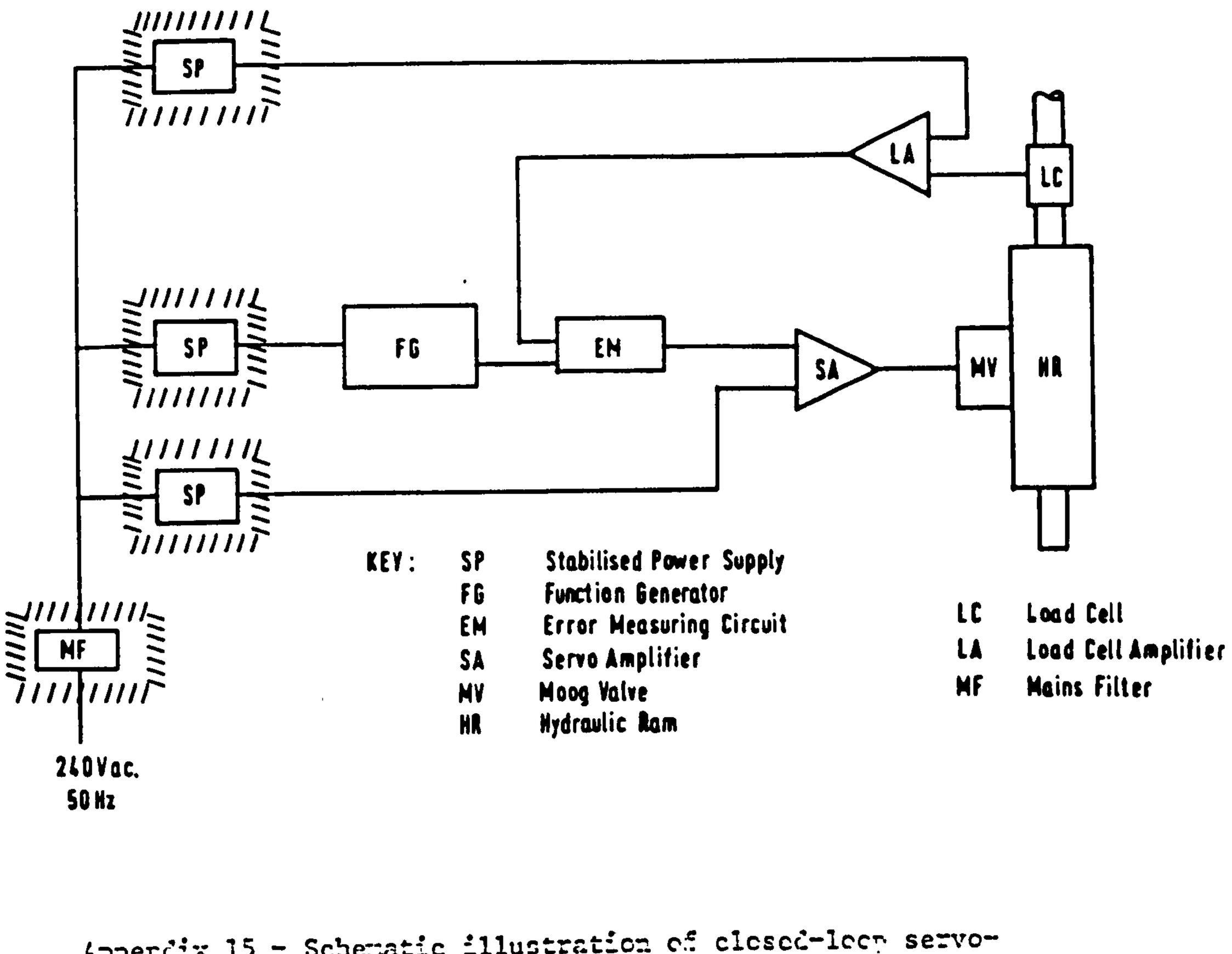

Appendix 15 - Schematic illustration of closed-loop servo-hydraulic load control system

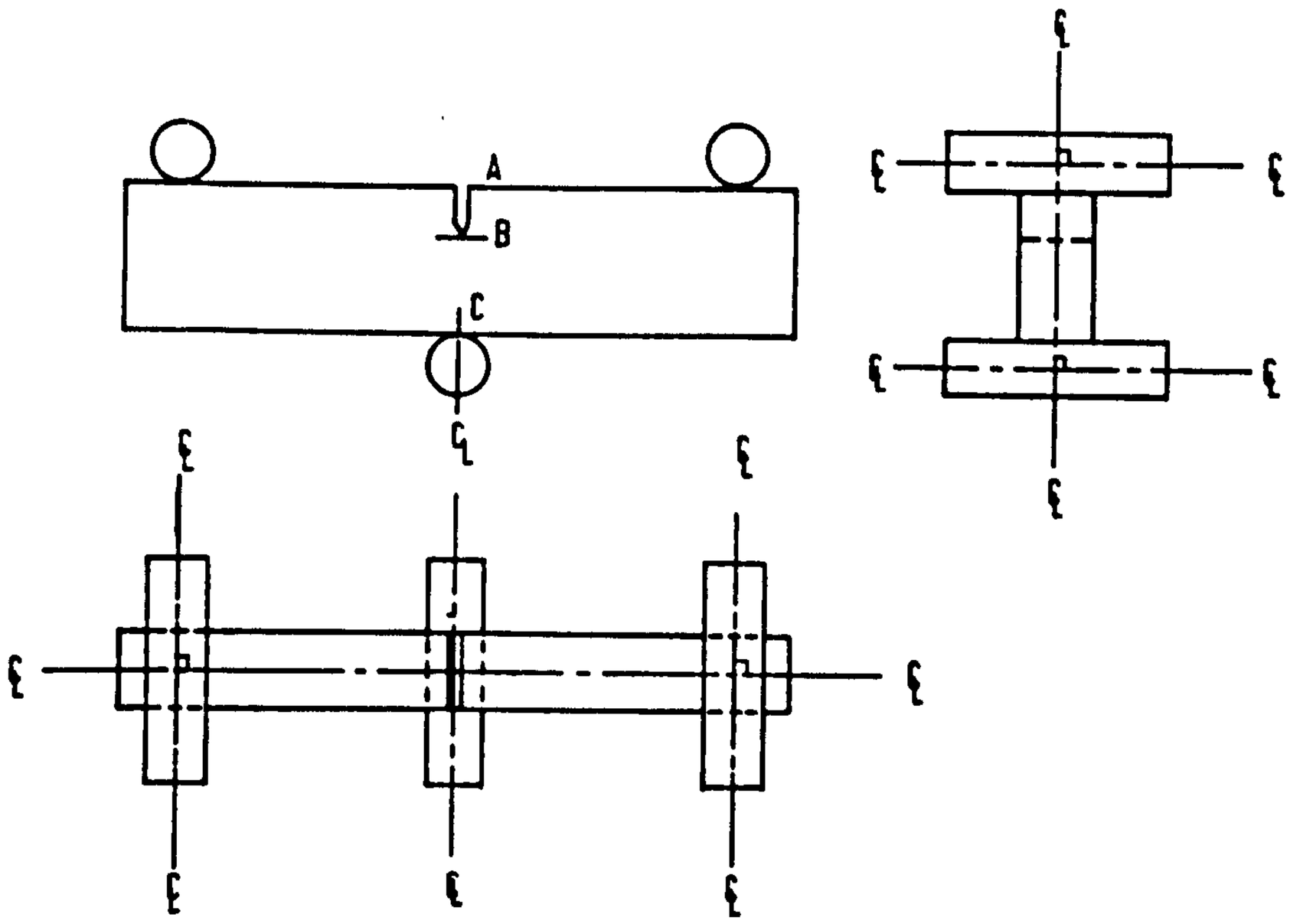

Appendix 16 – Schematic illustration of specimen reference marks and alignment in test machine